UNIVERSITAT POLITÈCNICA DE VALÈNCIA

Department of Mechanical and Materials Engineering

PhD Thesis

Advanced numerical techniques for the acoustic modelling of materials and noise control devices in the exhaust system of internal combustion engines

---

Presented by: MSc. Eva María Sánchez Orgaz

Supervised by: Dr. Francisco David Denia Guzmán

Valencia, March, 2016

PhD Thesis

Advanced numerical techniques for the acoustic modelling of materials and noise control devices in the exhaust system of internal combustion engines

for the degree of

Doctor in Engineering and Industrial Production

presented by

MSc. Eva María Sánchez Orgaz

at the

Department of Mechanical and Materials Engineering

Universitat Politècnica de València

Supervised by

Dr. Francisco David Denia Guzmán

Valencia, March, 2016

PhD THESIS

ADVANCED NUMERICAL TECHNIQUES FOR THE ACOUSTIC MODELLING OF MATERIALS AND NOISE CONTROL DEVICES IN THE EXHAUST SYSTEM OF INTERNAL COMBUSTION ENGINES

Presented by: MSc. Eva María Sánchez Orgaz

Supervised by: Dr. Francisco David Denia Guzmán

QUALIFYING COMMITTEE

PRESIDENT: Dr. Antonio J. Torregrosa Huguet

VOCAL: Dr. Wenbo Duan

SECRETARY: Dr. Jordi Romeu Garbí

Valencia, March, 2016

Abstract

This Thesis is focused on the development and implementation of general and efficient numerical methods for the acoustic modelling and design of noise control devices in the exhaust system of combustion engines. Special attention is paid to silencers, that can be divided into reactive and dissipative configurations. For the latter, significant differences are likely to appear in their acoustic behaviour, depending on the temperature variations within the absorbent material. Also, material heterogeneities associated with uneven filling processes and time degradation due to the exhaust gases, can alter the silencer attenuation performance. Therefore, numerical techniques considering all these features are required to guarantee an accurate prediction of the acoustic behaviour.

First, a literature review is carried out. This is mainly related to one-dimensional models and their associated matrix representation, as well as to acoustic models for absorbent materials and perforated surfaces. It is worth noting that plane wave model limitations make indispensable using alternative multidimensional methods, since the latter are valid for a wide frequency range and for silencers with complex geometries.

In addition to developing acoustic models to simulate exhaust silencers in general terms, the possibility of using new acoustic elements is also explored in this Thesis. These elements have as an objective being an interesting potential alternative to the fibrous absorbent materials commonly used in practice, whose negative impact on health is a current cause for concern. In this sense, and following earlier studies, the Thesis considers the use of microperforated surfaces and goes into detail about the study of surfaces manufactured by sintering. The latter present, in some cases, the particularity of having a nearly constant acoustic impedance, whose value depends, among others, on the thickness and porosity of the plates. Both kind of surfaces have been proved to be an interesting alternative to dissipative silencers; the microperforated surfaces in the low frequency range and the sintered screens in the mid and high frequency range.

General acoustic models, in which the wave equation permits to consider variable properties and mean flow, are considered. Thus, a finite element approach is first

proposed for the acoustic analysis of perforated dissipative silencers including a perforated duct with uniform axial mean flow and an outer chamber with heterogeneous absorbent material. The presence of material heterogeneities can be caused, for example, by the manufacturing process as well as by the degradation due to the soot particles contained in the exhaust gases. In this first approach, a variable bulk density is introduced in the model. On the other hand, property variations can be also produced by temperature gradients. In this second case, a hybrid finite element model has been derived for the acoustic analysis of perforated dissipative silencers including several effects simultaneously: (1) High temperature and thermal gradients in the central duct and the outer absorbent material; (2) A perforated passage carrying non-uniform axial mean flow. Independently of the reasons for the propagation media non-homogeneity, their properties vary with position. The material of the outer chamber can be characterized by means of its equivalent acoustic properties (complex density and speed of sound), considered coordinate-dependent in the context of the current investigation. This can be achieved via the introduction of a heterogeneous bulk density (and the corresponding material airflow resistivity variations) as well as by computing the resistivity distribution if the thermal gradients are significant. A finite element approach has been implemented to solve the pressure-based wave equation for a non-moving heterogeneous medium, associated with the problem of sound propagation in the outer chamber. On the other hand, the governing equation in the central duct has been written and solved in terms of an acoustic velocity potential to allow the presence of an axially inhomogeneous flow while overcoming some numerical issues of the pressure formulation found in earlier studies. The coupling between both regions and the corresponding acoustic fields has been carried out by means of a perforated duct and its acoustic impedance, adapted here to include absorbent material heterogeneities and mean flow effects simultaneously. It has been found that temperature gradients and bulk density heterogeneities can have a significant influence on the acoustic attenuation of an automotive silencer and so should be included in the theoretical models if accurate predictions are required. In some particular configurations, it may be relatively precise to approximate the temperature/bulk density distribution by using a uniform profile with an average value, specially for low resistivity materials. It has been shown, however, that this is not always possible and attenuation overestimation is likely to be predicted, mainly for high radial variations of temperature/bulk density and high material flow resistivities, if the temperature/bulk density distribution is not taken into account.

The use of optimization techniques for industrial devices is also relevant, since it leads to the production of elements with better characteristics. From a practical point of view, the material reduction usually means cost savings, which is very important, for example, in the automotive sector, where large series are manufactured. In activities related to transportation of people and goods, design criteria to achieve the optimum

shape or the maximum weight reduction of vehicle devices usually yield an energy saving. It is worth pointing out that in certain sectors (for example, aeronautical, aerospace, automotive and naval industries), the requirements of optimum shape and minimum weight are very relevant and, in some cases, absolutely indispensable. Evolutionary algorithms (EA) are emergent techniques able to obtain a solution, even in those problems in which the traditional optimization procedures have difficulties, such as multiple constraints or stochastic data. Nevertheless, the favourable characteristics of this kind of algorithms are achieved at the expense of carrying out a high number of evaluations of the objective function, which can be an important problem from a computational point of view. Optimization techniques are combined with the finite element method in the current work, the objective being to achieve the maximum attenuation in the frequency range of interest. A multichamber silencer optimization problem is defined and several analyses are carried out to obtain the most suitable configuration meeting the design constraints for each particular application.

The presence of material heterogeneities due to uneven filling processes or temperature gradients has been considered through a full multidimensional finite element method, although this approach is traditionally thought to be very time-consuming. Under certain assumptions of axial uniformity, several techniques have been developed with a view to reducing the computational effort of a full three-dimensional finite element analysis for dissipative silencers with temperature gradients and a central perforated passage carrying mean flow. These are based on a suitable decomposition of the acoustic field into a set of transversal and axial modes within each silencer subdomain, and a matching procedure of the corresponding modal expansions at the silencer geometrical discontinuities through the continuity conditions of the acoustic pressure and axial velocity. The relative computational efficiency and accuracy of predictions for three matching techniques are studied, including collocation at nodes and Gauss points and also mode-matching with weighted integration. All the techniques provide accurate predictions of the silencer attenuation and outperform the computational expenditure of a finite element computation. Some differences are found among the various schemes in terms of computational speed and solution accuracy. Although more accuracy is expected with the mode-matching method, the computational cost required rapidly increases with the number of modes. For a given computational effort, the most precise technique seems to be the nodal point collocation method, which has a slight advantage over Gauss scheme.

Resumen

La presente Tesis se centra en el desarrollo e implementación de métodos generales y eficientes para el modelado y diseño acústico de componentes de la línea de escape de motores de combustión interna. Merecen una especial atención los silenciadores, que se pueden dividir en configuraciones reactivas y disipativas. Estas últimas pueden llegar a presentar diferencias significativas en el comportamiento acústico debido a las variaciones de temperatura en el interior del material absorbente. La atenuación producida por el silenciador también puede sufrir alteraciones debido a las heterogeneidades que presenta el material asociadas al llenado irregular de la cámara y a la degradación de las fibras producida por el paso del tiempo. Por lo tanto, para obtener una predicción precisa del comportamiento acústico del silenciador considerando todas estas características es necesaria la utilización de técnicas numéricas.

En primer lugar, se lleva a cabo una revisión bibliográfica. Esta recopilación recoge principalmente los modelos unidimensionales y su representación matricial asociada, así como modelos acústicos de materiales absorbentes y superficies perforadas. Merece la pena destacar que las limitaciones inherentes a los modelos de onda plana hacen indispensable la utilización de métodos multidimensionales alternativos, ya que los últimos son válidos para un amplio rango de frecuencias, así como para silenciadores con geometrías complejas.

Además de desarrollar modelos acústicos para simular silenciadores de escape en términos generales, también se explora la posibilidad de utilizar nuevos elementos acústicos. Éstos tienen como objetivo ser una alternativa potencialmente interesante a los materiales fibrosos comúnmente utilizados en la práctica, cuyo impacto negativo sobre la salud es una fuente de preocupación en la actualidad. En este sentido, y siguiendo estudios previos, la Tesis considera el uso de superficies microperforadas y profundiza en el estudio de superficies fabricadas mediante sinterización. Estas últimas, en algunos casos, presentan la particularidad de tener una impedancia acústica prácticamente constante, cuyo valor depende, entre otras cosas, del espesor y la porosidad de las placas. Ambos tipos de superficies han demostrado ser una alternativa interesante a los silenciadores perforados disipativos; las superficies

microperforadas en el rango de bajas frecuencias y las superficies sinterizadas en el rango de medias y altas frecuencias.

En la presente Tesis se consideran modelos acústicos generales, en los que la ecuación de ondas permite considerar propiedades variables y flujo medio. Así pues, se propone un enfoque en elementos finitos para el análisis acústico de silenciadores disipativos perforados incluyendo un conducto perforado con flujo medio axialmente uniforme y una cámara exterior con material absorbente heterogéneo. La presencia de heterogeneidades puede ser causada, por ejemplo, por el proceso de fabricación, así como por la degradación causada por las partículas de hollín inmersas en los gases de escape. En este primer modelo, se introduce una densidad variable. Por otro lado, las variaciones de las propiedades también pueden ser producidas por los gradientes de temperatura. En este segundo caso, se ha desarrollado un modelo de elementos finitos mixto para el análisis acústico de silenciadores disipativos perforados que incluye varios efectos simultáneamente: (1) elevada temperatura y gradientes térmicos en el conducto central y el material absorbente externo; (2) un conducto central que canaliza flujo medio axial no uniforme. Independientemente de las causas de la heterogeneidad de los medios de propagación, sus propiedades varían con la posición. El material de la cámara exterior se puede caracterizar por medio de sus propiedades acústicas equivalentes (densidad y velocidad del sonido) complejas, consideradas dependientes de las coordenadas en el contexto de la presente investigación. Esto se puede lograr gracias a la introducción de una densidad heterogénea (y las correspondientes variaciones de la resistividad) así como al cálculo de la distribución de la resistividad si los gradientes térmicos son significativos. Se ha implementado un modelo de elementos finitos para resolver la ecuación de ondas basada en una formulación en presión para un medio heterogéneo sin flujo medio, asociado al problema de propagación del sonido en la cámara exterior. Por otro lado, la ecuación en el conducto central se ha planteado y resuelto en términos de potencial acústico de velocidad que considera la existencia de flujo medio a la par que evita algunos problemas numéricos hallados en estudios previos al utilizar una formulación en presiones. El acoplamiento entre ambas regiones y los correspondientes campos acústicos se ha llevado a cabo mediante un conducto perforado y su correspondiente impedancia acústica, que aquí ha sido adaptada para poder incluir las heterogeneidades del material absorbente y los efectos del flujo medio simultáneamente. Se ha visto que los gradientes de temperatura y las heterogeneidades de la densidad influyen notablemente en la atenuación acústica de un silenciador de automoción y por lo tanto, deben incluirse en los modelos teóricos. En algunas configuraciones particulares puede ser relativamente preciso aproximar el campo de temperatura o la variación de densidad utilizando una distribución uniforme con un valor promediado, especialmente para materiales de baja resistividad. Sin embargo, se ha demostrado que esto no siempre es posible y los cálculos sobrestiman la atenuación, principalmente debido a las variaciones radiales de temperatura/densidad

y las elevadas resistividades del material, si la distribución de temperatura/densidad no se tiene en cuenta.

La utilización de técnicas de optimización para componentes industriales también es relevante, ya que conduce a la producción de elementos con mejores características. Desde un punto de vista práctico, la disminución de material normalmente conlleva una reducción en los costes, lo que es muy importante, por ejemplo, en el sector del automóvil, donde se fabrican grandes series. En actividades relacionadas con el transporte de personas y bienes, el criterio de diseño para conseguir la forma óptima o la máxima reducción de peso de los componentes del vehículo normalmente conlleva un ahorro energético. Es importante destacar que en ciertos sectores (por ejemplo, en las industrias aeronáutica, aeroespacial, de la automoción y naval) el requerimiento de forma óptima y peso mínimo es muy relevante, y en algunos casos, absolutamente indispensable. Los algoritmos evolutivos (AE) son técnicas emergentes debido a su capacidad de obtener una solución, incluso en aquellos problemas en los que los procedimientos de optimización tradicionales tienen dificultades, como restricciones múltiples o datos estocásticos. No obstante, las características favorables de este tipo de algoritmos se consiguen a expensas de llevar a cabo un elevado número de evaluaciones de la función objetivo, lo que puede ser un problema importante desde un punto de vista computacional. Las técnicas de optimización se combinan con el método de elementos finitos en el presente trabajo, siendo el objetivo lograr la máxima atenuación posible en el rango de frecuencias de interés. Se define un problema de optimización de un silenciador multicámara y se llevan a cabo varios análisis para obtener la configuración más adecuada para cada aplicación que cumpla las restricciones de diseño.

La presencia de heterogeneidades en el material debidas a un proceso irregular de llenado de la cámara o a gradientes de temperatura se ha considerado mediante el método de elementos finitos, aunque este enfoque tradicionalmente se ha caracterizado por consumir un elevado tiempo de cálculo. Bajo ciertas suposiciones de uniformidad axial, se han desarrollado varias técnicas con vistas a reducir el coste computacional de un análisis 3D de elementos finitos para silenciadores disipativos con gradientes de temperatura y un conducto central que canaliza el flujo. Éstas se basan en la descomposición del campo acústico en un conjunto de modos axiales y transversales dentro de cada subdominio del silenciador, y un procedimiento de ajuste de las correspondientes expansiones modales en las discontinuidades geométricas del silenciador mediante las condiciones de continuidad de la presión acústica y la velocidad axial. Se estudia la eficiencia computacional y precisión de los cálculos para tres técnicas de ajuste, incluyendo colocación en nodos y puntos de Gauss y también ajuste modal con integración ponderada. Todas las técnicas proporcionan resultados precisos de la atenuación del silenciador y logran mejores resultados en cuanto a coste computa-

cional que los cálculos de elementos finitos. Se han encontrado algunas diferencias entre los diferentes métodos en términos de velocidad de cálculo y precisión de la solución. Aunque se obtiene más precisión con el método de ajuste modal, el coste computacional requerido aumenta rápidamente con el número de modos. Para un coste computacional dado, la técnica más precisa parece ser el método de colocación puntual en nodos, con una ligera ventaja sobre la colocación en puntos de Gauss.

Resum

La present Tesi es centra en el desenvolupament i implementació de mètodes generals i eficients per al modelatge i disseny acústic de components de la línia d'escapament de motors de combustió interna. Mereixen una especial atenció els silenciadors, que es poden dividir en configuracions reactives i dissipatives. Aquestes últimes poden arribar a presentar diferències significatives en el comportament acústic a causa de les variacions de temperatura a l'interior del material absorbent. L'atenuació produïda pel silenciador també pot patir alteracions a causa de les heterogeneïtats que presenta el material associades a l'ompliment irregular de la cambra i a la degradació de les fibres produïda pel pas del temps. Per tant, per obtenir una predicció precisa del comportament acústic del silenciador considerant totes aquestes característiques és necessària la utilització de tècniques numèriques.

En primer lloc, es porta a terme una revisió bibliogràfica. Aquesta recopilació recull principalment els models unidimensionals i la seua representació matricial associada, així com models acústics de materials absorbents i superfícies perforades. Val la pena destacar que les limitacions inherents als models d'ona plana fan indispensable la utilització de mètodes multidimensionals alternatius, ja que els últims són vàlids per a un ampli rang de freqüències, així com per a silenciadors amb geometries complexes.

A més de desenvolupar models acústics per simular silenciadors d'escapament en termes generals, també s'explora la possibilitat d'utilitzar nous elements acústics. Aquests tenen com a objectiu ser una alternativa potencialment interessant als materials fibrosos comunament utilitzats en la pràctica, l'impacte negatiu dels quals sobre la salut és una font de preocupació en l'actualitat. En aquest sentit, i seguint estudis previs, la Tesi considera l'ús de superfícies microperforades i aprofundeix en l'estudi de superfícies fabricades mitjançant sinterització. Aquestes últimes, en alguns casos, presenten la particularitat de tenir una impedància acústica pràcticament constant, el valor de la qual depèn, entre altres coses, del gruix i la porositat de les plaques. Tots dos tipus de superfícies han demostrat ser una alternativa interessant als silenciadors dissipatius perforats; les superfícies microperforades en el rang de baixes freqüències i les superfícies sinteritzades en el rang de mitjanes i altes freqüències.

En la present Tesi es consideren models acústics generals, en els que l'equació d'ones permet considerar propietats variables i flux mig. Així doncs, es proposa un enfocament en elements finits per a l'anàlisi acústica de silenciadors dissipatius perforats incloent un conducte perforat amb flux mig axialment uniforme i una cambra exterior amb material absorbent heterogeni. La presència d'heterogeneïtats pot ser causada, per exemple, pel procés de fabricació, així com per la degradació causada per les partícules de sutge immerses en els gasos d'escapament. En aquest primer model, s'introdueix una densitat variable. D'altra banda, les variacions de les propietats també poden ser produïdes pels gradients de temperatura. En aquest segon cas, s'ha desenvolupat un model d'elements finits mixt per a l'anàlisi acústic de silenciadors dissipatius perforats que inclou diversos efectes simultàniament: (1) elevada temperatura i gradients tèrmics en el conducte central i el material absorbent extern; (2) una conducció central que canalitza flux mig axial no uniforme. Independentment de les causes de l'heterogeneïtat dels medis de propagació, les seves propietats varien amb la posició. El material de la cambra exterior es pot caracteritzar per mitjà de les seues propietats acústiques equivalents (densitat i velocitat del so) complexes, considerades dependents de les coordenades en el context de la present investigació. Això es pot aconseguir gràcies a la introducció d'una densitat heterogènia (i les corresponents variacions de la resistivitat) així com al càlcul de la distribució de la resistivitat si els gradients tèrmics són significatius. S'ha implementat un model d'elements finits per a resoldre l'equació d'ones basada en una formulació en pressió per a un medi heterogeni sense flux mig, associat al problema de propagació del so a la cambra exterior. D'altra banda, l'equació en el conducte central s'ha plantejat i resolt en termes de potencial acústic de velocitat que considera l'existència de flux mig a l'una que evita alguns problemes numèrics trobats en estudis previs al utilitzar una formulació en pressions. L'acoblament entre les dues regions i els corresponents camps acústics s'ha dut a terme mitjançant un conducte perforat i la seua impedància acústica, que aquí ha sigut adaptada per poder incloure les heterogeneïtats del material absorbent i els efectes del flux mig simultàniament. S'ha vist que els gradients de temperatura i les heterogeneïtats de la densitat influeixen notablement en l'atenuació acústica d'un silenciador d'automoció i per tant, s'han d'incloure en els models teòrics. En algunes configuracions particulars pot ser relativament precís aproximar el camp de temperatura o la variació de densitat utilitzant una distribució uniforme amb un valor mig, especialment per a materials de baixa resistivitat. No obstant això, s'ha demostrat que no sempre és possible i els càlculs sobreestimen l'atenuació, principalment a causa de les variacions radials de temperatura/densitat i les elevades resistivitats del material, si la distribució de temperatura/densitat no es té en compte.

La utilització de tècniques d'optimització per a components industrials també és rellevant, ja que condueix a la producció d'elements amb millors característiques. Des d'un punt de vista pràctic, la disminució de material normalment comporta una reducció

en els costos, el que és molt important, per exemple, en el sector de l'automòbil, on es fabriquen grans sèries. En activitats relacionades amb el transport de persones i béns, el criteri de disseny per aconseguir la forma òptima o la màxima reducció de pes dels components del vehicle normalment comporta un estalvi energètic. És important destacar que en certs sectors (per exemple, en les indústries aeronàutica, aeroespacial, de l'automoció i naval) el requeriment de forma òptima i pes mínim és molt rellevant, i en alguns casos, absolutament indispensable. Els algoritmes evolutius (AE) són tècniques emergents a causa de la seua capacitat d'obtenir una solució, fins i tot en aquells problemes en què els procediments d'optimització tradicionals tenen dificultats, com restriccions múltiples o dades estocàstiques. No obstant això, les característiques favorables d'aquest tipus d'algoritmes s'aconsegueixen a costa de dur a terme un elevat nombre d'avaluacions de la funció objectiu, el que pot ser un problema important des d'un punt de vista computacional. Les tècniques d'optimització es combinen amb el mètode dels elements finits en el present treball, sent l'objectiu aconseguir la màxima atenuació possible en el rang de freqüències d'interès. Es defineix un problema d'optimització d'un silenciador multicambra i es duen a terme diverses anàlisis per obtenir la configuració més adequada per a cada aplicació que complisca les restriccions de disseny.

La presència d'heterogeneïtats en el material degudes a un procés irregular d'ompliment de la cambra o gradients de temperatura s'ha considerat mitjançant el mètode dels elements finits, encara que aquest enfocament tradicionalment s'ha caracteritzat per consumir un elevat temps de càlcul. Sota certes suposicions d'uniformitat axial, s'han desenvolupat diverses tècniques amb vista a reduir el cost computacional d'una anàlisi 3D d'elements finits per silenciadors dissipatius amb gradients de temperatura i un conducte central que canalitza el flux. Aquestes es basen en la descomposició del camp acústic en un conjunt de modes axials i transversals dins de cada subdomini del silenciador, i un procediment d'ajust de les corresponents expansions modals en les discontinuïtats geomètriques del silenciador mitjançant les condicions de continuïtat de la pressió acústica i la velocitat axial. S'estudia la relativa eficiència computacional i precisió dels càlculs per a tres tècniques d'ajust, incloent col·locació en nodes i punts de Gauss i també ajust modal amb integració ponderada. Totes les tècniques proporcionen resultats precisos de l'atenuació del silenciador i aconsegueixen millors resultats quant a cost computacional que els càlculs d'elements finits. S'han trobat algunes diferències entre els diferents mètodes en termes de velocitat de càlcul i precisió de la solució. Encara que s'obté més precisió amb el mètode d'ajust modal, el cost computacional requerit augmenta ràpidament amb el nombre de modes. Per a un cost computacional donat, la tècnica més precisa sembla ser el mètode de col·locació puntual en nodes, amb un lleuger avantatge sobre la col·locació en punts de Gauss.

Dedicated to my parents and sister

Acknowledgments

First and foremost, I would like to express my gratitude to my supervisor Dr. Francisco D. Denia for his continuous support during these four years, as well as for his encouragement, his numerous suggestions and all the transmitted knowledge.

I would also like to thank all members of the Mechanical Engineering Group who have contributed immensely to my personal and professional development. This group has been a source of support and motivation, especially Dr. Juan José Ródenas and Dr. José Albelda who guided me in my first steps into the research world. Also Dr. Ana Pedrosa for her excellent advice and Carlos Orero for his contribution on the experimental part of the Thesis.

In addition, I would like to extend my gratitude to my PhD mates for their friendship and support; as well as to Fede, Angels, Eva and Marga because without them finishing this PhD would have been impossible.

Dr. Ray Kirby requires a special mention for all his help and kindness during my research stay at Brunel University.

I devote innermost appreciation to my family because they have always been by my side loving and supporting me during these four years.

Finally, I want to express my gratitude to all the people who have contributed to a greater or a lesser extent to the development of this work.

Contents

Chapter 1

Introduction

Summary:

In this chapter, some problems associated with the noise emitted by the running of internal combustion engines are presented. Also, the development of accurate and efficient numerical tools for the modelling and calculation of the acoustic performance of dissipative silencers is justified. The scope of the Thesis is explained, as well as the structure used to obtain the main objectives of this work.

1.1 Motivation and background

In the last decades, concerns about the acoustic environmental pollution have considerably increased. In cities, one of the main sources of noise are vehicles, whose emissions of sound are due to the noise produced by reciprocating internal combustion engines, by the interaction of the tyres with the roadbed, etc.

For vehicles using combustion engines, the exhaust system is one of the main sources of noise. For this reason, silencers have a special relevance as they reduce the sound to levels allowed by the legislation in force. The incorporation of absorbent materials increases the attenuation levels achieved by the silencer in the mid and high frequency range [57, 126]. To facilitate the evacuation of the exhaust gases and decrease the swept of the absorbent material, configurations normal to the flow are avoided. In the last years, however, new configurations have been explored as an alternative to traditional dissipative silencers to reduce the harmful effects of fibrous materials on human health and the environment. One of the alternatives that seems especially interesting is based on the combination of multichamber configurations and microperforated surfaces [8, 64].

Regarding the modelling and acoustic analysis of silencers, the most widely used methodologies are the three-dimensional techniques [44–47, 62, 160, 161, 174, 178] that have displaced the one-dimensional models [126] because of their higher accuracy and versatility. While multidimensional analytical approaches [1, 15, 61, 66, 104, 158, 159] are useful for relatively simple geometries, numerical techniques, such as the finite element method (FEM) [44–47, 62, 103, 105, 160, 161] and the boundary element method (BEM) [178, 181], have been more widely used than analytical methods as they permit more general and complex calculations. Comparing FEM and BEM, it can be observed that the FEM is more versatile than the BEM when dealing with general problems that include, for example, material heterogeneities and non-uniform mean flow convective effects [181]. One of the main disadvantages of these numerical methods is their high computational cost as the number of degrees of freedom increases. For this reason, alternative techniques arise to palliate this drawback. Some authors take benefit from the fact that most automotive silencers present an arbitrary but axially uniform cross section, thus allowing the proposal of some approaches to be more efficient from a computational point of view. Glav [80, 81] considered the wave equation, in the absence of mean flow, at the cross section of dissipative silencers (without perforated duct) and obtained its associated eigenvalue problem. Once this problem was analytically solved, he applied a point collocation technique to axially couple the acoustic fields (acoustic pressure and velocity) and then obtain the full pressure field to compute the attenuation achieved by the silencer. Afterwards, Kirby

combined the finite element method (more versatile than analytical techniques) with a point collocation approach [100, 105] and the mode-matching method [101] to obtain the transmission loss of perforated dissipative silencers in the presence of mean flow.

Another important factor to consider is that, in spite of the fact that traditionally the properties within the silencer (bulk density of the absorbent material, temperature field, etc.) have been considered uniform [54, 126, 155, 158], in real applications they can present strong variations. These heterogeneities can have a notable influence on the acoustic performance of the silencer [16, 62, 138, 160, 178].

Nowadays, due to the demands of markets and manufacturing companies, finding the optimal component for each application is becoming an important factor for the automotive industry in order to determine the most suitable configuration that meets the design constraints. For that reason, optimization techniques have experimented a rapid growth and can be classified in different ways. The most common classification divides the algorithms that guide the optimization process into deterministic and stochastic algorithms [37–39, 56]. The main advantage of the deterministic approaches is their high speed of convergence, while the stochastic algorithms allow a greater exploration of the search space. Besides, stochastic algorithms present a better behaviour against noise. For this reason, during recent years these methods, and more specifically the evolutionary algorithms such as the genetic ones [24, 38, 56, 183], have become especially relevant.

1.2 Objectives

The aim of the present Thesis is to obtain advanced acoustical models for fundamental components of the exhaust system in internal combustion engines, such as silencers. Therefore, it is expected to extend and complete the models available in the literature. In order to achieve this aim, the following partial objectives are proposed:

- Experimental characterization of the acoustic behaviour of sintered surfaces and exploration of potential applications as an alternative to the traditional perforated dissipative silencer.

- Development and implementation of in-house FE models that allow the multidimensional simulation of perforated dissipative silencers containing heterogeneous materials and mean flow. Several approaches are proposed to deal with this design situation which are of practical interest. In the first model, the bulk density of the absorbent material is considered to be heterogeneous. This fact

leads to spatial variations in the material resistivity, which also affects the characteristic impedance of the perforated duct. The influence of the material bulk density heterogeneities on the attenuation will be studied. A second model is also proposed, where the existence of thermal gradients within the silencer is considered. These temperature variations modify the properties of the different propagation media: air in the central duct and absorbent material within the chamber. In addition, the mean flow confined within the central duct will also be non-uniform from an axial point of view, leading to the corresponding variations of the perforated screen impedance and additional convective terms in the formulation. The effects of high temperatures as well as thermal gradients within the silencer on the acoustic attenuation performance of perforated dissipative configurations will be studied in detail.

- Development and implementation of in-house three-dimensional finite element (FE) models to compute the acoustic attenuation performance of multichamber silencers to achieve as much attenuation as possible in the desired frequency range by using different surfaces and the most suitable geometry.

- Development and implementation of accurate and efficient numerical techniques to study the acoustic performance of perforated dissipative silencers of arbitrary, but uniform, cross section in the presence of transversal thermal gradients and mean flow. Two different approaches are proposed for reducing the computational expenditure of a full three-dimensional FE calculation. The first combines a two-dimensional FE eigenvalue problem with the point collocation (PC) method while in the second approach, PC is replaced by the mode-matching (MM) technique.

1.3   Organization and development of the Thesis

The Thesis is focused on three different subjects with a view to completing the existing models, as well as filling some gaps found in the bibliography: (1) Modelling and characterization of sintered surfaces and optimization of multichamber silencers incorporating them; (2) Advanced numerical FE models to consider different kinds of heterogeneities in the propagation media within the silencer; (3) Computationally efficient methods to study any geometry with an arbitrary, but axially uniform, cross section, considering the presence of transversal thermal gradients. The organization and main structure of the work consist of six chapters.

In Chapter 1, the targets and the organization of this Thesis are described.

In Chapter 2, the bases of the acoustic theory applied to ducts and silencers are presented, with special emphasis on plane wave models and their associated matrix representation. In this chapter, the main part of the nomenclature is defined, as well as the variables used within the Thesis. Some silencer typologies used in practice and their fundamental properties are described. In addition, some relevant characteristics of perforated and microperforated surfaces are described, and the properties of a number of commonly used fibrous absorbent material models are presented. Also, some details are provided for the basic equations that characterize the wave propagation in media other than air. Besides, the way of quantifying the sound attenuation by means of different indicators is discussed. Finally, the models described are applied to some particular silencer configurations.

In Chapter 3, a generalization of the absorbent material models described in Chapter 2 is carried out to obtain more realistic results and predictions. These models consider that the material properties are heterogeneous. Non-homogeneity can be due to several causes, such as temperature variations within the silencer, uneven filling of the chamber during manufacturing, material degradation over time due to the exhaust gases, etc. Also, sintered surfaces are modelled, characterized and explored as a possible potential alternative to the traditional perforated dissipative silencers.

In Chapter 4, the finite element method (FEM) is applied to the computation of the acoustic attenuation performance for perforated dissipative silencers. Three different formulations are proposed: (1) A 3D pressure-based approach; (2) A 3D velocity potential-based technique; (3) A hybrid method combining approaches (1) and (2) to consider the heterogeneities associated with properties of the different propagation media (air and absorbent material). As previously mentioned, these heterogeneities can be due to the silencer manufacturing process (chamber filling with fibrous absorbent material) or to its operating conditions (fibre degradation/pollution, thermal gradients, etc.). The hybrid formulation is applied, on the one hand, to predict the attenuation in the presence of temperature gradients and, on the other hand, to study the influence of the bulk density variations on the acoustic attenuation. Also, a practical shape optimization procedure is presented and applied to a multichamber silencer with different geometries in order to obtain the most suitable configuration for the cases under study.

In Chapter 5, two computationally efficient numerical techniques are detailed with a view to reducing the computational expenditure of a full multidimensional FE calculation. Thus, one of the main advantages of these methods is that they permit obtaining the attenuation of silencers with an arbitrary, but axially uniform, cross section with less computational effort. As will be shown, axial and transversal solutions of the wave equation are combined. First, the FEM is employed in a two-dimensional

problem to extract the eigenvalues and associated eigenvectors for the silencer cross section. Mean flow as well as transversal temperature gradients and the corresponding thermal-induced material heterogeneities are included in the model. The main hypothesis is that the acoustic impact of axial temperature variations is small compared to transversal gradients. PC and MM schemes are then used to couple the acoustic fields (pressure and axial acoustic velocity) at the geometric discontinuities between the silencer chamber and the inlet and outlet pipes. Transmission loss predictions are compared favourably with a general FE approach, offering a reduction in the computational effort. The methods are applied to some common automotive silencer configurations and the influence of the temperature field on the silencer acoustic behaviour is studied.

In Chapter 6, the conclusions of the work are summarized and some potential future lines of investigation are briefly described.

Chapter 2

Fundamentals: wave equation and acoustic characterization

Summary:

In this chapter, the governing equations of sound propagation and the fundamentals of acoustics theory are applied to ducts and silencers, emphasizing the traditional plane wave models and their associated matrix representation that is detailed for certain relevant elements such as ducts with uniform section, expansions and contractions. A review of the literature is carried out regarding the characterization of perforated elements and a number of common absorbent materials used in practical applications. A description of the usual silencer typologies used in the exhaust systems and their basic characteristics is presented. Also, the definition of some sound attenuation indicators is provided to evaluate the acoustic behaviour of silencers. Then, the quantification of the sound attenuation produced by the configurations of interest is considered for purely reactive and resonant geometries and also dissipative configurations. The chapter ends with an exposition of the inherent limitations related to the plane wave models, which justify the development of more accurate modelling techniques.

2.1   Introduction

The physical phenomena associated with sound wave propagation can be described by means of the appropriate mathematical equations [49, 125, 144]. These equations are more or less complex depending on the number of simplifying hypotheses taken into account when their deduction is carried out. Simplifying hypotheses always have to be justified by means of the suitable experimental verifications and their basic function is to reduce the complexity of the equations with a view to simplifying obtaining the solution. In this section, the mathematical expressions of these equations are shown. These expressions are relations that define the behaviour over time (or frequency) and space of the pressure, velocity, density or any other variable of the acoustic problem considered. Once the equations of interest are defined, such as the wave equation, their solution can obtained analytically [126] or numerically [181]. The basic drawback of analytic solutions lies in the fact that these can be only obtained in certain cases; for example, for simple geometries such as rectangular, circular or conical domains, thus limiting their generalization (although, fortunately, these geometries are commonly used in practical applications related to ducts and silencers). On the other hand, analytical techniques present some advantages: the mathematical treatment can be easier under certain assumptions, computation times can be strongly reduced and some useful conclusions and parametric guidelines for silencer design can be inferred [82, 85, 158]. Also, by means of simple models where the analytical solution is valid, it is possible to define improved strategies for a more general design technique such as the FEM [19, 43, 138]. Some physical models are shown in the next sections for the acoustic computation of silencers. First, general behaviour equations are considered; appropriate simplifying hypotheses are applied in Section 2.2.

2.1.1   Models for the acoustic calculation

Different models can be considered for the study of the acoustic attenuation of silencers [35, 126]. Here, two models are presented: (1) The non-linear fluid-dynamic model; (2) The linear acoustic model. Although the former is more general, it is beyond the scope of the current investigation and only the latter approach is considered in this Thesis. The fluid-dynamic model is no longer used in this work and therefore, only some relevant characteristics will be explained. The choice between these models is related to their characteristics, which are exposed below.

I. Dynamic model

The solution of a general fluid-dynamic problem requires a simultaneous consideration of three equations:

- Continuity equation

- Dynamic equilibrium equation

- Energy equation

Also necessary is the inclusion of an equation of state, an internal energy equation and a viscosity equation. Finally, the suitable relations between fluid velocity, pressure, temperature, density, internal energy and viscosity are considered.

The continuity equation can be written as [89]

$$\frac{\partial \rho}{\partial t} + \frac{\partial}{\partial x}(\rho u) + \frac{\partial}{\partial y}(\rho v) + \frac{\partial}{\partial z}(\rho w) = 0 \tag{2.1}$$

that can be expressed in vector form as:

$$\frac{\partial \rho}{\partial t} + \nabla^T (\rho \vec{u}) = 0 \tag{2.2}$$

u, v and w being the components of the velocity $\vec{u}$ in x, y and z, respectively, ρ the density, t the time and $\nabla^T = \{\vec{i}\ \partial/\partial x\ \ \vec{j}\ \partial/\partial y\ \ \vec{k}\ \partial/\partial z\}$. Equation 2.1 is met for any fluid that satisfies the continuity hypothesis.

The dynamic equilibrium equation, in a Newtonian fluid [89], can be written as

$$\rho a_x = \rho B_x - \frac{\partial p}{\partial x} + \frac{\partial}{\partial x}\left(2\mu\frac{\partial u}{\partial x} + \left(\zeta - \frac{2}{3}\mu\right)\nabla^T \vec{u}\right)$$
$$+ \frac{\partial}{\partial y}\left(\mu\left(\frac{\partial u}{\partial y} + \frac{\partial v}{\partial x}\right)\right) + \frac{\partial}{\partial z}\left(\mu\left(\frac{\partial u}{\partial z} + \frac{\partial w}{\partial x}\right)\right) \tag{2.3}$$

$$\rho a_y = \rho B_y - \frac{\partial p}{\partial y} + \frac{\partial}{\partial y}\left(2\mu\frac{\partial v}{\partial y} + \left(\zeta - \frac{2}{3}\mu\right)\nabla^T \vec{u}\right)$$
$$+ \frac{\partial}{\partial z}\left(\mu\left(\frac{\partial v}{\partial z} + \frac{\partial w}{\partial y}\right)\right) + \frac{\partial}{\partial x}\left(\mu\left(\frac{\partial v}{\partial x} + \frac{\partial u}{\partial z}\right)\right) \tag{2.4}$$

$$\rho a_z = \rho B_z - \frac{\partial p}{\partial z} + \frac{\partial}{\partial z}\left(2\mu\frac{\partial w}{\partial z} + \left(\zeta - \frac{2}{3}\mu\right)\nabla^T \vec{u}\right)$$
$$+ \frac{\partial}{\partial x}\left(\mu\left(\frac{\partial w}{\partial x} + \frac{\partial u}{\partial z}\right)\right) + \frac{\partial}{\partial y}\left(\mu\left(\frac{\partial w}{\partial y} + \frac{\partial v}{\partial z}\right)\right) \tag{2.5}$$

where ρB_x, ρB_y y ρB_z are volumetric forces, μ corresponds to the dynamic viscosity and ζ is the second viscosity coefficient, whose value is zero for monoatomic gases. The accelerations in the x, y and z axes are $a_x = Du/Dt$, $a_y = Dv/Dt$ y $a_z = Dw/Dt$ respectively, D/Dt being the total or material derivative, defined as

$$\frac{D}{Dt} = \frac{\partial}{\partial t} + u\frac{\partial}{\partial x} + v\frac{\partial}{\partial y} + w\frac{\partial}{\partial z} \tag{2.6}$$

In the case of non-isothermal flows where the viscosity depends on the temperature, the continuity equations and dynamic equilibrium are coupled with the energy equation, and all the equations have to be simultaneously solved. In general, the energy equation can be written as

$$\frac{\partial}{\partial x}\left(\kappa\frac{\partial T}{\partial x}\right) + \frac{\partial}{\partial y}\left(\kappa\frac{\partial T}{\partial y}\right) + \frac{\partial}{\partial z}\left(\kappa\frac{\partial T}{\partial z}\right) + \frac{\partial Q}{\partial t} + \Phi_d - \nabla^T \vec{q}_r$$
$$= \frac{\partial}{\partial x}\left(pu\right) + \frac{\partial}{\partial y}\left(pv\right) + \frac{\partial}{\partial z}\left(pw\right) + \frac{\rho}{2}\frac{D}{Dt}\left(u^2 + v^2 + w^2\right) + \rho\frac{DE}{Dt} \tag{2.7}$$

and expresses the existing equilibrium between the incoming, the outgoing and the accumulated energy. In equation 2.7 κ represents the thermal conductivity, T the temperature, Q the heat generated in the fluid per volume unity, E the internal energy, $\vec{q}_r$ the vector of heat radiation flux and Φ_d is the heat dissipation function, given by

$$\Phi_d = \lambda\left(\frac{\partial u}{\partial x} + \frac{\partial v}{\partial y} + \frac{\partial w}{\partial z}\right)^2 + 2\mu\left(\left(\frac{\partial u}{\partial x}\right)^2 + \left(\frac{\partial v}{\partial y}\right)^2 + \left(\frac{\partial v}{\partial z}\right)^2\right)$$
$$+ \mu\left(\left(\frac{\partial w}{\partial y} + \frac{\partial v}{\partial z}\right)^2 + \left(\frac{\partial u}{\partial z} + \frac{\partial w}{\partial x}\right)^2 + \left(\frac{\partial v}{\partial x} + \frac{\partial u}{\partial y}\right)^2\right) \tag{2.8}$$

where $\lambda = \zeta - 2/3\mu$. As can be seen, the value of Φ_d is zero for non-viscous flows.

In order to completely specify the flow problem, it is necessary to include three additional equations. These are the equations of state, the internal energy and the viscosity equations [89], which can be written in general form as

$$\rho = \rho(p, T) \tag{2.9}$$

$$E = E(p, T) \tag{2.10}$$

$$\mu = \mu(p, T) \tag{2.11}$$

To obtain the solution of a general flow problem, the procedure can be as follows: given the domain, the fluid properties, the equations (2.1), (2.3)-(2.5), (2.7)-(2.11),

and a suitable set of boundary and initial conditions, search the velocity fields u, v and w, as well as the pressure p, temperature T, density ρ, internal energy E and the viscosity μ [89]. Therefore, the solution requires solving eight equations with eight unknowns. This is a complex situation, whose difficulty increases because the acting forces or the temperature can deform the boundary domain. A solution of this kind is complex and remains beyond the scope of this Thesis.

II. Linear acoustic model

The linear acoustic model owes its name to the hypotheses formulated to obtain the wave equation, or in the case of harmonic behaviour, the Helmholtz equation [126], which results in linearizing and combining the continuity, dynamic equilibrium and constitutive equations of the fluid. The linearizing procedure is based on the fact that the increment of pressure and density (and velocity, in the case of a moving medium) of the particles is small with respect to its average or equilibrium value. It is evident that this restricts the application range of the wave equation, so that it is only valid in the study of acoustic phenomena of small amplitude. For silencers this is useful since the excitation systems do not usually exceed 140 dB [58, 124].

2.2   Wave equation

Due to the importance of the linearized wave equation in this Thesis, its deduction will be carried out in this section. Then, by solving the linearized equation, the behaviour of the fundamental acoustic variables will be characterized. In order to simplify the nomenclature in this chapter and in subsequent chapters, total variables are denoted here with subscript T, subscript 0 being used for the average values, while notation without any subscript is retained for the acoustic perturbation variables used in the linearization procedure.

To start with, the initial hypotheses considered to obtain the wave equation are given [126]:

- It is supposed that the fluid in which the wave propagates is ideal (non-viscous), and more specifically an ideal gas.

- The wave propagation process is considered adiabatic. There is a very small interchange of thermal energy between the particles of a fluid, their entropy

remaining almost invariable. Therefore, in an acoustic perturbation the particles do not interchange energy. Indeed, during the fluid compression process an increase of the temperature is generated and inversely, in the expansion, the temperature decreases. At a given instant the propagation of a longitudinal wave would produce heat transfer from a condensation to a rarefaction, separated by half wavelength $\lambda/2$. The quantity of heat transferred depends on the thermal conductivity of the fluid. In the audible frequency range (20-20000 Hz), most of the acoustic perturbations have a relatively large wavelength λ and a thermal conductivity small enough to produce an appreciable heat transfer and therefore, the wave propagation is considered adiabatic. This hypothesis, together with the previous idealization, lead to an isotropic process, verifying the relation

$$p_T = Constant \cdot \rho_T^{\gamma} \tag{2.12}$$

γ being the ratio between the specific heat capacity at constant pressure and the specific heat capacity at constant volume [14, 30]

- Small variations in the pressure, density and velocity functions of the particle are assumed. So, the problem can be linearized and a small acoustic amplitude is superposed to the pressure, the density and the average velocity, resulting in

$$\rho_T = \rho_0 + \rho \tag{2.13}$$

$$p_T = p_0 + p \tag{2.14}$$

$$\vec{u}_T = \vec{u}_0 + \vec{u} \tag{2.15}$$

where ρ, p and $\vec{u}$ are considered small when compared with the average value.

In general, the fluid has a non-zero average velocity resulting in the well-known convective wave equation. For a non-moving medium, particles have only a vibratory motion around their equilibrium position that provokes the propagation of the acoustic perturbation without a net motion of the fluid [140].

2.2.1 Non-moving medium

The ideal fluid hypothesis does not consider the viscosity effects, so the Navier-Stokes equations (2.3)-(2.5) are expressed as

$$\rho_T \frac{Du_T}{Dt} = \rho_T B_x - \frac{\partial p_T}{\partial x} \tag{2.16}$$

$$\rho_T \frac{Dv_T}{Dt} = \rho_T B_y - \frac{\partial p_T}{\partial y} \tag{2.17}$$

$$\rho_T \frac{Dw_T}{Dt} = \rho_T B_z - \frac{\partial p_T}{\partial z} \tag{2.18}$$

known as Euler equations [179]. If these equations are written in vector form one obtains

$$\rho_T \frac{D\vec{u}_T}{Dt} = \rho_T \vec{B} - \nabla p_T \tag{2.19}$$

From certain thermodynamic considerations [49], the following expression can be deduced

$$\frac{Dp_T}{Dt} = c_0^2 \frac{D\rho_T}{Dt} \tag{2.20}$$

where c_0 is the speed of sound in the air and is given by

$$c_0^2 = \left(\frac{\partial p_T}{\partial \rho_T} \right)_s \tag{2.21}$$

s being the entropy and taking the derivative for constant entropy. For an ideal gas, taking into account the expression given by (2.12), equation (2.21) remains as

$$c_0^2 = \left(\frac{\partial p_T}{\partial \rho_T} \right)_s = \frac{\gamma (p_0 + p)}{\rho_0 + \rho} \approx \frac{\gamma p_0}{\rho_0} \tag{2.22}$$

On the basis of the total derivative definition given by equation (2.6), the continuity equation (2.1) can be written as

$$\frac{D\rho_T}{Dt} + \rho_T \nabla^T \vec{u}_T = 0 \tag{2.23}$$

Combining equations (2.20) and (2.23), results in

$$\frac{Dp_T}{Dt} + \rho_T c_0^2 \nabla^T \vec{u}_T = 0 \tag{2.24}$$

Neglecting the gravity terms, the Euler equation (2.19), yields

$$\rho_T \frac{D\vec{u}_T}{Dt} = -\nabla p_T \tag{2.25}$$

Then the time-derivative of the expression (2.24) can be expressed as

$$\frac{D^2 p_T}{Dt^2} + \frac{D}{Dt} \left(\rho_T c_0^2 \nabla^T \vec{u}_T \right) \tag{2.26}$$

The linear governing equations of the acoustic perturbations are determined from first-order terms of the initial non-linear equations. The zeroth-order terms are cancelled since the environmental variables of the medium correspond to a valid state thereof. For example, given that zeroth-order terms have to be satisfied in the absence of perturbation, for the Euler equations (2.25), this yields

$$\rho_0 \left(u_0 \frac{\partial u_0}{\partial x} + v_0 \frac{\partial u_0}{\partial y} + w_0 \frac{\partial u_0}{\partial z} \right) + \frac{\partial p_0}{\partial x} = 0$$
$$\rho_0 \left(u_0 \frac{\partial v_0}{\partial x} + v_0 \frac{\partial v_0}{\partial y} + w_0 \frac{\partial v_0}{\partial z} \right) + \frac{\partial p_0}{\partial y} = 0 \tag{2.27}$$
$$\rho_0 \left(u_0 \frac{\partial w_0}{\partial x} + v_0 \frac{\partial w_0}{\partial y} + w_0 \frac{\partial w_0}{\partial z} \right) + \frac{\partial p_0}{\partial z} = 0$$

whose integration provides the Bernouilli equation for a steady flow [179].

In the case of a non-moving medium, the mean flow velocity is zero and it can be considered that $\vec{u}_T = \vec{u}$ [126, 140]. Then, the expression (2.27) yields $\nabla p_0 = 0$, the linearization of the equation (2.24) gives

$$\frac{\partial p}{\partial t} + \rho_0 c_0^2 \nabla^T \vec{u} = 0 \tag{2.28}$$

and for the Euler equation (2.25) the following expression is obtained

$$\rho_0 \frac{\partial \vec{u}}{\partial t} = -\nabla p \tag{2.29}$$

Combining the expressions (2.28) and (2.29), and eliminating $\vec{u}$, leads to the wave equation in the absence of flow [140]

$$\nabla^2 p - \frac{1}{c_0^2} \frac{\partial^2 p}{\partial t^2} = 0 \tag{2.30}$$

where the acoustic field of interest is the acoustic pressure perturbation p. As will be shown in Section 2.2.2, this equation is a particular case of the convective wave equation after considering $\vec{u}_0 = 0$. Assuming harmonic behaviour, the pressure is expressed as $p = Pe^{j\omega t}$, and substituting it in the wave equation results in the Helmholtz equation [126]

$$\nabla^2 P + k_0^2 P = 0 \tag{2.31}$$

where $k_0 = \omega/c_0$ is the wavenumber, P the complex acoustic pressure amplitude (function of the spatial coordinates), $\omega = 2\pi f$ the angular frequency and j the imaginary unit.

For a propagation medium whose density ρ_0 and speed of sound c_0 vary with position, an appropriate generalization of equation (2.30) is [140]

$$\rho_0 \nabla \left(\frac{1}{\rho_0} \nabla p \right) - \frac{1}{c_0^2} \frac{\partial^2 p}{\partial t^2} = 0 \tag{2.32}$$

2.2.2 Moving medium

In those situations in which ρ_0 and c_0 are constant, and considering a steady flow field (in general a function of the coordinates x, y and z), equation (2.27) can be combined with (2.26) and (2.25), providing the convective wave equation [140]

$$
\begin{aligned}
\nabla^2 p - \frac{1}{c_0^2} \frac{D^2 p}{Dt^2} + 2\rho_0 &\left(\frac{\partial u_0}{\partial x} \frac{\partial u}{\partial x} + \frac{\partial v_0}{\partial x} \frac{\partial u}{\partial y} + \frac{\partial w_0}{\partial x} \frac{\partial u}{\partial z} + \frac{\partial u_0}{\partial y} \frac{\partial v}{\partial x} \right. \\
&\left. + \frac{\partial v_0}{\partial y} \frac{\partial v}{\partial y} + \frac{\partial w_0}{\partial y} \frac{\partial v}{\partial z} + \frac{\partial u_0}{\partial z} \frac{\partial w}{\partial x} + \frac{\partial v_0}{\partial z} \frac{\partial w}{\partial y} + \frac{\partial w_0}{\partial z} \frac{\partial w}{\partial z} \right) = 0
\end{aligned}
\tag{2.33}
$$

the variables being the acoustic velocity $\vec{u}$ and the acoustic pressure p (the mean flow field is supposed to be known), and $\nabla^2 = \partial^2/\partial x^2 + \partial^2/\partial y^2 + \partial^2/\partial z^2$ is the Laplacian operator. In compact form this yields [140]

$$\nabla^2 p - \frac{1}{c_0^2} \frac{D^2 p}{Dt^2} + 2\rho_0 \sum_{ij} \frac{\partial u_{0j}}{\partial x_i} \frac{\partial u_i}{\partial x_j} = 0 \tag{2.34}$$

with $i, j = 1, 2, 3$, and $u_{01} = u_0$, $u_{02} = v_0$, $u_{03} = w_0$, $u_1 = u$, $u_2 = v$ and $u_3 = w$. For a uniform mean flow case, without spatial variation, the classic convective equation is recovered [126]

$$\nabla^2 p - \frac{1}{c_0^2} \frac{D^2 p}{Dt^2} = 0 \tag{2.35}$$

in which the mean flow velocity field is assumed to be known and the acoustic pressure p is the only unknown. The total derivative in equations (2.34) and (2.35) is given by

$$\frac{D}{Dt} = \frac{\partial}{\partial t} + u_0 \frac{\partial}{\partial x} + v_0 \frac{\partial}{\partial y} + w_0 \frac{\partial}{\partial z} \tag{2.36}$$

No equation of comparable simplicity to (2.35) is known to exist, however, when the ambient medium is moving and the ambient velocity field varies with position. A simple wave equation for inhomogeneous moving media has been given for a somewhat special case [140], this being when the ambient flow is irrotational and steady, and

when the entropy per unit mass has the same value at every point and for all time. The appropriate dependent wave field amplitude is the velocity potential ϕ for the acoustic part of the flow [43, 140]. Thus, the previous hypotheses lead to

$$\vec{u} = \nabla \phi \tag{2.37}$$

where ϕ is a potential function. In this way, the following expression is obtained

$$\nabla^2 \phi - \frac{1}{c_0^2} \frac{D^2 \phi}{Dt^2} = 0 \tag{2.38}$$

in which the only variable is the acoustic velocity potential ϕ. This equation can also be applied for a non-moving medium, just considering that the mean flow velocity is zero. The relation between the acoustic pressure and the acoustic velocity potential is given by [126, 140]

$$p = -\rho_0 \frac{D\phi}{Dt} \tag{2.39}$$

The mean flow velocity field can be obtained from the mean flow velocity potential ϕ_0, which satisfies the Laplace equation

$$\nabla^2 \phi_0 = 0 \tag{2.40}$$

by means of an expression similar to that given by equation (2.37)

$$\vec{u}_0 = \nabla \phi_0 \tag{2.41}$$

in spite of the fact that this approximation can considerably differ from the real flow field [6, 50].

If ρ_0 and c_0 vary with position, the resulting wave equation is [140]

$$\frac{1}{\rho_0} \nabla \left(\rho_0 \nabla \phi \right) - \frac{D}{Dt} \left(\frac{1}{c_0^2} \frac{D\phi}{Dt} \right) = 0 \tag{2.42}$$

Equations (2.32) and (2.42) have great importance for their consideration within this Thesis.

2.3 One-dimensional acoustics of ducts

In practice, an important and common assumption to solve the wave equation is based on the consideration of a one-dimensional propagation, resulting in the traditional

plane wave models. These have been profusely used in the acoustic literature [27, 55, 70, 135]. Therefore, some relevant information to model the acoustic behaviour of silencers is presented in this section. Munjal's works [126] are a remarkable source of information.

2.3.1 Non-moving medium

First, the case of a stationary medium is considered. The results presented are extended in the following section to consider a moving medium (see Section 2.3.2). Starting from equation (2.35), and assuming harmonic solution $p = Pe^{j\omega t}$, the Helmholtz equation is derived (2.31). Supposing a rigid wall duct with its axis parallel to the z direction, and assuming that the propagation only depends on this coordinate, a non-moving medium equation can be written as

$$\frac{\partial^2 P}{\partial z^2} + k_0^2 P = 0 \tag{2.43}$$

whose solution is [126]

$$P(z) = P^+ e^{-jk_0 z} + P^- e^{jk_0 z} \tag{2.44}$$

P^+ and P^- being complex wave amplitudes associated with the progressive and regressive plane wave, respectively. Therefore, the propagation is described as the sum of two components: one that advances in the positive direction of z and another in the opposite direction. Starting from Euler equation (2.29), the acoustic velocity can be written as

$$U = \frac{-1}{j\rho_0\omega} \frac{\partial P}{\partial z} \tag{2.45}$$

so

$$U(z) = \frac{1}{\rho_0 c_0} \left(P^+ e^{-jk_0 z} - P^- e^{jk_0 z} \right) = \frac{1}{Z_0} \left(P^+ e^{-jk_0 z} - P^- e^{jk_0 z} \right) \tag{2.46}$$

where Z_0 is known as the characteristic impedance of the medium. Sometimes it is convenient to use as a second acoustic variable the mass flow V instead of the velocity. For a duct of transversal section S, the relation between both variables is given by

$$V = \rho_0 S U \tag{2.47}$$

which can be rewritten as

$$V(z) = \frac{S}{c_0} \left(P^+ e^{-jk_0 z} - P^- e^{jk_0 z} \right) = \frac{1}{Y_0} \left(P^+ e^{-jk_0 z} - P^- e^{jk_0 z} \right) \tag{2.48}$$

$Y_0 = c_0/S$ being the characteristic impedance of the duct. Wave amplitudes P^+ and P^- are determined from the boundary conditions applied to the duct. This will be detailed in Section 2.4.

The one-dimensional Helmholtz equation (2.43) has been deduced assuming an ideal fluid. The consideration of plane wave models permits the introduction of the viscous effects without losing the simplicity of the associated solution. Thus, in the case of a viscous propagation medium, the wavenumber and the characteristic impedance of the duct are complex numbers. Therefore, the wavenumber k_0 used in equations (2.44), (2.46) and (2.48) is now defined as a complex propagation constant β [55, 126]

$$\beta = (k_0 + \alpha) - j\alpha = k - j\alpha \tag{2.49}$$

where α is the acoustic pressure attenuation constant, whose definition depends on the consideration of the heat transfer through the duct wall. For a circular duct of radius R it can be expressed as [55]

$$\alpha = \frac{1}{Rc_0}\sqrt{\frac{\mu\omega}{2\rho_0}}\left(1 + \frac{\gamma - 1}{\sqrt{\gamma Pr}}\right) \tag{2.50}$$

Pr being the Prandtl number that is defined as $\mu C_p/\kappa$, where μ is the dynamic viscosity, C_p the specific heat capacity at constant pressure and κ the thermal conductivity of the duct walls. If the thermal transfer through the walls of the duct is not considered, equation (2.50) can be rewritten as

$$\alpha = \frac{1}{Rc_0}\sqrt{\frac{\mu\omega}{2\rho_0}} \tag{2.51}$$

Finally, the pressure and the mass flow can be described as

$$P(z) = P^+ e^{-\alpha z - jk_0 z} + P^- e^{\alpha z + jk_0 z} \tag{2.52}$$

$$V(z) = \frac{1}{Y}\left(P^+ e^{-\alpha z - jk_0 z} - P^- e^{\alpha z + jk_0 z}\right) \tag{2.53}$$

where [126]

$$Y = Y_0\left(1 - \frac{\alpha}{k_0} + j\frac{\alpha}{k_0}\right) \tag{2.54}$$

The ratio α/k_0 is small, particularly at high frequencies, in such a way that except for very long ducts, the effect of the viscothermal attenuation can be neglected.

2.3.2 Moving medium

For a one-dimensional treatment of the problem, a duct of rigid walls can be supposed aligned with the z axis in the presence of a uniform mean flow in the same direction,

defined by the velocity U_{mf}. The relative propagation velocity of the wave with respect to the medium is still c_0, whereas in a non-moving system of reference, the progressive wave advances with a velocity $U_{mf} + c_0$, and the regressive wave has a velocity $U_{mf} - c_0$. In this case the waves are swept downstream by the fluid in motion, which is known as the convective effect. The classic convective wave equation (2.34) can be written as

$$\frac{\partial^2 p}{\partial z^2} - \frac{1}{c_0^2} \frac{D^2 p}{Dt^2} = 0 \tag{2.55}$$

and the total derivative (2.36) is now

$$\frac{D}{Dt} = \frac{\partial}{\partial t} + U_{mf} \frac{\partial}{\partial z} \tag{2.56}$$

Combining the previous expressions, yields

$$\left(1 - M^2\right) \frac{\partial^2 p}{\partial z^2} - 2\frac{M}{c_0} \frac{\partial^2 p}{\partial z \partial t} - \frac{1}{c_0^2} \frac{\partial^2 p}{\partial t^2} = 0 \tag{2.57}$$

where $M = U_{mf}/c_0$ is the Mach number. The harmonic version of the equation (2.57) is [49]

$$\left(1 - M^2\right) \frac{\partial^2 P}{\partial z^2} - 2jk_0 M \frac{\partial P}{\partial z} + k_0^2 P = 0 \tag{2.58}$$

The solution sought for equation (2.58) has the form

$$P\left(z\right) = P^+ e^{-j\frac{k_0}{1+M}z} + P^- e^{j\frac{k_0}{1-M}z} \tag{2.59}$$

By using Euler equation (2.25), the axial acoustic velocity is related to the pressure by means of

$$\rho_0 \left(j\omega U + U_{mf} \frac{\partial U}{\partial z}\right) = -\frac{\partial P}{\partial z} \tag{2.60}$$

and this can be expressed as

$$U\left(z\right) = \frac{1}{Z_0} \left(P^+ e^{-j\frac{k_0}{1+M}z} - P^- e^{j\frac{k_0}{1-M}z}\right) \tag{2.61}$$

while the mass flow is

$$V\left(z\right) = \frac{1}{Y_0} \left(P^+ e^{-j\frac{k_0}{1+M}z} - P^- e^{j\frac{k_0}{1-M}z}\right) \tag{2.62}$$

The characteristic impedances of the medium and the duct, Z_0 and Y_0, are defined in the same way as in the case of a non-moving propagation medium.

Similarly to the study carried out for a quiescent medium in Section 2.3.1, the viscothermal effects of the fluid can be included in order to consider both the additional aeroacoustic losses due to the turbulent friction and the convective effects of the mean flow. In this case, the wavenumber is given by [126]

$$\beta^{\pm} \approx \mp \left(\frac{\alpha + \xi M + jk}{1 \pm M} \right) \tag{2.63}$$

where the symbols $+$ and $-$ refer to the progressive and regressive propagation components respectively. In this expression, $\xi = F/(2d)$, F being the Froude factor and d the duct diameter. For exhaust systems, Munjal [126] proposes the value given by Lee's formula

$$F = 0.0072 + \frac{0.612}{Re^{0.35}} \qquad Re < 4 \cdot 10^5 \tag{2.64}$$

where $Re = U_{mf} d\rho_0 / \mu$ is the Reynolds number.

The acoustic pressure can be written as

$$P(z) = P^{+} e^{-\frac{\alpha + \xi M + jk}{1+M} z} + P^{-} e^{\frac{\alpha + \xi M + jk}{1-M} z} \tag{2.65}$$

In this solution, it can be observed that the total aeroacoustic attenuation in a moving medium depends on the Mach number, and is also a sum of the contributions of the viscothermal and turbulent flow friction effects. Also, the factors $1 \pm M$ that represent the convective effect of the mean flow have an influence on both the attenuation coefficient and the wavenumber [126]. The following notation can be introduced

$$\alpha^{\pm} = \frac{\alpha + \xi M}{1 \pm M} = \frac{\alpha(M)}{1 \pm M} \tag{2.66}$$

$$k^{\pm} = \frac{k}{1 \pm Mk} \tag{2.67}$$

with $k = k_0 + \alpha$. The value of $\alpha(M)$, equal for the perturbations in both directions of the flow, can be considered as the real coefficient of the aeroacoustic attenuation for a moving medium.

With the previous notation, the mass flow can be expressed as

$$V(z) = \frac{1}{Y} \left(P^{+} e^{-\alpha^{+} z - jk^{+} z} - P^{-} e^{\alpha^{-} z + jk^{-} z} \right) \tag{2.68}$$

where the characteristic impedance of the duct is [126]

$$Y = Y_0 \left(1 - \frac{\alpha + \xi M}{k_0} + j \frac{\alpha + \xi M}{k_0} \right) \tag{2.69}$$

However, according to Dokumaci [69], the wavenumber is given by $k_0 K^{\pm}$, where the propagation constant K can be written as

$$K = \sqrt{1 + ((1+j)/\kappa)(1 + (\gamma - 1)/\sqrt{Pr})\sqrt{2}} \qquad (2.70)$$

γ being the ratio of specific heat coefficients, Pr the Prandtl number, $\kappa = r\sqrt{\rho_0 \omega/\mu}$ the shear wavenumber, μ the dynamic viscosity coefficient, s the thermal conductivity, r the duct radius while the propagation constant $K^{\pm}$ is defined as

$$K^{\pm} = \frac{K}{1 \pm MK} \qquad (2.71)$$

where the symbols $+$ and $-$ refer again to the progressive and regressive propagation components respectively. Thusm, the acoustic pressure can be expressed as

$$P(z) = P^{+} e^{-jk_0 K^{+} z} + P^{-} e^{-jk_0 K^{-} z} \qquad (2.72)$$

Regarding the previous procedure, it is worth noting that there are several implicit simplifications with the purpose of assessing the aeroacoustic attenuation coefficient. Equations (2.65) and (2.69) should be considered as an approximation of the wave propagation in a viscous moving medium [126]. Nevertheless, these equations are very useful in engineering because of the similarity between the equations corresponding to a viscous quiescent medium and those of an inviscid moving flow, previously detailed.

2.4   Plane wave models. Matrix representation

Once the solution of the wave equation is obtained considering the one-dimensional theory, matrix methods can be developed to assess the acoustic performance of the elements belonging to the exhaust system. The global acoustic response of an exhaust system depends on the working conditions and to evaluate it several considerations have to be taken into account, including the noise generation source, the influence of the external conditions and the elements arranged in the exhaust system. Matrix methods can be applied in order to obtain a characterization that only depends on the behaviour of the component under study and provides a quantification of its intrinsic characteristics. The definition of each element can be obtained separately

through the well-known four-pole matrix [58, 126]. Thus, a complex acoustic system can be decomposed into several subcomponents, each one having its corresponding behaviour matrix. The global response of the system is obtained from the combination of all the matrices involved. This philosophy can be applied to silencers, which can be modelled as a series of chambers, resonators, geometric discontinuities, etc., connected by ducts. It is supposed that, although the acoustic field can be multidimensional within the different subcomponents, plane wave conditions hold in the connecting interfaces among the different devices involved.

2.4.1 Generalities
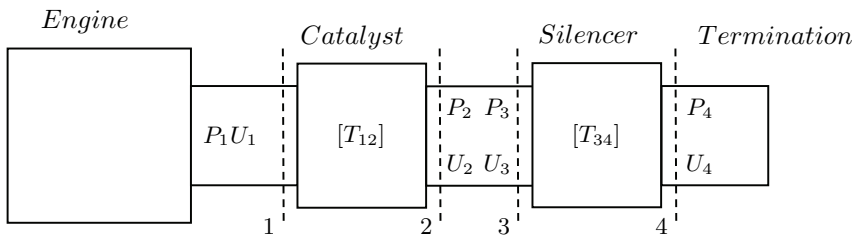
Figure 2.1: Scheme of an exhaust system.

A simplified scheme of an acoustic system is shown in Figure 2.1, consisting of an engine (main source of noise), a catalyst, a silencer and some additional elements connected downstream (termination).

The matrix definition of a given device, as for example the catalyst, implies the choice of the variables of interest at the inlet section (plane 1) and outlet section (plane 2). A commonly used formulation in practice consists of considering the pressure and axial velocity at planes 1 and 2, that are related by means of the following expression

$$\begin{Bmatrix} P_1 \\ U_1 \end{Bmatrix} = \begin{bmatrix} A^c & B^c \\ C^c & D^c \end{bmatrix} \begin{Bmatrix} P_2 \\ U_2 \end{Bmatrix} = \begin{bmatrix} T_{12} \end{bmatrix} \begin{Bmatrix} P_2 \\ U_2 \end{Bmatrix} \tag{2.73}$$

which constitutes the basis of the transfer matrix approach. The acoustic perturbation at a point of the duct, defined by the state vector $\{P_1 \ U_1\}^T$, is related to the perturbation at another point, downstream with respect to the first point, defined by the state vector $\{P_2 \ U_2\}^T$, by means of the transfer matrix $[T_{12}]$ of the device placed between planes 1 and 2. In general it is admitted that for any system, provided that the wave is plane in planes 1 and 2, a transfer matrix such as that defined in equation

(2.73) can be found. An immediate property that will be used hereafter consists of the possibility of computing the transfer matrix of a full system from the matrices of each subsystem, just by carrying out the sorted multiplication of these, as they relate to two state vectors associated with specific points. This property is basic, and the versatility of the method when representing complex systems lies in it.

The four-pole transfer matrix can be obtained by means of the calculation of the acoustic system under study with suitable boundary conditions. These conditions are based on the physical meaning of each of the matrix poles, which is simple as it can be deduced from the previous expressions, obtained from equation (2.73)

$$A^c = \left. \frac{P_1}{P_2} \right|_{U_2=0} \tag{2.74}$$

$$B^c = \left. \frac{P_1}{U_2} \right|_{P_2=0} \tag{2.75}$$

$$C^c = \left. \frac{U_1}{P_2} \right|_{U_2=0} \tag{2.76}$$

$$D^c = \left. \frac{U_1}{U_2} \right|_{P_2=0} \tag{2.77}$$

The condition $P_2 = 0$ is equivalent to the consideration of an ideal open end in plane 2 and the condition $U_2 = 0$ corresponds to an ideal rigid closed end. Both conditions can be used without any difficulty in the numerical computation of the acoustic problem, regardless of the level of complexity. Also, they indicate the possibility of estimating the approximate values of the four poles from experiments with two different boundary conditions..

The transfer matrices of some common elements usually found in silencers are obtained in the next sections for illustration purposes.

2.4.2   Transfer matrix of a duct

A duct of length L and cross section S, as shown in Figure 2.2, is considered first. In order to obtain the transfer matrix of the duct, the following definitions of pressure and acoustic velocity, given by (2.44) and (2.46), are taken into account

$$P(z) = P^+ e^{-jk_0 z} + P^- e^{jk_0 z}$$

$$U\left(z\right) = \frac{1}{Z_0}\left(P^+ e^{-jk_0 z} - P^- e^{jk_0 z}\right)$$
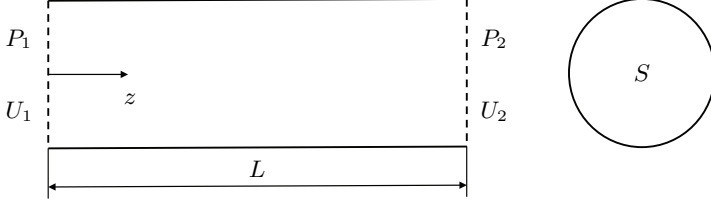
Figure 2.2: Duct with uniform cross section.

Taking into account equations (2.74)-(2.77), two analyses have to be carried out with their associated boundary conditions. The process can begin with $U_2 = 0$, combined with an arbitrary excitation P_i (for convenience a value equal to unity is usually considered), giving

$$P\left(z = 0\right) = P_1 = P_i = P^+ + P^- = 1 \tag{2.78}$$

$$U\left(z = L\right) = U_2 = \frac{1}{Z_0}\left(P^+ e^{-jk_0 L} - P^- e^{jk_0 L}\right) \tag{2.79}$$

whose solution is

$$P^+ = \frac{1}{2}\frac{\cos\left(k_0 L\right) + j\sin\left(k_0 L\right)}{\cos\left(k_0 L\right)} \tag{2.80}$$

$$P^- = \frac{1}{2}\frac{\cos\left(k_0 L\right) - j\sin\left(k_0 L\right)}{\cos\left(k_0 L\right)} \tag{2.81}$$

which completely defines the pressure $P(z)$ and the velocity $U(z)$ in the duct. Thus, the terms A and C of the transfer matrix are

$$A = \left.\frac{P_1}{P_2}\right|_{U_2=0} = \cos\left(k_0 L\right) \tag{2.82}$$

$$C = \left.\frac{U_1}{P_2}\right|_{U_2=0} = \frac{j}{Z_0}\sin\left(k_0 L\right) \tag{2.83}$$

The calculation of B and D involves the consideration of $P_2 = 0$, yielding

$$P(z = 0) = P_1 = P_i = P^+ + P^- = 1 \tag{2.84}$$

$$P(z = L) = P_2 = P^+ e^{-jk_0 L} + P^- e^{jk_0 L} = 0 \tag{2.85}$$

so that

$$P^+ = \frac{-j}{2} \frac{\cos(k_0 L) + j\sin(k_0 L)}{\sin(k_0 L)} \tag{2.86}$$

$$P^- = \frac{1}{2} \frac{\sin(k_0 L) + j\cos(k_0 L)}{\sin(k_0 L)} \tag{2.87}$$

and therefore

$$B = \frac{P_1}{U_2}\bigg|_{P_2=0} = jZ_0 \sin(k_0 L) \tag{2.88}$$

$$D = \frac{U_1}{U_2}\bigg|_{P_2=0} = \cos(k_0 L) \tag{2.89}$$

Then, for a duct, the expression is

$$\begin{Bmatrix} P_1 \\ U_1 \end{Bmatrix} = \begin{bmatrix} \cos(k_0 L) & jZ_0 \sin(k_0 L) \\ \dfrac{j}{Z_0} \sin(k_0 L) & \cos(k_0 L) \end{bmatrix} \begin{Bmatrix} P_2 \\ U_2 \end{Bmatrix} \tag{2.90}$$

A similar approach, considering as variables the pressure and the mass flow, gives

$$\begin{Bmatrix} P_1 \\ V_1 \end{Bmatrix} = \begin{bmatrix} \cos(k_0 L) & jY_0 \sin(k_0 L) \\ \dfrac{j}{Y_0} \sin(k_0 L) & \cos(k_0 L) \end{bmatrix} \begin{Bmatrix} P_2 \\ V_2 \end{Bmatrix} \tag{2.91}$$

If there is mean flow, the same procedure can be applied starting from equations (2.59) and (2.61) for the pressure and velocity, which after further manipulations, yields [126]

$$\begin{Bmatrix} P_1 \\ U_1 \end{Bmatrix} = e^{-jM\frac{k_0}{1-M^2}L} \begin{bmatrix} \cos\left(\dfrac{k_0}{1-M^2}L\right) & jZ_0 \sin\left(\dfrac{k_0}{1-M^2}L\right) \\ \dfrac{j}{Z_0} \sin\left(\dfrac{k_0}{1-M^2}L\right) & \cos\left(\dfrac{k_0}{1-M^2}L\right) \end{bmatrix} \begin{Bmatrix} P_2 \\ U_2 \end{Bmatrix} \tag{2.92}$$

The four poles of a duct are shown in Figure 2.3 to explain their main characteristics. The length of the duct is $L = 0.3$ m and the mean flow velocities are given by the Mach numbers $M = 0$, $M = 0.1$ and $M = 0.2$. It is worth noting that, in a duct, A and D overlap, and the same happens with B/Z_0 and $Z_0 C$. When no mean flow exists, the imaginary part of A and D is zero, as well as the real part of B and C. Nevertheless, the presence of mean flow originates phase differences in the waves that make the aforementioned parts different from zero. Besides, the mean flow modifies the parts that are initially non-zero for $M = 0$. This effect increases for higher frequencies.
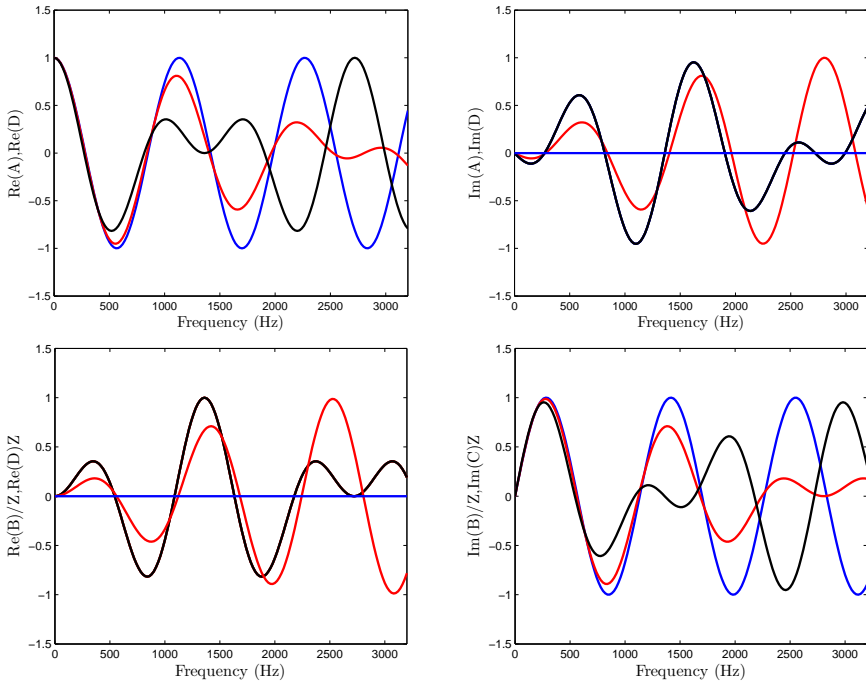
Figure 2.3: Real and imaginary parts of the four poles for a duct with length $L = 0.3$ m: ——, $M = 0$; ——, $M = 0.1$; ——, $M = 0.2$.

2.4.3 Transfer matrix at expansions and contractions

This case is especially interesting because it constitutes the fundamental element of the attenuation mechanism in reactive silencers [26, 126]. A sketch of two geometric discontinuities consisting of an expansion ($S_1 < S_2$) and a contraction ($S_1 > S_2$) is shown in Figure 2.4.
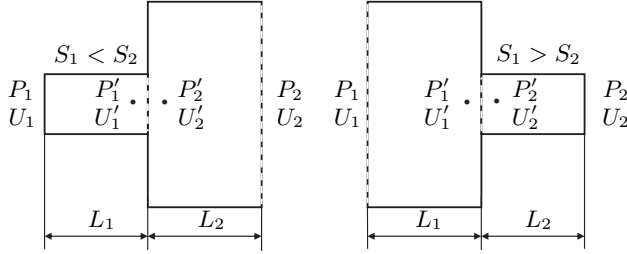
Figure 2.4: Geometric discontinuities between ducts.

In the absence of mean flow, the relationship between the acoustic variables at both sides of the geometric discontinuity can be written as

$$P_1' = P_2' \tag{2.93}$$

$$\rho_0 S_1 U_1' = \rho_0 S_2 U_2' \tag{2.94}$$

which means that the acoustic pressure and the mass flow do not change at the geometric discontinuity. Now, these expressions can be written in matrix form as

$$\begin{Bmatrix} P_1' \\ U_1' \end{Bmatrix} = \begin{bmatrix} 1 & 0 \\ 0 & S_2/S_1 \end{bmatrix} \begin{Bmatrix} P_2' \\ U_2' \end{Bmatrix} \tag{2.95}$$

$$\begin{Bmatrix} P_1' \\ V_1' \end{Bmatrix} = \begin{bmatrix} 1 & 0 \\ 0 & 1 \end{bmatrix} \begin{Bmatrix} P_2' \\ V_2' \end{Bmatrix} \tag{2.96}$$

This simple representation of the area change is very useful to model a silencer in matrix form, as it is usually formed of different geometric discontinuities. Nevertheless, it should be noted that the representation given by expressions (2.95) and (2.96) is approximated, since in every section change the acoustic pressure and velocity fields have to be necessarily continuous, leading to the generation of multidimensional phenomena [73, 96, 147]. These phenomena take on special relevance as the frequency increases and therefore, the previous matrices are only valid in the low frequency range.

However, the plane wave models allow their approximated consideration, valid in the low frequency range, according to a length correction factor [96, 137, 147, 153]. Thus, the expression (2.96)

$$\begin{Bmatrix} P_1' \\ V_1' \end{Bmatrix} = \begin{bmatrix} 1 & 0 \\ 0 & 1 \end{bmatrix} \begin{Bmatrix} P_2' \\ V_2' \end{Bmatrix}$$

can be modified to include the length correction δ, resulting in

$$\begin{Bmatrix} P_1' \\ V_1' \end{Bmatrix} = \begin{bmatrix} 1 & \dfrac{j\omega\delta}{S_1} \\ 0 & 1 \end{bmatrix} \begin{Bmatrix} P_2' \\ V_2' \end{Bmatrix} \tag{2.97}$$

The values of δ depend on the frequency and the geometries defining the area discontinuity [59, 126, 137].

Once the matrix associated with the area change is known, it is possible to relate the acoustic variables at plane 1 to the corresponding variables at plane 2 (see Figure 2.4), by simply multiplying in an orderly way the matrices belonging to each element, that is

$$\begin{Bmatrix} P_1 \\ U_1 \end{Bmatrix} = \begin{bmatrix} \cos\left(k_0 L_1\right) & jZ_0 \sin\left(k_0 L_1\right) \\ \dfrac{j}{Z_0}\sin\left(k_0 L_1\right) & \cos\left(k_0 L_1\right) \end{bmatrix} \begin{bmatrix} 1 & 0 \\ 0 & \dfrac{S_2}{S_1} \end{bmatrix} \begin{bmatrix} \cos\left(k_0 L_2\right) & jZ_0 \sin\left(k_0 L_2\right) \\ \dfrac{j}{Z_0}\sin\left(k_0 L_2\right) & \cos\left(k_0 L_2\right) \end{bmatrix} \begin{Bmatrix} P_2 \\ U_2 \end{Bmatrix} \tag{2.98}$$

2.5 Perforated plates and ducts

Perforated elements are a usual component in silencers [120, 126, 168]; in practical applications, they can appear with diverse configurations such as completely or partially perforated ducts and plates.

The usual characterization of perforated elements is based on the concept of acoustic impedance, defined as the ratio of the acoustic pressure drop to the normal velocity through the perforations [120, 126]. In general, the impedance is difficult to model; but it can be approximately described as a complex function of several parameters such as the orifice diameter d_h, thickness t_p and porosity σ, which is the ratio of perforated area to the total surface [108, 139, 168]. Also, it can depend on the mean flow through the holes or grazing the holes, and the material backing the perforations [171]. Acoustic attenuation phenomena involve different effects associated with the area change that the fluid particles undergo when passing through the perforations. The process implies reflection and transmission of the waves and energy dissipation due to friction. The acoustic fields near the perforated element can be relatively complex [122], above all in the presence of mean flow [172], in such a way that the treatment received in the literature is always simplified, according to the concept of impedance presented in Section 2.5.1.

2.5.1 Characteristic impedance of a perforated surface

The impedance of a perforated element is the ratio between the acoustic pressure jump at both sides of the surface and the acoustic velocity across the holes,

$$Z_p = \frac{P_i - P_o}{\bar{U}} = R_0 + jX_0 \tag{2.99}$$

where P_i is the acoustic pressure at the orifice inlet, P_o the acoustic pressure at the orifice outlet and $\bar{U}$ is the average acoustic velocity through the hole. The acoustic impedance can be expressed in terms of the resistance R_0 and the reactance X_0, real and imaginary parts of the impedance respectively.

In a linear regime, for applications where the acoustic pressure levels are considered to be low, the acoustic impedance is linearly related to the pressure difference between both sides of the perforated duct. However, in the case of perforated plates for silencer applications, the fluid dynamics of the holes can exhibit non-linear features when exposed to sound pressure levels typical of combustion engines [123]. Experimental measurements carried out at the orifices show a quadratic behaviour [92]. In these cases the acoustic impedance depends on the velocity through the orifices [67, 92].

A review of the existing literature shows that there are many impedance models available [64, 102, 108], whose results can sometimes present important discrepancies [108]. In this section, an exposition of the models most commonly used is carried out. Many of these models have been experimentally validated. The first and simplest case corresponds to a perforated element placed within a non-moving medium. The following expression can be found in references [169, 171]

$$Z_p = \rho_0 c_0 \frac{6 \cdot 10^{-3} + jk_0 \left(t_p + 0.75 d_h \right)}{\sigma} \tag{2.100}$$

The real or resistive part, associated with the acoustic energy losses, remains almost invariable. The imaginary or reactive part, which depends on the frequency and geometric characteristics of the perforated surface, is determined by means of the following expression

$$X_0 = \rho_0 \omega \frac{\left(t_p + 0.75 d_h \right)}{\sigma} \tag{2.101}$$

Porosity has a considerable influence on the acoustic impedance, since it appears in the expression (2.100) at the denominator. To avoid the overestimation of the impedance associated with this model, a correction factor $F(\sigma)$ is considered in recent references

[59, 66, 104] to take into account the interaction between orifices. This interaction can be translated into a reduction of the reactive part of the impedance

$$Z_p = \rho_0 c_0 \frac{6 \cdot 10^{-3} + jk_0 \left(t_p + 0.75 d_h F\left(\sigma\right)\right)}{\sigma} \tag{2.102}$$

Better results are achieved substituting $0.75 d_h$ by $0.85 d_h F(\sigma)$ whereby the expression (2.100) can be written as [59, 66, 104]

$$Z_p = \rho_0 c_0 \frac{6 \cdot 10^{-3} + jk_0 \left(t_p + 0.85 d_h F\left(\sigma\right)\right)}{\sigma} \tag{2.103}$$

The correction factor $F(\sigma)$ is calculated through formulae such as the Ingard's interaction factor [91]

$$F_I\left(\sigma\right) = 1 - 0.7\sqrt{\sigma} \tag{2.104}$$

or the Fok's expression [27]

$$F_F\left(\sigma\right) = 1 - 1.41\sqrt{\sigma} + 0.34\left(\sqrt{\sigma}\right)^3 + 0.07\left(\sqrt{\sigma}\right)^5 \tag{2.105}$$

In this Thesis, the correction factor $F(\sigma)$ is calculated as the average of the values obtained by the expressions (2.104) and (2.105) [27]

$$F\left(\sigma\right) = 0.5\left(F_I\left(\sigma\right) + F_F\left(\sigma\right)\right) \tag{2.106}$$

In the non-linear regime [92, 171] the increase of the acoustic pressure till values over 120 dB (the pressure amplitude in internal combustion engines can exceed 140 dB [67]) involves a non-linear increase of the resistance while the reactance tends to decrease, also in a non-linear form, but to a lower degree when compared to the resistance.

The consideration of mean flow makes it more difficult to obtain the impedance associated with perforated elements. Therefore, sometimes experimental measurements are carried out to obtain empirical models of the acoustic behaviour close to the orifices. In the perforated surfaces exposed to the tangential mean flow, defined by the Mach number M, turbulences are generated that modify the local impedance [108] changing the pattern of the acoustic energy distribution through the orifices as a consequence of the convective effects. The resistance of the orifices tends to increase as the mean flow is higher, whereas the reactance tends to slightly decrease [108, 143].

According to an empirical model, Garrison *et al.* [76] obtained the following expression

$$Z_p = \left(1 + 1.9M\right)R_0 + j\left(1 - 1.65M\right)X_0 \tag{2.107}$$

Rao and Munjal [143] carried out tests to assess the effects of the mean flow in some typologies of perforated ducts by applying conditions of tangential flow velocity similar to those existing in automotive silencers. The empirical expression that determines the acoustic impedance under these conditions is

$$Z_p = \rho_0 c_0 \frac{7.337 \cdot 10^{-3} \left(1 + 72.23M\right) + j2.2245 \cdot 10^{-5} \left(1 + 51t_p\right) \left(1 + 204d_h\right) f}{\sigma}$$
(2.108)

in which the mean flow affects the resistive part of the model. The ranges defined for the validity of this expression are $0.05 \leq M \leq 0.2$ for the tangential flow velocity, $3\% \leq \sigma \leq 10\%$ for the porosity, 1 mm $\leq t_p \leq 3$ mm for the thickness of the perforated surface and 1.75 mm $\leq d_h \leq 7$ mm for the orifice diameter.

Sullivan [169], according to the empirical model of Garrison *et al.*, modified his impedance model without mean flow (2.100) to include the effect of the normal mean flow velocity on the resistive component. This effect is similar to that produced in a plug silencer where the flow is forced to pass through the orifices and the velocity presents two components: a component tangential to the surface, whose value is maximum at the inlet and zero at the plug, and a normal or transversal component $\bar{U}_0$ considered uniform [58, 169]

$$Z_p = \rho_0 c_0 \frac{2.57 \dfrac{\bar{U}_0}{c_0} + jk_0 \left(t + 0.75d_h\right)}{\sigma}$$
(2.109)

An empirical expression developed by Bauer [25] additionally relates the viscous effects of the medium to the Mach number M in the modification of the resistive part of the acoustic impedance

$$Z_p = \rho_0 c_0 \frac{\dfrac{\sqrt{8\mu\rho_0\omega}}{\rho_0 c_0} \left(1 + \dfrac{t_p}{d_h}\right) + 0.3M + 1.15\dfrac{\bar{U}_0}{c_0} + jk_0 \left(t_p + 0.25d_h\right)}{\sigma}$$
(2.110)

Jayaraman and Yam [95] modify the impedance model of Sullivan for plugs (2.100) when considering the tangential mean flow as an influential part of the variation of the resistance

$$Z_p = \frac{\rho_0 c_0}{\sigma} \left(\frac{0.514d}{\sigma} \frac{M}{l} + j4.8 \cdot 10^{-5} f\right)$$
(2.111)

where d is the diameter of the duct and l its length. It is worth noting that the magnitude M/l is the axial gradient of the mean flow Mach number, which is variable since the Mach number linearly decreases from a maximum value M at the inlet of the perforated duct to zero over the perforated length l [82].

Another group of expressions that consider the variation of the resistive part of the acoustic impedance according to the flow resistance R_f and the correction length factor δ/δ_0 is proposed by Kooi and Sarin [106], Cummings [51] and Kirby and Cummings [102]. The flow resistance R_f can be expressed as follows [42]

$$R_f = \frac{\Delta P}{U} \tag{2.112}$$

where ΔP is the difference in pressure at both sides of the porous sample and U the velocity through the sample.

Kooi and Sarin [106] propose

$$\frac{R_f c_0}{f d_h} = \frac{1}{4}\left(5 - \frac{t_p}{d_h}\right)\left(9.9\frac{u^*}{f d_h} - 3.2\right) \tag{2.113}$$

where R_f corresponds to the average flow resistance in the orifice area and u^* is the friction velocity, a parameter written in units of velocity that is often used as a scaling parameter for the fluctuating component of velocity in turbulent flow, and can be obtained as [152]

$$u^* = \sqrt{\frac{\tau_w}{\rho_0}} \tag{2.114}$$

where τ_w is the shear stress at the wall and ρ_0 the fluid density. The length correction factor is obtained as

$$\frac{\delta}{\delta_0} = \begin{cases} 0.92 - 0.75\dfrac{u^*}{f t_p} + 0.11\left(\dfrac{u^*}{f t_p}\right)^2 , & 0.2 \le \dfrac{u^*}{f t_p} \le 3.5 \\[3mm] -0.04 , & \dfrac{u^*}{f t_p} > 3.5 \end{cases} \tag{2.115}$$

in which δ represents the length correction in the presence of mean flow and δ_0 the length correction in the absence of mean flow. Cummings [51] expresses R_f as

$$\frac{R_f c_0}{f d_h} = \left(12.52\left(\frac{t_p}{d_h}\right)^{-0.32} - 2.44\right)\frac{u^*}{f d_h} - 3.2 \tag{2.116}$$

and the length correction factor as

$$\frac{\delta}{\delta_0} = \begin{cases} 1 , & \dfrac{u^*}{f t_p} \le 0.12\dfrac{d_h}{t_p} \\[3mm] \left(1 + 0.6\dfrac{t_p}{d_h}\right) e^{\left(-\left(\frac{u^*}{f t_p} - 0.12\frac{d_h}{t_p}\right)/\left(0.25 + \frac{t_p}{d_h}\right)\right)} - 0.6\dfrac{t_p}{d_h} , & \dfrac{u^*}{f t_p} > 0.12\dfrac{d_h}{t_p} \end{cases} \tag{2.117}$$

Kirby and Cummings [102], modified the resistive part and obtained

$$\frac{R_f c_0}{f d_h} = \left(26.16 \left(\frac{t_p}{d_h} \right)^{-0.169} - 20 \right) \frac{u^*}{f d_h} - 4.055 \tag{2.118}$$

while their length correction factor yields

$$\frac{\delta}{\delta_0} = \begin{cases} 1 \, , & \dfrac{u^*}{f t_p} \leq 0.18 \dfrac{d_h}{t_p} \\[3ex] \left(1 + 0.6 \dfrac{t_p}{d_h} \right) e^{\left(-\left(\frac{u^*}{f t_p} - 0.18 \frac{d_h}{t_p} \right) / \left(1.8 \frac{t_p}{d_h} \right) \right)} - 0.6 \dfrac{t_p}{d_h} \, , & \dfrac{u^*}{f t_p} > 0.18 \dfrac{d_h}{t_p} \end{cases} \tag{2.119}$$

For these three last cases, the resistive part of the dimensionless acoustic impedance R_0 is the sum of the flow resistance R_f and the viscous losses R_ν due to the turbulent flow. Therefore

$$R_0 = R_f + R_\nu \tag{2.120}$$

where

$$R_\nu = \frac{\sqrt{8\nu\omega}}{c_0} \frac{t_p}{d_h} \tag{2.121}$$

and ν represents the kinematic viscosity. The reactive part of the dimensionless acoustic impedance X_0 depends on the length correction factor δ/δ_0

$$X_0 = k_0 \left(t_p + \frac{\delta}{\delta_0} 0.85 d_h \right) \tag{2.122}$$

Due to the difference of parameters considered in both groups of impedances, Lee and Ih [108] bring them together in one empirical expression whose normalized resistive part is

$$R_0 = \rho_0 c_0 \frac{a_0 \left(1 + a_1 \left| f - f_0 \right| \right) \left(1 + a_2 M \right) \left(1 + a_3 d_h \right) \left(1 + a_4 t_p \right)}{\sigma} \tag{2.123}$$

where $a_0 = 3.94 \cdot 10^{-4}$, $a_1 = 7.84 \cdot 10^{-3}$, $a_2 = 14.9$, $a_3 = 296$ and $a_4 = -127$. Note that some of this coefficients have dimensions. In this resistive part, the critical frequency f_0 is related to the mean flow velocity Mach number M and the diameter of the orifice d_h as

$$f_0 = \phi_1 \frac{1 + \phi_2 M}{1 + \phi_3 d_h} \tag{2.124}$$

The coefficients are given by $\phi_1 = 412$, $\phi_2 = 104$ and $\phi_3 = 274$. These values are obtained according to a non-linear regression analysis of the results from experimental tests (that consider f_0, M and d_h). The resistance is a decreasing function of the frequency until a minimum value is reached at the critical frequency, from which it starts to increase. The reactive part is influenced by the mean flow velocity and the frequency, among others, yielding

$$X_0 = \rho_0 c_0 \frac{b_0 \left(1 + b_1 d_h\right) \left(1 + b_2 t_p\right) \left(1 + b_3 M\right) \left(1 + b_4 f\right)}{\sigma} \qquad (2.125)$$

where $b_0 = -6 \cdot 10^{-3}$, $b_1 = 194$, $b_2 = 432$, $b_3 = -1.72$ and $b_4 = -6.62 \cdot 10^{-3}$. As for the resistive part, some of these coefficients have dimensions. Reactance increases with frequency and its magnitude generally decreases as the flow Mach number M increases. The valid range of values for each of these parameters is as follows: 60 Hz$\leq f \leq$ 4000 Hz, for the frequency, $0 \leq M \leq 0.2$, for the mean flow velocity, 2 mm$\leq d_h \leq$ 9 mm, for the diameter of the orifices, 1 mm $\leq t_p \leq$ 5 mm, for the thickness of the plate and $2.79\% \leq \sigma \leq 22.3\%$ for the porosity. Similar to previous works [180], it has been considered that the coefficients involved in expressions (2.123)-(2.125) do not depend on the temperature. Equations (2.123) and (2.125) have been used in this Thesis, as well as in some of the associated contributions. Further details will be given in Section 3.2 in order to include the effect of the absorbent material and its heterogeneities.

2.5.2 Characteristic impedance of microperforated surfaces

Silencers with microperforated ducts are currently under study as a possible alternative to the traditional perforated dissipative silencers, since they help to avoid the potentially harmful effects of the absorbent materials on human health [8, 64]. Another relevant characteristic is that they are lighter than dissipative silencers. In this section, the model developed by Allam and Åbom [8] for microperforated surfaces is briefly described. This model is based on the results obtained by Maa [112, 114, 115], who published the first attempts to comprehensively characterize these kinds of surface. Maa defined the microperforated area as a perforated surface where the size of the orifice and the ratio of the perforated screen provide an impedance whose real part is close to the characteristic impedance of the air (approx. 400 Pa s/m in Standard Temperature and Pressure). The thickness of a microperforated plate must be around 1 mm, the porosity a value around 1% and the hole diameter a submillimetric value.

Maa [112, 114, 115] modelled a microperforated surface with circular orifices as if it were composed of a grid of tiny tubes, separated by distances much higher than their diameter. Nevertheless, these distances are small when compared to the incident

wavelength. Maa developed an impedance model for microperforated surfaces according to Rayleigh's model for ducts of small length [144] and Crandall's simplifications [48]. The equation of motion for the air (in a duct sufficiently short in comparison to the wavelength) is given by

$$j\omega\rho_0 u_h - \frac{\mu}{r}\frac{\partial}{\partial r}\left(r\frac{\partial}{\partial r}u_h\right) = \frac{\Delta p}{t_p} \tag{2.126}$$

Δp being the pressure difference between the ends of the duct (with the same thickness t_p as the surface), ρ_0 the air density, μ its viscosity coefficient and r the radial coordinate of the duct in cylindrical coordinates. This equation can be solved for the particle velocity u_h, and the ratio of Δp to the average value of $\bar{u}_h$ over the cross section of the duct giving as a result the specific acoustic impedance of the short duct [115]

$$Z = \frac{\Delta p}{\bar{u}_h} = j\omega\rho_0 t_p \left(1 - \frac{2}{\kappa\sqrt{-j}}\frac{J_1\left(\kappa\sqrt{-j}\right)}{J_0\left(\kappa\sqrt{-j}\right)}\right)^{-1} \tag{2.127}$$

where $\kappa = d_h\sqrt{\omega/(4\nu)}$ is the shear wavenumber that depends on the diameter of the tube d_h, the angular frequency ω, as well as on the kinematic viscosity ν. J_0 and J_1 are the Bessel functions of the first kind and zeroth and first-order [8]. The normalized impedance of a microperforated plate can be obtained by dividing the specific impedance Z by the characteristic impedance of the air $\rho_0 c_0$ and the porosity σ, obtaining the following expression

$$z = \frac{Z}{\rho_0 c_0 \sigma} = \frac{j\omega t_p}{\sigma c_0}\left(1 - \frac{2}{\kappa\sqrt{-j}}\frac{J_1\left(\kappa\sqrt{-j}\right)}{J_0\left(\kappa\sqrt{-j}\right)}\right)^{-1} \tag{2.128}$$

It is necessary to include an end correction to model the orifices [125]. This theoretical correction can be decomposed into external resistive and a reactive terms. Ingard [91] suggested the utilization of the values proposed by Rayleigh [144] to assess the resistive part due to the friction of the airflow over the screen surface: $R_s = 1/2\sqrt{2\omega\rho_0\mu}$, μ being the dynamic viscosity. According to some measurements previously carried out, Guo *et al.* [83] determined that the correction value proposed by Ingard and equal to $4R_s$ provides better results for orifices with sharp edges, while for rounded edges an improvement is obtained using the correction proposed by Maa [115], given by $2R_s$. Then, the total external resistivity can be written as

$$r = \frac{2\alpha R_s}{\sigma\rho_0 c_0} \tag{2.129}$$

where α is a factor that depends on the kind of edge of the orifice, its value being 2 for a rounded orifice edge and 4 when it is sharp.

When the air is impulsed within the small ducts composing the microperforated surface, the performance of the orifices can be assimilated to a piston behaviour. According to the literature [8, 48, 164], the mass reactance due to the piston sound radiation in both ends of the duct is $0.85d$. Thus, the normalized expression for the external reactance can be written as

$$\chi = \frac{\delta \omega}{\sigma c_0} \tag{2.130}$$

Besides, a non-linear orifice behaviour can exist, modifying both the acoustic resistance and reactance. This fact was studied by Sivian [164], who observed that the acoustic resistance is higher as the particle velocity in the holes increases. This is due to the vorticity produced by the high sound intensity at the orifice outlet, dissipating acoustic energy; however, the reactance starts to decrease. This non-linear term was quantified by Maa [113] as $z_{non-lin} = |\hat{u}_h|/(\sigma c_0)$, $|\hat{u}_h|$ being the absolute value of the particle velocity within the holes. For the resistive part, this term can be directly added as an external term to the real part of expression (2.128), while for the reactive term Maa [113] proposed an empirical formula, which is multiplied by the end correction term $\delta(1 + z_{non-lin})^{-1}$.

Finally, the normalized full expression of the resistive part for the microperforated surface is

$$r_{mp} = \mathrm{Re}\left(\frac{j\omega t_p}{\sigma c_0} \left(1 - \frac{2}{\kappa\sqrt{-j}} \frac{J_1\left(\kappa\sqrt{-j}\right)}{J_0\left(\kappa\sqrt{-j}\right)} \right)^{-1} \right) + \frac{2\alpha R_s}{\sigma \rho_0 c_0} + \frac{|\hat{u}_h|}{\sigma c_0} \tag{2.131}$$

while the reactive part is

$$\chi_{mp} = \mathrm{Im}\left(\frac{j\omega t_p}{\sigma c_0} \left(1 - \frac{2}{\kappa\sqrt{-j}} \frac{J_1\left(\kappa\sqrt{-j}\right)}{J_0\left(\kappa\sqrt{-j}\right)} \right)^{-1} \right) + \frac{\delta \omega \left(1 + \dfrac{|\hat{u}_h|}{\sigma c_0} \right)^{-1}}{\sigma c_0} \tag{2.132}$$

Expressions (2.131) and (2.132) are valid for porosities below 5%, for which the interaction between holes is negligible.

2.6   Absorbent materials

Absorbent materials are widely used in a great variety of applications to improve the sound attenuation. The main function of the absorbent materials is the reduction of

the amplitudes of the acoustic fields associated with the wave propagation phenomena by dissipation of the acoustic energy [29]. Natural and artificial fibres, as well as polymeric and ceramic foams are commonly used materials in practical applications [10, 18, 117–119]. In exhaust systems, chambers incorporating absorbent materials are denominated dissipative silencers [126].

In a silencer, the absorbent material that wraps one or several perforated ducts can be characterized on many occasions as an isotropic structure. There exist internal cavities or interconnected pores in the structure, randomly distributed, in which the air can move [146]. The path followed by the air through a porous structure, when mean flow is considered, is generally defined by a tortuous path. If the flow is not turbulent, the air volume passing through the material is directly proportional to the difference of pressure that originates the flow [14].

The acoustic attenuation is produced, on the one hand, by the reflection of the acoustic wave, and on the other by the viscous losses at the interstices. Depending on the method used in the silencer manufacturing process, the variation of the material density can generate heterogeneity, anisotropy and spatial variation of the acoustic properties [16, 29, 149].

The incorporation of absorbent materials in vehicle exhaust systems has traditionally presented some problems associated with the degradation of their properties over time, the high temperatures they are subjected to and soiling due to the particles from the exhaust gases [74]. Also, the loss of material produced by the gas flow swept has to be considered in some configurations. In order to avoid this problem, Selamet *et al.* [155] proposed filling the outer chamber of a dissipative silencer with continuous strand fibres of texturized fibreglass. The texturization process separates 4000 filament roving strands of fibreglass into individual filaments by turbulent air flow. The degree to which the strands are separated into individual filaments affects both the complex-valued wavenumber and the impedance of the absorbent material. The physical and chemical properties of various materials and their relative durability in simulated automotive silencer operations are described by Huff [88]. Despite the improvements of the material properties and the increasing interest not only in reducing the noise levels under the legal limits, but also in the sound quality, having promoted use of the absorbent materials as a part of the silencers over recent decades [47, 65, 100, 138, 155, 159, 160], recent studies [5, 8, 64, 182] have raised an interesting trend that promotes the search of less polluting alternatives.

2.6.1   Introduction

Some of the most important properties of absorbent materials can be summarized in steady airflow resistivity, material density, porosity, tortuosity, elasticity, as well as fibre orientation in the case of a fibrous material. The resistivity is one of the most significant magnitudes in the characterization of absorbent materials. To measure the resistivity of an absorbent material, a sample is placed in a duct, and a differential pressure induces a steady flow of air [10]. The flow resistivity R is given by

$$R = \frac{\Delta P}{u \Delta l} \qquad (2.133)$$

where ΔP is the difference in pressure at both sides of the porous sample, Δl corresponds to the thickness and u is the velocity through the sample. This last magnitude can be measured with a Pitot-Static tube.

It should be pointed out that fibrous materials are generally anisotropic [12, 21]. For example, in a panel of absorbent material the fibres generally lie in planes parallel to the surface of the material. The flow resistivity in the normal direction is different from that in the planar direction. In the former case, air flows perpendicularly to the surface of the panel while in the latter case it flows parallel to the surface of the layer [10]. The normal flow resistivity is larger than the planar flow resistivity. For a fibrous material, the resistivity depends, among others, on the porosity σ and dynamic viscosity μ [10, 120], the size of the material fibres, their shape and orientation, as well as on the tortuosity q [14, 28].

Materials such as fibreglass consist of an elastic frame which is surrounded by air [10]. The porosity σ of an absorbent material is the ratio of the air volume V_a to the total volume of porous material V_m

$$\sigma = \frac{V_a}{V_m} \qquad (2.134)$$

2.6.2   Material characterization

The quantities involved in the sound propagation within a porous material can be defined locally, on a microscopic scale, considering for instance cylindrical pores having a circular cross section, as functions of the distance to the axis of the pores. However, studying the sound propagation in porous materials on a microscopic scale is difficult due to the complex geometries of the frames. Only the mean values of the quantities involved are of practical interest. The averaging must be performed on a macroscopic scale, on a homogenization volume with dimensions sufficiently large for the average

to be significant. At the same time, these dimensions must be much smaller than the acoustic wavelength. The description of sound propagation in a porous material can be complicated by the fact that sound also excites and moves the frame of the material. If the frame is motionless, in a first step, the air inside the porous medium can be replaced on the macroscopic scale by an equivalent free fluid. This equivalent fluid has a complex effective density ρ_m and a complex bulk modulus K_m. The wavenumber k_m and the characteristic impedance Z_m of the equivalent fluid are also complex [10, 57, 134]. This model can be used for a number of fibrous materials used by industry in the manufacturing process of silencers [65, 138, 149, 155, 156, 180]. The second model, also known as the poroelastic approach, is based on Biot's theories [32, 33] and was adapted by Allard et al. [11] to the acoustic problem. In this model, the elasticity of the solid phase is considered, which has a significant interaction with the spaces filled by air or another gas [131]. Delany and Bazley [57] carried out experimental studies including a wide assortment of absorbent materials for which analytical expressions were obtained to define the impedance Z_m and the wavenumber k_m as a function of frequency and resistivity. Later, several authors [104, 138, 155], according to this approach, extended the results to additional materials and carried out numerous studies of the acoustic behaviour of silencers with absorbent materials. Delany and Bazley's expressions [57] can be adapted and written as

$$Z_m = Z_0 \left(1 + a_5 \left(\frac{f \rho_0}{R} \right)^{a_6} - j a_7 \left(\frac{f \rho_0}{R} \right)^{a_8} \right) \tag{2.135}$$

$$k_m = k_0 \left(1 + a_3 \left(\frac{f \rho_0}{R} \right)^{a_4} - j a_1 \left(\frac{f \rho_0}{R} \right)^{a_2} \right) \tag{2.136}$$

where $Z_0 = \rho_0 c_0$ represents the characteristic impedance of the fluid medium, $k_0 = 2\pi f/c_0$ is the air wavenumber, f the frequency and R the resistivity of the absorbent material. The a_i coefficients, $i = 1, 2, ..., 8$, depend on the material under consideration and are obtained from a curve fitting process following laboratory measurements [100, 155]. Additional properties, depending on the previous expressions, complement the characterization of the absorbent material, such as the complex speed of sound and the complex density. These are defined by

$$c_m = \frac{\omega}{k_m} \tag{2.137}$$

$$\rho_m = \frac{Z_m}{c_m} = \frac{Z_m k_m}{\omega} \tag{2.138}$$

However, the empirical power-law of Delany and Bazley [57] produces non-physical predictions at low frequencies. To overcome this problem Kirby and Cummings [103] proposed a semi-empirical model which combines the empirical power-law of Delany and Bazley with a theoretical microstructure model at low frequencies. Values for the

propagation constant $\tilde{\Gamma}$ and characteristic impedance Z_m were given by Kirby and Cummings as [103]

$$\tilde{\Gamma} = j\sqrt{\gamma q^2(\omega)} \left(\frac{(\ln(1-\sigma) + 1 + 2\sigma)\,\sigma\ln(1-\sigma) + \sigma^2 + 3\sigma^3/2 + \sigma^4/3}{(\ln(1-\sigma) + \sigma + \sigma^2/2)^2} \right.$$
$$\left. - \left(\frac{\gamma-1}{\gamma}\right) Pr - j\frac{\sigma}{2\pi\xi_f q_0^2 s^2(\omega)} \right)^{\frac{1}{2}} \tag{2.139}$$

$$\frac{Z_m}{\rho_0 c_0} = j\sqrt{\frac{q^2(\omega)}{\gamma\sigma^2}} \left(\frac{(\ln(1-\sigma) + 1 + 2\sigma)\,\sigma\ln(1-\sigma) + \sigma^2 + 3\sigma^3/2 + \sigma^4/3}{(\ln(1-\sigma) + \sigma + \sigma^2/2)^2} \right.$$
$$\left. - \left(\frac{\gamma-1}{\gamma}\right) Pr - j\frac{\sigma}{2\pi\xi_f q_0^2 s^2(\omega)} \right)^{\frac{1}{2}} \tag{2.140}$$

where σ is the porosity of the porous material, ξ_f is a dimensionless frequency parameter ($\xi_f = \rho_0 f/R$, where f is the frequency and R the flow resistivity of the bulk porous material), γ is the ratio of specific heats for air, Pr is the Prandtl number and the tortuosity $q^2(\omega)$ and shape factor $s^2(\omega)$ are given by

$$q^2(\omega) = \frac{\left(\left(1 + a_3\xi_f^{a_4}\right)\left(1 + a_5\xi_f^{a_6}\right) - a_1 a_7\xi_f^{(a_2+a_8)}\right)\left(\ln(1-\sigma) + \sigma + \sigma^2/2\right)^2}{(\ln(1-\sigma) + 1 + 2\sigma)\ln(1-\sigma) + \sigma + 3\sigma^2/2 + \sigma^3/3} \tag{2.141}$$

$$s^2(\omega) = \frac{q^2(\omega)}{2\pi\xi_f q_0^2 \left(a_1\xi_f^{a_2}\left(1 + a_5\xi_f^{a_6}\right) + a_7\xi_f^{a_8}\left(1 + a_3\xi_f^{a_4}\right)\right)} \tag{2.142}$$

where a_i are the Delany and Bazley's [57] coefficients obtained experimentally for a particular absorbent material. Regarding equations (2.139) and (2.140), it is worth remarking that a transition value exists for ξ_f, denoted as ξ_{f_0}, below which $q^2(\omega)$ must be set equal to $q_0^2(\omega)$, q_0 being the steady flow tortuosity, in equations [103].

2.6.3 Additional considerations

I. Effect of the absorbent material on the acoustic impedance of the perforated duct

Perforated surfaces give, from a structural point of view, rigidity to the silencer and support to the absorbent material. They also prevent the material from being swept by the exhaust gases. From an acoustical point of view, the most significant effect of

the material in contact with the perforations is to increase the reactance, or imaginary part, of the acoustic impedance of the perforated surface [36, 94].

Several studies have been carried out to determine the acoustic impedance of perforated elements in contact with porous materials in both the absence and presence of mean flow. One of the main targets of these analytical works is to determine the effect of absorbent materials on the perforated element impedance. Initially, Bolt [34] focused his investigation on the variation of the reactance of perforated elements in contact with the absorbent material. This author indicated that an increase in the number of holes in contact with the absorbent material tends to improve the absorption coefficient at low frequencies; on the other hand, at high frequencies the opposite trend was observed. Ingard and Bolt [94] showed that the combination of absorbent material and perforated elements is equivalent to a Helmholtz resonator. Callaway and Ramer [36] and Ingard [93] increased the real part of the perforated screen impedance leaving a free space between the surface and the absorbent material.

Some empirical works combine the acoustic properties of the perforated surfaces and the absorbent materials to obtain the absorption coefficient. For example, Davern [54] considered the effect of the porosity, perforated plate thickness, density of the absorbent material, free space, and the contact between the absorbent material and perforated surfaces on the absorption coefficient.

Additional semi-empirical studies are oriented to establish the characteristics of the interaction between perforated surface-absorbent material, emphasizing the computation of the impedance of perforated surfaces. In this sense Kirby and Cummings [102], as previously mentioned, developed a semi-empirical formulation for the computation of the acoustic impedance of perforated elements in contact with the absorbent material, taking into account the presence of a grazing mean flow. It is worth noting that orifice interaction effects were negligible in the tests reported by the authors [102]. This model combined the empirical formulation proposed by Delany and Bazley [57] for the characterization of absorbent materials with a microstructural theoretical model [11] at low frequencies. These authors presented a semi-empirical predictive model, combining the formulae for the perforated duct impedance in the absence of a porous medium with the predicted bulk acoustic properties of the absorbent material. This prediction method for the perforated duct impedance in the presence of a porous medium is based on the heuristic assumption that the hydrodynamic effects of grazing flow on the orifice resistance and end correction on the side of the orifice facing the flow are unaltered by the presence of the porous medium, which has the principal effect of changing the mass end correction on the side of the orifice facing the porous material. For a single orifice with no porous backing and no mean flow

present, the normalized mass end correction is given by [102]

$$\chi = 0.425 k_0 d_h \tag{2.143}$$

d_h being the hole diameter and k_0 the air wavenumber.

The equivalent mass end correction when a porous material is present is obtained [94] by substituting the properties of air for the properties of the porous medium, namely,

$$\chi_m = 0.425 Z_m d_h \tilde{\Gamma} / (\rho_0 c_0) \tag{2.144}$$

Note that the end correction is now complex, and has a resistive component. The perforated duct impedance is given in terms of the empirically-predicted impedance [102]

$$\tilde{\xi}_p = \frac{1}{\sigma} \left(\xi'_p - 0.425 k_0 d_h + \frac{0.425 d_h Z_m \tilde{\Gamma}}{\rho_0 c_0} \right) \tag{2.145}$$

ξ'_p being the dimensionless impedance of an orifice in the absence of absorbent material.

Selamet *et al.* [155] modified the expression of the perforated plate impedance presented by Sullivan and Crocker [171] in view of the work by Kirby and Cummings [102] as

$$\tilde{Z}_p = \rho_0 c_0 \frac{\left(6 \cdot 10^{-3} + j k_0 \left(t_p + 0.375 \left(1 + \frac{Z_m}{Z_0} \frac{k_m}{k_0} \right) d_h \right) \right)}{\sigma} \tag{2.146}$$

Later, Denia *et al.* [66] also proposed an expression by modifying the expression of the perforated duct of Sullivan and Crocker [171] to incorporate the effect of the absorbent material

$$\tilde{Z}_p = \rho_0 c_0 \frac{\left(6 \cdot 10^{-3} + j k_0 \left(t_p + 0.425 \left(1 + \frac{Z_m}{Z_0} \frac{k_m}{k_0} \right) d_h F\left(\sigma \right) \right) \right)}{\sigma} \tag{2.147}$$

where $F(\sigma)$ is the correction factor related to the acoustic interaction between holes.

The results obtained with both formulae (2.146) and (2.147) show good agreement when compared with experimental results [66, 155].

II. Moving medium

The exhaust gases at the silencer inlet can induce a flow field in the absorbent material. Although the corresponding flow velocities are usually small from a practical point of

view, sometimes the acoustic behaviour of the material can be modified. Considering that the absorbent material is initially homogeneous and has isotropic properties, a non-uniform mean flow field can generate anisotropy and heterogeneities [138].

Although the knowledge about the acoustic behaviour of perforated surfaces in the presence of grazing flow is still improvable, it is found that the magnitude of the resistance increases in general with the mean flow Mach number, but the rate of the decrease of resistance with frequency is nearly the same for a very low Mach number condition. However, the decreasing trend of resistance for higher frequencies changes at a certain frequency, at which the resistance is nearly zero. This special frequency f_0 is denominated critical frequency in resistance and is different for each flow velocity condition. Reactance, however, increases with frequency and its magnitude generally decreases as the flow Mach number increases [108]. Kirby and Cummings [102] studied perforated plates subjected to grazing flow and backed by porous media, and obtained expressions (2.118) and (2.119) considering the influence of the mean flow in the term χ_p. In addition, expression (2.147) [66] can be applied for a mean flow case, which leads to

$$\tilde{Z}_p = \rho_0 c_0 \frac{\left(\xi_p' + j0.425 k_0 d_h \left(\frac{\rho_m}{\rho_0} - 1 \right) F\left(\sigma \right) \right)}{\sigma} \tag{2.148}$$

ξ_p' being the dimensionless impedance of an orifice in the absence of absorbent material but including the presence of mean flow, whose resistive and reactive parts are given by expressions (2.120) and (2.122).

As previously indicated, another relevant formulation of the acoustic impedance for a perforated surface in the presence of mean flow was presented by Lee and Ih [108]. The resistive and reactive parts R_0 and X_0, are calculated by means of (2.123) and (2.125), respectively. The final expression is given by

$$\tilde{Z}_p = \rho_0 c_0 \left(\xi_p' + \frac{j0.425 k_0 d_h \left(\frac{\rho_m}{\rho_0} - 1 \right) F\left(\sigma \right)}{\sigma} \right) \tag{2.149}$$

To characterize the perforated element in the presence of mean flow and absorbent material, equation (2.149) will be used along the Thesis.

2.7 Silencers

A silencer is, generally, a passive element, connected to a source of noise, whose function is to attenuate the sound level to acceptable values in both the duct and the surrounding environment. The acoustic response of the silencers depends on the phenomena that produce the sound attenuation [26, 126]. Silencers can be divided into two main groups: reactive and dissipative configurations [31, 126].

2.7.1 Reactive configurations

In reactive silencers the attenuation is mainly produced when a part of the incident energy is reflected back to the source at the area changes and other geometrical particularities producing a destructive wave interference [126, 142]. However, a simple area change does not result in any loss of power in the course of transmission [126]. A typical example is a simple expansion chamber, composed of an inlet tube, a central chamber and an outlet duct, as can be observed in Figure 2.5. The energy dissipated in this case is almost negligible.
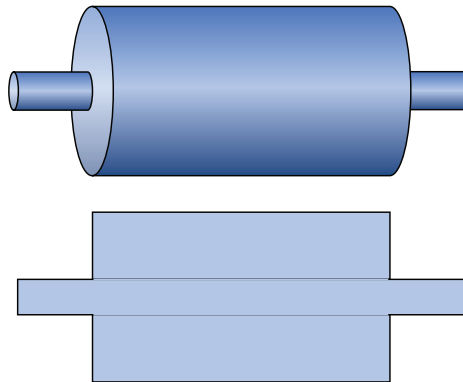

Figure 2.5: Reactive silencer with a simple expansion chamber.

2.7.2 Dissipative configurations

In dissipative silencers, the main attenuation phenomena (in addition to those associated with the aforementioned geometric discontinuities) are produced by the utilization of absorbent materials with a high specific surface (specifically in the form of fibres or pores). The absorbent material dissipates the wave propagation into heat [126] by the viscous boundary layer effect. In this case, the propagation of the acoustic wave produces a linear relationship between pressure drop and velocity. Also, dissipative characteristics can be obtained (although to a lower degree) by introducing perforated ducts and plates that favour the dissipation of energy during the propagation of the acoustic wave in the perforations [102]. For the case of perforated ducts in the presence of flow, the turbulent losses give an equivalent acoustic flow resistance which will be proportional to the mean flow speed reflecting the quadratic pressure drop. Figure 2.6 shows a scheme of a dissipative silencer.
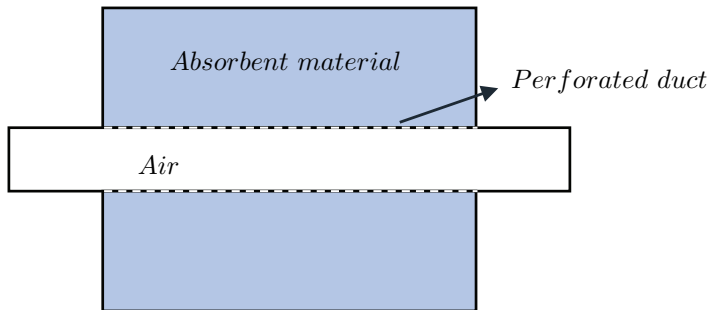
Figure 2.6: Perforated dissipative silencer with absorbent material.

In reality, all the reactive silencers produce some dissipation as a consequence of the energy losses associated with any real fluid when it circulates within the ducts, area changes, etc. In the same way, dissipative silencers have associated reactive effects due to the presence of expansions and contractions. In the literature, it is frequent to find the silencers containing perforated elements in the category of reactive configurations. Anyway, the dissipation introduced by these components cannot be negligible in certain configurations [8, 9, 64].

Hybrid silencers can also be included within configurations with dissipation, since they combine the geometric and attenuation characteristics of resonators and dissipative silencers, providing a combination of reactive and dissipative effects. Some works have

demonstrated the benefit of combining both types of behaviour in hybrid mufflers, i.e., reactive and dissipative effects for low and high frequencies respectively, which may lead to a broadband attenuation performance including resonant peaks at particular frequencies that can be pre-selected by the designer [59, 60, 66, 116].

2.8 Sound attenuation in silencers

The quantification of the sound attenuation in silencers requires the introduction of some basic concepts related to the energy associated with an acoustic wave, together with the definition of the suitable indicators of the noise reduction level. The deduction of the energy expressions involves the consideration of some thermodynamic relationships [126] to obtain a number of useful equations in terms of the acoustic fields considered here. As the presence of flow is relevant, its effect has to be included in the equations.

2.8.1 Energetic considerations

A duct in which the acoustic wave propagates in the presence of mean flow with velocity U_{mf} is considered first. In general harmonic behaviour is assumed, the values of interest being obtained from the temporal average along a period of the instantaneous acoustic fields. The acoustic intensity I associated with the wave, defined as the energy that passes through the duct cross section by time unit and surface, is given by [126]

$$I = \langle pu \rangle + \frac{U_{mf}}{\rho_0} \langle p\rho \rangle + U_{mf}\rho_0 \langle u^2 \rangle + U_{mf}^2 \langle u\rho \rangle \qquad (2.150)$$

where $\langle \rangle$ indicates the temporal average, this equation being only valid for plane waves and uniform mean flow. Now, using the expression (2.21), the density perturbation can be removed from equation (2.150), resulting in

$$I = \langle pu \rangle + \frac{M}{\rho_0 c_0} \langle p^2 \rangle + M\rho_0 c_0 \langle u^2 \rangle + M^2 \langle pu \rangle \qquad (2.151)$$

The acoustic power W can be obtained by simply integrating the intensity over the cross section,

$$W = \int_S I dS = \int_S \left(\langle pu \rangle + \frac{M}{\rho_0 c_0} \langle p^2 \rangle + M\rho_0 c_0 \langle u^2 \rangle + M^2 \langle pu \rangle \right) dS \qquad (2.152)$$

Considering harmonic behaviour of the waves results

$$Pe^{j\omega t} = \left(P^+ + P^-\right) e^{j\omega t} = \left(\left|P^+\right| e^{j\alpha_p} + \left|P^-\right| e^{j\alpha_r}\right) e^{j\omega t} \tag{2.153}$$

$$Ue^{j\omega t} = \frac{1}{\rho_0 c_0} \left(P^+ - P^-\right) e^{j\omega t} = \frac{1}{\rho_0 c_0} \left(\left|P^+\right| e^{j\alpha_p} - \left|P^-\right| e^{j\alpha_r}\right) e^{j\omega t} \tag{2.154}$$

and carrying out the temporal integration over a period $T = 2\pi/\omega$, expression (2.152) can now be written as

$$W = W(\omega) = \frac{S}{2\rho_0 c_0} \left(\left|P^+\right|^2 (1+M)^2 - \left|P^-\right|^2 (1-M)^2\right) \tag{2.155}$$

In the previous expression the distinction between the power associated with the progressive and the regressive wave can be clearly observed. In the absence of mean flow, $M = 0$ is considered.

2.8.2 Sound attenuation parameters in silencers

One of the basic targets of acoustic modelling is to obtain the sound attenuation produced by a device of the exhaust system, that can be measured in terms of one of the following parameters:

- Insertion loss (IL): this parameter provides information about the acoustic behaviour of a device (e.g. silencer or catalyst) coupled with an acoustic source and a termination. Therefore, its value will be determined by the characteristics of the whole system. It is defined as the difference in dB between the power level measured at a point before and after inserting the device between the measurement point and the noise source. Thus, if W_1 is the acoustic power without the device and W_2 with the device inserted, the following expression can be obtained [126]

$$IL = 10 \log \left(\frac{W_1}{W_2}\right) \tag{2.156}$$

- Transmission loss (TL): this is independent of the source and requires an anechoic termination at the downstream end. It is defined as difference between the power level incident on the device and that transmitted downstream into an anechoic termination. If P_1^+ is the incident pressure and P_2^+ the transmitted one, the following expression is obtained in the absence of flow [126]

$$TL = 10 \log \left(\frac{S_1 \left|P_1^+\right|^2}{S_2 \left|P_2^+\right|^2}\right) = 20 \log \left(\left(\frac{S_1}{S_2}\right)^{\frac{1}{2}} \left|\frac{P_1^+}{P_2^+}\right|\right) \tag{2.157}$$

- Level difference (LD): this is the difference in sound pressure levels between two arbitrarily selected points in the exhaust pipe and the tail pipe. It does not required an anechoic termination. If P_1 is the pressure upstream and P_2 is the value downstream, it yields [126]

$$LD = 20 \log \left(\left| \frac{P_1}{P_2} \right| \right) \tag{2.158}$$

In this Thesis the transmission loss is used as an acoustic characterization of the silencers, since it does not involve the source and the radiation impedances, given that it represents the difference between the incident and the transmitted acoustic energy considering an anechoic termination. Thus, the fact that this parameter does not depend on the termination is interesting when the objective is to obtain the acoustic transmission behaviour of an element or a set of elements in isolation of the terminations. Therefore, this parameter will be used from now on in this Thesis.

2.9 Applications

In this section, the transmission loss of reactive and dissipative silencers is computed in order to show the basic sound attenuation characteristics. Both types of silencer has been widely studied in the literature [46, 56, 65, 105, 126, 158]. Particularly, the dissipative configuration have been profusely studied from a multidimensional point of view in subsequent chapters. Since the characteristics of the behaviour are described by means of the transfer matrix method, the assessment of the TL from the four poles of a generic acoustic device is initially described. Thus, a matrix relating the variables at the inlet and the outlet of the device (denoted by subscripts 1 and 2 respectively) is considered.

$$\begin{Bmatrix} P_1 \\ U_1 \end{Bmatrix} = \begin{bmatrix} A & B \\ C & D \end{bmatrix} \begin{Bmatrix} P_2 \\ U_2 \end{Bmatrix} \tag{2.159}$$

According to equations (2.44) and (2.46), the following expressions are obtained

$$P_1 = P_1^+ + P_1^- \tag{2.160}$$

$$U_1 = U_1^+ + U_1^- = \frac{1}{\rho_0 c_0}(P_1^+ - P_1^-) \tag{2.161}$$

and therefore

$$P_1^+ = \frac{P_1 + \rho_0 c_0 U_1}{2} \tag{2.162}$$

Given an anechoic termination

$$P_2 = P_2^+ = \rho_0 c_0 U_2 \tag{2.163}$$

Using the TL definition given by expression (2.157), it is obtained that

$$TL = 20 \log \left(\left(\frac{S_1}{S_2} \right)^{\frac{1}{2}} \left| \frac{P_1 + \rho_0 c_0 U_1}{2 P_2} \right| \right) = 20 \log \left(\left(\frac{S_1}{S_2} \right)^{\frac{1}{2}} \left| \frac{P_1 + \rho_0 c_0 U_1}{2 \rho_0 c_0 U_2} \right| \right) \tag{2.164}$$

and considering now equation (2.159), the TL can be written as

$$TL = 20 \log \left(\left(\frac{S_1}{S_2} \right)^{\frac{1}{2}} \left| \frac{A + \dfrac{B}{\rho_0 c_0} + \rho_0 c_0 C + D}{2} \right| \right) \tag{2.165}$$

A similar procedure can be followed considering the four poles that relate pressure and mass flow, obtaining

$$TL = 20 \log \left(\left(\frac{S_1}{S_2} \right)^{\frac{1}{2}} \left| \frac{A + \dfrac{S_2 B}{c_0} + \dfrac{c_0 C}{S_1} + \dfrac{S_2 D}{S_1}}{2} \right| \right) \tag{2.166}$$

2.9.1 *TL* of a simple expansion chamber

A silencer similar to the one shown in Figure 2.5 is considered. This geometry consists of an inlet duct, a central chamber and an outlet duct, whose lengths and cross sectional areas are, respectively, L_1, L_2, L_3, S_1, S_2 and S_3,. The global transfer matrix of the silencer, considering pressures and velocities, is obtained by multiplying the matrices of the ducts and area changes, given by expressions (2.90) and (2.95) respectively, which yields

$$\begin{Bmatrix} P_1 \\ U_1 \end{Bmatrix} = \begin{bmatrix} A_1 & B_1 \\ C_1 & D_1 \end{bmatrix} \begin{bmatrix} 1 & 0 \\ 0 & \dfrac{S_2}{S_1} \end{bmatrix} \begin{bmatrix} A_2 & B_2 \\ C_2 & D_2 \end{bmatrix} \begin{bmatrix} 1 & 0 \\ 0 & \dfrac{S_3}{S_2} \end{bmatrix} \begin{bmatrix} A_3 & B_3 \\ C_3 & D_3 \end{bmatrix} \begin{Bmatrix} P_3 \\ U_3 \end{Bmatrix} = \begin{bmatrix} A & B \\ C & D \end{bmatrix} \begin{Bmatrix} P_3 \\ U_3 \end{Bmatrix} \tag{2.167}$$

Rearranging the previous expression and applying the TL definition given by equation (2.165), results in

$$TL = 10 \log \left(\frac{m_2}{4 m_1} \left(1 + \frac{m_1}{m_2} \right)^2 + \frac{m_2}{4 m_1} (m_1^2 - 1) \left(1 - \frac{1}{m_2^2} \right) \sin^2(k_0 L_2) \right) \tag{2.168}$$

with $m_1 = S_2/S_1$ y $m_2 = S_2/S_3$. Obviously, the attenuation is zero for $m_1 = m_2 = 1$.

In order to illustrate the acoustic attenuation performance of this kind of silencer, the configurations presented in Table 2.1 are considered. The silencers are composed of pipes with a circular cross section, which can be defined by their radii and lengths.

Geometry	R_1 (m)	R_2 (m)	R_3 (m)	L_2 (m)
1	0.0268	0.0886	0.0268	0.3
2	0.0268	0.0886	0.0268	0.15
3	0.0268	0.0532	0.0268	0.15

Table 2.1: Dimensions of simple expansion chambers.

The results obtained are shown in Figure 2.7, where it can be observed that the TL consists of a series of domes of attenuation with constant width and pass bands. The maximum value of attenuation of the attenuation curves appear at frequencies $f = (2n + 1)c_0/(4L_2)$, $n = 0, 1, 2, ...$ due to the existence of $2n + 1$ quarter-waves within the chamber. The troughs or pass bands are associated with a frequency $f = nc_0/(2L_2)$, $n = 0, 1, 2, ...$, which implies that n half-wavelengths appear inside the silencer chamber. As the length increases, the number of attenuation domes is higher in the frequency range under consideration. Regarding the maximum amplitude of attenuation, this is proportional to the relation between the chamber and the duct section, with the increasing area ratio leading to higher silencer attenuation.
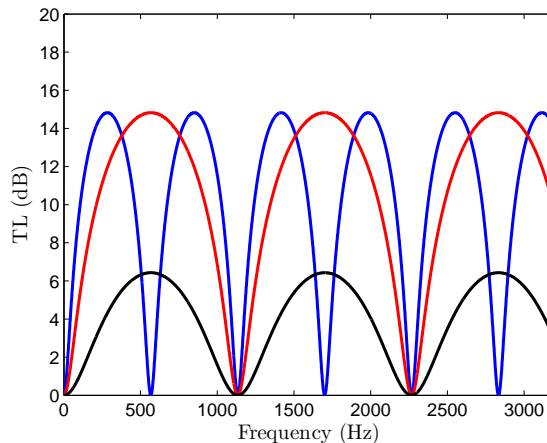

Figure 2.7: TL of a reactive silencer: ——, Geometry 1; ——, Geometry 2; ——, Geometry 3.

2.9.2   *TL* of perforated dissipative silencer

A perforated dissipative silencer was previously depicted in Figure 2.6. The silencer is composed of a central airway carrying mean flow and a surrounding chamber containing absorbent material. It is assumed that no mean flow exists within the chamber (or, if present, its influence on the silencer attenuation is considered negligible), which is consistent with the literature [100, 126, 170].

The following model is an extension of the matrix approach presented by Munjal [126], including absorbent material within the chamber. Thus, considering that equations of continuity (2.23) and dynamic equilibrium (2.25) can be expressed at any section of the duct as [126]

$$U_{mf_1}\frac{\partial \rho_1}{\partial z} + \rho_0\frac{\partial U_1}{\partial z} + \frac{4\rho_0}{d_1}U = -j\omega\rho_1 \tag{2.169}$$

$$\rho_0\left(j\omega U_1 + U_{mf_1}\frac{\partial U_1}{\partial z}\right) = -\frac{\partial P_1}{\partial z} \tag{2.170}$$

At the chamber, the corresponding equations can be written as follows [177]

$$\tilde{\rho}\frac{\partial U_2}{\partial z} - \frac{4d_1\tilde{\rho}_2}{d_2^2 - d_1^2}U = -j\omega\tilde{\rho}_2 \tag{2.171}$$

$$j\omega\tilde{\rho}U_2 = -\frac{\partial P_2}{\partial z} \tag{2.172}$$

d_1 and d_2 being the diameters of the duct and the chamber respectively, ρ_0 and $\tilde{\rho}$ the average values of the air and the material equivalent densities, U_{mf_1} the mean flow velocity, and U_1, U_2, ρ_1, $\tilde{\rho}_2$, P_1, and P_2 the acoustic perturbations. The pressure condition over the perforated plate can be written as

$$U(z) = \frac{P_1(z) - P_2(z)}{\tilde{Z}_p} \tag{2.173}$$

where the impedance $\tilde{Z}_p$ has to be adapted to the presence of absorbent material, as has been indicated in Section 2.6.3. In addition, a continuity condition is required. In this case, a kinematic continuity condition is considered, where radial velocity is the same at each side of the orifices leading to $U_1 = -U_2$ [104].

Finally, supposing a perfect gas behaviour, the expression (2.20) can be considered to eliminate the densities ρ_1 and $\tilde{\rho}_2$ and it is repeated here for clarity,

$$\frac{DP_T}{Dt} = c_0^2\frac{D\rho_T}{Dt} \tag{2.174}$$

where ρ_T and P_T are the total density and pressure. In the same way, the velocities U_1, U_2 and U can be eliminated resulting in

$$\frac{\partial^2 P_1}{\partial z^2} + \left(\frac{-M_1}{1-M_1^2} \left(j2k_0 + \frac{4\rho_0 c_0}{d_1 \tilde{Z}_p} \right) \right) \frac{\partial P_1}{\partial z} + \left(\frac{1}{1-M_1^2} \left(k_0^2 - \frac{4jk_0\rho_0 c_0}{d_1 \tilde{Z}_p} \right) \right) P_1$$
$$+ \left(\frac{M_1}{1-M_1^2} \left(\frac{4j\rho_0 c_0}{d_1 \tilde{Z}_p} \right) \right) \frac{\partial P_2}{\partial z} + \left(\frac{1}{1-M_1^2} \left(\frac{4jk_0\rho_0 c_0}{d_1 \tilde{Z}_p} \right) \right) P_2 = 0$$
$$\text{(2.175)}$$

$$\left(\frac{4d_1}{d_2^2 - d_1^2} \left(\frac{jk_0\tilde{\rho}c_0}{\tilde{Z}_p} \right) \right) P_1 + \frac{\partial P_2^2}{\partial z^2} + \left(\tilde{k}^2 - \frac{4d_1}{d_2^2 - d_1^2} \left(\frac{jk_0\tilde{\rho}c_0}{\tilde{Z}_p} \right) \right) P_2 = 0 \quad \text{(2.176)}$$

The previous equations can be written in matrix form as follows

$$\begin{bmatrix} D^2 + \alpha_1 D + \alpha_2 & \alpha_3 D + \alpha_4 \\ \alpha_5 & D^2 + \alpha_6 \end{bmatrix} \begin{Bmatrix} P_1 \\ P_2 \end{Bmatrix} = \begin{Bmatrix} 0 \\ 0 \end{Bmatrix} \quad \text{(2.177)}$$

where $D = \partial/\partial z$. Thus, the coefficients are

$$\begin{aligned}
\alpha_1 &= \frac{-M_1}{1-M_1^2} \left(j2k_0 + \frac{4\rho_0 c_0}{d_1 \tilde{Z}_p} \right) & \alpha_2 &= \frac{1}{1-M_1^2} \left(k_0^2 - \frac{4jk_0\rho_0 c_0}{d_1 \tilde{Z}_p} \right) \\
\alpha_3 &= \frac{M_1}{1-M_1^2} \left(k_0^2 - \frac{4\rho_0 c_0}{d_1 \tilde{Z}_p} \right) & \alpha_4 &= \frac{1}{1-M_1^2} \left(\frac{4jk_0\rho_0 c_0}{d_1 \tilde{Z}_p} \right) \\
\alpha_5 &= \frac{4d_1}{d_2^2 - d_1^2} \left(\frac{jk_0\tilde{\rho}c_0}{\tilde{Z}_p} \right) & \alpha_6 &= \tilde{k}^2 - \frac{4d_1}{d_2^2 - d_1^2} \left(\frac{jk_0\tilde{\rho}c_0}{\tilde{Z}_p} \right)
\end{aligned} \quad \text{(2.178)}$$

$k_0 = \omega/c_0$ and $\tilde{k} = \omega/\tilde{c}$ being the air and absorbent material wavenumbers respectively. Now equation (2.177) is reordered, which yields

$$\begin{Bmatrix} D^2 P_1 \\ D^2 P_2 \\ DP_1 \\ DP_2 \end{Bmatrix} + \begin{bmatrix} \alpha_1 & \alpha_3 & \alpha_2 & \alpha_4 \\ 0 & 0 & \alpha_5 & \alpha_6 \\ -1 & 0 & 0 & 0 \\ 0 & -1 & 0 & 0 \end{bmatrix} \begin{Bmatrix} DP_1 \\ DP_2 \\ P_1 \\ P_2 \end{Bmatrix} = \begin{Bmatrix} 0 \\ 0 \\ 0 \\ 0 \end{Bmatrix} \quad \text{(2.179)}$$

that can be written in general form as $\{P'\} = [A(z)]\{P\}$. Then, starting from (2.179) and computing the four pole matrix of the silencer, the acoustic attenuation can be easily calculated. The general solution can be written as

$$\{P\} = \sum_{i=1}^{4} \{\psi\}_i C_i e^{\beta_i z} \quad \text{(2.180)}$$

where β_i are the eigenvalues and $\{\psi\}$ the eigenvectors associated with matrix $-[A]$.

Then, normalizing the vectors, their first components have a unit value and the solution of equation (2.179) is

$$\frac{\partial P_1}{\partial z} = \sum_{i=1}^{4} \psi_{1,i} C_i e^{\beta_i z} = \sum_{i=1}^{4} C_i e^{\beta_i z} \tag{2.181}$$

$$\frac{\partial P_2}{\partial z} = \sum_{i=1}^{4} \psi_{2,i} C_i e^{\beta_i z} \tag{2.182}$$

$$P_1 = \sum_{i=1}^{4} \psi_{3,i} C_i e^{\beta_i z} \tag{2.183}$$

$$P_2 = \sum_{i=1}^{4} \psi_{4,i} C_i e^{\beta_i z} \tag{2.184}$$

while the velocity field can be written as [126]

$$U_1 = \sum_{i=1}^{4} K_i e^{\beta_i z} \tag{2.185}$$

where coefficients K_i can be obtained by substituting (2.181) and (2.185) in equation (2.170), which yields

$$K_i = -\frac{C_i}{\rho_0 (j\omega + U_{mf_1}\beta_i)} \tag{2.186}$$

On the other hand, the velocity in the chamber can be expressed as

$$U_2 = \sum_{i=1}^{4} -\frac{\psi_{2,i} C_i}{\tilde{\rho} j\omega} e^{\beta_i z} \tag{2.187}$$

Now, multiplying equations (2.185) and (2.187) by the characteristic impedance of air, yields

$$\rho_0 c_0 U_1 = \sum_{i=1}^{4} -\frac{C_i}{jk_0 + M_1\beta_i)} e^{\beta_i z} \tag{2.188}$$

$$\rho_0 c_0 U_2 = \sum_{i=1}^{4} -\frac{\psi_{2,i} C_i \rho_0}{jk_0 \tilde{\rho}} e^{\beta_i z} \tag{2.189}$$

and expressions (2.183), (2.184), (2.188) and (2.189) can be written in compact form as

$$\begin{Bmatrix} P_1(z) \\ P_2(z) \\ \rho_0 c_0 U_1(z) \\ \rho_0 c_0 U_2(z) \end{Bmatrix} = \begin{bmatrix} A(z) \end{bmatrix} \begin{Bmatrix} C_1 \\ C_2 \\ C_3 \\ C_4 \end{Bmatrix} \tag{2.190}$$

where $[A(z)]$ can be assessed from equations (2.183) and (2.182).

Then, considering that the axial velocity is zero at both sides of the chamber, i.e. $U_2(0) = 0$ and $U_2(L) = 0$, the previous expression can be rewritten as

$$\begin{Bmatrix} P_1(0) \\ P_2(0) \\ \rho_0 c_0 U_1(0) \\ \rho_0 c_0 U_2(0) \end{Bmatrix} = \begin{bmatrix} A(0) \end{bmatrix} \begin{bmatrix} A(L) \end{bmatrix}^{-1} \begin{Bmatrix} P_1(L) \\ P_2(L) \\ \rho_0 c_0 U_1(L) \\ \rho_0 c_0 U_2(L) \end{Bmatrix} = \begin{bmatrix} MT \end{bmatrix} \begin{Bmatrix} P_1(L) \\ P_2(L) \\ \rho_0 c_0 U_1(L) \\ \rho_0 c_0 U_2(L) \end{Bmatrix} \tag{2.191}$$

where the components of matrix $[MT]$ have been obtained as $[A(0)][A(L)^{-1}]$.

Once the boundary conditions are substituted in equation (2.191), the definition of the transfer matrix provided by (2.159) is taken into account, giving

$$\begin{Bmatrix} P_1(0) \\ P_2(0) \end{Bmatrix} = \begin{bmatrix} A & B \\ C & D \end{bmatrix} \begin{Bmatrix} P_1(L) \\ P_2(L) \end{Bmatrix} \tag{2.192}$$

the poles being

$$A = MT_{11} - \frac{MT_{41}}{MT_{42}} MT_{12} \qquad B = \rho_0 c_0 \left(MT_{13} - \frac{MT_{43}}{MT_{42}} MT_{12} \right)$$

$$C = \frac{1}{\rho_0 c_0} \left(MT_{31} - \frac{MT_{41}}{MT_{42}} MT_{32} \right) \qquad D = MT_{33} - \frac{MT_{43}}{MT_{42}} MT_{32} \tag{2.193}$$

where the terms MT_{ij} belong to the matrix defined in expression (2.191). Then, once the poles of the transfer matrix are obtained, the TL corresponding to the perforated dissipative silencer is obtained by substituting them into expression (2.165).

Some results are finally provided considering a geometry defined by the following values: $d_1 = 0.0268$ m, $d_2 = 0.0886$ m and $L = 0.3$ m, while the main parameters related to the perforated pipe and the absorbent material are $t_p = 0.001$ m, $d_h = 0.0035$ m, $\sigma = 11\%$ and $R = 4896$ rayl/m respectively. The impedance of the perforated duct is computed by means of the expression (2.149). In addition, the absorbent material considered is Owens Corning texturized fibreglass, which can be characterized by the wavenumber k_m and the complex impedance Z_m, whose general expressions

have been given in equations (2.136) and (2.135) respectively. Theses expressions are particularized here for the Owens Corning texturized fibreglass as [155]

$$Z_m = Z_0 \left(1 + 0.09534 \left(\frac{f\rho_0}{R} \right)^{-0.754} - j0.08504 \left(\frac{f\rho_0}{R} \right)^{-0.732} \right) \tag{2.194}$$

$$k_m = k_0 \left(1 + 0.16 \left(\frac{f\rho_0}{R} \right)^{-0.577} - j0.18897 \left(\frac{f\rho_0}{R} \right)^{-0.595} \right) \tag{2.195}$$

The mean flow effect on the TL is depicted in Figure 2.8 and two different trends can be found. At low frequencies the attenuation is higher for low Mach numbers, while at high frequencies the opposite tendency is found. It is also worth noting that the introduction of a dissipative fibre increases the attenuation and eliminates simultaneously the pass bands that appear in a reactive chamber (see Figure 2.7).
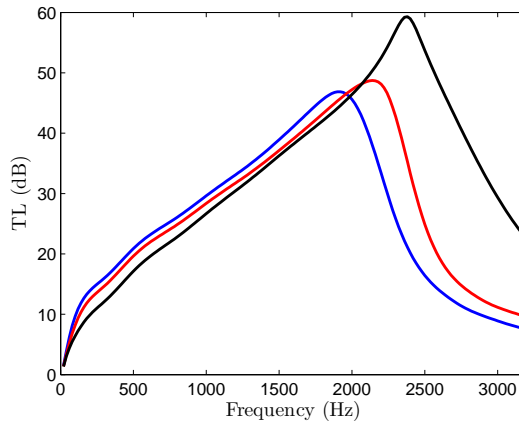
Figure 2.8: TL of a dissipative silencer: ———, $M = 0$; ———, $M = 0.1$; ———, $M = 0.2$.

2.10   Limitations

The plane wave hypothesis supposes that the sound pressure is uniform across the duct cross section [49]. This is valid if the axial dimension of the duct is large enough compared to its transversal dimensions. Besides, the frequency has to be lower than the first cut-on frequency, corresponding to the first non-planar pressure mode of the duct. Multidimensional modes start to propagate when the frequency is over this cut-on value and the plane wave hypothesis is no longer valid.

On the other hand, the acoustic field is also multidimensional at geometric discontinuities of silencers (as previously indicated, a silencer can be understood as several ducts of different dimensions interconnected in a particular, suitable configuration), even at frequencies below the cut-on frequencies, due to the appearance of evanescent modes that are rapidly attenuated but clearly modify the acoustic behaviour of the silencer [153].

Figure 2.9 shows the TL of an expansion chamber (whose geometry is defined as Geometry 1 in Table 2.1) computed by means of the FEM and the plane wave model. If both of them are compared, it can be observed that at low frequencies the results obtained are quite similar. However, at high frequencies the discrepancies between both methodologies are considerable due to the propagation of higher order modes.
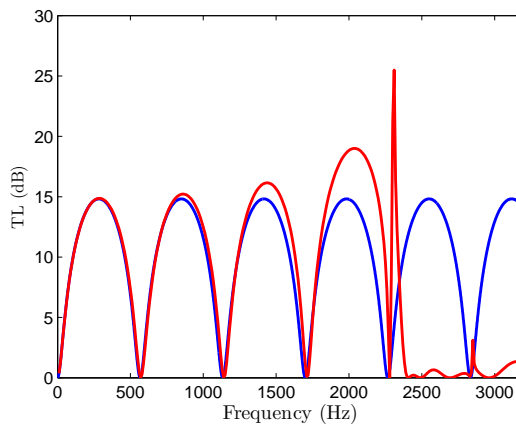
Figure 2.9: *TL* of a reactive silencer: ——, plane wave; ——, FEM.

2.11 Conclusions

In this chapter, the fundamental equations of the acoustic behaviour of a fluid and their linear associated models have been introduced, considering certain hypotheses, in order to simplify the mathematical approach. Besides, several matrix representations commonly used in the literature have been presented. These representations have been adapted and applied to certain elements belonging to silencers (ducts, area changes, *etc.*) to quantify their acoustic attenuation. Also, a review of the literature for the models that permit characterizing perforated elements in the presence of absorbent materials has been carried out. These models are the basis of the approaches that

will be presented in Section 3.2, where thermal-induced heterogeneities within the silencer and non-uniform properties of the absorbent material are considered in order to obtain more realistic and accurate results of acoustic behaviour. Also, a review of models for microperforated silencers has been undertaken, since these configurations are likely to be a good alternative to the traditional perforated dissipative silencers in some practical applications, such as multichamber silencers (as will be shown, for example, in Sections 4.7.3 and 4.7.4).

Some relevant silencer configurations have been presented, as well as the phenomena that originate the acoustic attenuation and the parameters usually considered for its assessment. The noise reduction in reactive and perforated dissipative geometries has been evaluated by means of the transfer matrix representation.

Finally, the deficiencies related to the plane wave model have been shown. For reactive and dissipative silencers, this model is likely to be no longer valid even at low frequencies because multidimensional evanescent and propagating higher order modes can appear, modifying the acoustic performance of the silencer. Therefore, a multidimensional approach is required, which justifies the necessity for new models including this phenomena. For this reason, the mathematical approaches presented in this Thesis are based on 3D full FE formulations, as well as on other models that consider a combination of a 2D FE formulation with the collocation point technique or the mode-matching method to reduce the computational effort required by full 3D FE calculations.

Chapter 3

Extended models for absorbent materials and sintered surfaces

Summary:

In this chapter, an extension of the existing absorbent material models is presented in order to increase their accuracy, assuming more realistic working conditions. Therefore, the models consider the variation of the propagation media properties due to the heterogeneous bulk density of the absorbent material or to the presence of thermal gradients. This fact affects the acoustic impedance of the perforated surface making it also coordinate-dependent. Thus, the usual definition of acoustic impedance is modified to include this dependence. On the other hand, sintered surfaces are presented as a potential alternative to the traditional configuration of a perforated dissipative silencer. Sintered surfaces are characterized via experimental measurements and a model for the acoustic impedance is also proposed according to the results obtained in the laboratory. Finally, the attenuation of reactive and dissipative configurations is quantified.

3.1 Introduction

The acoustic behaviour of dissipative silencers strongly depends on the properties of the absorbent material. In many design applications, it is necessary to predict accurately their acoustic performance for a wide frequency range and general working conditions. From a practical and computational point of view, it is easier for the silencer designer to consider homogeneous materials. Nevertheless, this assumption is often far from reality, since material properties can present significant spatial variations. Therefore, it can be important to take the presence of heterogeneities into account when modelling bulk reacting fibrous materials, as these variations are expected to considerably affect the acoustic performance of the silencer [16, 160, 161]. Material heterogeneity can be due to the fact that, within the silencer, the mean flow fields are non-uniform [138], and considerable thermal gradients can appear [71, 98, 178] as a result of the uneven filling process of the chamber [16, 160, 161]. Thus, the properties of the propagation media vary from one point to another within the silencer, which notably affects the acoustic behaviour of the silencer. Usually, a bulk reacting fibrous material can be characterized by means of its wavenumber and characteristic impedance [57, 108]. In this chapter, the definition of these two properties are analyzed in detail when: (1) The bulk density of the absorbent material is heterogeneous; (2) Thermal gradients exist within the silencer. In addition, the possible laws for the density and temperature field variations proposed are detailed.

On the other hand, the use of nearly constant impedance surfaces, as sintered screens, is proposed since they permit the considerable reduction in the sound emissions, in the mid and high frequency range [64]. Following the principles of microperforated silencers (see Section 2.5.2), this alternative can be useful in some practical applications to avoid the potentially harmful effects of some fibres on human health (additional considerations related to the weight and cost of the silencer are also interesting, but beyond the scope of the current investigation).

3.2 Models for the absorbent material with variable properties

In this section, two models of absorbent material including heterogeneous properties are described. The first model considers the variation of the properties due to a heterogeneous bulk density of the absorbent material, whereas the second takes into account the influence of the temperature gradients on the different propagation media

properties. In addition, the influence of the heterogeneous properties on the acoustic impedance of a perforated surface is also described.

3.2.1 Absorbent material with heterogeneous bulk density

As previously indicated, the presence of heterogeneities can produce significant spatial variations of material properties. These heterogeneities can be caused by an uneven filling of the chamber; for example, when the fibre is rolled around the central duct or it is pushed into the chamber. Selamet *et al.* [160] studied a dissipative silencer containing two concentric annular layers of absorbent material with different airflow resistivities in the absence of mean flow. In this work, a 2D analytical approach was used to compute the wavenumbers and transversal pressure modes in the central airway and chamber. Finally, the transmission loss was obtained through the application of the mode-matching technique by considering the continuity conditions of the acoustic pressure and axial velocity at the geometrical discontinuities. A good agreement was found between the results derived from this method and FE calculations. In a later work from the same authors [161], the acoustic effect of voids inside the silencer, modelled by means of axially staggering filled/empty segments in the outer chamber, was studied by considering a similar approach to the previous reference [160]. In this case, the method provided good correlation with both experimental measurements and FE calculations. Antebas *et al.* [16, 17] presented a pressure-based FE approach to compute the transmission loss of perforated dissipative silencers including a continuously-varying bulk density distribution. In these investigations, a linear function was proposed to model the axial variation of the bulk density, leading to heterogeneous material properties such as the flow resistivity, equivalent complex density and speed of sound. Some numerical issues were found at very low frequencies in the presence of a moving propagation medium [17]. On the other hand, anisotropy is likely to appear for silencers manufactured in such a way that the fibres are aligned in a specific direction or when a strongly directional mean flow exists within the absorbent material. Peat and Rathi [138] presented an FE approach to model the acoustic behaviour of dissipative silencers with anisotropic and heterogeneous properties caused by an induced flow, even if the material is initially isotropic and homogeneous. Despite being usual to place a perforated surface to protect the fibre and reduce the static pressure losses, it was not considered in this study.

Heterogeneities can also be caused by the soot particles contained in the exhaust gases from the engine [7]. From a modelling point of view, this can lead to a variable material resistivity, and therefore to a coordinate-dependent equivalent density and speed of

sound [10, 16, 17]. The presence of a perforated screen [123, 171] has an impact on the silencer performance, and the fibrous backing material has a considerable effect on the acoustic impedance of the perforations [102, 107]. Therefore, material heterogeneities are expected to produce spatial variations of the perforated duct impedance. Sullivan and Crocker studied the acoustic behaviour of a perforated surface in the absence of absorbent material [171]. Kirby and Cummings [102] presented empirical formulae for the acoustic impedance of a perforated surface with absorbent material located close to one side of the plate in the presence of mean flow. More relevant information describing the influence of the fibrous material on the acoustic performance of a perforated surface can be found in the work of Lee *et al.* [107].

On the other hand, Pedrosa [139] carried out several experiments in order to study the influence of the bulk density distribution and the filling process of the chamber on the acoustic attenuation. This author rolled the dissipative fibre around a central grid placed within a chamber and ensured the bulk density of the fibre was different in each test, while keeping the mass constant. The quantity of fibre used was 0.469 kg, its resistivity being 5321 rayl/m at 25 °C. The transmission loss curves obtained after the different filling processes of the chamber are shown in Figure 3.1.
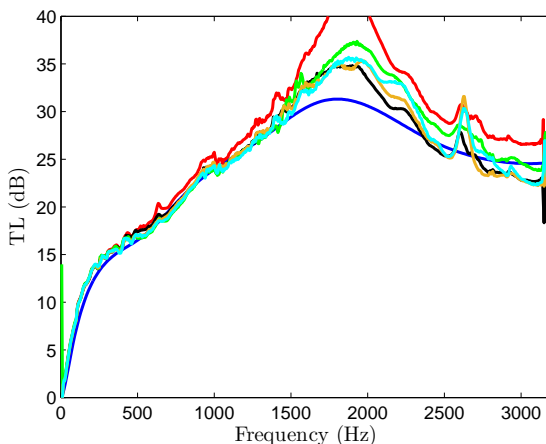
Figure 3.1: Transmission loss of a dissipative silencer with bulk density variation and constant mass (0.469 kg): ————, FE computation; ————, ————, ————, ————, ————, Experimental measurements with different bulk density distributions.

The blue line represents the theoretical transmission loss with a homogeneous bulk density, while the rest of the curves have been experimentally obtained after filling the chamber manually several times with the same quantity of fibre. It can be observed that at low frequencies the results of the different experiments are very similar.

Nevertheless, at high frequencies the discrepancies are significant. Therefore, it can be concluded that including the bulk density variations of the fibre in a dissipative silencer model is important to achieve an accurate prediction of its acoustic performance. The attenuation achieved by the silencer can be computed using numerical techniques, since some authors [161] found good agreement between them and experimental measurements. Further details of the numerical method (FEM) applied to determine the acoustic behaviour of a silencer including bulk density variations will be given in Section 4.5.1.

I. Variation of the properties

As mentioned in Section 2.6, an absorbent material can be characterized by its equivalent acoustic properties, as the wavenumber $k_m = \omega/c_m$ and characteristic impedance $Z_m = \rho_m c_m$, both complex and coordinate-dependent [10, 57]. These properties are usually uniform in the literature, since a homogeneous steady airflow resistivity R is assumed [59, 158]. This means that the bulk density of the absorbent material also has to be constant, since its relationship with the material resistivity is given by the following expression [103]

$$R = A_1 \rho_b^{A_2} \tag{3.1}$$

where coefficients A_1 and A_2 depend on the material and can be obtained from a curve fitting process following experimental data.

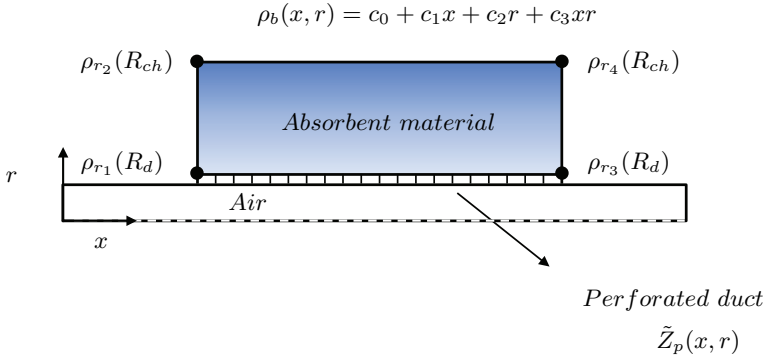$$\rho_b(x,r) = c_0 + c_1 x + c_2 r + c_3 x r$$

Figure 3.2: Bulk density distribution of the absorbent material for an axisymmetric silencer.

The bulk density is usually considered constant in the literature [57, 66, 102, 104, 107]. However, the heterogeneities that appear during the manufacturing process of the silencer lead to spatial variations of the bulk density. As can be observed in

E.M. Sánchez-Orgaz

Figure 3.2, an axisymmetric silencer is considered for computational purposes and the heterogeneous bulk density distribution can be approximated by a bilinear function as $\rho_b(x,r) = c_0 + c_1 x + c_2 r + c_3 xr$ [149], where x and r are the axial and radial coordinates respectively. With a view to obtaining the coefficients c_i, the density value in four points of the chamber is required. In this case, the distribution can be computed from the values ρ_{r_i}, $i = 1, 2, ..., 4$ (see Figure 3.2).

This leads to heterogeneous resistivity of the absorbent material [16, 17, 160, 161], which according to equation $R = A_1 \rho_b(\mathbf{x})^{A_2}$ depends on the coordinates and therefore, expressions (2.135) and (2.136) can be expressed as

$$Z_m = Z_0 \left(1 + a_5 \left(\frac{f\rho_0}{R(\mathbf{x})} \right)^{a_6} - ja_7 \left(\frac{f\rho_0}{R(\mathbf{x})} \right)^{a_8} \right) \qquad (3.2)$$

$$k_m = k_0 \left(1 + a_3 \left(\frac{f\rho_0}{R(\mathbf{x})} \right)^{a_4} - ja_1 \left(\frac{f\rho_0}{R(\mathbf{x})} \right)^{a_2} \right) \qquad (3.3)$$

where $Z_0 = \rho_0 c_0$ is the characteristic impedance of the air and f is the frequency.

II. Acoustic impedance of the perforated surface

The impedance of the perforated plate is considerably affected by the absorbent material [102]. Therefore, the heterogeneities presented by the fibre have to be included in the acoustic model of the perforated surface to guarantee the accuracy of the computations. Also, the impedance depends on the mean flow [108, 126]. As shown previously, the perforated duct impedance is given by

$$\tilde{Z}_p = \rho_0 c_0 \left(\xi_p' + \frac{j0.425 k_0 d_h \left(\frac{\rho_m(\mathbf{x})}{\rho_0} - 1 \right) F(\sigma)}{\sigma} \right) \qquad (3.4)$$

where ξ_p' is the dimensionless impedance of the perforated surface considering the influence of the mean flow without taking into account the absorbent material (for further details see Section 2.6.3)

$$\xi_p' = \frac{Z_p}{\rho_0 c_0} = \frac{R_0 + jX_0}{\rho_0 c_0} \qquad (3.5)$$

In the computations carried out in the current investigation, the perforated duct is parallel to the x axis and is then the only relevant coordinate.

3.3 Absorbent material with thermal-induced heterogeneity

The temperature distribution in the silencer is strongly related to a number of parameters, such as the geometrical configuration, thermal conductivities and convection heat transfer coefficients determining the surface heat flux from the metallic housing to the surrounding air. In addition, convection coefficients depend on numerous fluid properties, flow conditions, vehicle speed and also the geometries of the surfaces involved [90]. Engine load and speed are relevant parameters as well, and significant temperature modifications can be found by running the engine at idle condition or accelerating to a certain speed. In reference [71], a method is developed for estimating the temperature profiles of the exhaust gases from the surface temperatures of the exhaust piping. Concerning the silencer, the corresponding axial temperature gradient $\Delta T_{ax} = T_i - T_o$ (T_i and T_o being the inlet and outlet temperatures, respectively) associated with different vehicle models is shown to vary over a wide interval. Engines running at idle and free accelerated conditions are considered. In this latter case, the particular ranges presented in [71] at a speed of 2000 rpm are 40 °C ∼ 200 °C for ΔT_{ax}, 240 ∼ 725 °C for T_i, and 200 °C ∼ 650 °C for T_o. Reference [73] shows the axial temperature gradient along an exhaust system of a single-cylinder four-stroke engine. A reactive silencer is presented whose temperature variation is $\Delta T_{ax} = 200$ °C approximately, with $T_i = 510$ °C and $T_o = 315$ °C. Transversal temperature variations ΔT_{rad} can also be significant in exhaust silencers, and thermal gradients higher than 100 °C can be found in the literature [87], resulting in complex profiles of the relevant acoustic properties. The presence of high temperature and strong thermal gradients in dissipative silencers modifies their acoustic attenuation performance. Therefore, it is important to consider them in order to assess the silencer attenuation [65].

3.3.1 Variation of the properties

The temperature distribution within the silencer, causative of the variation of the properties of the different propagation media [65, 127, 167], is modelled according to the silencer region under analysis. In this case, an axisymmetric configuration, as shown in Figure 3.3, is considered for computational purposes:

- A constant temperature is assumed within the inlet and the outlet ducts due to their small dimensions in comparison with the rest of the silencer. The temperature values are defined as T_i and T_o respectively.

- In the central perforated duct, a linear variation depending on the x coordinate is assumed, while the radial variation of temperature is neglected because the radius of the duct is much smaller than the outer radius of the chamber. Thus, the gradient in the central duct can be written as

$$T_d(x) = b_0 + b_1 x \qquad (3.6)$$

b_0 and b_1 being the coefficients of the polynomial that defines the temperature field.

- At the outer chamber with absorbent material, the temperature varies according to the expression

$$T_{ch}(x, r) = c_0 + c_1 x + c_2 r + c_3 xr + c_4 r^2 + c_5 xr^2 \qquad (3.7)$$

combining a linear variation along the axial direction and a quadratic law in the radial coordinate, defined from the temperatures values T_{r_i}, $i = 1, 2, ..., 6$. Note that this quadratic function is used to interpolate the approximate logarithmic temperature distribution through a cylindrical domain [90].
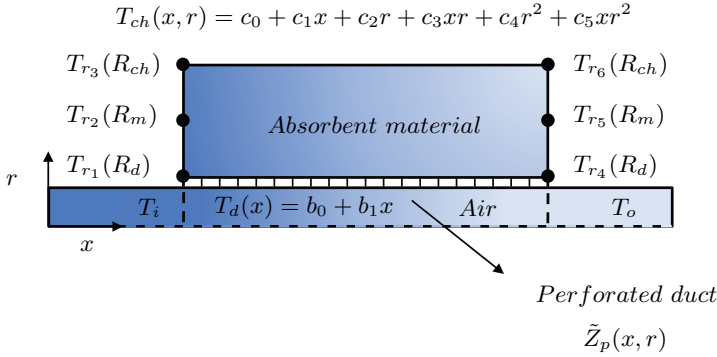
Figure 3.3: Temperature field within an axisymmetric silencer.

For a given temperature distribution, the density $\rho_0(\mathbf{x})$ and speed of sound $c_0(\mathbf{x})$ can be easily evaluated at each integration point assuming the ideal gas law, as shown in the work of Dokumaci [68], where the local dependence of these properties on the mean flow velocity is not taken into account since the flow velocities under consideration are relatively low.

On the other hand, the characteristic properties of the absorbent material depend on the resistivity that spatially varies as a consequence of the existing thermal gradients.

Consequently, the local resistivity can be calculated at each point of the dissipative chamber as [65]

$$R(T(\mathbf{x})) = R(T_0)\frac{\mu(T(\mathbf{x}))}{\mu(T_0)} \tag{3.8}$$

μ being the dynamic viscosity of the air (whose reference value can be approximately $\mu(T_0) = 1.84 \cdot 10^{-5}$ Pa·s for $T_0 = 25\,°\text{C}$). For a continuously varying temperature field $T(\mathbf{x})$, the viscosity $\mu(T(\mathbf{x}))$ can be computed by means of Sutherland's equation [152]

$$\mu(T(\mathbf{x})) = 1.458 \cdot 10^{-6}\frac{(273.15 + T(\mathbf{x}))^{1.5}}{273.15 + T(\mathbf{x}) + S} \tag{3.9}$$

where the Sutherland's constant S is a characteristic of the gas. The value considered for air is $S = 110.4$ K.

However, as far as the temperature increases, expressions (3.8) and (3.9) lead to an overestimation of the material resistivity when compared to Christie's power law [41, 180]

$$R(T(\mathbf{x})) = R(T_0)\left(\frac{T(\mathbf{x}) + 273.15}{T_0 + 273.15}\right)^{0.6} \tag{3.10}$$

For example, an approximate deviation of 10% has been found at 500 °C. Williams *et al.* [180] have recently provided further experimental validation to the use of equation (3.10). These authors have shown that the data measured at different temperatures collapse well onto Delany and Bazley curves if equation (3.10) is used for relating temperature and resistivity, and therefore the 0.6 power law will be used hereafter.

Then, once the resistivity is obtained, the impedance and the wavenumber of the absorbent material can be calculated by means of equations (3.2) and (3.3). Now, the equivalent density and speed of sound computation at each integration point is straightforward as they can be obtained as $\rho_m = Z_m/c_m$ and $c_m = \omega/k_m$.

II. Perforated surface acoustic impedance

The dimensionless impedance of a perforated surface in the presence of a grazing mean flow can be expressed as [108]

$$\xi'_p(\mathbf{x}) = \frac{Z_p(\mathbf{x})}{\rho_0(\mathbf{x})c_0(\mathbf{x})} = \frac{R_0(\mathbf{x}) + jX_0(\mathbf{x})}{\rho_0(\mathbf{x})c_0(\mathbf{x})} \tag{3.11}$$

where the dependence on the coordinates has been explicitly indicated. Note that the tilde has been intentionally omitted from $Z_p(\mathbf{x})$ to indicate that the effect of the absorbent material is not included in the acoustic behaviour of the holes.

This expression depends on R_0 and X_0, as defined in equations (2.123) and (2.125) [108]. Nevertheless, it is worth remarking that the Mach number $M(\mathbf{x})$ is now coordinate-dependent due to the axial temperature gradient. So, the previous expressions based on the model of Lee and Ih (see Section 2.6.3) are redefined assuming that they can be extended to situations where the Mach number varies with position, giving

$$R_0(\mathbf{x}) = \rho_0(\mathbf{x})c_0(\mathbf{x})\frac{a_0\left(1 + a_1\left|f - f_0(\mathbf{x})\right|\right)\left(1 + a_2 M(\mathbf{x})\right)\left(1 + a_3 d_h\right)\left(1 + a_4 t_p\right)}{\sigma} \tag{3.12}$$

$$X_0(\mathbf{x}) = \rho_0(\mathbf{x})c_0(\mathbf{x})\frac{b_0\left(1 + b_1 d_h\right)\left(1 + b_2 t_p\right)\left(1 + b_3 M(\mathbf{x})\right)\left(1 + b_4 f\right)}{\sigma} \tag{3.13}$$

The critical frequency can now be expressed as follows

$$f_0(\mathbf{x}) = \frac{\phi_1(1 + M(\mathbf{x})\phi_2)}{(1 + \phi_3 d_h)} \tag{3.14}$$

If the effect of the absorbent material on the perforated surface is also included, Lee and Ih's model results in

$$\tilde{Z}_p(\mathbf{x}) = \rho_0(\mathbf{x})c_0(\mathbf{x})\left(\xi_p'(\mathbf{x}) + \frac{j0.425 k_0(\mathbf{x}) d_h\left(\dfrac{\rho_m(\mathbf{x})}{\rho_0(\mathbf{x})} - 1\right) F\left(\sigma\right)}{\sigma}\right) \tag{3.15}$$

where, as in equation (3.4), the dependence on the coordinates has been considered to model the presence of heterogeneities in the properties of the material, as well as in the mean flow Mach number. The equation (3.15) simultaneously includes the influence of the mean flow and the absorbent material on the acoustic impedance of the perforated screen. It should be noted that $\mathbf{x} = x$, since the perforated duct is parallel to the x axis.

3.4 Sintered surface model

The sintered surfaces are presented as a potential alternative to the traditional configuration of perforated dissipative silencer that is commonly used in internal combustion engines. In this section, the experimental methodology used to characterize sintered surfaces is described. In the experiments carried out the mean flow has not been taken into account. Most of the methods found in the bibliography characterize an

absorbent material according to its characteristic impedance [107, 166, 173]. Nevertheless, these methods can be easily adapted to obtain the acoustic impedance of a surface as will be shown later.

3.4.1   Material characterization

In particular one of the most common methods to acoustically characterize an absorbent material is the transfer matrix method [2, 166], which has been adapted in the present work to characterize sintered surfaces. A scheme of the setup used to obtain the acoustic impedance of the sintered samples is shown in Figure 3.4, while the real setup can be observed in Figure 3.5.

Figure 3.4: Scheme of the experimental setup for the characterization of material samples by means of the transfer matrix method.

In this setup the impedance pipe is supplied with four microphones and a loudspeaker (see Figure 3.4). The loudspeaker generates noise within the pipe that passes through the sintered surface placed in the sample holder (see Figure 3.6) and continues towards the outlet pipe.

Regarding the microphones, two are placed upstream and two downstream of the samples, their function being to pick up the sound pressure data (P_1, P_2, P_3, P_4) at
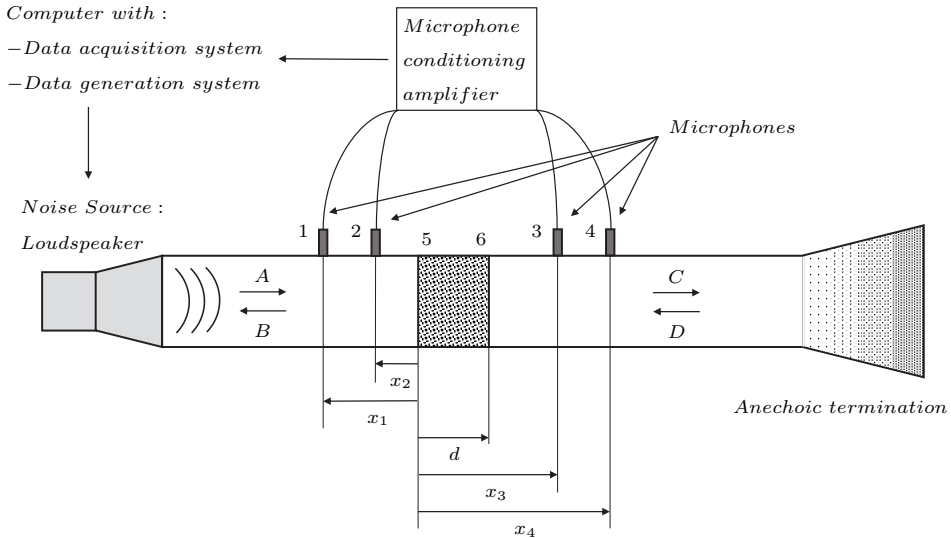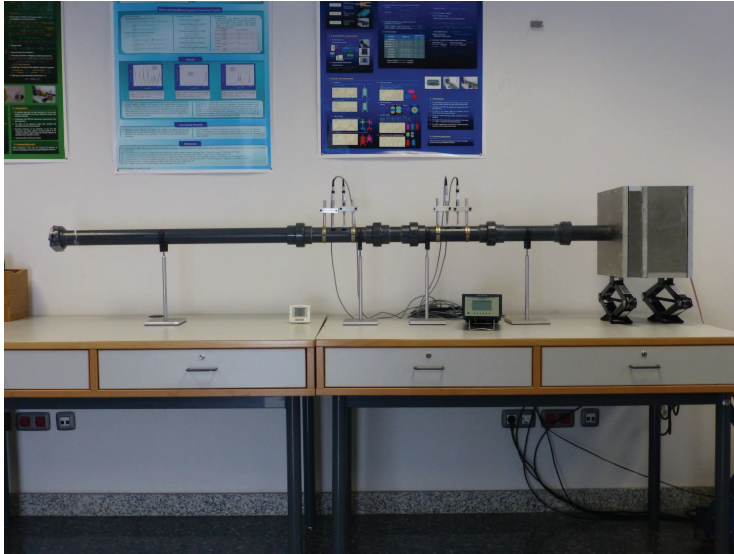
Figure 3.5: Picture of the experimental setup for the characterization of material samples by means of the transfer matrix method.

Figure 3.6: Sample holder for the study of the sintered plates.

the corresponding microphones locations. The pressures can be written as

$$P_1 = Ae^{-jk_0x_1} + Be^{jk_0x_1} \tag{3.16}$$

$$P_2 = Ae^{-jk_0x_2} + Be^{jk_0x_2} \tag{3.17}$$

$$P_3 = Ce^{-jk_0x_3} + De^{jk_0x_3} \tag{3.18}$$

$$P_4 = Ce^{-jk_0x_4} + De^{jk_0x_4} \tag{3.19}$$

where k_0 is the wavenumber of the air, x_1, x_2, x_3 and x_4 are the distances from each microphone until the face of the sample, while d is the thickness of the sample under study.

Then, solving the system composed of equations (3.16)-(3.19) yields

$$A = \frac{j(P_1 e^{jk_0x_2} - P_2 e^{jk_0x_1})}{2\sin(k_0(x_1 - x_2))} \tag{3.20}$$

$$B = \frac{j(P_2 e^{-jk_0x_1} - P_1 e^{jk_0x_2})}{2\sin(k_0(x_1 - x_2))} \tag{3.21}$$

$$C = \frac{j(P_3 e^{jk_0x_4} - P_4 e^{jk_0x_3})}{2\sin(k_0(x_3 - x_4))} \tag{3.22}$$

$$D = \frac{j(P_4 e^{-jk_0x_3} - P_3 e^{jk_0x_4})}{2\sin(k_0(x_3 - x_4))} \tag{3.23}$$

The transfer matrix between sections 5 and 6 can be expressed as

$$\begin{Bmatrix} P \\ U \end{Bmatrix}_{x=0} = \begin{bmatrix} A_{56} & B_{56} \\ C_{56} & D_{56} \end{bmatrix} \begin{Bmatrix} P \\ U \end{Bmatrix}_{x=d} \tag{3.24}$$

Thus, the above expression of the pressure and velocity (3.24) can be obtained from their progressive and regressive components

$$P|_{x=0} = A + B \tag{3.25}$$

$$U|_{x=0} = \frac{A - B}{\rho_0 c_0} \tag{3.26}$$

$$P|_{x=d} = Ce^{-jk_0d} + De^{jk_0d} \tag{3.27}$$

$$U|_{x=d} = \frac{Ce^{-jk_0d} - De^{jk_0d}}{\rho_0 c_0} \tag{3.28}$$

where ρ_0 is the density of the air and c_0 is the speed of sound.

In the transfer matrix four unknowns appear, so two additional equations will be required. To obtain those expressions there are two alternatives. The first one involves carrying out a new test with, for example, a different outlet condition. A second approach consists of assuming that the system is symmetric and reciprocal [166]. This assumption has been shown to provide good results for absorbent materials, and the associated hypotheses are valid as long as the mean flow is not considered. In the particular case of these surfaces, the performance of this second method is more than enough to obtain an accurate estimation of the acoustic impedance. The conditions of symmetry and reciprocity can be written as

$$A_{56} = D_{56} \tag{3.29}$$

$$A_{56}D_{56} - B_{56}C_{56} = 1 \tag{3.30}$$

The solution of the previous system (3.25)-(3.30) yields

$$A_{56} = \frac{P|_{x=d}\, U|_{x=d} + P|_{x=0}\, U|_{x=0}}{P|_{x=0}\, U|_{x=d} + P|_{x=d}\, U|_{x=0}} \tag{3.31}$$

$$B_{56} = \frac{P|_{x=0}^2 - P|_{x=d}^2}{P|_{x=0}\, U|_{x=d} + P|_{x=d}\, U|_{x=0}} \tag{3.32}$$

$$C_{56} = \frac{U|_{x=0}^2 - U|_{x=d}^2}{P|_{x=0}\, U|_{x=d} + P|_{x=d}\, U|_{x=0}} \tag{3.33}$$

$$D_{56} = \frac{P|_{x=d}\, U|_{x=d} + P|_{x=0}\, U|_{x=0}}{P|_{x=0}\, U|_{x=d} + P|_{x=d}\, U|_{x=0}} \tag{3.34}$$

For a homogeneous and isotropic material, the transfer matrix is given according to its properties by

$$\begin{bmatrix} A_{56} & B_{56} \\ C_{56} & D_{56} \end{bmatrix} = \begin{bmatrix} \cos(k_m d) & jZ_m \sin(k_m d) \\ \dfrac{j\sin(k_m d)}{Z_m} & \cos(k_m d) \end{bmatrix} \tag{3.35}$$

from where k_m and Z_m can be obtained as

$$k_m = \frac{\arccos A_{56}}{d} \tag{3.36}$$

$$Z_m = \rho_m c_m = \sqrt{\frac{B_{56}}{C_{56}}} \tag{3.37}$$

It should be noted that for a surface, the transfer matrix (3.24) can be easily simplified, since the thickness of the sample tends to zero, leading to the following expression

$$
\begin{Bmatrix} P \\ U \end{Bmatrix}_{x=0} = \begin{bmatrix} 1 & Z_p \\ 0 & 1 \end{bmatrix} \begin{Bmatrix} P \\ U \end{Bmatrix}_{x=d}
\tag{3.38}
$$

Then, the acoustic impedance of the sintered surface can be obtained as

$$
Z_p = \frac{P_{x=0} - P_{x=d}}{U_{x=0}} = \frac{P_{x=0} - P_{x=d}}{U_{x=d}}
\tag{3.39}
$$

as long as the sample is symmetric. Nevertheless, the experimentally determined acoustic velocities $U_{x=0}$ and $U_{x=d}$ at the sintered surface may not be exactly identical in experiments. Therefore, according to Lee *et al.* [107], an average of the two velocities can be used for the calculation of the sintered screen impedance as

$$
Z_p = \frac{P_{x=0} - P_{x=d}}{\dfrac{U_{x=0} + U_{x=d}}{2}}
\tag{3.40}
$$

In order to reduce the errors due to the measurement system, the microphones have to be calibrated previously. Seybert and Ross [162] suggested that the calibration has to be carried out flushing the microphones in the same plane and placing them at one end of the propagation duct, in such a way that they remain under the same pressure wave from the excitation source. The dimensions of the propagation duct permit considering plane wave propagation at the position where the microphones are placed, and therefore, the corresponding pressure measurements should have the same amplitude and phase offset. The discrepancies that appear between the collected data can be used to achieve a relative calibration with respect to one of the microphones arbitrarily chosen. In this case, the calibration is made with respect to microphone 1.

Thus, the transfer function between microphones 1 and 2, both excited by random noise is [154]

$$
H_{12}(f) = \sum_{p=1}^{N_{mean}} \frac{S_{12}(f)}{S_{11}(f)}
\tag{3.41}
$$

$S_{12}(f)$ and $S_{11}(f)$ being the cross spectrum between microphones 1 and 2 and the autospectrum of microphone 1 respectively, i.e. $S_{12} = FFT(P_2)\overline{FFT(P_1)}$ and $S_{11} = FFT(P_1)\overline{FFT(P_1)}$, where P_1 and P_2 are the pressure measurements obtained by microphones 1 and 2, FFT is the fast Fourier transform and N_{mean} is the number of averaged measurements. $H_{12}(f)$ is complex in general, so the gain of the measures of the microphones and the phase offset can be written as

$$
|H_{12}|
\tag{3.42}
$$

$$\phi_{12}(f) = \arctan\left(\frac{\text{Im}[H_{12}(f)]}{\text{Re}[H_{12}(f)]}\right) \tag{3.43}$$

The spectra obtained from the pressure time signals achieved during the material or surface test can be corrected with the frequency response determined at the calibration test by dividing the non-corrected measurements by H_{12}. It is worth noting that microphone 1 does not require any correction, since it is the reference microphone.

Microphones 3 and 4 are calibrated following a similar process to the one considered for the calibration of microphone 2.

3.4.2 Sintered surface acoustic impedance

A metallic sintered material is obtained from compacted spherical powder and heated to a high temperature (about 20% - 30% below the melting point of the mixture). During this process, an atomic diffusion between the particles is produced and coalescence of the microspheres to the solid state appears, resulting in a chemical link. The sintering process is carried out in continuous ovens, where the velocity and chemical composition of the atmosphere are controlled. The temperatures are usually between 750 °C and 1300 °C depending on the material and the required characteristics. Nevertheless, the samples characterized in the present Thesis have not been compacted in order to obtain a more porous surface. In this case, the samples characterized at the acoustic testing bench are circular plates manufactured with bronze (see Figure 3.7), their thickness being 0.001 m, 0.002 m and 0.003 m. Besides, several microsphere sizes of the powder were characterized, the nomenclature being FB12, FB24, FB40 and FB60, where the numerical code indicates the size of the pores among the microspherical particles (see also Table 3.1).

Granularity	Mean microsphere diameter (μm)	Mean pore size (μm)
FB12	65	12
FB24	120	24
FB40	200	40
FB60	300	60

Table 3.1: Filtered normalized granularities of the bronze sintered plates.
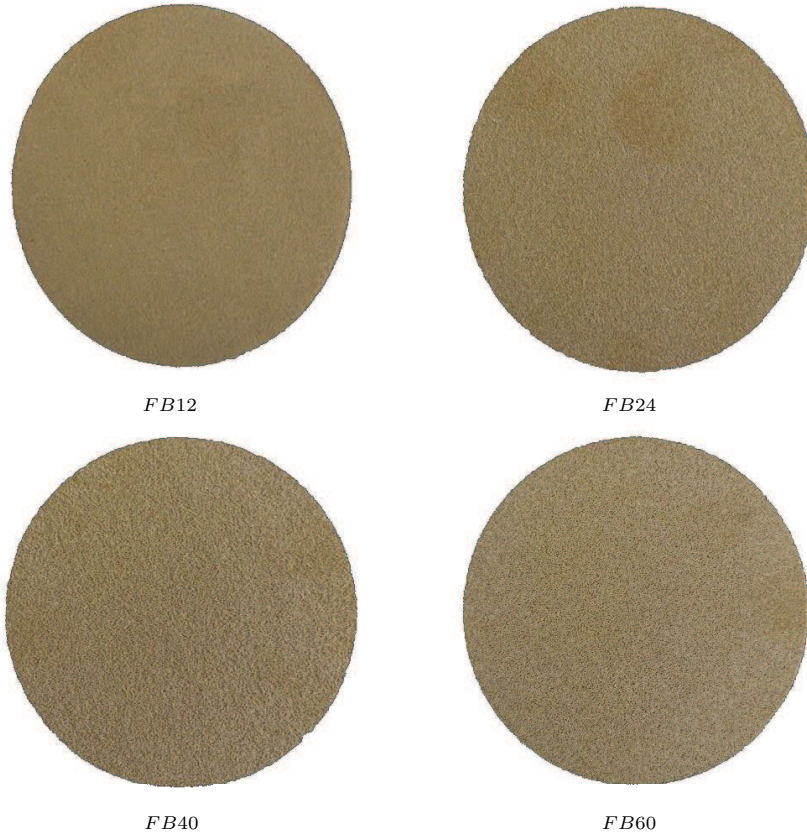
Figure 3.7: Bronze sintered plates of 0.002 m in thickness.

The estimation of the porosity has been carried out through the computation of the bulk density of the plate, as

$$\sigma(\%) = 100(1 - \frac{\rho_b}{\rho_{sp}}) \tag{3.44}$$

the bulk density being

$$\rho_b = \frac{m}{V} = \frac{m}{\frac{\pi \phi^2}{4} t} \tag{3.45}$$

ϕ being the diameter of the plate, t its thickness and ρ_{sp} the specific density of the base material. In this case, the base of the samples is a bronze 90/10 (CDA C90700 - ASTM B505), with 90% copper and 10% tin, the specific density value being $\rho_{sp} = 8770 \ kg/m^3$.

The plate thicknesses have been measured with a calliper, showing quite disperse values, mainly for the thinner samples. This is due to the uneven geometry of the plates produced by the material heterogeneity and the manufacturing process, which contributes to the existence of uncertainty over the porosity value, this being high in some cases, as can be observed in Table 3.2.

The relative error made when computing the bulk density of the sintered material e_{ρ_b} has been obtained considering the propagation of uncertainty of the different variables as

$$e_{\rho_b} = \sqrt{\left(\frac{e_m}{V}\right)^2 + \left(\frac{me_v}{V^2}\right)^2} \qquad (3.46)$$

where m is the mass, V is the volume, and e_m and e_v are their respective uncertainties. Therefore, the relative error on the porosity can be computed as

$$e_\sigma = \frac{e_{\rho_b}}{\rho_{sp}}100 \qquad (3.47)$$

e_σ being the uncertainty on the porosity.

Thickness (m)	Granularity	Porosity (%)	Relative error (%)
0.001	FB12	33.38	5.0
0.001	FB24	41.94	2.7
0.001	FB40	46.24	0.9
0.001	FB60	49.79	2.0
0.002	FB12	32.19	2.5
0.002	FB24	36.95	1.3
0.002	FB40	41.06	1.7
0.002	FB60	43.36	0.8
0.003	FB12	31.76	2.6
0.003	FB24	34.63	2.0
0.003	FB40	39.48	0.9
0.003	FB60	40.34	2.1

Table 3.2: Porosity and relative error (%) of the bronze sintered plates.

Some images of the bronze plates taken with the microscope are shown in Figure 3.8, where the different sizes of the samples, as well as the necks joining the spheric powder particles can be observed. The neck growth and densification of the particles is provoked by atomic diffusion during the heating process (when the temperature exceeds 1/2 of the melting point of the substance) [132].
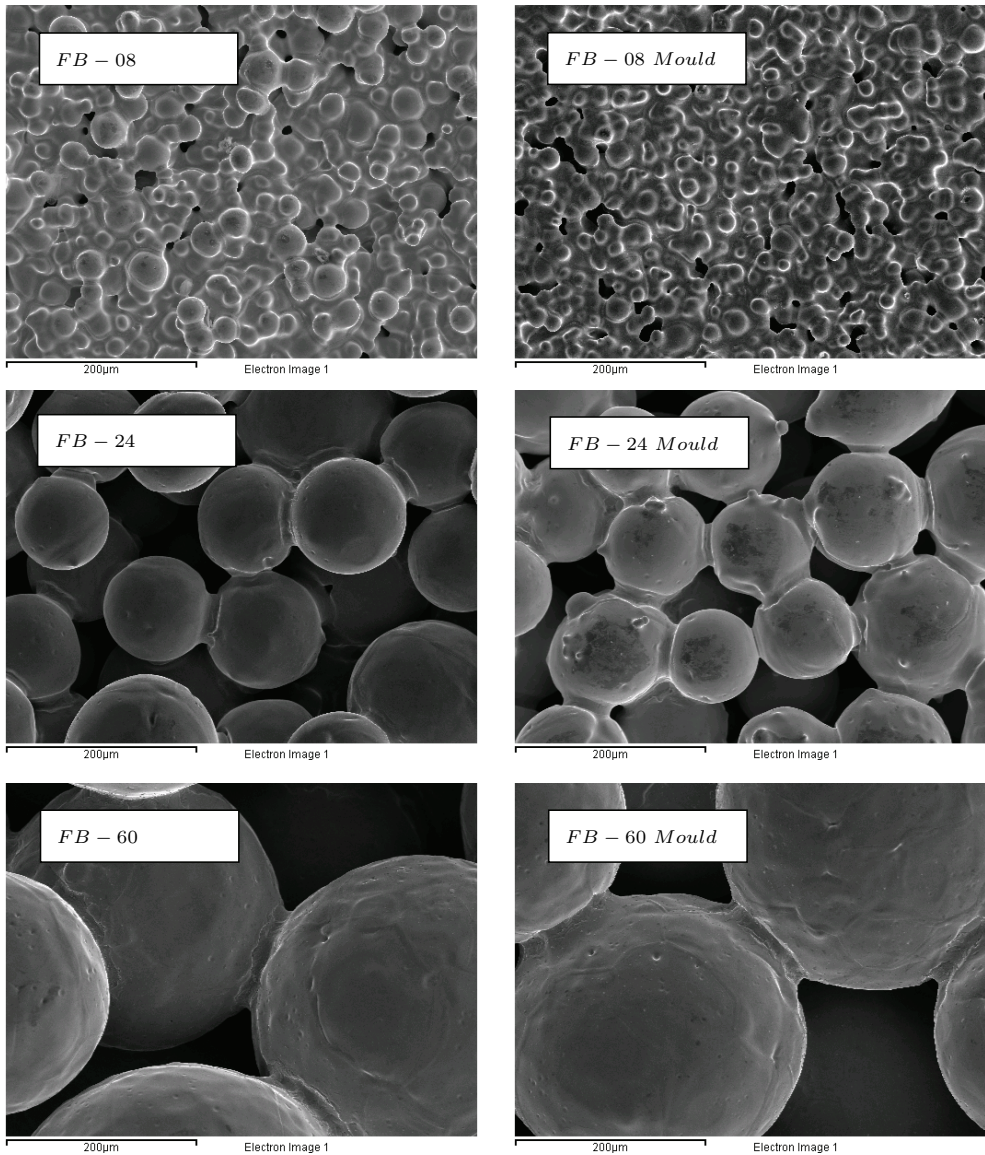
Figure 3.8: 500x microscope view of bronze sintered plates of 0.002 m in thickness. Top layer on the left and bottom layer (mould) on the right: FB08, FB24 and FB60.

Several tests have been carried out to determine the acoustic impedance of the sintered plates, the results being depicted in Figures 3.9-3.12. In comparing them, it can be observed that as the mean pore size decreases, the plate gradually behaves as a more *rigid* acoustic element and the acoustic impedance increases. The sound reflections are stronger, the measurements exhibit relevant irregularities and the acoustic trends are far from being clear, as can be observed in Figures 3.9 and 3.10, where the acoustic impedance of samples FB12 and FB24 are depicted, and therefore, their application as perforated ducts in automotive silencers is not likely to be interesting. The situation improves for larger pore size, as can be seen in Figures 3.11 and 3.12 for samples FB40 and FB60. In these two cases, a more consistent and uniform acoustic behaviour is found. The real part of the acoustic impedance Z_p is relatively *flat* in the frequency range under investigation, while the imaginary part increases slowly for higher frequencies, its value being lower than the real one.

For a given thickness, the impedance increases as the sphere and pore size decrease as can be deduced from Figures 3.13-3.15. In addition, if the design parameters are combined in a proper way, samples with similar normalized acoustic impedance can be obtained. Examples where the sphere size and thickness can be combined to obtain (approximately) similar results are given in Figures 3.16 and 3.17. Finally, it is important to remark that all the samples present a common characteristic, as indicated previously: all of them present a real part of the normalized acoustic impedance that is nearly constant, whereas the imaginary part shows a certain dependence on the frequency, its value being lower than the real one.

3.4.3   Sintered surface acoustic model

Sintered surfaces can be modelled by means of semi-phenomenological models as demonstrated by Li *et al.* [109]. These authors presented an acoustical model of sintered bronze material based on the work developed by Allard and Atalla [10] for porous materials, where the absorbent medium was modelled as an equivalent fluid characterized by its complex effective density ρ_m and complex bulk modulus K_m. As mentioned in Section 2.6.1, the wave propagation in the equivalent fluid depends on several parameters such as porosity σ, tortuosity q and steady airflow resistivity R. In addition, it also depends on microstructural properties such as the viscous characteristic length Λ and thermal characteristic length Λ'. The first is the ratio of the volume to the surface area in the pores, weighted by the square of the microscopic velocity of a non-viscous liquid in the pores, while the second is the ratio of the pore volume to the surface. It is obvious that the thermal characteristic length will be larger or equal to the viscous characteristic length [86]. The sintered bronze is composed of

Figure 3.9: Normalized acoustic impedance for plates FB12 and different thickness: ——, $\text{Re}(Z_p)$, $t = 0.001$ m; – – –, $\text{Im}(Z_p)$, $t = 0.001$ m; ——, $\text{Re}(Z_p)$, $t = 0.002$ m; – – –, $\text{Im}(Z_p)$, $t = 0.002$ m; ——, $\text{Re}(Z_p)$, $t = 0.003$ m; – – –, $\text{Im}(Z_p)$, $t = 3$ mm.
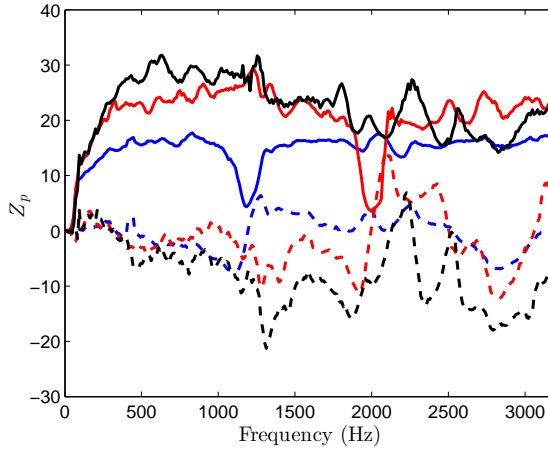

Figure 3.10: Normalized acoustic impedance for plates FB24 and different thickness: ——, $\text{Re}(Z_p)$, $t = 0.001$ m; – – –, $\text{Im}(Z_p)$, $t = 0.001$ m; ——, $\text{Re}(Z_p)$, $t = 0.002$ m; – – –, $\text{Im}(Z_p)$, $t = 0.002$ m; ——, $\text{Re}(Z_p)$, $t = 0.003$ m; – – –, $\text{Im}(Z_p)$, $t = 0.003$ m.
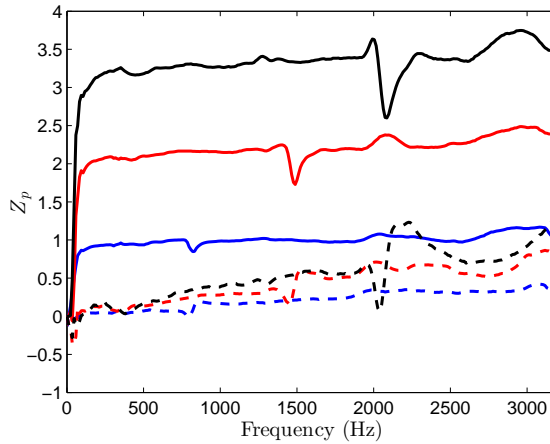
Figure 3.11: Normalized acoustic impedance for plates FB40 and different thickness: ——, Re(Z_p), $t = 0.001$ m; – – –, Im(Z_p), $t = 0.001$ m; ——, Re(Z_p), $t = 0.002$ m; – – –, Im(Z_p), $t = 0.002$ m; ——, Re(Z_p), $t = 0.003$ m; – – –, Im(Z_p), $t = 0.003$ m.
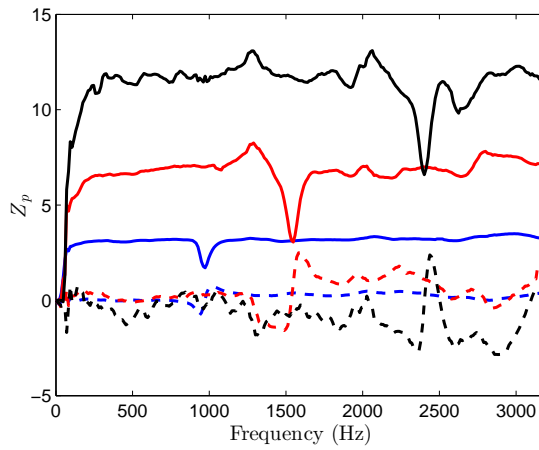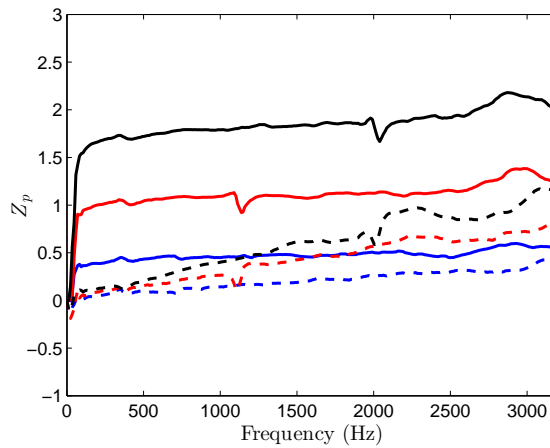

Figure 3.12: Normalized acoustic impedance for plates FB60 and different thickness: ——, Re(Z_p), $t = 0.001$ m; – – –, Im(Z_p), $t = 0.001$ m; ——, Re(Z_p), $t = 0.002$ m; – – –, Im(Z_p), $t = 0.002$ m; ——, Re(Z_p), $t = 0.003$ m; – – –, Im(Z_p), $t = 0.003$ m.
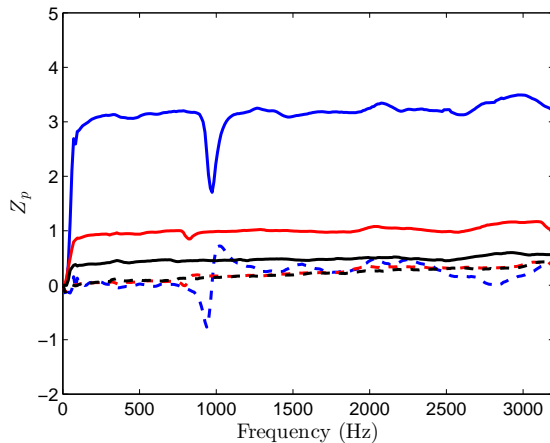
Figure 3.13: Normalized acoustic impedance for plates of 0.001 m in thickness: ──────, Re(Z_p), FB24; ─ ─ ─, Im(Z_p), FB24; ──────, Re(Z_p), FB40; ─ ─ ─, Im(Z_p), FB40; ──────, Re(Z_p), FB60; ─ ─ ─, Im(Z_p), FB60.
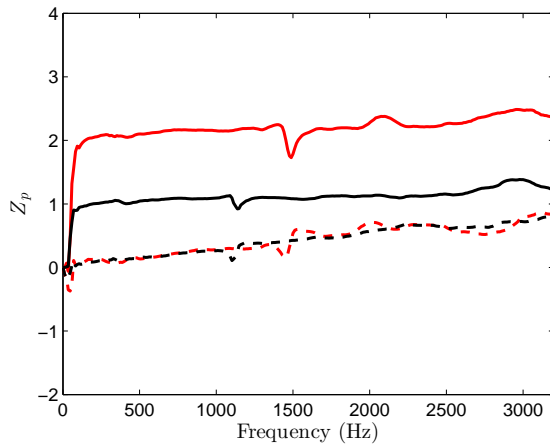
Figure 3.14: Normalized acoustic impedance for plates of 0.002 m in thickness: ──────, Re(Z), FB40; ─ ─ ─, Im(Z_p), FB40; ──────, Re(Z_p), FB60; ─ ─ ─, Im(Z_p), FB60.
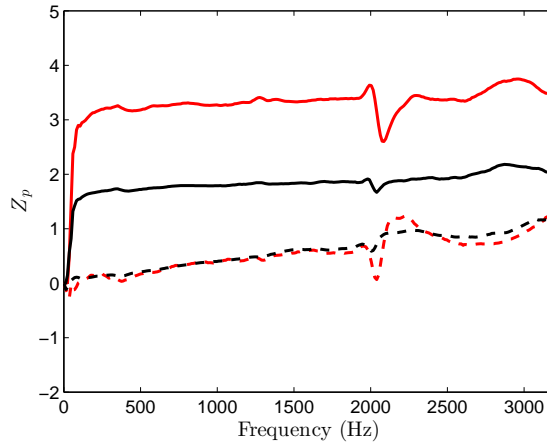
Figure 3.15: Normalized acoustic impedance for plates of 0.003 m in thickness: ———, $\text{Re}(Z_p)$, FB40; – – –, $\text{Im}(Z_p)$, FB40; ———, $\text{Re}(Z_p)$, FB60; – – –, $\text{Im}(Z_p)$, FB60.
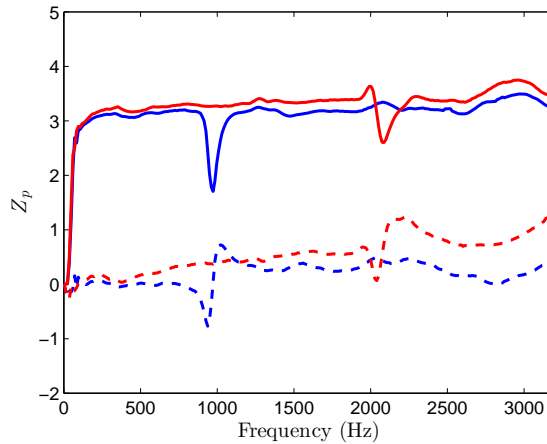
Figure 3.16: Normalized acoustic impedance of FB24 and FB40 plates: ———, $\text{Re}(Z_p)$, $t = 0.001$ m, FB24; – – –, $\text{Im}(Z_p)$, $t = 0.001$ m, FB24; ———, $\text{Re}(Z_p)$, $t = 0.003$ m, FB40; – – –, $\text{Im}(Z_p)$, $t = 0.003$ m, FB40.
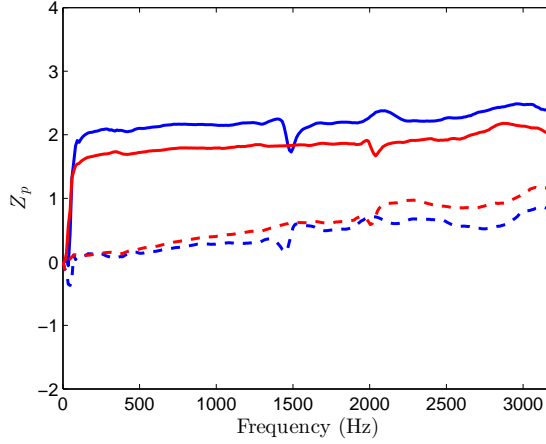
Figure 3.17: Normalized acoustic impedance of FB40 and FB60 plates: ——, $\mathrm{Re}(Z_p)$, $t = 0.002$ m, FB40; — — —, $\mathrm{Im}(Z_p)$, $t = 0.002$ m, FB40; ——, $\mathrm{Re}(Z_p)$, $t = 0.003$ m, FB60; — — —, $\mathrm{Im}(Z_p)$, $t = 0.003$ m, FB60.

small particles and can be assumed to be a porous material having a rigid frame [109]. Once the complex density and bulk modulus are known, the characteristic impedance Z_m and wavenumber k_m of the sintered material can be obtained as

$$Z_m = \sqrt{K_m \rho_m} \qquad (3.48)$$

$$k_m = \omega \sqrt{\frac{\rho_m}{K_m}} \qquad (3.49)$$

while the sound speed in the porous material can be written as

$$c_m = \frac{\omega}{k_m} = \sqrt{\frac{K_m}{\rho_m}} \qquad (3.50)$$

Open pores allow considerable sound dissipation via friction because of the significant increase in air velocity when the air travels by the small channels connecting them [84]. The contribution of the small holes to the sound dissipation is much more significant than that produced by viscous and thermal losses in the large pores [111].

Umnova *et al.* [175, 176] developed a cell-based model to assess the acoustic properties of packings of spheres. In a first approximation [175], these authors derived expressions for the permeability, tortuosity and characteristic length in terms of the dynamic drag. In a second work [176], Umnova *et al.* obtained a new relationship between the complex compressibility with a high volume of spheres by combining a

cell model with a coupled phase approach; through its combination with an analytical expression for complex density inferred a model for the prediction of bulk density characteristics. As an alternative and in the same work, the previous model was combined and a semi-empirical approach for the frequency dependence of dynamic density and its extension to the frequency dependence of dynamic compressibility for granular materials was proposed. These works [175, 176] were validated by comparing the theoretical results with experimentally measured data of sintered bronze spheres and fused glass beds, obtaining good agreement.

In the present Thesis a model based on the works of Umnova *et al.* [175, 176] and Li *et al.* [109] is presented. According to Umnova *et al.*, complex density can be evaluated as

$$\rho_m = \rho_0 q \left(1 + \frac{-j\mu\sigma}{\omega\rho_0 c_0 q} \sqrt{1 + \frac{\omega\rho_0 4q^2 k_p^2}{-j\mu\Lambda^2\sigma^2}} \right) \tag{3.51}$$

ρ_0 and c_0 being the air density and speed of sound, μ the dynamic viscosity, σ the porosity, q the tortuosity, k_p the steady state thermal permeability and Λ the viscous characteristic length. Tortuosity can be defined as

$$q = 1 + \frac{1-\sigma}{2\sigma} \tag{3.52}$$

while permeability is

$$k_p = \frac{\mu}{R} \tag{3.53}$$

where R is the flow resistivity given by

$$R = \frac{9\mu(1-\sigma)}{2R_{part}\sigma} = \frac{5(1-\Theta)}{5 - 9\sqrt[3]{\Theta} + 5\Theta - \Theta^2} \tag{3.54}$$

and finally Λ can be written as

$$\Lambda = \frac{4(1-\Theta)\sigma q R_{part}}{9(1-\Theta)} \tag{3.55}$$

where R_{part} is the particle radius and Θ the cell parameter radius, which can be estimated as follows

$$\Theta = \frac{3(1-\sigma)}{\pi\sqrt{2}} \tag{3.56}$$

On the other hand, the complex bulk modulus can be estimated as [109]

$$K_m = \frac{\gamma P_0}{\gamma - \dfrac{\gamma - 1}{1 + \dfrac{8\mu}{j\omega\rho_0 Pr\Lambda^2} \sqrt{1 + \dfrac{j\omega\rho_0 Pr\Lambda'^2}{16\mu}}}} \tag{3.57}$$

where γ is the specific heat capacity ratio, P_0 the atmospheric pressure, Pr the Prandtl number ($Pr = 0.71$), ω the angular frequency, while, as indicated previously, Λ' is the characteristic thermal dimension and can be defined, according to Umnova *et al.* [176], as

$$\Lambda' = \frac{3\Lambda}{2q(1 - \Theta)} \tag{3.58}$$

Once all these parameters are known, the sintered material is fully characterized and the acoustic impedance of the sintered surface can be modelled as

$$Z_p = j\omega\rho_m t \frac{1}{\sigma} \tag{3.59}$$

t being the thickness of the perforated plate.

As an example, some values of the model parameters are provided in Table 3.3 with a view to having an order of magnitude.

q	κ_p (m^2)	R (rayl/m)	Λ (m)	Θ	Λ' (m)
1.7395	$9.3638 \cdot 10^{-11}$	$1.9244 \cdot 10^5$	$4.6823 \cdot 10^{-5}$	0.4028	$6.7616 \cdot 10^{-5}$

Table 3.3: Some values of the sintered model parameters for the FB60 plate of 0.001 m in thickness.

In order to validate the model, a comparison of the theoretical values of the sintered surface impedance with those obtained through experimentally measured data is carried out in Figures 3.18 and 3.19.

The results predict a nearly constant real part of the sintered plate impedance, showing the same trend observed in the acoustic measurements. However, some discrepancies appear between the curves obtained theoretically and experimentally, except for the 3 mm plate, where good agreement can be observed. The differences found between both sets of results can probably be due, among others, to the uncertainty in the dimensional measurements of the sintered plate, which causes an error when obtaining the porosity of the samples. Regarding the imaginary part, the theoretical and experimental results show the same tendency, since both increase with frequency, but the agreement is improvable. Again, it can be observed that some differences appear between the model and the curves experimentally obtained, except for the thickest plate, for which the agreement is good up to 2000 Hz. It is worth noting that the reactance of this kind of perforated screen is usually smaller than the real part of the acoustic impedance [20]. From now on, the attenuation computations of silencers incorporating sintered surfaces will consider only the resistive component of the impedance for simplicity.
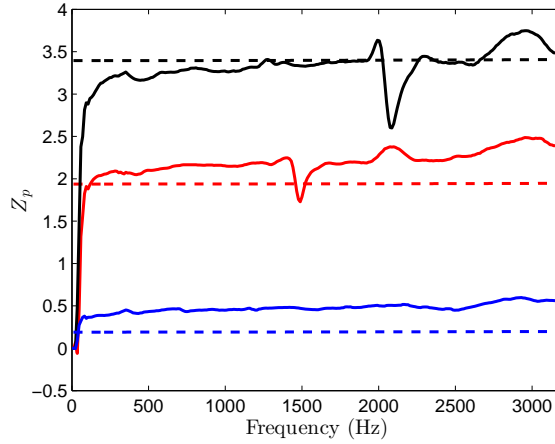
Figure 3.18: Real part of the normalized acoustic impedance for FB40 and FB60 plates and different thickness: $- - -$, Re(Z_p), FB60, $t = 1$ mm, theoretical; ———, Re(Z_p), FB60, $t = 1$ mm, experimental; $- - -$, Re(Z_p), FB40, $t = 2$ mm, theoretical; ———, Re(Z_p), FB40, $t = 2$ mm, experimental; $- - -$, Re(Z_p), FB40, $t = 3$ mm, theoretical; ———, Re(Z_p), FB40, $t = 3$ mm, experimental.
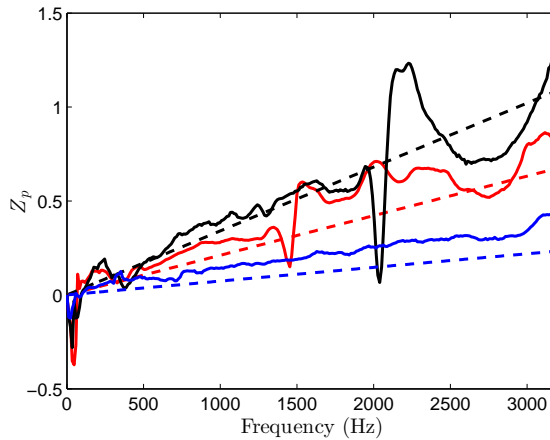
Figure 3.19: Imaginary part of the normalized acoustic impedance for FB40 and FB60 plates and different thickness: $- - -$, Im(Z_p), FB60, $t = 1$ mm, theoretical; ———, Im(Z_p), FB60, $t = 1$ mm, experimental; $- - -$, Im(Z_p), FB40, $t = 2$ mm, theoretical; ———, Im(Z_p), FB40, $t = 2$ mm, experimental; $- - -$, Im(Z_p), FB40, $t = 3$ mm, theoretical; ———, Im(Z_p), FB40, $t = 3$ mm, experimental.

3.5 Applications

In this section, the models developed are applied to several geometries of circular cross section to study their acoustic attenuation. First, a traditional configuration of perforated dissipative silencer with variable properties (density and temperature) is considered and, in addition, an alternative configuration of sintered silencer is presented. In the latter configuration the central sintered duct acts, in any way, as a kind of perforated duct, with a nearly constant acoustic impedance. All the transmission loss computations have been carried out by means of the FEM. More details of the formulation used will be given in Chapter 4. Thus, the results presented here have to be considered as a brief introduction to those that will be presented later.

3.5.1 Perforated dissipative silencers

Here, the acoustic attenuation of perforated dissipative silencers with variable properties is studied. The geometric dimensions of the configuration under study are shown in Table 3.4 and the characteristics that define the perforated duct are $\sigma = 0.2$, $d_h = 0.0035$ m and $t_p = 0.001$ m. The fibre considered in both cases is Owens-Corning texturized fibreglass [155], whose resistivity is $R = 4896$ rayl/m for a density of value $\rho = 100$ kg/m^3.
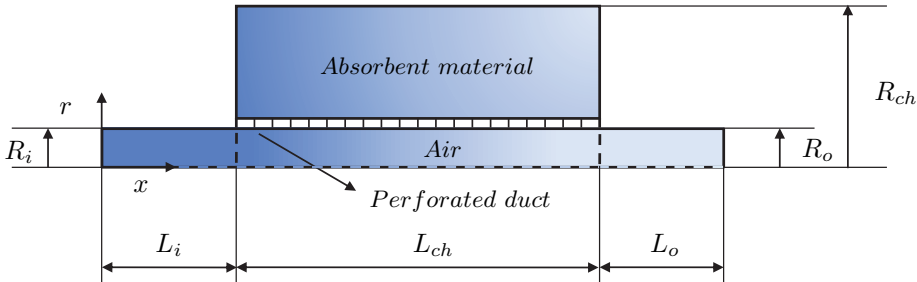
Figure 3.20: Geometry under study.

Geometry	L_i/L_o (m)	R_i/R_o (m)	L_{ch} (m)	R_{ch} (m)
1	0.1	0.0268	0.3	0.091875
2	0.1	0.0268	0.3	0.05
3	0.1	0.0268	0.5	0.091875

Table 3.4: Geometry under study: L, length; R, radius; i, inlet section; o, outlet section; ch, chamber.

I. Variable density distribution

Several density distributions are considered in order to obtain the attenuation achieved by the silencer in the absence of mean flow. In this case all the computations have been carried out considering configuration 2 and the density distributions are defined in Table 3.5 (see also Figure 3.2 for more details). Cases 1, 2 and 3 are uniform, while 4 is variable. It is worth noting that the density value corresponding to case 2 is the same as the average density of distribution 4.

Case	$\rho_{r_1}(R_d)$	$\rho_{r_2}(R_{ch})$	$\rho_{r_3}(R_d)$	$\rho_{r_4}(R_{ch})$	R_{avg}
1	100	100	100	100	4896
2	200	200	200	200	17378
3	300	300	300	300	36461
4	300	300	100	100	18476

Table 3.5: Density distributions (kg/m^3) under study and average resistivity (rayl/m).

From the results depicted in Figure 3.21 it can be deduced that, as density increases, the transmission loss achieved is higher in general, except some frequency bands associated with attenuation peaks. This is due to the low resistivity of the fibre, which is increased with the filling density. Besides, it can be observed that as density increases the peak of maximum attenuation is shifted to lower frequency values. A possible explanation for the highest attenuation value achieved with distribution 2 could be found in the appearance of a resonance. On the other hand, when the density is variable the results obtained are between those obtained with uniform density distributions. Thus, considering only the average value of the density distribution, the attenuation would be overestimated. Therefore, the variations of density considerably affect the attenuation of the silencer and have to be considered in the computations.
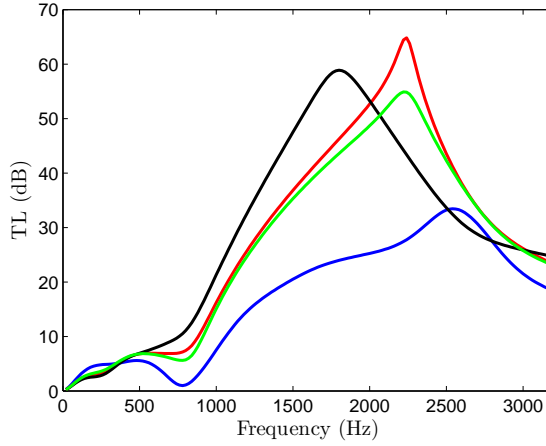
Figure 3.21: Transmission loss of a dissipative silencer with different filling density distributions of absorbent material: ——, case 1; ——, case 2; ——, case 3; ——, case 4.

II. Variable temperature field

The configuration studied in this section is the first of those shown in Table 3.4. The temperatures used to compute the corresponding fields, following the scheme of Figure 3.3, are shown in Table 3.6. Also, an extra computation at 25 °C has been included for illustrative purposes. To study the temperature effect, the attenuation achieved by the silencer subjected to a simple axially-varying thermal field has been computed and compared with two uniform fields, whose temperature values are equal to those at the inlet and outlet sections. The presence of mean flow has been neglected in all the computations.

Case	T_{r_1} °C	T_{r_2} °C	T_{r_3} °C	T_{r_4} °C	T_{r_5} °C	T_{r_6} °C
1	25	25	25	25	25	25
2	300	300	300	300	300	300
3	500	500	500	500	500	500
4	500	500	500	300	300	300

Table 3.6: Temperature fields under study.

The results obtained for the different computations are depicted in figure 3.22. It can be observed that, as the temperature increases, the attenuation achieved is higher. This can be due to the low resistivity of this fibre, since it increases with the tem-

perature. This effect happens above all at high frequencies, where the performance of the silencer shows bigger differences in the transmission loss (at low frequencies no significant changes in the transmission loss appear). It should be noted that high temperatures notably affect the acoustic behaviour of the silencer, and therefore they should be included as a design parameter in the computations. Besides, as could be expected, the axial temperature gradient affects the transmission loss, that lies between the lines related to fields 2 and 3 (minimum and maximum temperatures of field 4 respectively).
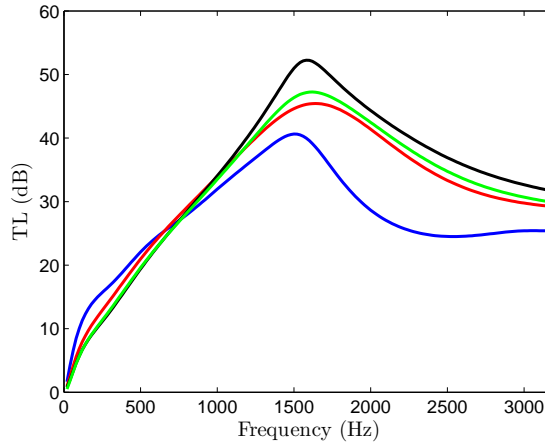
Figure 3.22: Transmission loss of a dissipative silencer at different temperatures: ――, case 1; ;――, case 2; ――, case 3; ――, case 4.

3.5.2 Silencers incorporating sintered ducts

In this section, the configuration under study is composed of a sintered central duct surrounded by a chamber. The sintered duct is modelled by means of its acoustic impedance. In this particular case, the value of the impedance is considered constant and equal to the characteristic impedance of air. The configurations of the silencer under study are geometries 1 and 3 of those shown in Table 3.4. Two extra computations have been carried out for comparison purposes considering geometry 1. The first one has been carried out taking into account a reactive silencer and the second a perforated dissipative silencer with Owens-Corning texturized fibreglass. The characteristics of the perforated duct are $\sigma = 0.2$, $d_h = 0.0035$ m and $t_p = 0.001$ m. A comparison of the attenuation performance achieved by these configurations is shown in Figure 3.23, where the silencer with a sintered duct shows a similar behaviour to

the reactive silencer with domes and pass bands, but its attenuation is higher in the whole frequency range. Another important characteristic is that the transmission loss increases with the frequency. On the other hand, when compared to the dissipative configuration, it can be observed that at very low frequencies the attenuation achieved by the silencer with a sintered duct is higher. Anyway, in this particular comparison the dissipative silencer exhibits the best acoustic performance. As it will be shown later in Chapter 4, silencers incorporating sintered surfaces strongly improve their sound attenuation if multichamber configurations are considered [8].
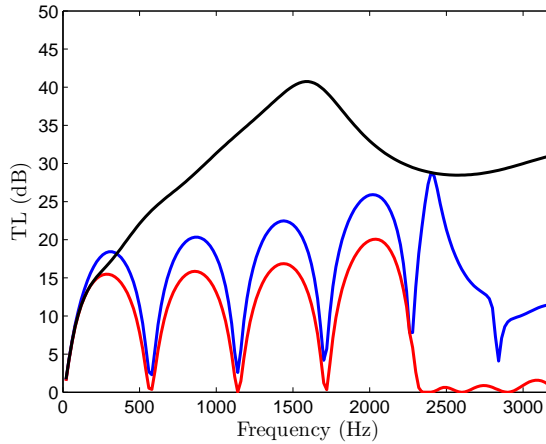
Figure 3.23: Transmission loss comparison of silencer incorporating a central sintered duct with other configurations: ———, sintered silencer; ———, reactive silencer; ———, perforated dissipative silencer.

Two sintered silencers with different chamber lengths have been considered to analyse the influence of this parameter on the attenuation. The results obtained are depicted in Figure 3.24. It can be observed that as the chamber length increases, the number of domes increases and the troughs are shifted to lower frequencies [157]. It is also remarkable that at high frequencies the transmission loss is higher.
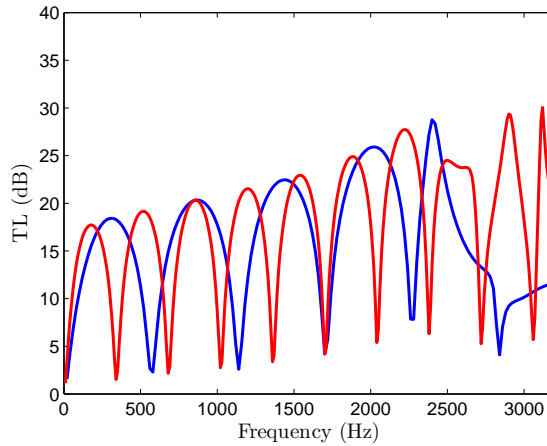
Figure 3.24: Transmission loss of silencer with a central sintered duct: ———, $L = 0.3$ m; ———, $L = 0.5$ m.

3.6 Conclusions

In this chapter, a number of models have been presented to include the presence of thermal gradients, as well as bulk density heterogeneities of the absorbent material, in the computation of silencer attenuation performance. Mathematical laws for these variations have been presented and the effects of these spatial heterogeneities have been included in the perforated duct impedance model through the material resistivity. Some results have been provided, which show that not considering the variations of the temperature and filling density variations, in the computations of the attenuation supposes a lack of accuracy in the predictions. Therefore, they should be included to obtain more realistic and accurate models.

Sintered materials have been experimentally characterized showing a nearly constant impedance (mainly the most important part, i.e., the real one). In addition, a theoretical model of the sintered surface impedance has been presented and compared with the experimental results, showing a good agreement in some cases of practical interest. Finally, the attenuation achieved by silencers incorporating sintered ducts has been compared to other configurations, such as a reactive geometry and a perforated dissipative silencer, showing that for some particular applications the former can be a potential alternative. In this sense, further results confirming this idea will be presented in the next chapter. In addition, another possible advantage of sintered

configurations when compared to dissipative devices is related to the reduction of the silencer weight as well as the pollution associated with the fibres.

Chapter 4

Advanced numerical techniques for the acoustic modelling of dissipative silencers

Summary:

In this chapter, the FEM is applied to the acoustic modelling of silencers with absorbent material considering several formulations: (1) A 3D pressure-based approach; (2) A 3D velocity potential-based technique; (3) A hybrid method combining approaches (1) and (2). The most relevant steps of the method for the three formulations, such as the weighted residual method and the matrix formulation of its integral form, are detailed. The wave propagation modelling is included within the absorbent materials. Also, the coupling between the outer chamber of the silencer and the central airway by means of plates and perforated ducts is considered in the presence of mean flow. In addition, non-homogeneous propagation media are taken into account in the hybrid formulation (variable bulk density of the absorbent material and thermal gradients within the silencer). Finally, the FEM is applied to different configurations of interest to study the influence on the TL, on the one hand, of the bulk density variations of the dissipative fibre and on the other hand, of the high temperatures within the silencer and their associated gradients. The main objective of the numerical tools proposed in this chapter is to correct and complete the deficiencies and gaps found in the available commercial programs, since they do not permit the consideration of variable temperature fields or density distributions within the absorbent materials in the presence of mean flow.

4.1 Introduction

The FEM is a numerical tool capable of tackling many problems in engineering, without the usual limitations of the analytical techniques regarding complex geometries, non-uniform properties or complex boundary conditions. The main drawback of this method, however, is its high computational cost.

Due to the limitations of the plane wave method (see Section 2.10) application of the FEM is carried out to study the acoustic behaviour of silencers. In this Thesis, the FEM is fundamentally used to compute sound attenuation of silencers under more realistic working conditions. Nevertheless, it is also used as a validation tool of some methodologies that will be presented later (see Chapter 5).

The first application of the FEM was carried out for the computation of structures [186], and was later extended to acoustic applications by Gladwell *et al.* [77–79] and Craggs [44, 45]. The first works with FEs were limited to the solution of the Helmholtz wave equation in a non-moving medium and without considering the dissipative phenomena. Young and Crocker [184, 185] applied the FEM to the study of silencers without a perforated duct in the absence of mean flow. Later, Craggs [46] considered the inclusion of the dissipative phenomena in a variational-based approach, and solved it by means of the FEM. The same author considered the existence of a locally reacting absorbent material when considering an acoustic impedance boundary condition without taking into account the presence of mean flow [47], this approach being valid only for small thicknesses.

The convective effect produced by the mean flow was studied by several authors. Sigman *et al.* [163] and Abrahamson [3] included the mean flow in the models, considering the velocity potential as a variable. The advantage of this formulation is based on the fact that including the gradients of the mean flow field is quite easy when compared to pressure formulation, since solving the problem requires only one variable. Astley and Eversman [19] carried out the analysis of non-uniform ducts with mean flow using a pressure and velocity formulation and a simplified mean flow field. Ross [145] presented the application of the FEM for the study of silencers with perforated regions. However, this author only included the mean flow effect on the impedance, neglecting the convective effect. Peat [136] applied this method to a convective wave equation formulated in terms of velocity potential and obtained the four poles of a duct.

On the other hand, it is worth noting that in the analysis of the acoustic behaviour of silencers at high frequencies, the variation of the pressure field distribution is con-

siderable over small regions and therefore, a refined FE mesh is required. This fact supposes an increment of the degrees of freedom, which involves an important increase of the computation time. Cummings [52] developed a variational method applying the Rayleigh-Ritz formulation, which can be adapted to geometries with uniform cross section for the fundamental mode. The point collocation technique was implemented by Kirby [100, 105] and was also focused on geometries of arbitrary, but axially uniform, cross section combining a transversal eigenvalue problem (solved by means of the FEM) and a modal scheme at discrete points of the geometric discontinuities. The techniques presented by Cummings [52] and Kirby [100, 105] achieve enough accuracy for an acoustic analysis till the mid frequency range.

The FEM is one of the most widely used techniques in silencer modelling, mainly in geometries with a complex cross section. There are two possibilities for the FE formulation, either starting from a differential formulation or from a variational principle. In the first case, the FEM is considered as a weighted residual method, such as the Galerkin approach, and in the second as a variational technique, such as the Rayleigh-Ritz method.

Nevertheless, few works in the literature consider the influence of the heterogeneous properties of the propagation media on the transmission loss computations of silencers by means of numerical techniques. Peat and Rathi [138] studied the influence of the absorbent material and the mean flow on the acoustic performance of a silencer, assessing the steady flow field in the absorbent material induced by the mean flow of the central duct. Selamet *et al.* [160] applied the FEM to validate an analytic method based on a modal analysis to obtain the attenuation of dissipative expansion chambers lined with two concentric layers of fibrous material. Antebas *et al.* [17] applied a pressure FE formulation to obtain the transmission loss of a dissipative silencer in the presence of mean flow. In these investigations, a linear function was proposed to model the axial variation of the bulk density, leading to heterogeneous material properties such as flow resistivity, equivalent complex density and speed of sound [17]. Some numerical issues were found at very low frequencies in the presence of a moving propagation medium, that will be later prevented by considering the aforementioned combination of pressure and velocity potential. Wang *et al.* [178] combined a segmentation procedure and the BEM to compute the transmission loss of reactive expansion chambers with uniform mean flow and a linear temperature gradient.

The aim of the current chapter is to obtain a suitable formulation that permits assessing the acoustic performance of dissipative silencers in the presence of mean flow under more realistic working conditions, such as the influence of the heterogeneous

properties of the different propagation media, due for example to temperature gradients, thus extending the existing models of FE.

4.2 Application of the finite element method to the convective wave equation

In this section, the FEM is applied to the convective wave equation. The results are obtained considering the existence of mean flow, and are also valid for the non-flow case by just omitting the terms associated with the velocity of the moving medium. The weighted residual method in combination with the Galerkin approach will be applied because of its generality. A domain without absorbent material is initially considered. This will be included in Section 4.4.

4.2.1 Pressure formulation

A simple situation is considered first with the purpose of introducing the numerical techniques. To achieve this goal, a generic silencer is shown in Figure 4.1. The acoustic domain is denoted by Ω and its associated boundary by Γ.
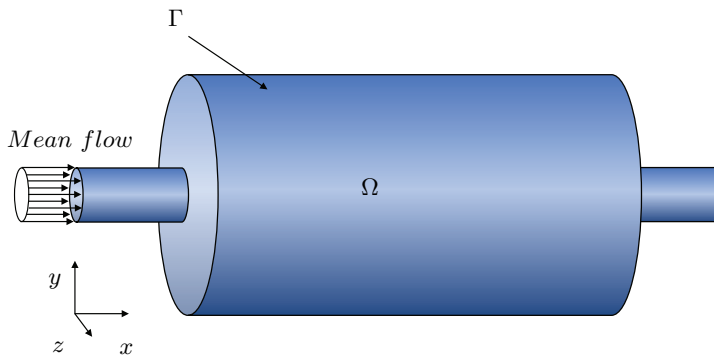
Figure 4.1: Generic silencer.

The sound propagation within the silencer is governed, in the presence of uniform mean flow, by the following equation [140]

$$\nabla^2 p - \frac{1}{c_0^2}\frac{D^2 p}{Dt^2} = 0 \tag{4.1}$$

Now, considering harmonic waves, $p = Pe^{j\omega t}$, results in

$$
\begin{aligned}
\left(1 - \frac{U_{mf}^2}{c_0^2}\right)\frac{\partial^2 P}{\partial x^2} &+ \left(1 - \frac{V_{mf}^2}{c_0^2}\right)\frac{\partial^2 P}{\partial y^2} + \left(1 - \frac{W_{mf}^2}{c_0^2}\right)\frac{\partial^2 P}{\partial z^2} \\
&- 2\frac{U_{mf}V_{mf}}{c_0^2}\frac{\partial^2 P}{\partial x \partial y} - 2\frac{U_{mf}W_{mf}}{c_0^2}\frac{\partial^2 P}{\partial x \partial z} - 2\frac{V_{mf}W_{mf}}{c_0^2}\frac{\partial^2 P}{\partial y \partial z} \\
&- 2j\omega\frac{U_{mf}}{c_0^2}\frac{\partial P}{\partial x} - 2j\omega\frac{V_{mf}}{c_0^2}\frac{\partial P}{\partial y} - 2j\omega\frac{W_{mf}}{c_0^2}\frac{\partial P}{\partial z} + k_0^2 P = 0
\end{aligned}
\tag{4.2}
$$

The mean flow velocity field $\vec{U}_{mf} = U_{mf}\vec{i} + V_{mf}\vec{j} + W_{mf}\vec{k}$ is assumed to be known and uniform. Also, as it will be shown later, the computations with perforated ducts will consider the flow field parallel to the x-axis. Equation (4.2) is multiplied by a weighting function Ψ and integrated over the problem domain Ω. As usual in this kind of problem, Green's theorem is applied, reducing the existing degree of derivation in the unknown function leading to

$$\int_\Omega (\nabla\Psi)^T [D]\nabla P \mathrm{d}\Omega + \frac{2j\omega}{c_0^2}\int_\Omega \Psi\vec{U}_{fm}^T \nabla P \mathrm{d}\Omega - k_0^2\int_\Omega \Psi P \mathrm{d}\Omega - \int_\Gamma \Psi\frac{\partial P}{\partial n}\vec{n}^T [D]\vec{n}\mathrm{d}\Gamma = 0 \tag{4.3}$$

where $[D]$ is the matrix defined as

$$[D] = \begin{bmatrix} 1 - \dfrac{U_{mf}^2}{c_0^2} & -\dfrac{U_{mf}V_{mf}}{c_0^2} & -\dfrac{U_{mf}W_{mf}}{c_0^2} \\[2mm] -\dfrac{V_{mf}U_{mf}}{c_0^2} & 1 - \dfrac{V_{mf}^2}{c_0^2} & -\dfrac{V_{mf}W_{mf}}{c_0^2} \\[2mm] -\dfrac{W_{mf}U_{mf}}{c_0^2} & -\dfrac{W_{mf}V_{mf}}{c_0^2} & 1 - \dfrac{W_{mf}^2}{c_0^2} \end{bmatrix} \tag{4.4}$$

$\vec{n}$ being the outward unit normal vector to the boundary Γ. If the domain is discretized in N_e elements of volume Ω_e and both P and Ψ present C^0 continuity, equation (4.3)

can be rewritten as

$$\sum_{e=1}^{N_e} \int_{\Omega^e} (\nabla \Psi^{(e)})^T [D] \nabla P^{(e)} \mathrm{d}\Omega + \frac{2j\omega}{c_0^2} \sum_{e=1}^{N_e} \int_{\Omega^e} \Psi^{(e)} \vec{U}_{fm}^T \nabla P \mathrm{d}\Omega$$

$$- k_0^2 \sum_{e=1}^{N_e} \int_{\Omega^e} \Psi^{(e)} P^{(e)} \mathrm{d}\Omega - \sum_{e=1}^{N_e} \int_{\Gamma \cap \Gamma^e} \Psi^{(e)} \frac{\partial P^{(e)}}{\partial n} \vec{n}^T [D] \mathrm{d}\Gamma = 0 \tag{4.5}$$

The FE nodal interpolation for an element e results in

$$P^{(e)} = [N]\{P^{(e)}\} \tag{4.6}$$

where $[N]$ is the vector of shape functions and $\{P^{(e)}\}$ is the vector that contains the nodal values of the unknown function, this being the pressure. On the other hand, using the Galerkin formulation, the weighting function can be expressed as follows

$$\Psi^{(e)} = [N]\{\Psi^{(e)}\} \tag{4.7}$$

Developing equation (4.5) and taking into account expressions (4.6) and (4.7) yields

$$\sum_{e=1}^{N_e} \{\Psi^{(e)}\}^T \int_{\Omega^e} [B]^T [D][B] \mathrm{d}\Omega \{P^{(e)}\} + \sum_{e=1}^{N_e} \{\Psi^{(e)}\}^T \int_{\Omega^e} \frac{2\omega j}{c_0^2} [N]^T \vec{U}_{fm}^T [B] \mathrm{d}\Omega \{P^{(e)}\}$$

$$- \sum_{e=1}^{N_e} \{\Psi^{(e)}\}^T \int_{\Omega^e} k_0^2 [N]^T [N] \mathrm{d}\Omega \{P^{(e)}\} - \sum_{e=1}^{N_e} \{\Psi^{(e)}\}^T \int_{\Gamma \cap \Gamma^e} [N]^T \frac{\partial P^{(e)}}{\partial n} \vec{n}^T [D] \vec{n} \mathrm{d}\Gamma = 0 \tag{4.8}$$

$[B]$ being the matrix of the shape function derivatives, expressed as

$$[B] = \begin{bmatrix} \dfrac{\partial N_1}{\partial x} & \dfrac{\partial N_2}{\partial x} & \cdots & \dfrac{\partial N_{N_{pe}}}{\partial x} \\[2ex] \dfrac{\partial N_1}{\partial y} & \dfrac{\partial N_2}{\partial y} & \cdots & \dfrac{\partial N_{N_{pe}}}{\partial y} \\[2ex] \dfrac{\partial N_1}{\partial z} & \dfrac{\partial N_2}{\partial z} & \cdots & \dfrac{\partial N_{N_{pe}}}{\partial z} \end{bmatrix} \tag{4.9}$$

where N_{pe} is the number of nodes per element.

Expression (4.8) can be written in compact form as

$$\sum_{e=1}^{N_e} \{\Psi^{(e)}\}^T [k^{(e)}]\{P^{(e)}\} + j\omega \sum_{e=1}^{N_e} \{\Psi^{(e)}\}^T [c^{(e)}]\{P^{(e)}\}$$

$$- \omega^2 \sum_{e=1}^{N_e} \{\Psi^{(e)}\}^T [m^{(e)}]\{P^{(e)}\} - \sum_{e=1}^{N_e} \{\Psi^{(e)}\}^T \{f^{(e)}\} = 0 \tag{4.10}$$

where the following nomenclature has been introduced for element matrices

$$[k^{(e)}] = \int_{\Omega^e} [B]^T[D][B]\mathrm{d}\Omega \tag{4.11}$$

$$[c^{(e)}] = \frac{2}{c_0^2} \int_{\Omega^e} [N]^T \vec{U}_{fm}^T [B]\mathrm{d}\Omega \tag{4.12}$$

$$[m^{(e)}] = \frac{1}{c_0^2} \int_{\Omega^e} [N]^T[N]\mathrm{d}\Omega \tag{4.13}$$

$$[f^{(e)}] = \int_{\Gamma \cap \Gamma^e} [N]^T \frac{\partial P^{(e)}}{\partial n} \vec{n}^T[D]\vec{n}\mathrm{d}\Gamma \tag{4.14}$$

Assembling the element matrices, the global matrices of the problem can be obtained leading to the following system

$$\{\Psi\}^T(([K] + j\omega[C] - \omega^2[M])\{P\} - \{F\}) = \{0\} \tag{4.15}$$

The previous equation is valid for any weighting function, yielding

$$([K] + j\omega[C] - \omega^2[M])\{P\} = \{F\} \tag{4.16}$$

Now, Dirichlet boundary conditions [138] have to be considered, which involves that the pressure value is known in part of boundary Γ. These conditions can be easily imposed in equation (4.16), considering that the value $P = \tilde{P}$ is prescribed in the nodes belonging to the corresponding boundary.

Then, the pressure nodal values can be obtained solving the system of equations represented by expression (4.16) together with the Dirichlet conditions. The acoustic velocity can be obtained in any element e, once the pressure field is solved, by means of the Euler equations (2.19). If there is no mean flow, it can be expressed as

$$\vec{U}^{(e)} = -\frac{1}{j\rho_0\omega}[B]\{P^{(e)}\} \tag{4.17}$$

However, in the presence of mean flow the procedure is more laborious. For example, to obtain the velocity nodal values $\{U^{(e)}\}$ in the x-axis direction, the corresponding expression is

$$-\frac{1}{\rho_0}\begin{bmatrix}\partial N_1/\partial x & \partial N_2/\partial x & ... & \partial N_{N_{pe}}/\partial x\end{bmatrix}\{P^{(e)}\} = (j\omega[N] + \vec{U}_{mf}^T[B])\{U^{(e)}\} \tag{4.18}$$

Thus, evaluating the previous expression at N_{pe} points, a system of N_{pe} equations with the same number of unknowns is obtained, which permits the calculation of $\{U^{(e)}\}$. In general, the procedure is quite simple, since it is only necessary to know the velocity at the inlet and the outlet sections to obtaining the TL or the transfer matrix of the silencer. For practical applications related to automotive silencers, it can be considered that in ducts containing those sections, the wave is plane at a distance enough from the geometric discontinuities associated with contractions and expansions. Therefore, knowing the pressure at two points of the duct, the velocity can be computed by means of expressions (2.59) and (2.61) of Chapter 2.

I. Load vector

A vector $\{F\}$ appears as a consequence of the existence of a pressure gradient in a part of boundary Γ (Neumann condition) [138]. Therefore, the natural boundary condition that results when $\{F\}$ is not taken into account corresponds to a zero normal velocity (rigid wall). Also, a normal velocity value of $\tilde{U}$ can be imposed at the inlet and outlet sections of the silencer, although its consideration is not necessary in a pressure formulation in the presence of mean flow. The implementation of this condition is significantly simplified in the problems treated in the present Thesis, since the inlet and the outlet sections of a silencer are usually plane and also perpendicular to an axis of the reference system. Generally, it can be considered that the inlet and outlet ducts are long enough and with a uniform cross section, which involves that the mean flow velocity is parallel to the duct and therefore, in this particular case, to the x axis. Thus, the velocity condition at the cross section can be written as

$$
\begin{aligned}
\{f^{(e)}\} &= \int_{\Gamma \cap \Gamma^e} [N]^T \frac{\partial P^{(e)}}{\partial n} \vec{n}^T [D] \vec{n} \mathrm{d}\Gamma \\
&= \int_{\Gamma \cap \Gamma^e} [N]^T \frac{\partial P^{(e)}}{\partial n} \begin{Bmatrix} 1 \\ 0 \\ 0 \end{Bmatrix}^T \begin{bmatrix} 1 - U_{fm}^2/c_0^2 & 0 & 0 \\ 0 & 1 & 0 \\ 0 & 0 & 1 \end{bmatrix} \begin{Bmatrix} 1 \\ 0 \\ 0 \end{Bmatrix} \mathrm{d}\Gamma \qquad (4.19) \\
&= -\rho_0 (1 - M^2) \int_{\Gamma \cap \Gamma^e} [N]^T \left(j\omega \tilde{U}^{(e)} + U_{mf} \frac{\partial [N]}{\partial x} \{\tilde{U}^{(e)}\} \right) \mathrm{d}\Gamma
\end{aligned}
$$

Then, to integrate equation (4.19), the distribution $\tilde{U}^{(e)}$ has to be evaluated. Although, as indicated previously, this boundary condition is not usually considered.

II. Imposition of the impedance condition

If part of the silencer boundary can be characterized by means of an acoustic impedance Z (for example, an anechoic termination or a locally reacting absorbent material), then

$$Z = \frac{P}{U} \tag{4.20}$$

U being the normal velocity to the boundary where the condition is applied. If the section is perpendicular to the x axis, the normal derivative of the pressure and the velocity can be related through the following expression

$$\frac{\partial P}{\partial n} = \frac{\partial P}{\partial x} = -\rho_0 \left(j\omega U + U_{fm} \frac{\partial U}{\partial x} \right) \tag{4.21}$$

and substituting expression (4.20) into (4.21), results

$$\frac{\partial P}{\partial n} = -\rho_0 \left(j\omega \frac{P}{Z} + \frac{U_{fm}}{Z} \frac{\partial P}{\partial n} \right) \tag{4.22}$$

Then, solving for the normal derivative of pressure yields

$$\frac{\partial P}{\partial n} = -\frac{\rho_0 j\omega P}{Z + \rho_0 U_{fm}} \tag{4.23}$$

and the load vector is

$$\{f^{(e)}\} = \int_{\Gamma \cap \Gamma^e} [N]^T \frac{\partial P^{(e)}}{\partial n} \vec{n}^T [D] \vec{n} \mathrm{d}\Gamma = (1 - M^2) \int_{\Gamma \cap \Gamma^e} [N]^T \left(-\frac{\rho_0 j\omega P}{Z + \rho_0 U_{fm}} \right) \mathrm{d}\Gamma \tag{4.24}$$

In order to compact the nomenclature, the following matrix is introduced

$$[c_Z^{(e)}] = \rho_0 \frac{1 - M^2}{Z + \rho_0 U_{fm}} \int_{\Gamma \cap \Gamma^e} [N]^T [N] \mathrm{d}\Gamma \tag{4.25}$$

Thus, the load vector can now be written as

$$\{f^{(e)}\} = -j\omega [c_Z^{(e)}] \{P^{(e)}\} \tag{4.26}$$

and the system of equations (4.16) yields

$$([K] + j\omega([C] + [C_Z]) - \omega^2 [M])\{P\} = \{F\} \tag{4.27}$$

For an anechoic termination of the silencer, the impedance is given by $Z = \rho_0 c_0$, while the matrix $[c_Z^{(e)}]$ can be expressed as

$$[c_Z^{(e)}] = \frac{1 - M}{c_0} \int_{\Gamma \cap \Gamma^e} [N]^T [N] \mathrm{d}\Gamma \tag{4.28}$$

III. Computation of the attenuation

Once the system of equations (4.16) is solved, the acoustic behaviour of the silencer at the frequency range of interest can be immediately evaluated. The TL can be computed by means of (2.157) considering an anechoic termination in the silencer outlet. When the inlet and outlet sections are not equal and the Mach numbers are different, the suitable modifications have to be done according to equation (2.156).

However, it is necessary to carry out two analyses to evaluate the poles of the transfer matrix (see Section 2.4.1). In this case, expressions (2.74)-(2.77) have to be applied. These are repeated here for convenience.

$$A = \left. \frac{P_1}{P_2} \right|_{U_2=0} \qquad B = \left. \frac{P_1}{U_2} \right|_{P_2=0} \qquad C = \left. \frac{U_1}{P_2} \right|_{U_2=0} \qquad D = \left. \frac{U_1}{U_2} \right|_{P_2=0}$$

4.2.2 Velocity potential formulation

Equations (2.38) and (2.40) are deduced from the more general equation [43]

$$\nabla^2 \phi_T - \frac{1}{c_0^2} \left(\frac{\partial^2 \phi_T}{\partial t^2} + \frac{\partial ((\nabla \phi_T)^T \nabla \phi_T)}{\partial t} + \frac{1}{2} (\nabla \phi_T)^T \nabla ((\nabla \phi_T)^T \nabla \phi_T) \right) = 0 \tag{4.29}$$

where ϕ_T is the total velocity potential function, which can be decomposed into a time-independent potential associated with the mean flow ϕ_{mf} and a small acoustic potential ϕ, satisfying

$$\frac{\partial \phi_{mf}}{\partial x} = U_{mf} \quad \frac{\partial \phi_{mf}}{\partial y} = V_{mf} \quad \frac{\partial \phi_{mf}}{\partial z} = W_{mf}$$
$$\frac{\partial \phi}{\partial x} = u \quad \frac{\partial \phi}{\partial y} = v \quad \frac{\partial \phi}{\partial z} = w \tag{4.30}$$

Equation (4.29) can be linearized considering that $\phi \ll \phi_{mf}$ and neglecting the terms of less influence, related to products of acoustic velocities. This leads to the

Laplace equation for the mean flow field

$$\nabla^2 \phi_{mf} = 0 \tag{4.31}$$

and to the convective wave equation valid for non-uniform mean flow (2.38)

$$\nabla^2 \phi - \frac{1}{c_0^2} \frac{D^2 \phi}{Dt^2} = 0 \tag{4.32}$$

Considering harmonic waves, i.e. $\phi = \Phi e^{j\omega t}$, the latter equation can be rewritten as

$$
\begin{aligned}
\left(1 - \frac{U_{mf}^2}{c_0^2}\right) \frac{\partial^2 \Phi}{\partial x^2} + \left(1 - \frac{V_{mf}^2}{c_0^2}\right) \frac{\partial^2 \Phi}{\partial y^2} + \left(1 - \frac{W_{mf}^2}{c_0^2}\right) \frac{\partial^2 \Phi}{\partial z^2} \\
- 2\frac{U_{mf}V_{mf}}{c_0^2} \frac{\partial^2 \Phi}{\partial x \partial y} - 2\frac{U_{mf}W_{mf}}{c_0^2} \frac{\partial^2 \Phi}{\partial x \partial z} - 2\frac{V_{mf}W_{mf}}{c_0^2} \frac{\partial^2 \Phi}{\partial y \partial z} \\
- \left(U_{mf}\frac{\partial U_{mf}}{\partial x} + V_{mf}\frac{\partial U_{mf}}{\partial y} + W_{mf}\frac{\partial U_{mf}}{\partial z}\right) \frac{\partial \Phi}{\partial x} \\
- \left(U_{mf}\frac{\partial V_{mf}}{\partial x} + V_{mf}\frac{\partial V_{mf}}{\partial y} + W_{mf}\frac{\partial V_{mf}}{\partial z}\right) \frac{\partial \Phi}{\partial y} \\
- \left(U_{mf}\frac{\partial W_{mf}}{\partial x} + V_{mf}\frac{\partial W_{mf}}{\partial y} + W_{mf}\frac{\partial W_{mf}}{\partial z}\right) \frac{\partial \Phi}{\partial z} \\
- 2j\omega \frac{U_{mf}}{c_0^2} \frac{\partial \Phi}{\partial x} - 2j\omega \frac{V_{mf}}{c_0^2} \frac{\partial \Phi}{\partial y} - 2j\omega \frac{W_{mf}}{c_0^2} \frac{\partial \Phi}{\partial z} + k_0^2 \Phi = 0
\end{aligned}
\tag{4.33}
$$

which can be solved once the mean flow velocity field is known. It is worth remarking that this equation includes terms of the mean flow velocity field gradient, contrarily to Coyette's formulation [43], in which they were neglected. However, this simplification does not seem completely justified because the same procedure could be followed with a pressure formulation, which is not correct for a non-uniform mean flow field. In the absence of the mean flow, the well-known Helmholtz equation is obtained

$$\nabla^2 \Phi + k_0^2 \Phi = 0 \tag{4.34}$$

I. Laplace equation

The mean flow velocity field can be evaluated by means of a formulation written in terms of velocity potential through the Laplace equation (4.31). By applying the weighted residuals method it yields

$$\int_\Omega \Psi \nabla^2 \phi_{mf} d\Omega = 0 \tag{4.35}$$

Ψ being the weighting function and Ω the domain considered. Following an analogue procedure to the pressure formulation case, Green's theorem is applied leading to

$$- \int_\Omega (\nabla \Psi)^T \nabla \phi_{mf} \mathrm{d}\Omega + \int_\Gamma \Psi (\nabla \phi_{mf})^T \vec{n} \mathrm{d}\Gamma = 0 \tag{4.36}$$

where Γ is the boundary of the domain under consideration and $\vec{n}$ is the outward normal unit vector. Two different parts can be distinguished in this boundary, Γ_1 and Γ_2, in which the Dirichlet and Neumann conditions are respectively applied. Thus, $\Gamma = \Gamma_1 \cup \Gamma_2$, $\Gamma_1 \cap \Gamma_2 = \emptyset$, and the weighting functions are only different from zero in Γ_2, where the Neumann condition is imposed as a velocity $\tilde{U}_{mf}$ normal to the boundary. Consequently, expression (4.36) can be written as

$$- \int_\Omega (\nabla \Psi)^T \nabla \phi_{mf} \mathrm{d}\Omega + \int_\Gamma \Psi \tilde{U}_{mf} \mathrm{d}\Gamma = 0 \tag{4.37}$$

Now, discretizing the domain into elements and approximating the unknown function to an element level by means of a nodal interpolation based on the shape functions $[N]$, the potential for any element can be expressed as

$$\phi_{mf}^{(e)} = [N]\{\Phi_{mf}^{(e)}\} \tag{4.38}$$

$\{\Phi_{mf}^{(e)}\}$ being the vector of potential nodal values. Following the same approach, the Galerkin formulation yields

$$\Psi_{mf}^{(e)} = [N]\{\Psi_{mf}^{(e)}\} \tag{4.39}$$

Then, expression (4.37) can be written as the sum of the weighted residuals of the N_e elements that compose the discretized domain

$$- \int_\Omega (\nabla \Psi)^T \nabla \phi_{mf} \mathrm{d}\Omega + \int_\Gamma \Psi \tilde{U}_{mf} \mathrm{d}\Gamma$$
$$= - \sum_{e=1}^{N_e} \int_{\Omega^e} (\nabla \Psi^{(e)})^T \nabla \phi_{mf}^{(e)} \mathrm{d}\Omega + \sum_{e=1}^{N_e} \int_{\Gamma_2 \cap \Gamma^e} \Psi^{(e)} \tilde{U}_{mf}^{(e)} \mathrm{d}\Gamma = 0 \tag{4.40}$$

and considering expressions (4.38) and (4.39) results in

$$- \sum_{e=1}^{N_e} \{\Psi^{(e)}\}^T \left(\int_{\Omega^e} [B]^T [B] \mathrm{d}\Omega \right) \{\Phi^{(e)}\} + \sum_{e=1}^{N_e} \{\Psi^{(e)}\}^T \left(\int_{\Gamma_2 \cap \Gamma^e} [N]^T \tilde{U}_{mf}^{(e)} \mathrm{d}\Gamma \right) = 0 \tag{4.41}$$

where $[B]$ is the derivative matrix of the shape functions defined in Section 4.2.1. If the following notation is introduced

$$[k^{(e)}] = \int_{\Omega^e} [B]^T [B] \mathrm{d}\Omega \tag{4.42}$$

$$[f^{(e)}] = \int_{\Gamma_2 \cap \Gamma^e} [N]^T \tilde{U}_{mf}^{(e)} \mathrm{d}\Gamma \tag{4.43}$$

equation (4.41) can be written as

$$\sum_{e=1}^{N_e} \{\Psi^{(e)}\}^T [k^{(e)}] \{\Phi^{(e)}\} - \sum_{e=1}^{N_e} \{\Psi^{(e)}\}^T [f^{(e)}] = 0 \tag{4.44}$$

Once the element vectors and matrices are expanded to the global dimensions of the problem, this yields

$$\{\Psi\}^T ([K]\{\Phi_{mf}\} - \{F\}) = \{0\} \tag{4.45}$$

The Dirichlet conditions $\tilde{\Phi}_{mf}$ applied at the nodes corresponding to surface Γ_1 can be introduced by removing the linearly dependent rows of matrix $[K]$, leading to the following system of equations

$$[K]\{\Phi_{mf}\} = \{F\} \tag{4.46}$$

Finally, the velocity potential at the nodes can be obtained solving this system, the velocity field being its gradient (4.30). However, the mean flow velocity field obtained by solving the Laplace equation can be far from reality. For this reason, it is necessary for the FE codes to permit importing the solution of the mean flow field computed with a CFD program (e.g., ANSYS Fluent [13]) and solving the convective wave equation considering this flow field.

II. Acoustic problem

Once the Laplace equation is solved and the mean flow velocity field is known, the previous procedure can be applied to equation (4.33). In order to simplify the nomenclature, the following notation is introduced

$$[D] = \begin{bmatrix} D_{11} & D_{12} & D_{13} \\ D_{21} & D_{22} & D_{23} \\ D_{31} & D_{32} & D_{33} \end{bmatrix} = \begin{bmatrix} 1 - U_{mf}^2/c_0^2 & -U_{mf}V_{mf}/c_0^2 & -U_{mf}W_{mf}/c_0^2 \\ -V_{mf}U_{mf}/c_0^2 & 1 - V_{mf}^2/c_0^2 & -V_{mf}W_{mf}/c_0^2 \\ -W_{mf}U_{mf}/c_0^2 & -W_{mf}W_{mf}/c_0^2 & 1 - W_{mf}^2/c_0^2 \end{bmatrix} \tag{4.47}$$

$$[G] = \begin{bmatrix} \partial D_{11}/\partial x & \partial D_{12}/\partial x & \partial D_{13}/\partial x \\ \partial D_{21}/\partial y & \partial D_{22}/\partial y & \partial D_{23}/\partial y \\ \partial D_{31}/\partial z & \partial D_{32}/\partial z & \partial D_{33}/\partial z \end{bmatrix} \tag{4.48}$$

$$[DU] = \begin{bmatrix} \partial U_{mf}/\partial x & \partial V_{mf}/\partial x & \partial W_{mf}/\partial x \\ \partial U_{mf}/\partial y & \partial V_{mf}/\partial y & \partial W_{mf}/\partial y \\ \partial U_{mf}/\partial z & \partial V_{mf}/\partial z & \partial W_{mf}/\partial z \end{bmatrix} \tag{4.49}$$

Now, multiplying equation (4.33) by a weighting function Ψ, integrating over the domain Ω and applying the Green's theorem yields

$$\int_{\Omega} (\nabla\Psi)^T [D]\nabla\Phi \mathrm{d}\Omega + \int_{\Omega} \Psi \begin{Bmatrix} 1 \\ 1 \\ 1 \end{Bmatrix}^T [G]\nabla\Phi \mathrm{d}\Omega + \int_{\Omega} \Psi \vec{U}_{mf}^T [DU]\nabla\Phi \mathrm{d}\Omega$$
$$+ \frac{2j\omega}{c_0^2} \int_{\Omega} \Psi \vec{U}_{mf}^T \nabla\Phi \mathrm{d}\Omega - k_0^2 \int_{\Omega} \Psi\Phi \mathrm{d}\Omega - \int_{\Gamma} \Psi \frac{\partial\Phi}{\partial n} \vec{n}^T [D]\vec{n} \mathrm{d}\Gamma = 0 \tag{4.50}$$

Then, the integration domain can be discretized and, after taking into account interpolations similar to those given by equations (4.38) and (4.39), the previous expression can be rewritten as

$$\sum_{e=1}^{N_e} \{\Psi^{(e)}\}^T [k^{(e)}]\{\Phi^{(e)}\} + j\omega \sum_{e=1}^{N_e} \{\Psi^{(e)}\}^T [c^{(e)}]\{\Phi^{(e)}\}$$
$$- \omega^2 \sum_{e=1}^{N_e} \{\Psi^{(e)}\}^T [m^{(e)}]\{\Phi^{(e)}\} - \sum_{e=1}^{N_e} \{\Psi^{(e)}\}\{f^{(e)}\} = 0 \tag{4.51}$$

where the following nomenclature has been introduced

$$[k^{(e)}] = \int_{\Omega^e} [B]^T [D][B]\mathrm{d}\Omega + \int_{\Omega^e} [N]^T \begin{Bmatrix} 1 \\ 1 \\ 1 \end{Bmatrix}^T [G][B]\mathrm{d}\Omega + \int_{\Omega^e} [N]^T \vec{U}_{mf}^T [DU][B]\mathrm{d}\Omega \tag{4.52}$$

$$[c^{(e)}] = \frac{2}{c_0^2} \int_{\Omega^e} [N]^T \vec{U}_{mf}^T [B]\mathrm{d}\Omega \tag{4.53}$$

$$[m^{(e)}] = \frac{1}{c_0^2} \int_{\Omega^e} [N]^T [N]\mathrm{d}\Omega \tag{4.54}$$

$$\{f^{(e)}\} = \int_{\Gamma\cap\Gamma^e} [N]^T \tilde{U}^{(e)} \vec{n}^T [D]\vec{n}\mathrm{d}\Gamma \tag{4.55}$$

$\tilde{U}^{(e)}$ being the boundary condition of the acoustic velocity (derivative of the potential normal to the surface). Expanding the matrices and vectors and assembling them, the final system of equations is obtained

$$([K] + j\omega[C] - \omega^2[M]) = \{\Phi\} = \{F\} \tag{4.56}$$

whose solution gives the nodal values of the acoustic velocity potential. Then, the velocity of any element e can be calculated as

$$\vec{U}^{(e)} = [B]\{\Phi^{(e)}\} \tag{4.57}$$

and the pressure can be obtained, neglecting the product of acoustic velocities, as

$$P^{(e)} = -\rho_0 \left(j\omega[N]\{\Phi^{(e)}\} + \vec{U}_{mf}^T[B]\{\Phi^{(e)}\} \right) \tag{4.58}$$

III. Load vector

The load vector $\{F\}$ can be obtained by means of the integration of equation (4.55) enforcing a Neumann condition, or which is the same thing, a normal acoustic velocity condition. This condition can be easily implemented, since in this Thesis it is considered that the inlet and outlet sections of silencers are plane and perpendicular to an axis of the reference system. In addition, if it is considered that the inlet and outlet ducts have a uniform section and are long enough, the mean flow velocity can be assumed to be uniform and one-directional. For ducts whose inlet and outlet sections, where the acoustic velocity continuity conditions are applied, are parallel to the x axis, the load vector $\{f^{(e)}\}$ can be defined as follows

$$\{f^{(e)}\} = \int_{\Gamma \cap \Gamma^e} [N]^T \tilde{U}^{(e)} \begin{Bmatrix} 1 \\ 0 \\ 0 \end{Bmatrix}^T \begin{bmatrix} 1 - U_{mf}^2/c_0^2 & 0 & 0 \\ 0 & 1 & 0 \\ 0 & 0 & 1 \end{bmatrix} \begin{Bmatrix} 1 \\ 0 \\ 0 \end{Bmatrix} d\Gamma$$

$$= (1 - M^2) \int_{\Gamma \cap \Gamma^e} [N]^T \tilde{U}^{(e)} d\Gamma \tag{4.59}$$

The diameter of the inlet and outlet ducts is usually small enough to assume plane wave conditions, leading to

$$\{f^{(e)}\} = (1 - M^2)\tilde{U}^{(e)} \int_{\Gamma \cap \Gamma^e} [N]^T d\Gamma \tag{4.60}$$

If the previous hypotheses are not verified, the integral (4.55) has to be evaluated. Finally, it is worth noting that the rigid wall condition (zero normal velocity) is the natural condition of the problem and its implementation is not necessary.

IV. Imposition of the pressure condition

One of the main drawbacks of the velocity potential approach is that the field of interest in acoustics is usually the pressure. This makes the post-processing of the results necessary by means of expression (4.58), which involves a lower accuracy in the results. Besides, the application of the pressure condition is carried out through a Robin condition [121], according to the potential function and its normal derivative, which supposes that it is affected by a discretization error. Thus, a pressure value $\tilde{P}$ is applied to the boundary, starting from the following relationship

$$P = -\rho_0 \left(j\omega\Phi + \vec{U}_{mf}^T \nabla\Phi \right) \tag{4.61}$$

and assuming the previous hypotheses, in which at the inlet and outlet sections, the acoustic velocity $\tilde{U}$ and mean flow velocity $\tilde{U}_{mf}$ are perpendicular to the surface, yielding

$$\tilde{P} = -\rho_0 \left(j\omega\Phi + \tilde{U}_{mf}\tilde{U} \right) \tag{4.62}$$

Solving for $\tilde{U}$ gives

$$\tilde{U} = -\frac{\tilde{P}}{\rho_0\tilde{U}_{mf}} - \frac{j\omega\Phi}{\tilde{U}_{mf}} \tag{4.63}$$

Therefore, the load vector is

$$\{f^{(e)}\} = \int_{\Gamma\cap\Gamma^e} [N]^T \tilde{U}^{(e)} \vec{n}^T [D]\vec{n}\mathrm{d}\Gamma = (1-M^2)\int_{\Gamma\cap\Gamma^e} [N]^T \left(-\frac{\tilde{P}^{(e)}}{\rho_0\tilde{U}_{mf}} - \frac{j\omega\Phi^{(e)}}{\tilde{U}_{mf}} \right) \mathrm{d}\Gamma \tag{4.64}$$

which can be expressed as

$$\begin{aligned}
\{f^{(e)}\} = &-(1-M^2)\int_{\Gamma\cap\Gamma^e} [N]^T \frac{\tilde{P}^{(e)}}{\rho_0\tilde{U}_{mf}}\mathrm{d}\Gamma \\
&- (1-M^2)\int_{\Gamma\cap\Gamma^e} [N]^T \frac{j\omega\Phi^{(e)}}{\tilde{U}_{mf}}\mathrm{d}\Gamma = \{f_P^{(e)}\} - j\omega[c_P^{(e)}]\{\Phi^{(e)}\}
\end{aligned} \tag{4.65}$$

where the following notation has been introduced

$$\{f_P^{(e)}\} = -\frac{1-M^2}{\rho_0\tilde{U}_{mf}}\int_{\Gamma\cap\Gamma^e} [N]^T \tilde{P}^{(e)}\mathrm{d}\Gamma \tag{4.66}$$

$$[c_P^{(e)}] = -\frac{1-M^2}{\tilde{U}_{mf}}\int_{\Gamma\cap\Gamma^e} [N]^T [N]\mathrm{d}\Gamma \tag{4.67}$$

In addition, the fact of imposing a condition of pressure generates, on the one hand a load vector $\{f_P^{(e)}\}$ similar to that obtained when imposing velocity conditions, and on the other hand, a matrix $[c_P^{(e)}]$ that multiplies the nodal unknown vector and is obtained by integrating over the boundary where the pressure condition is enforced. Then, assembling the system yields

$$([K] + j\omega([C] + [C_P]) - \omega^2[M])\{\Phi\} = \{F\} + \{F_P\} \tag{4.68}$$

Finally, to transform the pressure condition into an equivalent normal velocity condition, the outward direction of the domain has to be the same as the positive direction of the reference system. If this does not happen the sign of the equations should be changed in expressions (4.66) and (4.67).

V. Imposition of the impedance condition

To impose an impedance condition (e.g. an anechoic termination) the procedure is similar to that followed for pressure. Starting from the definition of impedance (4.20) and combining it with expression (4.62), the following expression is obtained

$$Z = \frac{-\rho_0(j\omega\Phi + \tilde{U}_{mf}\tilde{U})}{\tilde{U}} \tag{4.69}$$

where the symbol $\sim$ denotes the values in the boundary. Thus,

$$\tilde{U} = -\frac{\rho_0 j\omega\Phi}{Z + \rho_0\tilde{U}_{mf}} \tag{4.70}$$

the load vector is

$$\{f^{(e)}\} = \int_{\Gamma\cap\Gamma^e} [N]^T \tilde{U}^{(e)} \vec{n}^T [D]\vec{n}\mathrm{d}\Gamma = (1 - M^2) \int_{\Gamma\cap\Gamma^e} [N]^T \left(-\frac{\rho_0 j\omega\Phi^{(e)}}{Z + \rho_0\tilde{U}_{mf}}\right) \mathrm{d}\Gamma \tag{4.71}$$

and it can be written as

$$\{f^{(e)}\} = -j\omega[c_Z^{(e)}]\{\Phi^{(e)}\} \tag{4.72}$$

where

$$[c_Z^{(e)}] = \rho_0 \frac{1 - M^2}{Z + \rho_0\tilde{U}_{mf}} \int_{\Gamma\cap\Gamma^e} [N]^T[N]\mathrm{d}\Gamma \tag{4.73}$$

Therefore, by imposing this boundary condition, a new matrix $[c_Z^{(e)}]$ appears. Expanding the matrices and vectors to the global dimension of the problem and assembling

again, the system (4.68) can be expressed as

$$([K] + j\omega([C] + [C_P] + [C_Z]) - \omega^2[M])\{\Phi\} = \{F\} + \{F_P\} \qquad (4.74)$$

where a pressure boundary condition is included. For the particular case of an anechoic termination $Z = \rho_0 c_0$, equation (4.73) is now

$$[c_Z^{(e)}] = \frac{1 - M}{c_0} \int_{\Gamma \cap \Gamma^e} [N]^T [N] \mathrm{d}\Gamma \qquad (4.75)$$

this matrix being equal to that obtained through the pressure formulation.

VI. Computation of the attenuation

The acoustic attenuation of the silencer can be assessed through the transmission loss expression (2.157). The parameters required to compute it are the pressure at the inlet and outlet sections and the velocity at the inlet section, while assuming an anechoic termination. The pressures and velocities can be calculated post-processing the velocity potential solution by means of equations (4.57) and (4.58).

Another way of studying the acoustic behaviour of the silencer is through its four poles and two different analyses have to be carried out (see Section 2.4.1). The definitions of the poles are (2.74)-(2.77)

$$A = \frac{P_1}{P_2}\bigg|_{U_2=0} \qquad B = \frac{P_1}{U_2}\bigg|_{P_2=0} \qquad C = \frac{U_1}{P_2}\bigg|_{U_2=0} \qquad D = \frac{U_1}{U_2}\bigg|_{P_2=0}$$

that can be rewritten as

$$A = \frac{j\omega\Phi_1 + \dfrac{\partial \Phi_{mf1}}{\partial n}\dfrac{\partial \Phi_1}{\partial n}}{j\omega\Phi_2}\Bigg|_{\frac{\partial \Phi_2}{\partial n}=0} \qquad (4.76)$$

$$B = \frac{-\rho_0\left(j\omega\Phi_1 + \dfrac{\partial \Phi_{mf1}}{\partial n}\dfrac{\partial \Phi_1}{\partial n}\right)}{\dfrac{\Phi_2}{\partial n}}\Bigg|_{\Phi_2=-\frac{1}{j\omega}\frac{\partial \Phi_{mf2}}{\partial n}\frac{\partial \Phi_2}{\partial n}} \qquad (4.77)$$

$$C = -\frac{\dfrac{\partial \Phi_1}{\partial n}}{\rho_0 j\omega\Phi_2}\Bigg|_{\frac{\partial \Phi_2}{\partial n}=0} \qquad (4.78)$$

$$D = \left. \frac{\dfrac{\partial \Phi_1}{\partial n}}{\dfrac{\Phi_2}{\partial n}} \right|_{\Phi_2 = -\frac{1}{j\omega} \frac{\partial \Phi_{mf2}}{\partial n} \frac{\partial \Phi_2}{\partial n}} \tag{4.79}$$

where the subscripts 1 and 2 refer to the inlet and outlet sections respectively. The normal derivatives of the potential function can be easily obtained, because in general the inlet and outlet sections are perpendicular to an axis of the reference system and therefore, the derivatives are the components of the velocity in the direction of this axis. Thus, the TL can be calculated from expression (2.165), which depends on the poles.

4.3   Coupled subdomains

The coupling between the central duct and the outer chamber is usually carried out, in the automotive industry, by means of a perforated screen that is modelled through its acoustic impedance Z_p [120, 126].

4.3.1   Pressure formulation

I. Non-moving medium

A silencer containing a perforated surface that connects the central duct with the chamber is shown in Figure 4.2. These two subdomains are denoted as Ω_1 and Ω_2, while Γ_1 and Γ_2 are their associated boundaries and Γ_p is the perforated surface placed between them. No mean flow is assumed in either of the subdomains.

The previous developments can be applied to each subdomain separately. Therefore, the system of equations (4.16) can be written as

$$\begin{aligned} ([K_1] + j\omega[C_1] - \omega^2[M_1])\{P_1\} &= \{F_1\} \\ ([K_2] + j\omega[C_2] - \omega^2[M_2])\{P_2\} &= \{F_2\} \end{aligned} \tag{4.80}$$

whereas the load vector at an element level will be

$$\{f^{(e)}\} = \int_{\Gamma \cap \Gamma^e} [N]^T \frac{\partial P^{(e)}}{\partial n} \vec{n}^T [D] \vec{n} \mathrm{d}\Gamma \tag{4.81}$$
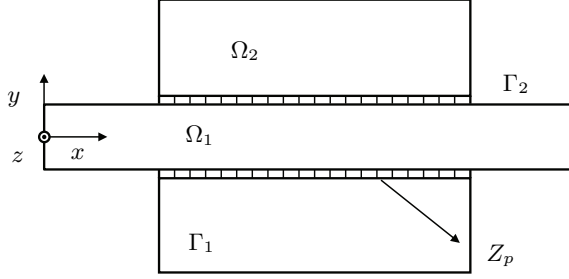
Figure 4.2: Silencer with two subdomains coupled by means of a perforated screen.

which in the absence of mean flow can be rewritten as

$$\{f^{(e)}\} = \int_{\Gamma \cap \Gamma^e} [N]^T \frac{\partial P^{(e)}}{\partial n} \mathrm{d}\Gamma \tag{4.82}$$

The acoustic impedance of a surface is defined as

$$Z_p = \frac{P_1 - P_2}{U} \tag{4.83}$$

where P_1 and P_2 are the acoustic pressures at each side of the perforated screen and U the normal acoustic velocity. The latter is assumed continuous when no mean exists [104]. At each side of the surface, pressure and normal velocity can be related by means of Euler's equation (2.19)

$$U_1 = \frac{-1}{j\rho_0\omega} \frac{\partial P_1}{\partial n} \qquad U_2 = \frac{-1}{j\rho_0\omega} \frac{\partial P_2}{\partial n} \tag{4.84}$$

When the outward normal velocity is considered to be continuous, it is met that $U_1 = -U_2$. Combining now equations (4.83) and (4.84), the following expressions are obtained

$$U = U_1 = \frac{-1}{j\rho_0\omega} \frac{\partial P_1}{\partial n} = \frac{P_1 - P_2}{Z_p} \qquad U = -U_2 = \frac{1}{j\rho_0\omega} \frac{\partial P_2}{\partial n} = \frac{P_1 - P_2}{Z_p} \tag{4.85}$$

Then, the load vectors can be evaluated as

$$\{f_1^{(e)}\} = \int_{\Gamma \cap \Gamma^e} [N]^T \left(-j\rho_0\omega \frac{P_1^{(e)} - P_2^{(e)}}{Z_p} \right) \mathrm{d}\Gamma \tag{4.86}$$

$$\{f_2^{(e)}\} = \int_{\Gamma \cap \Gamma^e} [N]^T \left(j\rho_0 \omega \frac{P_1^{(e)} - P_2^{(e)}}{Z_p} \right) d\Gamma \tag{4.87}$$

Considering the FE nodal interpolation, yields

$$\{f_1^{(e)}\} = \frac{-j\rho_0 \omega}{Z_p} \int_{\Gamma \cap \Gamma^e} [N]^T \left([N]\{P_1^{(e)}\} - [N]\{P_2^{(e)}\} \right) d\Gamma$$
$$= -j\omega [c_{11Z_p}^{(e)}]\{P_1^{(e)}\} + j\omega [c_{12Z_p}^{(e)}]\{P_2^{(e)}\} \tag{4.88}$$

$$\{f_2^{(e)}\} = \frac{j\rho_0 \omega}{Z_p} \int_{\Gamma \cap \Gamma^e} [N]^T \left([N]\{P_1^{(e)}\} - [N]\{P_2^{(e)}\} \right) d\Gamma$$
$$= j\omega [c_{21Z_p}^{(e)}]\{P_1^{(e)}\} - j\omega [c_{22Z_p}^{(e)}]\{P_2^{(e)}\} \tag{4.89}$$

As can be observed in expressions (4.88) and (4.89), the perforated surface provides new FE matrices multiplying the degrees of freedom of the problem. Assembling the matrices obtained at an element level and including the load vectors of the system, the following expression is obtained

$$\left(\begin{bmatrix} [K_1] & [0] \\ [0] & [K_2] \end{bmatrix} + j\omega \begin{bmatrix} [C_1] + [C_{11Z_p}] & -[C_{12Z_p}] \\ -[C_{21Z_p}] & [C_2] + [C_{22Z_p}] \end{bmatrix} \right.$$
$$\left. -\omega^2 \begin{bmatrix} [M_1] & [0] \\ [0] & [M_2] \end{bmatrix} \right) \begin{Bmatrix} \{P_1\} \\ \{P_2\} \end{Bmatrix} = \begin{Bmatrix} \{F_1\} \\ \{F_2\} \end{Bmatrix} \tag{4.90}$$

where the matrices generated by the coupling can be clearly observed. In compact form, the previous equation can be written as

$$([K] + j\omega([C] + [C_{Z_p}]) - \omega^2 [M])\{P\} = \{F\} \tag{4.91}$$

II. Moving medium

A silencer with a perforated duct is depicted in Figure 4.3. In the central duct a uniform mean flow is assumed, defined by its Mach number ($M = U_{mf}/c_0$) and parallel to the perforated screen. The mean flow that penetrates in the chamber is considered small, which permits neglecting the convective effect within the chamber. However, the influence of the mean flow on the impedance Z_p has to be considered to obtain accurate results when computing the attenuation performance.

Applying the FEM to the duct and chamber governing equations (see Section 4.3.1), the following expressions are obtained

$$([K_1] + j\omega[C_1] - \omega^2 [M_1])\{P_1\} = \{F_1\}$$
$$([K_2] + j\omega[C_2] - \omega^2 [M_2])\{P_2\} = \{F_2\} \tag{4.92}$$
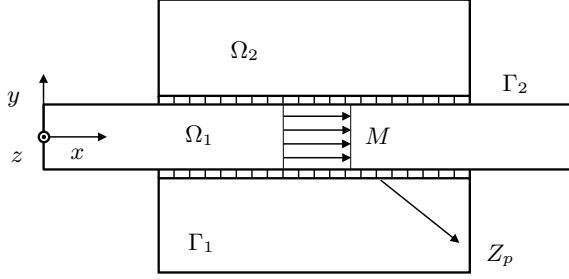
Figure 4.3: Silencer with a perforated pipe and mean flow.

As previously indicated, considering that the mean flow within the chamber is negligible and also that there are no impedance boundary conditions associated with the outer wall (i.e. a rigid wall is considered), leads to $[C_2] = [0]$. The coupling between the central airway and the chamber can be carried out through the load vectors $\{F_1\}$ and $\{F_2\}$. Then, at an element level and considering a perforated plate yields

$$\{f_1^{(e)}\} = \int_{\Gamma_p \cap \Gamma^e} [N]^T \frac{\partial P_1^{(e)}}{\partial n} \vec{n}^T [D] \vec{n} \mathrm{d}\Gamma = \int_{\Gamma_p \cap \Gamma^e} [N]^T \frac{\partial P_1^{(e)}}{\partial n} \mathrm{d}\Gamma \qquad (4.93)$$

$$\{f_2^{(e)}\} = \int_{\Gamma_p \cap \Gamma^e} [N]^T \frac{\partial P_2^{(e)}}{\partial n} \mathrm{d}\Gamma \qquad (4.94)$$

where $\{f_1^{(e)}\}$ does not depend explicitly on M, since the flow is parallel to the duct. In order to apply the condition associated with the perforated surface, several options can be taken into account [23, 104]. The first one considers continuity of the normal acoustic velocity ($U_1 = -U_2$) and the second continuity of the normal displacement with respect to the perforated duct ($\xi_1 = -\xi_2$). The velocities are related to the acoustic pressure by means of the Euler's equation (2.19)

$$\rho_0 \left(j\omega U_1 + U_{mf} \frac{\partial U_1}{\partial x} \right) = -\frac{\partial P_1}{\partial n} \qquad (4.95)$$

$$j\rho_0 \omega U_2 = -\frac{\partial P_2}{\partial n} \qquad (4.96)$$

whereas the displacement is related to the pressure through

$$\rho_0 \left(-\omega^2 \xi_1 + 2j\omega U_{mf} \frac{\partial \xi_1}{\partial x} + U_{mf}^2 \frac{\partial^2 \xi_1}{\partial x^2} \right) = -\frac{\partial P_1}{\partial n} \qquad (4.97)$$

$$- \rho_0 \omega^2 \xi_2 = -\frac{\partial P_2}{\partial n} \tag{4.98}$$

According to Kirby and Denia [104], good agreement between prediction and experiment was observed using continuity of displacement, whereas the TL tends to be overpredicted when using continuity of velocity. Continuity of acoustic radial displacement/velocity are commonly found in the literature, and it has been experimentally demonstrated that a realistic condition is between displacement and velocity [22]. In view of the good correlation between prediction and experiment observed by Elnady *et al.* [72] using continuity of velocity and the numerical advantages of its implementation, this condition will be retained here for all the silencer transmission loss calculations.

Also the continuity of the transversal component of the pressure gradient ($\partial P_1 / \partial n = -\partial P_2 / \partial n$) can be considered, this being the term that appears directly in the load vector. Nevertheless, the results given by this approach are not considered in the present Thesis, because the predictions underestimate the mean flow effect (according to some numerical computations not shown here).

Therefore, considering that normal velocity is continuous through the orifices of the perforated duct, the load vectors related to the acoustic impedance (4.83) through expressions (4.95) and (4.96) are

$$\{f_1^{(e)}\} = \int_{\Gamma_p \cap \Gamma^e} [N]^T \left(-j\rho_0 \omega \frac{P_1^{(e)} - P_2^{(e)}}{Z_p} - \rho_0 \frac{U_{mf}}{Z_p} \frac{\partial \left(P_1^{(e)} - P_2^{(e)} \right)}{\partial x} \right) d\Gamma \tag{4.99}$$

$$\{f_2^{(e)}\} = \int_{\Gamma_p \cap \Gamma^e} [N]^T \left(-j\rho_0 \omega \frac{P_1^{(e)} - P_2^{(e)}}{Z_p} \right) d\Gamma \tag{4.100}$$

Then, applying a FE interpolation, the following equations are obtained

$$\{f_1^{(e)}\} = -\frac{j\rho_0 \omega}{Z_p} \int_{\Gamma_p \cap \Gamma^e} [N]^T \left([N]\{P_1^{(e)}\} - [N]\{P_2^{(e)}\} \right) d\Gamma$$
$$- \frac{\rho_0 U_{mf}}{Z_p} \int_{\Gamma_p \cap \Gamma^e} [N]^T \left(\frac{\partial [N]}{\partial x}\{P_1^{(e)}\} - \frac{\partial [N]}{\partial x}\{P_2^{(e)}\} \right) d\Gamma$$
$$= -j\omega [c_{11Z_p}^{(e)}]\{P_1^{(e)}\} + j\omega [c_{12Z_p}^{(e)}]\{P_2^{(e)}\} - [k_{11Z_p}^{(e)}]\{P_1^{(e)}\} + [k_{12Z_p}^{(e)}]\{P_2^{(e)}\} \tag{4.101}$$

$$\{f_2^{(e)}\} = \frac{j\rho_0 \omega}{Z_p} \int_{\Gamma_p \cap \Gamma^e} [N]^T \left([N]\{P_1^{(e)}\} - [N]\{P_2^{(e)}\} \right) d\Gamma$$
$$= j\omega [c_{21Z_p}^{(e)}]\{P_1^{(e)}\} - j\omega [c_{22Z_p}^{(e)}]\{P_2^{(e)}\} \tag{4.102}$$

and the system of equations (4.92) results in

$$\left(\begin{bmatrix} [K_1] + [K_{11Z_p}] & -[K_{12Z_p}] \\ [0] & [K_2] \end{bmatrix} + j\omega \begin{bmatrix} [C_1] + [C_{11Z_p}] & -[C_{12Z_p}] \\ -[C_{21Z_p}] & [C_2] + [C_{22Z_p}] \end{bmatrix} \right.$$
$$\left. -\omega^2 \begin{bmatrix} [M_1] & [0] \\ [0] & [M_2] \end{bmatrix} \right) \left\{ \begin{matrix} \{P_1\} \\ \{P_2\} \end{matrix} \right\} = \left\{ \begin{matrix} \{F_1\} \\ \{F_2\} \end{matrix} \right\} \tag{4.103}$$

4.3.2 Velocity potential formulation

I. Moving medium

As happened with the pressure formulation, once the FEM is applied to the problem and considering the same subdomains as in Section 4.3.1, the following equations can be written according to the velocity potential

$$([K_1] + j\omega[C_1] - \omega^2[M_1])\{\Phi_1\} = \{\Phi_1\}$$
$$([K_2] + j\omega[C_2] - \omega^2[M_2])\{\Phi_2\} = \{\Phi_2\} \tag{4.104}$$

where it is assumed that the suitable boundary conditions have been applied, and the only thing left is to include the perforated duct influence. Thus, the load vectors can be written from expression (4.55) as

$$\{f_1^{(e)}\} = \int_{\Gamma_p \cap \Gamma^e} [N]^T \tilde{U}_1^{(e)} \mathrm{d}\Gamma \tag{4.105}$$

$$\{f_2^{(e)}\} = \int_{\Gamma_p \cap \Gamma^e} [N]^T \tilde{U}_2^{(e)} \mathrm{d}\Gamma \tag{4.106}$$

Similarly to the pressure formulation case, several alternatives of continuity can be considered. As indicated previously, the normal velocity continuity is selected in this work as boundary condition for the perforated screen. Therefore, this hypothesis meets $U_1 = -U_2$.

Therefore, following a similar approach to the pressure formulation detailed in Section 4.3.1, expressions (4.105) and (4.106) can be expressed as

$$\{f_1^{(e)}\} = \int_{\Gamma_p \cap \Gamma^e} [N]^T \left(\frac{P_1^{(e)} - P_2^{(e)}}{Z_p} \right) \mathrm{d}\Gamma \tag{4.107}$$

$$\{f_2^{(e)}\} = \int_{\Gamma_p \cap \Gamma^e} [N]^T \left(-\frac{P_1^{(e)} - P_2^{(e)}}{Z_p} \right) \mathrm{d}\Gamma \tag{4.108}$$

and taking into account expression (4.61) that relates the pressure to the velocity potential, yields

$$\{f_1^{(e)}\} = \int_{\Gamma_p \cap \Gamma^e} [N]^T \left(-j\rho_0\omega \frac{\Phi_1^{(e)} - \Phi_2^{(e)}}{Z_p} - \rho_0 \frac{U_{mf}}{Z_p} \frac{\partial \Phi_1^{(e)}}{\partial x} \right) d\Gamma \tag{4.109}$$

$$\{f_2^{(e)}\} = \int_{\Gamma_p \cap \Gamma^e} [N]^T \left(j\rho_0\omega \frac{\Phi_1^{(e)} - \Phi_2^{(e)}}{Z_p} + \rho_0 \frac{U_{mf}}{Z_p} \frac{\partial \Phi_1^{(e)}}{\partial x} \right) d\Gamma \tag{4.110}$$

Now applying FE nodal interpolation gives

$$
\begin{aligned}
\{f_1^{(e)}\} &= \frac{-j\rho_0\omega}{Z_p} \int_{\Gamma_p \cap \Gamma^e} [N]^T \left([N]\Phi_1^{(e)} - [N]\Phi_2^{(e)} \right) d\Gamma \\
&\quad - \frac{\rho_0}{Z_p} \int_{\Gamma_p \cap \Gamma^e} U_{mf}[N]^T \frac{\partial [N]}{\partial x} \{\Phi_1^{(e)}\} d\Gamma \\
&= -j\omega[c_{11Z_p}^{(e)}]\{\Phi_1^{(e)}\} + j\omega[c_{12Z_p}^{(e)}]\{\Phi_2^{(e)}\} - [k_{11Z_p}^{(e)}]\{\Phi_1^{(e)}\}
\end{aligned}
\tag{4.111}
$$

$$
\begin{aligned}
\{f_2^{(e)}\} &= \frac{j\rho_0\omega}{Z_p} \int_{\Gamma_p \cap \Gamma^e} [N]^T \left([N]\Phi_1^{(e)} - [N]\Phi_2^{(e)} \right) d\Gamma \\
&\quad + \frac{\rho_0}{Z_p} \int_{\Gamma_p \cap \Gamma^e} U_{mf}[N]^T \frac{\partial [N]}{\partial x} \{\Phi_1^{(e)}\} d\Gamma \\
&= j\omega[c_{21Z_p}^{(e)}]\{\Phi_1^{(e)}\} - j\omega[c_{22Z_p}^{(e)}]\{\Phi_2^{(e)}\} + [k_{21Z_p}^{(e)}]\{\Phi_1^{(e)}\}
\end{aligned}
\tag{4.112}
$$

Then, the following system can be obtained

$$
\left(
\begin{bmatrix}
[K_1] + [K_{11Z_p}] & [0] \\
-[K_{21Z_p}] & [K_2]
\end{bmatrix}
+ j\omega
\begin{bmatrix}
[C_1] + [C_{11Z_p}] & -[C_{12Z_p}] \\
-[C_{21Z_p}] & [C_2] + [C_{22Z_p}]
\end{bmatrix}
\right.
$$
$$
\left.
-\omega^2
\begin{bmatrix}
[M_1] & [0] \\
[0] & [M_2]
\end{bmatrix}
\right)
\begin{Bmatrix}
\{\Phi_1\} \\
\{\Phi_2\}
\end{Bmatrix}
=
\begin{Bmatrix}
\{F_1\} \\
\{F_2\}
\end{Bmatrix}
\tag{4.113}
$$

It can be observed that the stiffness submatrix $[K_{21Z_p}]$ changes of place when compared to pressure formulation. It is important to point out that a potential formulation permits considering a non-uniform mean flow field.

4.4 Configurations with absorbent material

The modelling of the sound wave propagation phenomena within an absorbent material in the absence of mean flow is relatively simple [120, 156, 160], since the air

properties (c_0 and ρ_0) can be replaced by the equivalent acoustic properties of the fibrous material, as the speed of sound c_m and the density ρ_m [10], so the procedure is analogous to that previously described in Section 4.3 and will be presented here for the sake of clarity.

When mean flow exists within the absorbent material, the computation procedure is more complex [53, 138]. First, the mean flow field (non-uniform in general) has to be determined. One of the main effects of the flow in the absorbent material is to cause acoustic anisotropy and non-homogeneity, even if the dissipative material itself is isotropic and homogeneous. Fortunately, for real applications there exists a perforated screen separating the mean gas flow from the absorbing material. In principle, the axial static pressure drop generated at the interface between the airway and the absorbent material should induce a mean flow in the material itself. It is unlikely, however, that these effects will be relevant when a perforated screen is present, as the latter will significantly reduce frictional effects at the interface between the airway and the material and so reduce the axial static pressure gradient over the silencer section [104]. Thus, when this hypothesis can be assumed, the modelling of the wave propagation in dissipative silencers by means of the FEM can be carried out in a relatively easy way. In this case, as a first approximation, it can be supposed that the wave propagation in the absorbent material is governed by

$$\frac{\partial^2 P}{\partial x^2} + \frac{\partial^2 P}{\partial y^2} + \frac{\partial^2 P}{\partial z^2} + k_m^2 P = 0 \tag{4.114}$$

where harmonic behaviour has been assumed. In equation (4.114) k_m is the complex wavenumber for the dissipative material, related to the equivalent speed of sound by means of [10]

$$k_m = \frac{\omega}{c_m} \tag{4.115}$$

Now, developing expression (4.114) similarly to the generic reactive silencer case (see Section 4.2.1), the compact weighted residual equation can be written as

$$\sum_{e=1}^{N_e} \{\Psi^{(e)}\}^T [k_m^{(e)}]\{P^{(e)}\} - \omega^2 \sum_{e=1}^{N_e} \{\Psi^{(e)}\}^T [m_m^{(e)}]\{P^{(e)}\} - \sum_{e=1}^{N_e} \{\Psi^{(e)}\}^T \{f_m^{(e)}\} = 0 \tag{4.116}$$

where the following nomenclature has been introduced

$$[k_m^{(e)}] = \int_{\Omega^e} [B]^T [I][B] \mathrm{d}\Omega \tag{4.117}$$

$$[m_m^{(e)}] = \frac{1}{c_m^2} \int_{\Omega^e} [N]^T [N] \mathrm{d}\Omega \tag{4.118}$$

$$[f_m^{(e)}] = \int_{\Gamma \cap \Gamma^e} [N]^T \frac{\partial P^{(e)}}{\partial n} \vec{n}^T \vec{n} \mathrm{d}\Gamma \qquad (4.119)$$

Now, assembling the element matrices to obtain the global matrices, yields

$$([K_m] - \omega^2[M_m])\{P\} = \{F_m\} \qquad (4.120)$$

Note that no damping matrix appears explicitly since the dissipative effects associated with the absorbent material are included in the *complex* speed of sound [10].

I. Non-moving medium

A perforated dissipative silencer consisting of a perforated central duct surrounded by a chamber with dissipative fibre is depicted in Figure 4.4. The volumes defining the silencer and its boundary surfaces are denoted as Ω_a, Ω_m, Γ_a and Γ_m respectively, whereas the perforated surface is denoted by Γ_p. In this section no mean flow is considered in the subdomains.
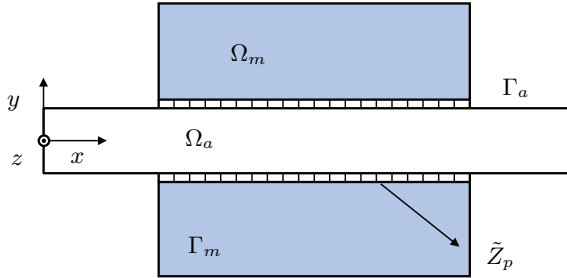
Figure 4.4: *Silencer with a perforated pipe and absorbent material.*

The wave equation (4.1) is met in the central duct, in which the total time derivative can be substituted by a partial derivative since $\vec{U}_{mf} = 0$. On the other hand, the sound behaviour in the absorbent material is governed by expression (4.114). Therefore, the equations corresponding to the duct (4.16) and the dissipative chamber (4.120) are

$$\begin{aligned}([K_a] + j\omega[C_a] - \omega^2[M_a]) &= \{P\} = \{F_a\} \\ ([K_m] + j\omega[C_m] - \omega^2[M_m]) &= \{P\} = \{F_m\}\end{aligned} \qquad (4.121)$$

Although no mean flow exists, a matrix $[C_a]$ can appear due to the assumption of an anechoic termination. Both subdomains are again coupled through the load vectors $\{F_a\}$ and $\{F_m\}$, which can be written at element level as

$$[f_a^{(e)}] = \int_{\Gamma_p \cap \Gamma^e} [N]^T \frac{\partial P_a^{(e)}}{\partial n} d\Gamma \tag{4.122}$$

$$[f_m^{(e)}] = \int_{\Gamma_p \cap \Gamma^e} [N]^T \frac{\partial P_m^{(e)}}{\partial n} d\Gamma \tag{4.123}$$

The normal velocity and the pressure at both sides of the perforated screen can be related by means of Euler's equation (2.19)

$$U_a = \frac{-1}{j\rho_0\omega} \frac{\partial P_a}{\partial n} \qquad U_m = \frac{-1}{j\rho_m\omega} \frac{\partial P_m}{\partial n} \tag{4.124}$$

ρ_m being the equivalent density of the absorbent material.

Following a similar procedure to the one presented at Section (4.3.1) and applying the normal velocity continuity condition, the following integral equations are obtained

$$\{f_a^{(e)}\} = \int_{\Gamma_p \cap \Gamma^e} [N]^T \left(-j\rho_0\omega \frac{P_a^{(e)} - P_m^{(e)}}{\tilde{Z}_p} \right) d\Gamma \tag{4.125}$$

$$\{f_m^{(e)}\} = \int_{\Gamma_p \cap \Gamma^e} [N]^T \left(j\rho_m\omega \frac{P_a^{(e)} - P_m^{(e)}}{\tilde{Z}_p} \right) d\Gamma \tag{4.126}$$

Then, considering the FE nodal interpolation yields

$$\begin{aligned}
\{f_a^{(e)}\} &= \frac{-j\rho_0\omega}{\tilde{Z}_p} \int_{\Gamma \cap \Gamma^e} [N]^T \left([N]\{P_a^{(e)}\} - [N]\{P_m^{(e)}\} \right) d\Gamma \\
&= -j\omega[c_{aaZ_p}^{(e)}]\{P_a^{(e)}\} + j\omega[c_{amZ_p}^{(e)}]\{P_m^{(e)}\}
\end{aligned} \tag{4.127}$$

$$\begin{aligned}
\{f_m^{(e)}\} &= \frac{j\rho_m\omega}{\tilde{Z}_p} \int_{\Gamma \cap \Gamma^e} [N]^T \left([N]\{P_a^{(e)}\} - [N]\{P_m^{(e)}\} \right) d\Gamma \\
&= j\omega[c_{maZ_p}^{(e)}]\{P_a^{(e)}\} - j\omega[c_{mmZ_p}^{(e)}]\{P_m^{(e)}\}
\end{aligned} \tag{4.128}$$

Therefore, at a global level of the problem, the system of equations is

$$\left(\begin{bmatrix} [K_a] + [0] & -[K_{amZ_p}] \\ [0] & [K_m] \end{bmatrix} + j\omega \begin{bmatrix} [C_a] + [C_{aaZ_p}] & -[C_{amZ_p}] \\ -[C_{maZ_p}] & [C_{mmZ_p}] \end{bmatrix} \right.$$
$$\left. -\omega^2 \begin{bmatrix} [M_a] & [0] \\ [0] & [M_m] \end{bmatrix} \right) \left\{ \begin{matrix} \{P_a\} \\ \{P_m\} \end{matrix} \right\} = \left\{ \begin{matrix} \{F_a\} \\ \{F_m\} \end{matrix} \right\} \tag{4.129}$$

and in compact form

$$([K] + j\omega([C] + [C_{Z_p}]) - \omega^2[M])\{P\} = \{F\} \tag{4.130}$$

II. Moving medium

The silencer shown in Figure 4.5 is considered, which presents a uniform mean flow field in the perforated duct. The flow is defined by means of its Mach number $M = U_{mf}/c_0$ and is assumed to be parallel to the perforated surface. No mean flow exists within the chamber [104], so the convective effect in the absorbent material can be neglected.
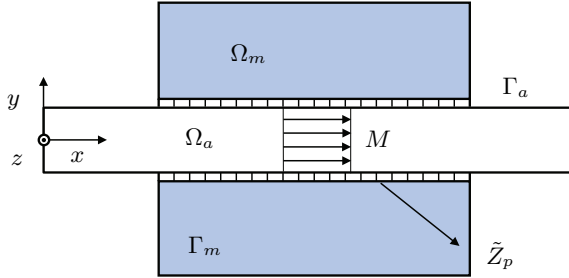
Figure 4.5: *Silencer with a perforated pipe and absorbent material.*

If the FEM is applied to the governing equations of the acoustic behaviour within the central duct and the chamber, the following expressions are obtained

$$\begin{aligned}
([K_a] + j\omega([C_a]) - \omega^2[M_a])\{P\} &= \{F_a\} \\
([K_m] - \omega^2[M_m])\{P\} &= \{F_m\}
\end{aligned} \tag{4.131}$$

Now, by coupling the air and the absorbent material regions by means of the load vectors $\{F_a\}$ and $\{F_m\}$ related to the perforated surface, this can be written at element level as

$$[f_a^{(e)}] = \int_{\Gamma_p \cap \Gamma^e} [N]^T \frac{\partial P_a^{(e)}}{\partial n} \vec{n}^T [D] \vec{n} \, \mathrm{d}\Gamma = \int_{\Gamma_p \cap \Gamma^e} [N]^T \frac{\partial P_a^{(e)}}{\partial n} \, \mathrm{d}\Gamma \tag{4.132}$$

$$[f_m^{(e)}] = \int_{\Gamma_p \cap \Gamma^e} [N]^T \frac{\partial P_m^{(e)}}{\partial n} \, \mathrm{d}\Gamma \tag{4.133}$$

where $\{f_a^{(e)}\}$ does not explicitly depend on the Mach number M because the flow is parallel to the duct.

In this case, as in Section 4.3.1, several alternatives can be considered for applying the condition associated with the perforated surface, such as the displacement or normal velocity continuity. As previously mentioned, the normal velocity continuity condition will be considered. Therefore, it is met that $U_a = -U_m$. These velocities are related through the Euler's equation (2.19)

$$\rho_0 \left(j\omega U_a + U_{mf} \frac{\partial U_a}{\partial x} \right) = -\frac{\partial P_a}{\partial n} \tag{4.134}$$

$$j\rho_m \omega U_m = -\frac{\partial P_m}{\partial n} \tag{4.135}$$

Then, the load vectors can be expressed as

$$\begin{aligned}
\{f_a^{(e)}\} &= \frac{-j\rho_0\omega}{\tilde{Z}_p} \int_{\Gamma_p \cap \Gamma^e} [N]^T \left([N]\{P_a^{(e)}\} - [N]\{P_m^{(e)}\} \right) \mathrm{d}\Gamma \\
&\quad - \frac{\rho_0 U_{mf}}{\tilde{Z}_p} \int_{\Gamma_p \cap \Gamma^e} [N]^T \left(\frac{\partial [N]}{\partial x}\{P_a^{(e)}\} - \frac{\partial [N]}{\partial x}\{P_m^{(e)}\} \right) \mathrm{d}\Gamma \\
&= -j\omega[c_{aaZ_p}^{(e)}]\{P_a^{(e)}\} + j\omega[c_{amZ_p}^{(e)}]\{P_m^{(e)}\} - [k_{aaZ_p}^{(e)}]\{P_a^{(e)}\} + j\omega[k_{amZ_p}^{(e)}]\{P_m^{(e)}\}
\end{aligned} \tag{4.136}$$

$$\begin{aligned}
\{f_m^{(e)}\} &= \frac{j\rho_m\omega}{\tilde{Z}_p} \int_{\Gamma \cap \Gamma^e} [N]^T \left([N]\{P_a^{(e)}\} - [N]\{P_m^{(e)}\} \right) \mathrm{d}\Gamma \\
&= j\omega[c_{maZ_p}^{(e)}]\{P_a^{(e)}\} - j\omega[c_{mmZ_p}^{(e)}]\{P_m^{(e)}\}
\end{aligned} \tag{4.137}$$

Thus, the final system of equations is

$$\left(\begin{bmatrix} [K_a] + [K_{aaZ_p}] & -[K_{amZ_p}] \\ [0] & [K_m] \end{bmatrix} + j\omega \begin{bmatrix} [C_a] + [C_{aaZ_p}] & -[C_{amZ_p}] \\ -[C_{maZ_p}] & [C_{mmZ_p}] \end{bmatrix} \right.$$
$$\left. -\omega^2 \begin{bmatrix} [M_a] & [0] \\ [0] & [M_m] \end{bmatrix} \right) \begin{Bmatrix} \{P_a\} \\ \{P_m\} \end{Bmatrix} = \begin{Bmatrix} \{F_a\} \\ \{F_m\} \end{Bmatrix} \tag{4.138}$$

4.5 Finite element hybrid formulation. Variable properties of the propagation media

The wave equation in its usual form is based on several assumptions such as the homogeneity of the propagation medium, the independence of the time and the absence

of mean flow [140].

$$\nabla^2 p - \frac{1}{c^2} \frac{\partial^2 p}{\partial t^2} = 0 \qquad (4.139)$$

Therefore, a more general form of the wave equation is required to study the acoustic performance of a silencer under realistic working conditions. Thus, in order to extend the existing models, a hybrid formulation has been developed to consider heterogeneous propagation media within a perforated dissipative silencer. These variations can be due to its working conditions (for example, temperature variations or soot particles [65, 150]), or to the manufacturing process (e.g. heterogeneities in the filling density of the fibre [16, 17, 149]).

4.5.1 Variable bulk density

Generally, the bulk density of the fibre contained in the chamber is not homogeneous due to the manufacturing process of perforated dissipative silencers [139, 155, 160]. The presence of material non-homogeneities can considerably affect the acoustic behaviour of the silencer [17, 149, 160, 161].
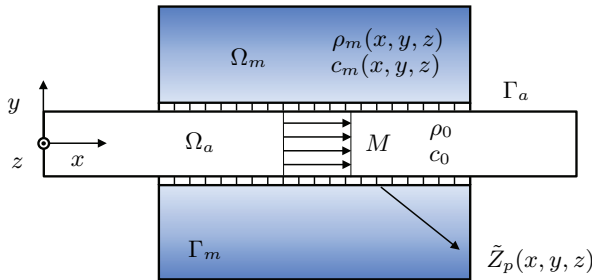
Figure 4.6: *Silencer with varying density distribution.*

A perforated dissipative silencer carrying mean flow can be observed in Figure 4.6. The volumes of the different subdomains are denoted by Ω_a and Ω_m and represent the air and absorbent material subregions respectively, whereas their boundaries are denoted as Γ_a and Γ_m and the perforated surface is Γ_p. The distribution of the fibre is represented through its bulk density (associated with a particular filling process during manufacturing) that is coordinate-dependent, so $\rho_b(x, y, z) = \rho_b(\mathbf{x})$. This implies that the equivalent complex density and the equivalent speed of sound will be affected resulting in $\rho_m(x, y, z) = \rho_m(\mathbf{x})$ and $c_m(x, y, z) = c_m(\mathbf{x})$, respectively,

leading to a spatially variable perforated duct acoustic impedance $\tilde{Z}_p(\mathbf{x})$ (see Section 3.2.1).

In the central airway carrying mean flow, the wave equation can be written in terms of acoustic velocity potential (see also expression (2.35)) as [43, 149]

$$\Delta\Phi_a - \frac{1}{c_0^2}D_t^2\Phi_a = 0 \qquad (4.140)$$

Δ being the Laplacian operator, c_0 the speed of sound in the air and Φ_a the acoustic velocity potential. Besides, the acoustic velocity is related to the potential as

$$\vec{U}_a = \{U_a \quad V_a \quad W_a\}^T = \nabla\Phi_a \qquad (4.141)$$

and D_t is the total time derivative

$$D_t = \frac{\partial}{\partial t} + U_{mf}^T\nabla \qquad (4.142)$$

where $\vec{U}_{mf} = \{U_{mf}\ V_{mf}\ W_{mf}\}^T = \{U_{mf}\ 0\ 0\}^T$, assuming that the mean flow is parallel to the x axis and therefore, to the perforated central duct. The acoustic pressure can be related to the velocity potential through the following expression (see also equation 2.39)

$$P_a = -\rho_0 D_t\Phi_a \qquad (4.143)$$

Assuming harmonic sound waves yields

$$\left(1 - \frac{U_{mf}^2}{c_0^2}\right)\frac{\partial^2\Phi_a}{\partial x^2} + \frac{\partial^2\Phi_a}{\partial y^2} + \frac{\partial^2\Phi_a}{\partial z^2} - \frac{2j\omega U_{mf}}{c_0^2}\frac{\partial\Phi_a}{\partial x} + \frac{\omega^2}{c_0^2}\Phi_a = 0 \qquad (4.144)$$

where ω is the angular frequency and j is the imaginary unit.

Regarding the dissipative chamber, the equivalent acoustic properties present a spatial dependence due to the heterogeneity of the absorbent material bulk density. Therefore, a suitable form of the wave equation, also assuming harmonic sound waves, is required [16, 65, 128, 140] and can be expressed in terms of pressure as

$$\nabla\left(\frac{1}{\rho_m}\nabla P_m\right) + \frac{\omega^2}{\rho_m c_m^2}P_m = 0 \qquad (4.145)$$

where the terms corresponding to the equivalent density and speed of sound explicitly appear.

Applying the FEM to equation (4.144) results in

$$
\sum_{e=1}^{N_a^e} \left(\int_{\Omega^e} (\nabla[N])^T [D] \nabla[N] \mathrm{d}\Omega + \frac{2j\omega U_{mf}}{c_0^2} \int_{\Omega^e} [N]^T \frac{\partial[N]}{\partial x} \mathrm{d}\Omega \right.
$$
$$
\left. - \frac{\omega^2}{c_0^2} \int_{\Omega^e} [N]^T [N] \mathrm{d}\Omega \right) \{\Phi_a{}^e\} = \sum_{e=1}^{N_a^e} \left(\int_{\Gamma^e} [N]^T \vec{n}^T [M] \nabla \Phi_a \mathrm{d}\Gamma \right)
\tag{4.146}
$$

$\vec{n}$ being the outward normal unit vector and $[D]$ a matrix defined as

$$
[D] = \begin{bmatrix} 1 - \dfrac{U_{mf}^2}{c_0^2} & 0 & 0 \\ 0 & 1 & 0 \\ 0 & 0 & 1 \end{bmatrix}
\tag{4.147}
$$

Expression (4.146) can be written in compact form as

$$
([K_a] + j\omega[C_a] - \omega^2[M_a]\{\Phi_a\} = \{F_a\}
\tag{4.148}
$$

where the following nomenclature has been introduced

$$
[K_a] = \sum_{e=1}^{N_a^e} \left(\int_{\Omega^e} (\nabla[N])^T [D] \nabla[N] \mathrm{d}\Omega \right)
\tag{4.149}
$$

$$
[M_a] = \sum_{e=1}^{N_a^e} \left(\frac{1}{c_0^2} \int_{\Omega^e} [N]^T [N] \mathrm{d}\Omega \right)
\tag{4.150}
$$

$$
[C_a] = \sum_{e=1}^{N_a^e} \left(\frac{2U_{mf}}{c_0^2} \int_{\Omega^e} [N]^T \frac{\partial[N]}{\partial x} \mathrm{d}\Omega \right)
\tag{4.151}
$$

$$
\{F_a\} = \sum_{e=1}^{N_a^e} \left(\int_{\Gamma^e} [N]^T \vec{n}^T [D] \nabla \Phi_a \mathrm{d}\Gamma \right)
\tag{4.152}
$$

The integral associated with the load term $\{F_a\}$ is calculated only over the inlet/outlet sections and the perforated duct. In addition, a rigid wall condition is assumed for the rest of surfaces.

If the FEM is now applied to expression (4.145), it yields

$$\sum_{e=1}^{N_m^e} \left(\int_{\Omega_m^e} \frac{1}{\rho_m} (\nabla[N])^T \nabla[N] \mathrm{d}\Omega - \omega^2 \int_{\Omega_m^e} \frac{1}{\rho_m c_m} [N]^T [N] \mathrm{d}\Omega \right) \{P_m{}^e\}$$
$$= \sum_{e=1}^{N_m^e} \left(\int_{\Gamma_m^e} \frac{1}{\rho_m} [N]^T \frac{\partial P_m}{\partial n} \mathrm{d}\Gamma \right) \tag{4.153}$$

and compacting the nomenclature leads to

$$([K_m] - \omega^2 [M_m]) \{P_m\} = \{F_m\} \tag{4.154}$$

where the following matrices have been defined

$$[K_m] = \sum_{e=1}^{N_m^e} \left(\int_{\Omega_m^e} \frac{1}{\rho_m} (\nabla[N])^T \nabla[N] \mathrm{d}\Omega \right) \tag{4.155}$$

$$[M_m] = \sum_{e=1}^{N_m^e} \left(\int_{\Omega_m^e} \frac{1}{\rho_m c_m} [N]^T [N] \mathrm{d}\Omega \right) \tag{4.156}$$

$$\{F_m\} = \sum_{e=1}^{N_m^e} \left(\int_{\Gamma_m^e} \frac{1}{\rho_m} [N]^T \frac{\partial P_m}{\partial n} \mathrm{d}\Gamma \right) \tag{4.157}$$

In this case, the integral of the previous expression (4.157) over Γ_m is carried out only over the perforated surface, since the chamber walls are considered rigid.

By combining equations (4.148) and (4.154) and taking into account the definition of the acoustic impedance of the perforated duct, the following expression is obtained

$$\tilde{Z}_p = \frac{P_a - P_m}{U} = \frac{-\rho_0 D_t \Phi_a - P_m}{U} \tag{4.158}$$

U being the normal acoustic velocity.

If continuity of the normal acoustic velocity is considered in the orifices of the perforated screen, the load vector corresponding to equation (4.152) is

$$\{F_a\} = \sum_{e=1}^{N_a^e} \left(\int_{\Gamma_a^e \cap \Gamma_p} [N]^T \frac{\partial \Phi_a}{\partial n} \mathrm{d}\Gamma \right) = \sum_{e=1}^{N_a^e} \left(\int_{\Gamma_a^e \cap \Gamma_p} [N]^T \frac{P_a - P_m}{\tilde{Z}_p} \mathrm{d}\Gamma \right)$$
$$= \sum_{e=1}^{N_a^e} \left(\int_{\Gamma_a^e \cap \Gamma_p} [N]^T \left(\frac{-\rho_0 j\omega \Phi_a - \rho_0 U_{mf} \partial \Phi_a / \partial x}{\tilde{Z}_p} - \frac{P_m}{\tilde{Z}_p} \right) \mathrm{d}\Gamma \right) \tag{4.159}$$

and compacting the notation after applying the FE discretization and nodal interpolation yields

$$\{F_a\} = -[K_{aaZ_p}]\{\Phi_a\} - [K_{amZ_p}]\{P_m\} - j\omega[C_{aaZ_p}]\{\Phi_a\} \tag{4.160}$$

where the following submatrices have been defined

$$[K_{aaZ_p}] = \sum_{e=1}^{N_a^e} \left(\rho_0 U_{mf} \int_{\Gamma_a^e \cap \Gamma_p} \frac{[N]^T}{\tilde{Z}_p} \frac{\partial[N]}{\partial x} \mathrm{d}\Gamma \right) \tag{4.161}$$

$$[K_{amZ_p}] = \sum_{e=1}^{N_a^e} \left(\int_{\Gamma_a^e \cap \Gamma_p} \frac{[N]^T[N]}{\tilde{Z}_p} \Gamma \right) \tag{4.162}$$

$$[C_{aaZ_p}] = \rho_0 \sum_{e=1}^{N_a^e} \left(\int_{\Gamma_a^e \cap \Gamma_p} \frac{[N]^T[N]}{\tilde{Z}_p} \Gamma \right) \tag{4.163}$$

On the other hand, the corresponding expression to equation (4.157) can be written as

$$\{F_m\} = \sum_{e=1}^{N_m^e} \left(\int_{\Gamma_m^e \cap \Gamma_p} \frac{[N]^T}{\rho_m} \frac{\partial P_m}{\partial n} \mathrm{d}\Gamma \right) = \sum_{e=1}^{N_m^e} \left(\int_{\Gamma_m^e \cap \Gamma_p} \frac{[N]^T}{\rho_m} \frac{\rho_m j\omega(P_a - P_m)}{\tilde{Z}_p} \mathrm{d}\Gamma \right)$$
$$= \sum_{e=1}^{N_m^e} \left(\int_{\Gamma_m^e \cap \Gamma_p} [N]^T \left(\frac{\rho_0 \omega^2 \Phi_a - \rho_0 j\omega U_{mf} \partial \Phi_a / \partial x}{\tilde{Z}_p} - \frac{j\omega P_m}{\tilde{Z}_p} \right) \mathrm{d}\Gamma \right) \tag{4.164}$$

that after applying a FE nodal interpolation can be expressed in compact form as

$$\{F_m\} = -j\omega[C_{mmZ_p}]\{P_m\} - j\omega[C_{maZ_p}]\{\Phi_a\} + \omega^2[M_{maZ_p}]\{\Phi_a\} \tag{4.165}$$

where the submatrices defined are now

$$[C_{mmZ_p}] = \sum_{e=1}^{N_m^e} \left(\int_{\Gamma_m^e \cap \Gamma_p} \frac{[N]^T[N]}{\tilde{Z}_p} \Gamma \right) \tag{4.166}$$

$$[C_{maZ_p}] = \rho_0 U_{mf} \sum_{e=1}^{N_m^e} \left(\int_{\Gamma_m^e \cap \Gamma_p} \frac{[N]^T[N]}{\tilde{Z}_p} \Gamma \right) \tag{4.167}$$

$$[M_{maZ_p}] = \rho_0 \sum_{e=1}^{N_m^e} \left(\int_{\Gamma_m^e \cap \Gamma_p} \frac{[N]^T[N]}{\tilde{Z}_p} \Gamma \right) \tag{4.168}$$

Finally, expressions (4.148), (4.154), (4.160) and (4.165) are combined. Considering a velocity potential boundary condition, as well as an anechoic termination with a view to obtaining the TL, the final system of equations in compact form is

$$\left(\begin{bmatrix} [K_a] + [K_{aaZ_p}] & [K_{amZ_p}] \\ [0] & [K_m] \end{bmatrix} + j\omega \begin{bmatrix} [C_a] + [C_{aaZ_p}] & [0] \\ [C_{maZ_p}] & [C_{mmZ_p}] \end{bmatrix} \right.$$
$$\left. -\omega^2 \begin{bmatrix} [M_a] & [0] \\ [M_{maZ_p}] & [M_m] \end{bmatrix} \right) \begin{Bmatrix} \{\Phi_a\} \\ \{P_m\} \end{Bmatrix} = \begin{Bmatrix} \{F_a\} \\ \{0\} \end{Bmatrix} \tag{4.169}$$

4.5.2 Non-uniform temperature field

A scheme of a perforated dissipative silencer carrying mean flow is presented in Figure 4.7. The silencer can be divided into two different regions, depending on the propagation media, i.e. air and absorbent material, which are denoted as Ω_a and Ω_m respectively, while their associated boundaries are represented by Γ_a and Γ_m, the perforated surface being Γ_p. In the duct, because of its dimensions, the temperature variation is considered only one-dimensional, as in references [65, 68, 97, 99, 178]. The temperature is maximum at the inlet section of the silencer and decreases along the flow path. However, a multidimensional temperature variation, which contemplates both axial and radial gradients, is considered within the chamber. As mentioned in Section 3.3, the temperature variations lead to heterogeneous properties of the different propagation media, and therefore, to a coordinate-dependent acoustic impedance of the perforated duct [65]. Also, the mean flow contained in the central airway is variable. The acoustic properties (air density and speed of sound) that characterize the propagation media are $\rho_0(x)$ and $c_0(x)$ for the air, and $\rho_m(x, y, z)$ and $c_m(x, y, z)$ for the dissipative fibre (see Section 3.3).

For a continuously varying temperature field, a suitable version of the wave equation is required to account for the heterogeneous properties of the wave propagation medium [65]. For flow velocity fields varying with position, a pressure-based equation will include spatial derivatives of the acoustic velocity and several dependent variables will be involved [140]. Therefore, a velocity potential formulation is proposed for the duct in order to avoid the above-mentioned drawback. Thus, the governing equation of the sound behaviour in the central airway is

$$\nabla(\rho_0 \nabla \Phi_a) - \rho_0 D_t \left(\frac{1}{c_0^2} D_t \Phi_a \right) = 0 \tag{4.170}$$
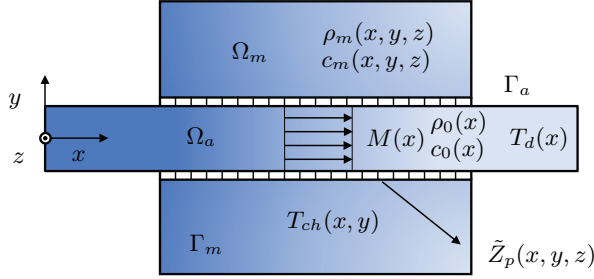
Figure 4.7: *Silencer with a varying temperature field.*

where the speed of sound c_0 and the air density ρ_0, as well as the flow, are non-homogeneous. In equation (4.170) Φ_a is the acoustic velocity potential so that

$$\vec{U}_a = \{U_a \quad V_a \quad W_a\}^T = \nabla\Phi_a \tag{4.171}$$

and D_t is the total time derivative defined as

$$D_t = \frac{\partial}{\partial t} + \vec{U}_{mf}^T \nabla \tag{4.172}$$

where $\vec{U}_{mf} = \{U_{mf} \quad V_{mf} \quad W_{mf}\}^T$. Besides, the relation between the acoustic pressure and the velocity potential is (see equation (2.39))

$$P_a = -\rho_0 D_t \Phi_a \tag{4.173}$$

Assuming a one-directional mean flow as in earlier studies [101, 104, 126], parallel to the x axis and transversally uniform, the velocity can be expressed as $\vec{U}_{mf} = \{U_{mf} \quad 0 \quad 0\}^T$. Thus, the total derivative can be rewritten as

$$D_t = \frac{\partial}{\partial t} + U_{mf}\frac{\partial}{\partial x} = j\omega + U_{mf}\frac{\partial}{\partial x} \tag{4.174}$$

where harmonic waves have been assumed, their angular frequency being ω.

Thus, the combination of the total derivative with equation (4.170) leads to [65]

$$\nabla(\rho_0\nabla\Phi_a) - \frac{\rho_0 U_{mf}^2}{c_0^2}\frac{\partial^2\Phi_a}{\partial x^2} - \frac{2\rho_0 j\omega U_{mf}}{c_0^2}\frac{\partial\Phi_a}{\partial x} - \rho_0 U_{mf}^2\frac{\partial\left(1/c_0^2\right)}{\partial x}\frac{\partial\Phi_a}{\partial x}$$
$$-\frac{\rho_0 U_{mf}}{c_0^2}\frac{\partial U_{mf}}{\partial x}\frac{\partial\Phi_a}{\partial x} - \rho_0 j\omega U_{mf}\frac{\partial\left(1/c_0^2\right)}{\partial x}\Phi_a + \frac{\rho_0\omega^2}{c_0^2}\Phi_a = 0 \tag{4.175}$$

Now, applying the weighted residuals method and the divergence theorem to expression (4.175) yields

$$
-\int_{\Omega_a} \rho_0 \nabla^T \Psi [D] \nabla \Phi_a d\Omega
$$

$$
+\int_{\Omega_a} \Psi \left(\frac{U_{mf}^2}{c_0^2} \frac{\partial \rho_0}{\partial x} + \frac{\rho_0 U_{mf}}{c_0^2} \frac{\partial U_{mf}}{\partial x} - \frac{2\rho_0 j\omega U_{mf}}{c_0^2} \right) \frac{\partial \Phi_a}{\partial x} d\Omega \qquad (4.176)
$$

$$
+\int_{\Omega_a} \Psi \left(-\rho_0 j\omega U_{mf} \frac{\partial \left(1/c_0^2\right)}{\partial x} + \frac{\rho_0 \omega^2}{c_0^2} \right) \Phi_a d\Omega + \int_{\Gamma_a} \rho_0 \Psi \vec{n}^T [D] \nabla \Phi_a d\Gamma = 0
$$

where, as indicated previously, the characteristic properties of air, c_0 and ρ_0, and the mean flow U_{mf} are variable. The normal unit vector to the surface Γ is $\vec{n}$, while the matrix $[D]$ is defined as

$$
[D] = \begin{bmatrix} 1 - \dfrac{U_{mf}^2}{c_0^2} & 0 & 0 \\ 0 & 1 & 0 \\ 0 & 0 & 1 \end{bmatrix} \qquad (4.177)
$$

Comparing equations (4.175) and (4.176), it is found that the product of the spatial derivatives of both the inverse of the squared speed of sound and the acoustic velocity potential cancels during the mathematical procedure. Also, it is important to point out that the relation $\rho_0 U_{mf} S = constant$ is satisfied, and since the cross section S of the central duct is uniform, the following expression can be deduced

$$
U_{mf} \frac{\partial \rho_0}{\partial x} + \rho_0 \frac{\partial U_{mf}}{\partial x} = 0 \qquad (4.178)
$$

Then, equation (4.176) can be rewritten in such a way that the two first terms of the second integral vanish leading to

$$
-\int_{\Omega_a} \rho_0 \nabla^T \Psi [D] \nabla \Phi_a d\Omega + \int_{\Omega_a} \Psi \left(-\frac{2\rho_0 j\omega U_{mf}}{c_0^2} \right) \frac{\partial \Phi_a}{\partial x} d\Omega
$$

$$
+\int_{\Omega_a} \Psi \left(-\rho_0 j\omega U_{mf} \frac{\partial \left(1/c_0^2\right)}{\partial x} + \frac{\rho_0 \omega^2}{c_0^2} \right) \Phi_a d\Omega \qquad (4.179)
$$

$$
+\int_{\Gamma_a} \rho_0 \Psi \vec{n}^T [D] \nabla \Phi_a d\Gamma = 0
$$

Applying now the FEM and considering the Galerkin approach yields

$$\sum_{e=1}^{N_a^e} \left(-\int_{\Omega_a^e} \rho_0 (\nabla[N])^T [D] \nabla[N] \mathrm{d}\Omega + \int_{\Omega_a^e} \left(-\frac{2\rho_0 j\omega U_{mf}}{c_0^2} \right) [N]^T \frac{\partial[N]}{\partial x} \mathrm{d}\Omega \right.$$

$$\left. + \int_{\Omega_a^e} \left(-\rho_0 j\omega U_{mf} \frac{\partial \left(1/c_0^2 \right)}{\partial x} + \frac{\rho_0 \omega^2}{c_0^2} \right) [N]^T [N] \mathrm{d}\Omega \right) \{\Phi_a^e\} \quad (4.180)$$

$$= \sum_{e=1}^{N_a^e} \int_{\Gamma_a^e} -\rho_0 [N]^T \vec{n}^T [D] \nabla \Phi_a \mathrm{d}\Gamma$$

which in compact form and changing the sign of the equation for more clarity can be expressed as

$$([K_a] + j\omega([C_{a_1}] + [C_{a_2}]) - \omega^2 [M_a])\{\Phi_a\} = \{F_a\} \quad (4.181)$$

where the following nomenclature has been used

$$[K_a] = \sum_{e=1}^{N_a^e} \int_{\Omega_a^e} \rho_0 (\nabla[N])^T [D] \nabla[N] \mathrm{d}\Omega \quad (4.182)$$

$$[M_a] = \sum_{e=1}^{N_a^e} \int_{\Omega_a^e} \frac{\rho_0}{c_0^2} [N]^T [N] \mathrm{d}\Omega \quad (4.183)$$

$$[C_{a_1}] = \sum_{e=1}^{N_a^e} \int_{\Omega_a^e} \frac{2\rho_0 U_{mf}}{c_0^2} [N]^T \frac{\partial[N]}{\partial x} \mathrm{d}\Omega \quad (4.184)$$

$$[C_{a_2}] = \sum_{e=1}^{N_a^e} \int_{\Omega_a^e} \rho_0 \omega U_{mf} \frac{\partial \left(1/c_0^2 \right)}{\partial x} \mathrm{d}\Omega \quad (4.185)$$

$$\{F_a\} = \sum_{e=1}^{N_a^e} \int_{\Gamma_a^e} \rho_0 [N]^T \vec{n}^T [D] \nabla \Phi_a \mathrm{d}\Gamma$$

$$= \sum_{e=1}^{N_a^e} \left(\int_{\Gamma_a^e \cap \Gamma_{bc}} \rho_0 [N]^T \left(1 - \frac{U_{mf}^2}{c_0^2} \frac{\partial \Phi_a}{\partial n} \right) \mathrm{d}\Gamma + \int_{\Gamma_a^e \cap \Gamma_p} \rho_0 [N]^T \frac{\partial \Phi_a}{\partial n} \mathrm{d}\Gamma \right) \quad (4.186)$$

$\Gamma_{bc} = \Gamma_i \cup \Gamma_o$ being the surface where the suitable inlet/outlet boundary conditions are applied.

The computation of the axial mean flow velocity is carried out considering the mass conservation law for a given Mach number M_i at the inlet section. The density ρ_0 and the speed of sound c_0 can be evaluated at each integration point by means of the

ideal gas law, as detailed in Section 3.3. The spatial derivative of c_0 can be calculated analytically or numerically, depending on the complexity of the temperature field. As can be inferred from the definition of $[C_{a_2}]$, the influence of this latter matrix on the silencer transmission loss is small when compared to the contributions from the rest of finite element matrices (this is also supported by additional calculations carried out with a number of parameters and temperature gradients).

On the other hand, the governing equation of the acoustic behaviour within the dissipative chamber in terms of pressure can be written as shown in the previous expression (4.145)

$$\nabla \left(\frac{1}{\rho_m} \nabla P_m \right) + \frac{\omega^2}{\rho_m c_m^2} P_m = 0 \tag{4.187}$$

The compact form of equation (4.187) after applying a FE interpolation, and following a similar procedure to that used for the variable density case (see equations (4.153)-(4.157)), can be expressed as

$$([K_m] - \omega^2 [M_m])\{P_m\} = \{F_m\} \tag{4.188}$$

To obtain the final system of equations, equations (4.181) and (4.188) have to be assembled. This assembly is carried out by means of the perforated duct impedance that is defined as

$$\tilde{Z}_p = \frac{P_a - P_m}{U} \tag{4.189}$$

which depends on several parameters such as the porosity, diameter of the orifices, thickness of the perforated screen, frequency and the mean flow. As discussed previously, different continuity conditions through the perforated surface such as the displacement or the normal acoustic velocity conditions can be considered, the latter being considered in the current formulation. Therefore, the load vector equation in the air domain is

$$\{F_a\} = \sum_{e=1}^{N_a^e} \int_{\Gamma_a^e \cap \Gamma_p} \rho_0 [N]^T \frac{\partial \Phi_a}{\partial n} d\Gamma = \sum_{e=1}^{N_a^e} \int_{\Gamma_a^e \cap \Gamma_p} \rho_0 [N]^T \frac{P_a - P_m}{\tilde{Z}_p} d\Gamma$$
$$= \sum_{e=1}^{N_a^e} \int_{\Gamma_a^e \cap \Gamma_p} \rho_0 [N]^T \left(\frac{-\rho_0 j \omega \Phi_a - \rho_0 U_{mf} \partial \Phi_a / \partial x}{\tilde{Z}_p} - \frac{P_m}{\tilde{Z}_p} \right) d\Gamma \tag{4.190}$$

Now, comparing equation (4.159) with the previous expression (4.190), it can be observed that in the latter the air density ρ_0 explicitly appears in the integral due to the formulation. This property is coordinate-dependent here, due to the thermal gradients under consideration, which lead to a heterogeneous air density within the central duct.

On the other hand, after considering a FE interpolation, equation (4.190) can be written in compact form as

$$\{F_a\} = -[K_{aaZ_p}]\{\Phi_a\} - [K_{amZ_p}]\{P_m\} - j\omega[C_{aaZ_p}]\{\Phi_a\} \tag{4.191}$$

The following matrices have been defined

$$[K_{aaZ_p}] = \sum_{e=1}^{N_a^e} \int_{\Gamma_a^e \cap \Gamma_p} \frac{\rho_0^2 U_{mf}[N]^T}{\tilde{Z}_p} \frac{\partial[N]}{\partial x} \mathrm{d}\Gamma \tag{4.192}$$

$$[K_{amZ_p}] = \sum_{e=1}^{N_a^e} \int_{\Gamma_a^e \cap \Gamma_p} \frac{\rho_0[N]^T[N]}{\tilde{Z}_p} \mathrm{d}\Gamma \tag{4.193}$$

$$[C_{aaZ_p}] = \sum_{e=1}^{N_a^e} \int_{\Gamma_a^e \cap \Gamma_p} \frac{\rho_0^2[N]^T[N]}{\tilde{Z}_p} \mathrm{d}\Gamma \tag{4.194}$$

whereas the load vector associated with the absorbent material formulation yields again equation (4.164)

$$\begin{aligned}
\{F_m\} &= \sum_{e=1}^{N_m^e} \int_{\Gamma_m^e \cap \Gamma_p} \frac{[N]^T}{\rho_m} \frac{\partial P_m}{\partial n} \mathrm{d}\Gamma = \sum_{e=1}^{N_m^e} \int_{\Gamma_m^e \cap \Gamma_p} \frac{[N]^T}{\rho_m} \frac{\rho_m j\omega(P_a - P_m)}{\tilde{Z}_p} \mathrm{d}\Gamma \\
&= \sum_{e=1}^{N_m^e} \int_{\Gamma_m^e \cap \Gamma_p} [N]^T \left(\frac{\rho_0\omega^2\Phi_a - \rho_0 j\omega U_{mf}\partial\Phi_a/\partial x}{\tilde{Z}_p} - \frac{j\omega P_m}{\tilde{Z}_p} \right) \mathrm{d}\Gamma
\end{aligned} \tag{4.195}$$

The latter equation can be rewritten after applying a FE nodal interpolation as

$$\{F_m\} = -j\omega[C_{mmZ_p}]\{P_m\} - j\omega[C_{maZ_p}]\{\Phi_a\} + \omega^2[M_{maZ_p}]\{\Phi_a\} \tag{4.196}$$

where the following notation has been considered

$$[C_{mmZ_p}] = \sum_{e=1}^{N_m^e} \int_{\Gamma_m^e \cap \Gamma_p} \frac{[N]^T[N]}{\tilde{Z}_p} \mathrm{d}\Gamma \tag{4.197}$$

$$[C_{maZ_p}] = \sum_{e=1}^{N_m^e} \int_{\Gamma_m^e \cap \Gamma_p} \frac{\rho_0 U_{mf}[N]^T}{\tilde{Z}_p} \frac{\partial[N]}{\partial x} \mathrm{d}\Gamma \tag{4.198}$$

$$[M_{maZ_p}] = \sum_{e=1}^{N_m^e} \int_{\Gamma_m^e \cap \Gamma_p} \frac{\rho_0[N]^T[N]}{\tilde{Z}_p} \mathrm{d}\Gamma \tag{4.199}$$

Then, the final system of equations can be written as

$$
\left(
\begin{bmatrix}
[K_a] + [K_{aaZ_p}] & [K_{amZ_p}] \\
[0] & [K_m]
\end{bmatrix}
+ j\omega
\begin{bmatrix}
[C_{a1}] + [C_{a2}] + [C_{aaZ_p}] & [0] \\
[C_{maZ_p}] & [C_{mmZ_p}]
\end{bmatrix}
\right.
$$
$$
\left.
-\omega^2
\begin{bmatrix}
[M_a] & [0] \\
[M_{maZ_p}] & [M_m]
\end{bmatrix}
\right)
\left\{
\begin{matrix}
\{\Phi_a\} \\
\{P_m\}
\end{matrix}
\right\}
=
\left\{
\begin{matrix}
\{F_{a_{bc}}\} \\
\{0\}
\end{matrix}
\right\}
\tag{4.200}
$$

where $\{F_{a_{bc}}\}$ corresponds to the part of the load vector $\{F_a\}$ in equation (4.186) calculated over the inlet/outlet sections with their corresponding boundary conditions, i.e. a velocity potential boundary condition and an anechoic termination respectively, while a rigid wall condition has been assumed for the remaining surfaces [126].

Several differences are found comparing the hybrid formulation for the cases of variable bulk density and the presence of thermal gradients. These differences are mainly due to the variation of the air density and speed of sound, as well as to a heterogeneous mean flow produced by the variation of temperature within the central duct of silencer, providing new submatrices (e.g. damping submatrices) and terms including these variations.

Finally, in order to solve the system of equations, a velocity potential boundary condition and an anechoic termination have been considered at the inlet and outlet sections respectively.

4.6 Shape optimization based on genetic algorithms

In shape optimization, making a decision that maximizes or minimizes a given criterion is required [40, 133, 165]. This decision is usually conditioned by several constraints.

The sequence of steps to follow in order to solve an optimization problem is:

1. Taking n points belonging to the search space, so that m new points are generated at each iteration (also called generation or population in some algorithms). Each one of these points represents a possible solution to the problem. In this step of generation of solutions, the algorithm has to be able to achieve any local improvement.

2. Evaluating if the restrictions and the objective function to maximize each one of the solutions are met.

3. Accepting the new solutions that in meeting the restrictions assume an improvement and can be reused as a new starting point. The rest of the solutions are rejected.

4. Repeating the previous steps till the stop criteria are met. These criteria are usually related to the maximum condition to reach or to the number of iterations previously determined by the user.

In order to assess the solutions obtained, an evaluation function has to be defined; in general, this is called the objective function. In this case, the main target is to obtain a silencer configuration that achieves the best acoustic characteristics, i.e. a TL as high as possible in a frequency range(s) prescribed by the user .

There are many algorithms that can guide the optimization process. For example, the genetic algorithms, which are going to be considered in the present Thesis due to their robustness, and the fact that are highly efficient for the solution of complex problems [37, 56, 110, 130, 148]. These algorithms are stochastic, which supposes that a certain degree of randomness can be introduced during the search process. This means that two different runs of the same algorithm will not necessarily obtain the same result. The main advantage of this kind of method lies in the fact that it can escape from local optima and make a wider search within the design space than deterministic methods. Also, they are not as affected as deterministic methods by the pollution generated during the process. Their main drawback is the high number of iterations required sometimes to obtain acceptable solutions [110, 133, 148].

The optimization processes based on genetic algorithms are composed of an upper and a lower level governed by the optimization algorithm and the numerical method used to analyse each one of the multiple solutions, respectively. In this case, the upper level used is the commercial program modeFRONTIER®, while the lower level is an in-house FE program [64] to compute the TL of multichamber silencers in the presence of mean flow. The latter parameter permits the quantification of the attenuation achieved by the silencer and can be used as an objective function [4, 24, 37, 56]. It is important to point out that the accuracy of the computation methods used has a notable influence on the solutions obtained by the optimization program [129, 148].

4.6.1   MOGA-II description

The commercial program modeFRONTIER® uses its own version of the Multi-Objective Genetic Algorithm, called MOGA-II [141]. It is an efficient version that uses a multi-

search smart elitism. This elitism operator is able to preserve some of the best so-lutions, without remaining stuck in a premature convergence at some local optima. The total number of evaluations carried out by the algorithm MOGA-II [141] is equal to the number of experimental designs defined (first generation randomly generated) multiplied by the generation number. The size of each analysis is defined, in general, by the computation resources available.

The parameters to specify by the user for the utilization of the mentioned algorithm are [141]:

- **Number of generations:** This value defines the maximum size of the simulation.

- **Probability of directional cross-over:** The cross-over operator is a recombination method in which the fathers produce offsprings by sharing information. The objective of this operator is to obtain individuals with better characteristics, while retaining the population diversity. The cross-over is considered as the main search operator in the genetic algorithms. This specific cross-over is an operator which gives efficiency to the algorithm. If this parameter is set to 1, only this operator is used. The search is efficient, but when highly non-linear problems are considered, the optimizer can remain stuck at the local optima solutions. The values 0 and 1 are not recommendable. The predetermined value is 0.5, although this value has to be increased when a problem is relatively smooth and decreased in the rest of the cases.

- **Probability of selection:** This value is the probability that design configurations are not changed during the evolution. Therefore, this parameter should be kept small in order to maintain the good diversity between points. If the value is one, no computation after the initial population will be carried out.

- **Probability of mutation:** This value shows the probability of a design configuration of being randomly changed. When the value is 1, the algorithm turns into a purely random search.

- **DNA string mutation ratio:** This value provides the percentage of the individual DNA that is perturbed by the mutation operator. The DNA of each individual is coded in a binary string; the mutation ratio defines the number of bits that mutate.

- **Elitism:** The elitism will ensure that the best solutions are preserved during the evolution.

On the other hand, the treatments for the constraints are:

- Assuring that a feasible solution is always better than a non-feasible solution and taking into account the intensity of the constraint violation. This can be done using *fuzzy* constraints for which a tolerance of violation is specified at a project level.

- By means of the addition of an objective for the problem equal to the number of violated constraints. This option is only relevant for over-constrained problems where a feasible solution does not exist and there are several constraints of relatively equivalent importance.

4.6.2   Variables, constraints and objective function of the problem

The definition of the variables and the objective function of the optimization problem is an important step, since the solution obtained depends on their definition. In this case, the problem to solve consists of obtaining the most suitable configuration of a multichamber silencer. In this case, the parameters defined as variables are the lengths of the different chambers, as well as their radii and the distances between two consecutive chambers (the thickness of the dividing plates). Also the properties defining the surface that separates the central duct from the outer chamber are considered as a variable. The different surfaces under consideration are:

- Microperforated central duct.
- Sintered central duct with nearly constant acoustic impedance.

These variables will be randomly generated by the program modeFRONTIER® that will send the information to a FE program fully developed in Matlab®. The coupling between the upper and lower levels is done through a macro that adapts the variables in such a way that the FE program can read them. In addition, the geometric constraints of the problem will be imposed in this macro. The total length of the multichamber silencer is considered constant, which seems reasonable because in many instances the space available in an car is limited. However, the lengths of the chambers could be variable, except for the last one, whose dimension will be imposed by the total dimensions of the configuration, which means that this will be calculated as the total length of the silencer minus the lengths of the different chambers and the distances between them.

On the other hand, modeFRONTIER® is a multi-objective program that can obtain a Pareto optimal frontier composed of the different optimal solutions computed; it is

then decision of the user to determine which is the most suitable for the purposes of the acoustic device because in many occasions the objectives are counterposed. In the present problem the main objective is to obtain the configuration of a multichamber silencer that achieves a higher sound attenuation in the frequency ranges of interest. The attenuation, in this case, has been quantified by means of the average TL obtained at the different frequencies. Nevertheless, when the average transmission loss is considered, the higher peaks of attenuation can be equilibrated with the troughs, and this is clearly a situation to avoid, since an attenuation as uniform and as high as possible is required in the frequency range under consideration for each particular design problem. Therefore, it should be pointed out that the maximization of the attenuation does not necessarily involve the minimization of the dispersion in the TL results and the deviation of the results has to be considered as another objective. This fact can reduce the convergence speed of the optimization procedure. Thus, it seems reasonable to combine both objectives and convert them into one. The new global objective function to maximize can be defined as the sum of the average of the obtained attenuations for each one of the frequencies belonging to the range under study plus the inverse of the standard deviation belonging to those results.

A scheme of the optimization procedure followed to obtain the suitable multichamber configuration is presented in Figure 4.8.
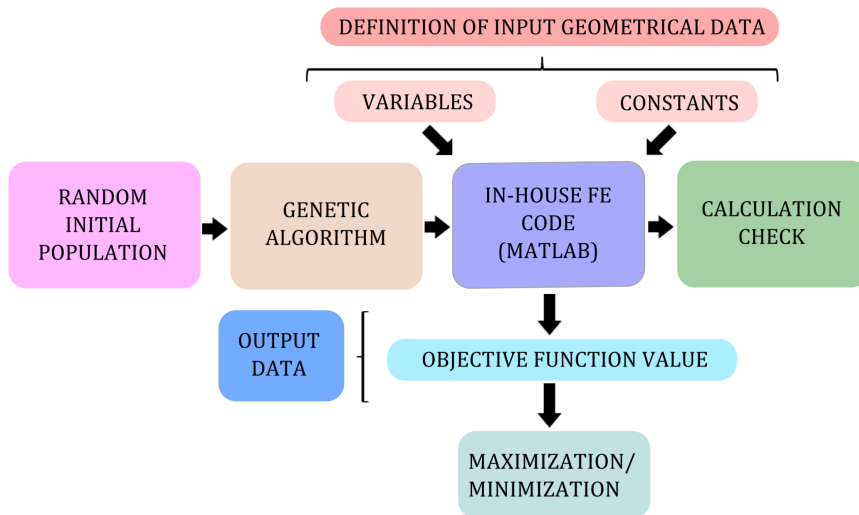
Figure 4.8: *Scheme of the optimization procedure.*

The values of the parameters belonging to MOGA-II, as well as the treatment of the constraints are listed below:

- Number of generations: 100

- Probability of cross-over: 0.5

- Probability of selection: 0.05

- Probability of mutation: 0.1

- Elitism: Enabled

- Treat constraints: Penalising objectives

- Random generator seed: 1

The above-defined figures are the default values of the program. These have been chosen because good results have been reported in a previous work for different kinds of problems [148].

4.7 Applications

In this section, the FEM is applied to a perforated dissipative configuration, in which the properties of the different propagation media are variable in order to study the acoustic performance of a silencer under more realistic conditions. Thus, the models developed in Chapter 3 have been included in the hybrid FE formulation (see Section 4.5) to consider on the one hand, the presence of a heterogeneous bulk density of absorbent material and on the other hand, the presence of thermal gradients, as well as the influence of high temperatures, on the attenuation. Also, a process of shape optimization of a multichamber silencer has been carried out to find the most suitable design for the configuration under study considering a FE standard pressure formulation (see Section 4.4).

4.7.1 Perforated dissipative silencer with variable bulk density of the absorbent material

As demonstrated in Section 3.5.1, the bulk density heterogeneities clearly modify the behaviour of a dissipative silencer. In the next sections, the axial and transversal density variations are studied separately in order to isolate the impact of each one of them. In addition, some calculations have been carried out to see the influence of a

more realistic and complex density distribution, including both kinds of variations. All the following results have been published in reference [149].

The silencer under study is an axisymmetric perforated dissipative configuration, whose geometric characteristics are defined in Table 4.1. The mesh considered to compute the silencer TL consists of eight-noded quadratic quadrilateral elements whose approximate size is 0.01 m to obtain an accurate solution. The characteristics of the perforated surface are $\sigma = 0.2$, $t_p = 0.001$ m, and $d_h = 0.0035$ m.

Geometry	L_i/L_o (m)	R_d (m)	L_{ch} (m)	R_{ch} (m)
1	0.1	0.0268	0.3	0.05

Table 4.1: Geometry under study: L, length; R, radius; i, inlet; o, outlet; d, duct; ch, chamber.

The fibre used in all the calculations is E fibreglass, whose characteristic impedance and wavenumber are defined as

$$Z_m(x) = Z_a \left(1 + 0.095 \left(\rho_0 f/R(x)\right)^{-0.669} - j0.169 \left(\rho_0 f/R(x)\right)^{-0.571}\right) \qquad (4.201)$$

$$k_m(x) = k_a \left(1 + 0.201 \left(\rho_0 f/R(x)\right)^{-0.583} - j0.220 \left(\rho_0 f/R(x)\right)^{-0.585}\right) \qquad (4.202)$$

and the presence of a $M{=}0.2$ mean flow is considered as well.

I. Effect of an axially-varying density on the attenuation

To study the influence of a linear axial variation of the bulk density on the silencer performance, several computations have been carried out. The corresponding values for the calculation of the axially-varying density distribution are listed in Table 4.2 (for further information see Figure 3.2). It should be noted that all the configurations present the same average density of value $\rho_{avg} = 200$ kg/m^3, which will be taken as a reference, and therefore an additional computation is included considering a uniform distribution with the aforementioned value for comparison purposes. In order to validate the hybrid formulation, the reference computation has been done twice to compare the results obtained with a calculation done with an in-house program based on a traditional pressure formulation.

$Case$	$\rho_{r_1}(R_d)$ kg/m³	$\rho_{r_2}(R_{ch})$ kg/m³	$\rho_{r_3}(R_d)$ kg/m³	$\rho_{r_4}(R_{ch})$ kg/m³
1	210	210	190	190
2	250	250	150	150
3	300	300	100	100

Table 4.2: Density values for the computation of the axially-varying density distributions.

The transmission loss predictions for the axially-varying densities are shown in Figure 4.9, as well as the results obtained for the uniform density. As can be observed, good agreement is shown between the TL predictions carried out for the uniform distribution computed by the hybrid formulation and the pressure FE formulation, since both curves are overlapped (circle blue line and solid blue line). In addition, the TL curves provided by case 1 and the uniform distribution are practically overlapped, due to the small bulk density variation considered in the former. It is also remarkable that increasing axial variations of the bulk density lead to higher transmission loss values in the mid frequency range, while at high frequencies an intersection point appears (at approximately 3200 Hz in Figure 4.9), where the trend seems to be the opposite and the attenuation values would be higher with larger axial variations. On the other hand, at low frequencies the influence of density variations on the attenuation seems to be not very relevant.
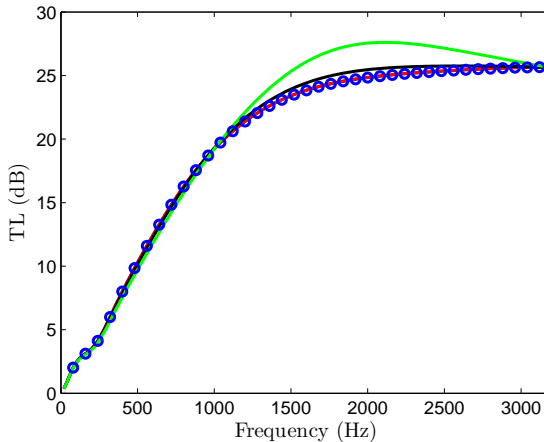

Figure 4.9: Transmission loss of a dissipative silencer with axially-varying density distributions (same average density of 200 kg/m³): ——, 200 kg/m³, hybrid formulation; ooo, 200 kg/m³, pressure formulation; ——, case 1, hybrid formulation; ——, case 2, hybrid formulation; ——, case 3, hybrid formulation.

II. Effect of a radially-varying density on the attenuation

To evaluate the acoustic performance of dissipative silencers incorporating a material with a linear radial variation of the bulk density, two kinds of function are considered, depending on whether the density increases (case a) or decreases (case b) with the radial coordinate. In both cases, three configurations are studied. The values for the calculation of the radial density distribution are listed in Table 4.3 (for further information see Figure 3.2), where all the configurations present the same average $\rho_{avg} = 200$ kg/m^3 as in Section 4.7.1. Also, an extra computation with uniform density considering this value is included. In all the calculations a mean flow of $M = 0.2$ has been considered.

Case	$\rho_{r_1}(R_d)$ kg/m^3	$\rho_{r_2}(R_{ch})$ kg/m^3	$\rho_{r_3}(R_d)$ kg/m^3	$\rho_{r_4}(R_{ch})$ kg/m^3
1a	164	230	164	230
2a	140	250	140	250
3a	103	280	103	280
1b	215	188	215	188
2b	240	168	240	168
3b	290	127	290	127

Table 4.3: Density values for the computation of the radially-varying density distributions.

Comparing Figures 4.9 and 4.10, it seems clear that the influence on the attenuation of radial variations is much higher than the influence of axial non-homogeneities. The uniform density distribution sets a frontier between cases a and b, the former (radially-varying) providing higher transmission loss. When considering the configurations belonging to case a, it can be observed that a higher attenuation is achieved for larger density variations from approximately 500 Hz to 3200 Hz (below 500 Hz the differences in the attenuation are not relevant). However, for configurations belonging to case b the opposite trend is found. Smaller density variations deliver higher attenuation values. This could be due to the fact that in case a, the density increases with the radius, which supposes that the material resistivity is lower near the perforated surface and the absorption of the sound energy is gradual as the acoustic wave penetrates the dissipative chamber, while in case b a higher resistivity near the perforated duct hinders the penetration of the sound wave in the outer chamber. This effect is considerable for the material considered here due to the high resistivity values that are presented by E fibreglass. For example, a bulk density of $\rho_b = 100$ kg/m^3 yields a resistivity of $R = 22155$ rayl/m, while a bulk density of $\rho_b = 300$ kg/m^3 gives $R = 158664$ rayl/m, which supposes that an increment of three times the density involves an increment in the resistivity of approximately seven times. Although in

principle, for less resistive materials, lower discrepancies are expected, the density variations should be included in the computations to achieve more accuracy in the transmission loss computations.
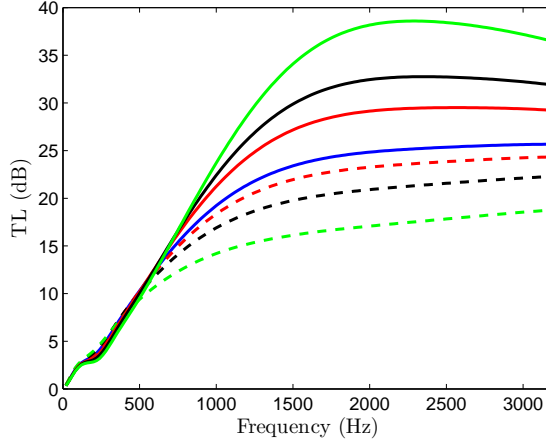
Figure 4.10: Transmission loss of a dissipative silencer with radially-varying density distributions (same average density of 200 kg/m^3): ——, 200 kg/m^3; ——, case 1a; ——, case 2a; ——, case 3a; – – –, case 1b; – – –, case 2b; – – –, case 3b.

III. Influence of a density distribution with axial and radial variations on the attenuation

In this section, more complex density distributions, including axial and radial variations, are studied. The values of density that define the distributions are detailed in Table 4.4 (for further information see Figure 3.2). In configuration 1c, the density increases from the radius of the perforated surface to the radius of the outer chamber, while an axial reduction appears from the inlet to the outlet section. On the other hand, in configuration 2c the density decreases in both the radial and the axial directions.

Case	$\rho_{r_1}(R_d)$ kg/m^3	$\rho_{r_2}(R_{ch})$ kg/m^3	$\rho_{r_3}(R_d)$ kg/m^3	$\rho_{r_4}(R_{ch})$ kg/m^3
1c	200	310	80	90
2c	330	258	150	78

Table 4.4: Density values for the computation of complex density distributions.

The results associated with the configurations listed in Table 4.4 are depicted in Figure 4.11. In all the density distributions under consideration, the average density is $\rho_{avg} = 200$ kg/m^3. Therefore, a computation with uniform density $\rho_b = 200$ kg/m^3 is also included for comparison purposes, as well as configurations 2a and 2b shown in Table 4.3, where only a radial variation of the bulk density is considered. Again, a value of $M = 0.2$ has been assigned for the mean flow Mach number.
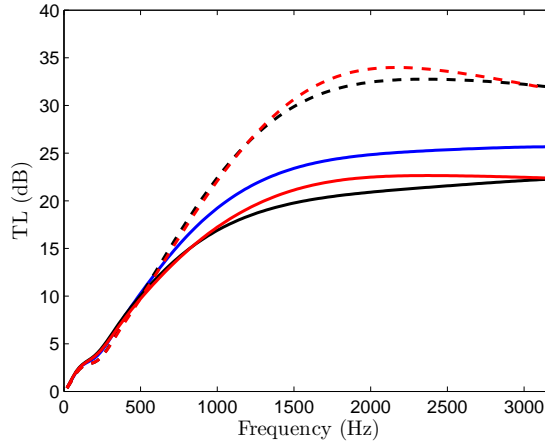
Figure 4.11: Transmission loss of a dissipative silencer with axial and radial variation of the bulk density (same average density of 200 kg/m^3): ——, 200 kg/m^3; – – –, case 1c; ——, case 2c; – – –, case 2a; ——, case 2b.

Configuration 1c provides higher attenuation than the uniform density case, as was expected according to previous results (see Section 4.7.1) and it also provides slightly larger transmission loss values than configuration 2a. The explanation can be found in the fact that configuration 2a does not consider the axial density variation (see Figure 4.9). Besides, configuration 2c provides lower transmission loss when compared to the uniform bulk density case, which is consistent with the results of radially decreasing density distributions (see Figure 4.10), but it yields larger TL than configuration 2b, since the latter does not include any axial variation. Finally, it is worth emphasizing that radial density variations have more influence on the attenuation than the axial ones. Thus, when both are simultaneously considered with a similar magnitude in the FE model, the prediction of the silencer behaviour is mainly dictated by the radial density distribution.

4.7.2 Perforated dissipative silencer subjected to thermal gradients

As shown in Section 3.5.1, thermal gradients significantly affect the behaviour of perforated dissipative silencers. In the next sections, the effects of high temperatures, as well as the influence of axial and radial gradients will be studied. All the results presented have been published in reference [65].

The geometry under study is an axisymmetric perforated dissipative silencer, whose characteristics are detailed in Table 4.5. The mesh considered to compute the silencer TL consists of eight-noded quadratic quadrilateral elements whose approximate size is 0.0075 m to obtain an accurate solution (this provides more than 10 quadratic elements per wavelength for the maximum frequency $f_{max} = 3200$ Hz considered in the simulations). The parameters defining the perforated surface are $\sigma = 0.2$, $t_p = 0.001$ m, and $d_h = 0.0035$ m.

Geometry	L_i/L_o (m)	R_d (m)	L_{ch} (m)	R_{ch} (m)
1	0.1	0.0268	0.3	0.091875

Table 4.5: Geometry under study: L, length; R, radius; i, inlet; o, outlet; d, duct; ch, chamber.

The materials used in the computations are E fibreglass, basalt wool and Owens-Corning texturized fibreglass, their properties being detailed in Table 4.6 (for further details see Section 2.6.2).

Material	E fibreglass	Basalt wool	Texturized fibreglass
a_1	0.220	0.218	0.189
a_2	-0.585	-0.605	-0.595
a_3	0.201	0.128	0.160
a_4	-0.583	-0.675	-0.577
a_5	0.095	0.060	0.095
a_6	-0.669	-0.766	-0.754
a_7	0.169	0.138	0.085
a_8	-0.571	-0.628	-0.0732

Table 4.6: Coefficients and exponents for the calculation of the equivalent acoustic properties for the absorbent materials under study.

The mean flow is defined by the Mach number at the inlet section M_i and the local value $M(x)$ is obtained considering continuity of mass flow.

I. Influence of axial temperature gradients on the attenuation

To assess the influence of axial gradients on the acoustic performance of dissipative silencers, the distributions detailed in Table 4.7 are studied (for further information see Figure 3.3). All these gradients have the same average value of temperature, given by $T_{avg} = 250$ °C. The inlet mean flow Mach number is given by $M_i = 0.1$.

Case	$T_{r_1}(R_d)$	$T_{r_2}(R_m)$	$T_{r_3}(R_{ch})$	$T_{r_4}(R_d)$	$T_{r_5}(R_m)$	$T_{r6}(R_{ch})$	T_{avg}
1a	300	300	300	200	200	200	250
2a	350	350	350	150	150	150	250
3a	400	400	400	100	100	100	250

Table 4.7: Temperatures (°C) for the definition of axial thermal gradients, cases 1a-3a.

The results obtained for the temperature fields detailed in Table 4.7 are depicted in Figure 4.12. Also a calculation with a uniform temperature field of value $T_{avg} = 250$ °C is included for comparison.
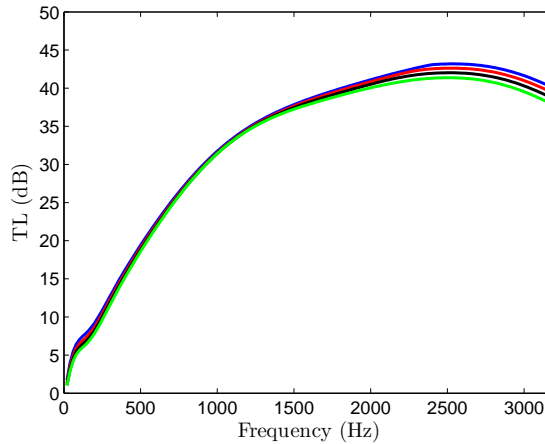

Figure 4.12: Transmission loss of a dissipative silencer containing basalt wool with axially-varying temperature distributions (same average temperature of 250 °C): ——, 250 °C, uniform; ——, case 1a; ——, case 2a; ——, case 3a.

As can be observed in Figure 4.12, higher axial thermal gradients lead to a reduction in the transmission loss at high frequencies, while no significant differences are found at low and mid frequencies, even for considerable gradients. For the cases under study, not taking into consideration the thermal gradients leads to a slight overestimation of the attenuation. The maximum discrepancy appears in case 3a at 3200 Hz, its value being approximately 5%. Therefore, it seems that including axial gradients and their associated thermal effects is only necessary if accurate predictions are required in the high frequency range, while an average temperature provides a reasonable accuracy at lower frequencies.

$Case$	$T_{r_1}(R_d)$	$T_{r_2}(R_m)$	$T_{r_3}(R_{ch})$	$T_{r_4}(R_d)$	$T_{r_5}(R_m)$	$T_{r_6}(R_{ch})$	T_{avg}
4a	400	400	400	200	200	200	300
5a	500	500	500	200	200	200	350

Table 4.8: Temperatures (°C) for the definition of axial thermal gradients, cases 4a and 5a.

Further transmission loss results appear in Figure 4.13, considering cases 1a and 4a-5a (see Table 4.8) for both E fibreglass and Owens-Corning texturized fibres. In the computations a value of $M_i = 0.1$ has been considered.
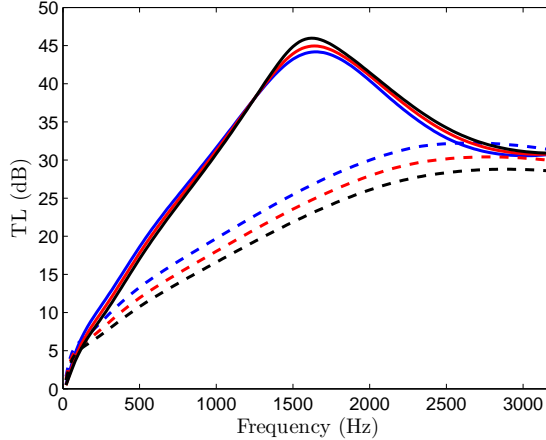
Figure 4.13: Transmission loss of a dissipative silencer with axially-varying temperature distributions: ──────, case 1a, Owens-Corning texturized fibreglass; ──────, case 4a, Owens-Corning texturized fibreglass; ──────, case 5a, Owens-Corning texturized fibreglass; ─ ─ ─, case 1a, E fibreglass; ─ ─ ─, case 4a, E fibreglass; ─ ─ ─, case 5a, E fibreglass.

Comparing the attenuation results delivered by both fibres it can be observed that E fibreglass achieves a lower transmission loss value in almost all the frequency range. For

this material of high resistivity the acoustic performance deteriorates as the axial gradient and average temperature increase. However, in the case of the Owens-Corning texturized fibreglass, it is worth emphasizing that the influence of the average temperature and its associated gradient is less relevant than in the E fibreglass case. For this less resistive material, a small difference in the silencer performance is observed initially when changing from case 1a to case 5a up to approximately 1250 Hz, where a transition point appears. Beyond this transition point, the previous trend changes and the acoustic behaviour shows a slight improvement when the temperature and the associated gradient increases, since the silencer seems more effective at attenuating sound in case 5a. Further computations show that the aforementioned transition frequency also appears for higher material resistivity (E fibreglass and basalt wool), but the associated frequencies are beyond the frequency limits considered in this Thesis.

As can be deduced from the previous results, material resistivity seems to be a very influential property when modelling thermal effects. The resistivity values detailed in Table 4.9 show that there are big differences between the different materials. From equation (3.10) it can be deduced that an increase in the average resistivity of the absorbent material is obtained for higher mean temperatures, in this case for configuration 5a.

Case	R_{avg} (rayl/m) E fibreglass	R_{avg} (rayl/m) Basalt wool	R_{avg} (rayl/m) Texturized fibreglass	T_{avg} (°C)
1a	43025	19348	6858	250
4a	45408	20420	7238	300
5a	47691	21447	7602	350

Table 4.9: Average resistivity and temperature for the absorbent materials.

Now, for isolating the impact of axial gradients corresponding to the E fibreglass and the Owens-Corning texturized fibres, several computations have been carried out and the results are shown in Figure 4.14. All the configurations present the same average value and in addition, a computation with uniform temperature is included for comparison.

For both materials, higher axial gradients lead to a slight reduction of the attenuation, mainly in the high frequency range. If the axial temperature is neglected, overestimations can reach 5%. This value is similar to that obtained for basalt wool in Figure 4.12.

Therefore, the average temperature has a great impact on the acoustic performance for very resistive materials (see Figure 4.13), while this effect is smaller for less resistive
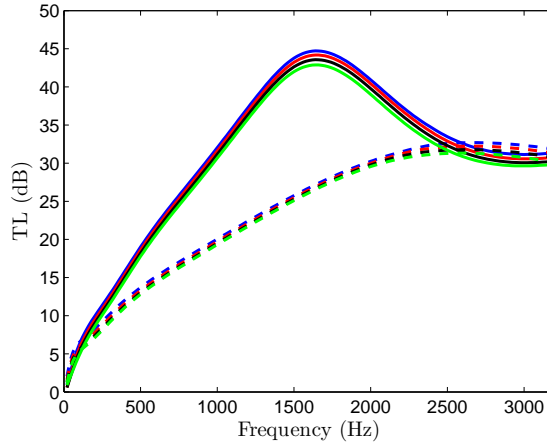
Figure 4.14: Transmission loss of a dissipative silencer with axially-varying temperature distributions (same average temperature of 250 °C): ——, 250 °C, uniform, Owens-Corning texturized fibreglass; ——, case 1a, Owens-Corning texturized fibreglass; ——, case 2a, Owens-Corning texturized fibreglass; ——, case 3a, Owens-Corning texturized fibreglass; – – –, 250 °C, uniform, E fibreglass; – – –, case 1a, E fibreglass; – – –, case 2a, E fibreglass; – – –, case 3a, E fibreglass.

materials. When the axial gradient has been studied separately (see Figures 4.12 and 4.14), lower influence is found in general, more concentrated in the high frequency range, and the resistivity does not seem to play such an important role.

II. Impact of radial temperature gradients

The values that define the radial temperature fields used in the transmission loss predictions are provided in Table 4.10 (for further information see Figure 3.3). The results of these calculations are shown in Figure 4.15. All of them present the same average value of 231 °C. In addition, an attenuation curve provided by a computation with uniform temperature field ($T = 231$ °C) has been included. Also a mean flow of $M_i = 0.1$ is considered in all the computations.

Figure 4.15 shows that considerable differences appear between the attenuation curves when considering radial gradients. Thus, it is clear that neglecting these temperature variations can lead to a systematic overestimation of the transmission loss, the effect being stronger as the gradients increase. Taking as reference the configuration with uniform temperature, the maximum difference for case 1b is 9% at 1980 Hz, for

Case	$T_{r_1}(R_d)$	$T_{r_2}(R_m)$	$T_{r_3}(R_{ch})$	$T_{r_4}(R_d)$	$T_{r_5}(R_m)$	$T_{r_6}(R_{ch})$	T_{avg}
1b	300	235	200	300	235	200	231
2b	410	242	150	410	242	150	231
3b	520	249	100	520	249	100	231

Table 4.10: Temperatures (°C) for the definition of radial thermal gradients, cases 1b-3b.

case 2b is given by 20% at 2060 Hz and finally, for case 3b the difference is 28% at 2160 Hz. Therefore, using an average value does not necessarily provide an accurate computation of the acoustic performance. Note that, although the particular values of radial temperature gradient used for 2b and 3b cases have been exaggerated deliberately, the heat transfer through the outer shell can be considerable, which justifies the need to include transverse temperature variations in the silencer noise attenuation calculations [65].

Figure 4.15: Transmission loss of a dissipative silencer containing E fibreglass with radially-varying temperature distributions (same average temperature of 231 °C): ———, 231 °C, uniform; ———, case 1b; ———, case 2b; ———, case 3b.

Two distributions with different radial gradients and mean temperatures are listed in Table 4.11 (see Figure 3.3), while the transmission loss results calculated for E fibreglass are depicted in Figure 4.16. Case 1b has also been included, as well as a computation considering a uniform field of 200 °C. As can be observed in the figure, the impact on the attenuation of high temperature and the associated radial gradient is relevant. The silencer attenuation drops as the temperature and thermal gradient are higher. A possible reason may be associated with a saturation effect due to

the high resistivity of E glass, which increases as the average temperature rises, and partially prevents the sound energy from penetrating the material for the frequency range under analysis.

Case	$T_{r_1}(R_d)$	$T_{r_2}(R_m)$	$T_{r_3}(R_{ch})$	$T_{r_4}(R_d)$	$T_{r_5}(R_m)$	$T_{r_6}(R_{ch})$	T_{avg}
4b	250	218	200	250	218	200	216
5b	350	253	200	350	253	200	247

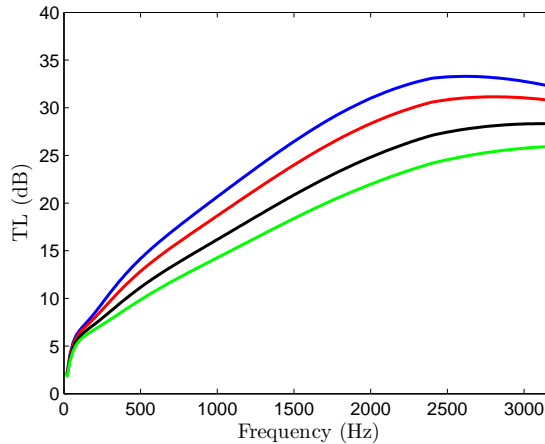Table 4.11: Temperatures (°C) for the definition of radial thermal gradients, cases 4b and 5b.

Figure 4.16: Transmission loss of a dissipative silencer containing E fibreglass with radially-varying temperature distributions: ——, 200 °C, uniform; ——, case 4b; ——, case 1b; ——, case 5b.

In Figure 4.17, a comparison between predictions for cases 1b, 2b and 3b is carried out considering Owens-Corning texturized fibreglass. Also a configuration with a uniform temperature value of 231 °C is included. The transmission loss curves appear to be quite similar in the frequency range depicted, with only some relevant differences close to 1500 Hz. At low frequencies, higher gradients lead to a systematic reduction of the attenuation performance, while an irregular influence is found in the mid and high frequency range. Thus, previous conclusions obtained from Figure 4.15 for the combination of radial gradient and E fibreglass no longer hold for materials with lower resistivity values, since only a slight influence of the radial gradient is found in general.
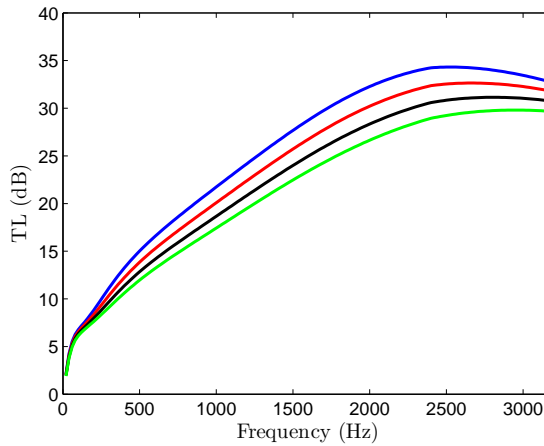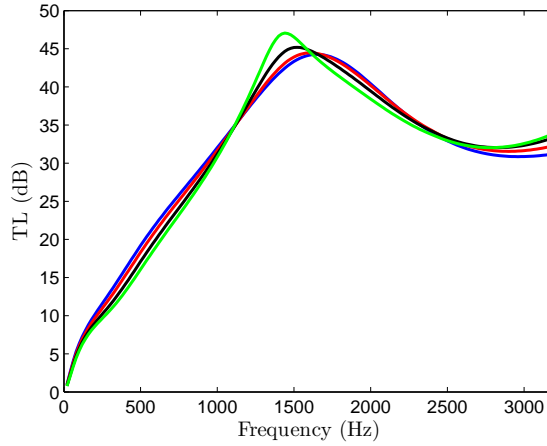
Figure 4.17: Transmission loss of a dissipative silencer containing Owens-Corning fibreglass with radially-varying temperature distributions (same average temperature of 231 °C): ——, 231 °C, uniform; ——, case 1b; ——, case 2b; ——, case 3b.

III. General thermal gradients and TL computations with average value

More general temperature fields are studied in this section, where both axial and radial gradients are considered simultaneously. The temperature values to compute the temperature field are detailed in Table 4.12 (for further information see Figure 3.3). All the configurations under study present the same average temperature given by $T_{avg} = 185$ °C. Previous results show that axial gradients do not have a relevant influence on the acoustic performance, while the radial thermal variations present a more significant influence for materials with a mid and high material airflow resistivity. Therefore, it is expected that the simultaneous presence of both gradients will modify the silencer attenuation performance for basalt wool and E fibreglass, while Owens-Corning texturized fibreglass will show a smaller effect.

Case	$T_{r_1}(R_d)$	$T_{r_2}(R_m)$	$T_{r_3}(R_{ch})$	$T_{r_4}(R_d)$	$T_{r_5}(R_m)$	$T_{r_6}(R_{ch})$	T_{avg}
1c	300	210	160	200	168	150	185
2c	400	254	175	200	129	90	185

Table 4.12: Temperatures (°C) for the definition of temperature fields, cases 1c and 2c.

The acoustic behaviour of a silencer considering general thermal gradients is depicted in Figure 4.18. The transmission loss associated with a uniform field defined by a value of 185 °C is also considered for comparison. The inlet mean flow Mach

number in the computations is $M_i = 0.1$. As expected, depending on the material, different trends are found. For the texturized fibreglass the maximum difference between the different predictions is approximately 2 dB, thus confirming the limited impact of the thermal gradient and justifying the use of a simplified approach with an average temperature value. For the E fibreglass, whose resistivity is high, it is worth emphasizing that, even when the average temperature is quite similar for all the calculations, the attenuation overprediction assuming a uniform temperature field can be significant. This effect becomes stronger as the thermal gradients are higher. The maximum TL difference between the uniform temperature field and case 1c is about 3 dB, while a higher discrepancy of about 5 dB is found at 1920 Hz between the uniform temperature predictions and case 2c. These results seem to indicate that, for general temperature fields including radial gradients in relatively resistive materials, an accurate and reliable prediction of the attenuation performance cannot be guaranteed if an average temperature value is considered.
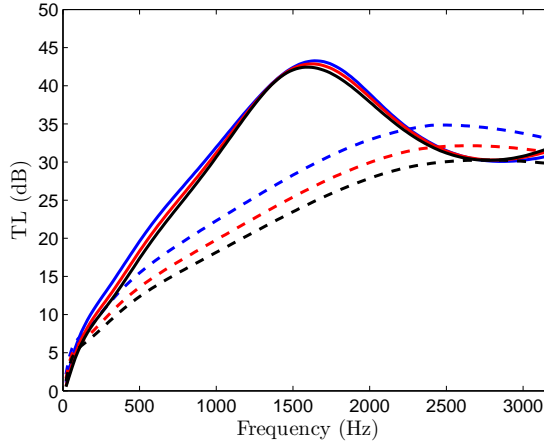
Figure 4.18: Transmission loss of a dissipative silencer with general temperature fields (same average temperature of 185 °C): ———, uniform, Owens-Corning fibreglass; ———, case 1c, Owens-Corning fibreglass; ———, case 2c, Owens-Corning fibreglass; ‑ ‑ ‑, uniform, E fibreglass; ‑ ‑ ‑, case 1c, E fibreglass; ‑ ‑ ‑, case 2c, E fibreglass.

IV. Considerations about mean flow

In order to study the influence of mean flow, several computations have been carried out considering the temperature fields detailed in Table 4.13 (for further information see Figure 3.3) and different Mach numbers: $M_i = 0$, 0.1 and 0.2. It should be

noted here that the two configurations under study present the same temperature distribution at the outlet section.

Case	$T_{r_1}(R_d)$	$T_{r_2}(R_m)$	$T_{r_3}(R_{ch})$	$T_{r_4}(R_d)$	$T_{r_5}(R_m)$	$T_{r_6}(R_{ch})$	T_{avg}
1d	400	335	300	300	235	200	281
2d	500	435	400	300	235	200	331

Table 4.13: Temperatures ($^\circ$C) for the definition of radial thermal gradients, cases 1d and 2d.

The results for basalt wool and the temperature distributions corresponding to cases 1d and 2d are shown in Figure 4.19.
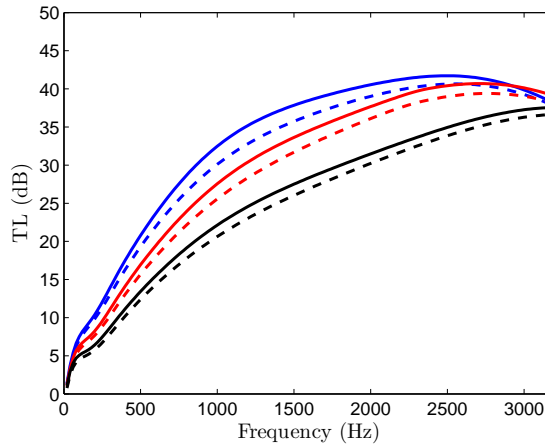
Figure 4.19: Transmission loss of a dissipative silencer containing basalt wool with general temperature fields and mean flow: ———, $M_i = 0$, case 1d; – – –, $M_i = 0$, case 2d; ———, $M_i = 0.1$, case 1d; – – –, $M_i = 0.1$, case 2d; ———, $M_i = 0.2$, case 1d; – – –, $M_i = 0.2$, case 2d.

In general, increasing the inlet Mach number while keeping the same temperature field yields a detrimental influence of the mean flow in almost all the frequency range under consideration, except in the highest part of the interval depicted in the figure. This is consistent with other results found in the literature [104] in the presence of mean flow at room temperature, where an increment in the mean flow velocity supposes a reduction in transmission loss. For a given inlet mean flow, higher average temperature and thermal gradients lead to lower attenuation in the frequency interval considered. However, the transition frequency for the case with $M_i = 0$ has shifted to lower frequencies and it is slightly higher than 3200 Hz (the intersection between the

solid blue line and dash blue line can be inferred from the figure 4.19). This transition shifts towards higher frequencies beyond the figure limits as the mean flow velocity rises. Note that, for a given thermal field, as the temperature decreases along the central passage, opposite density and speed of sound variations take place, resulting in a small reduction between the inlet and outlet Mach numbers.

4.7.3   Shape optimization in multichamber silencers

There are many geometric parameters that can have an influence over the acoustic performance of multichamber silencers such as the number of chambers, their lengths and radii and the thickness of dividing baffles. The characteristics of the central surfaces are also very influential, as well as the fibre in the particular case of a dissipative silencer. Therefore, in order to determine the optimal configuration of a multichamber silencer, a shape optimization procedure is a useful tool to obtain the most suitable design parameters for the case under study.

I. Optimization of a multichamber silencer with a sintered central duct of constant impedance

A three-chamber silencer is shown in Figure 4.20, where its main dimensions (see Table 4.14), as well as its different subdomains are defined. This silencer has been optimized, keeping the external geometry (the total length of the silencer $L_{tot} = L_{ch_1} + t_{ch_{12}} + L_{ch_2} + t_{ch_{23}} + L_{ch_3}$ and the chamber radii) and considering that the impedance of the sintered duct is a variable of the problem. In this case, the acoustic impedance of the sintered passage has been defined as $Z = AZ_0$, where A is a constant parameter, whose value is different for each individual of the population, and Z_0 is the characteristic impedance of air. The constant is defined in the interval between 0.05 and 4 with a step of 0.05. For this particular example, the frequency range of interest for carrying out the optimization process is 0 Hz - 1200 Hz.

Geometry	L_i/L_o	R_d	$L_{ch_{1-3}}$	$R_{ch_{1-3}}$	$t_{ch_{12-23}}$	L_{tot}
1	0.1	0.0268	0.183	0.0886	0.001	0.551

Table 4.14: Dimensions (m) of the three-chamber silencer with sintered duct.

The transmission loss achieved by some of the configurations obtained during the optimization process have been represented in Figure 4.21. As can be appreciated from the figure, in the frequency range of interest the most suitable configurations are
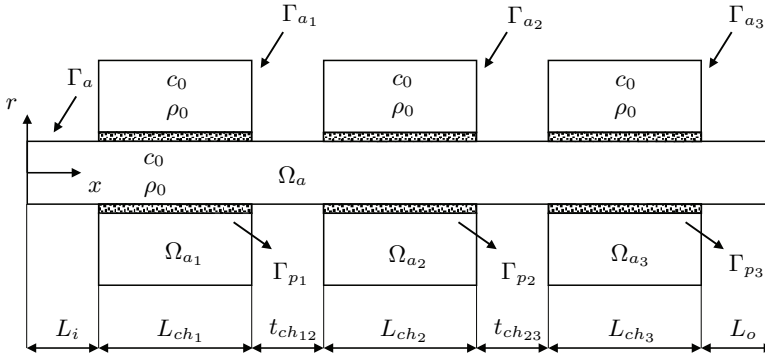
Figure 4.20: Three-chamber silencer with a central perforated duct.

those with impedances of value $Z = Z_0$ and $Z = 1.5Z_0$. In this case, the discrepancies between them in transmission loss are not very relevant in the frequencies under study (0 Hz - 1200 Hz). However, the configuration with $Z = 1.5Z_0$ provides better results in the frequency range between 1860 Hz and 2780 Hz approximately. Finally, at very high frequencies the best configuration is the one with an impedance given by $Z = 2Z_0$, from approximately 2780 Hz until 3200 Hz.
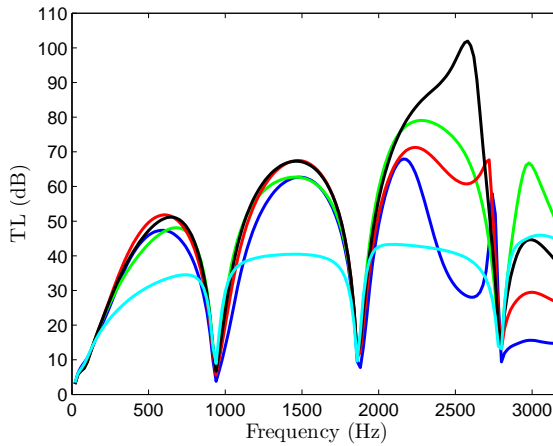
Figure 4.21: Transmission loss of a silencer with a sintered duct considering several impedance values: ———, A=0.5; ———, A=1; ———, A=1.5; ———, A=2; ———, A=4.

Note that TL values up to 100 dB could be unrealistic in practice due to viscosity of the air and the corresponding dissipative mechanisms.

II. Multichamber silencer optimization with a microperforated duct

Figure 4.23 depicts the TL of two three-chamber silencers (see Figure 4.22) including microperforated ducts with the same characteristics: $\sigma = 0.02$, $d_h = 0.001$ m and $t_p = 0.001$ m. The total length of the silencer is 0.551 m (the inlet and the outlet ducts are not included). The radius of the chamber is constant, while the length of the chambers and the thickness of the separating plates between them are variable. For this particular example, the frequency range in which the optimization process has been carried out is again 0 Hz - 1200 Hz. Thus, by optimizing the length of the chambers, the attenuation achieved at low frequencies increases, since the TL pass-band at approximately 1000 Hz (the chamber length equals half the wavelength) can be eliminated due to the acoustic effects produced when the chambers have different lengths. The dimensions of the silencer after the optimization procedure are detailed in Table 4.15.
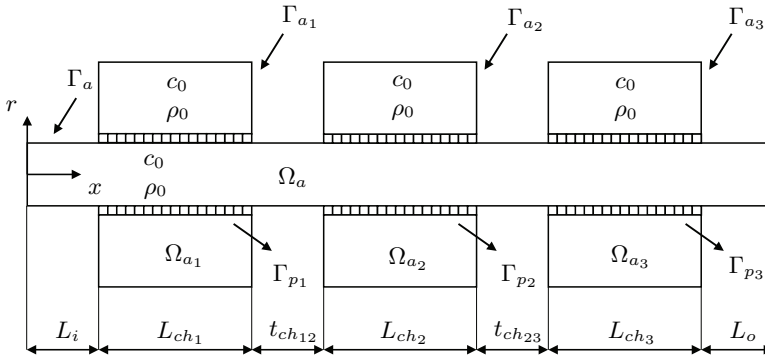
Figure 4.22: Three-chamber silencer with a central microperforated duct.

Geometry	L_i/L_o	R_d	L_{ch_1}	$t_{ch_{12}}$	L_{ch_2}	$t_{ch_{23}}$	L_{ch_3}	$R_{ch_{1-3}}$
Before	0.1	0.0268	0.0183	0.001	0.183	0.001	0.183	0.0886
After	0.1	0.0268	0.245	0.017	0.13	0.025	0.133	0.0886

Table 4.15: Dimensions (m) of the three-chamber silencer with microperforated duct.
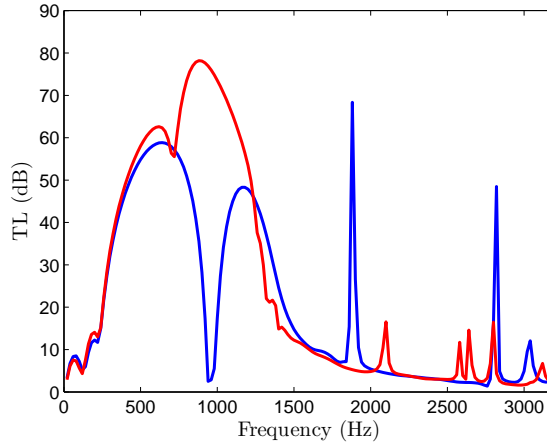
Figure 4.23: Transmission loss of multichamber silencer with a microperforated duct: ——, before optimization procedure; ——, after optimization procedure.

4.7.4 Comparison of surfaces

Figure 4.24 presents the comparison of the transmission loss associated with two multichamber silencers (both composed of three chambers). The first configuration has been computed twice. First considering a sintered central duct with an impedance of value $Z = 1.5Z_0$ and the second, with an impedance $Z = 2Z_0$. On the other hand, the second configuration under consideration is a perforated dissipative silencer containing Owens-Corning texturized fibreglass with $R = 4896$ rayl/m. The geometric characteristics of the silencers are detailed in Table 4.14. The characteristics of the perforated surface are $\sigma = 0.1$, $t_p = 0.001$ m, and $d_h = 0.0035$ m. As pointed out in Section 3.5.2, a sintered configuration improving the attenuation achieved at high frequencies by a perforated dissipative silencer can be found.

In addition, a four-chamber silencer is compared to a single chamber silencer considering different configurations according to their inner components, such as sintered ducts, microperforated surfaces and/or perforated ducts with absorbent material. The characteristics of the silencers are listed in Table 4.16. The total length is kept constant (0.3 m, not including inlet/outlet lengths) for all the silencers during the computations. For the four-chamber geometry, equal length is considered for all the subchambers within the silencer. The characteristics of the microperforated duct are $\sigma = 0.02$, $t_p = 0.001$ m, and $d_h = 0.001$ m, while the perforated duct is defined by $\sigma = 0.11$, $t_p = 0.001$ m, and $d_h = 0.003$ m.
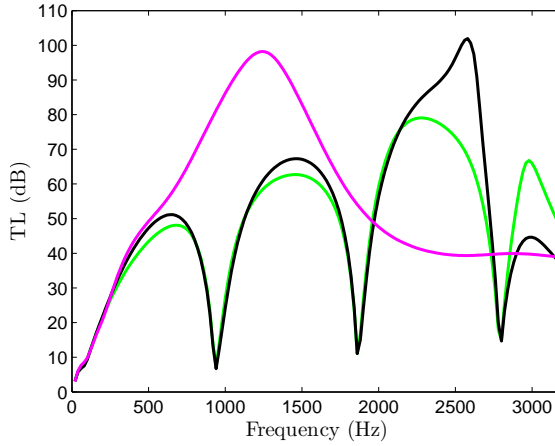
Figure 4.24: TL comparison of a silencer with a sintered duct and a perforated dissipative silencer: ▬▬, sintered duct, $Z = 1.5Z_0$; ▬▬, sintered duct, $Z = 2Z_0$; ▬▬, perforated dissipative silencer.

Geometry	L_i/L_o (m)	R_d (m)	L_{ch} (m)	R_{ch} (m)	t_{ch} (m)
1 chamber	0.1	0.0268	0.3	0.0886	-
4 chambers	0.1	0.0268	0.07425	0.0886	0.001

Table 4.16: Dimensions of the multichamber silencers.

Figure 4.25 shows that higher attenuation is obtained in general as the number of chambers increases [8], except in the low frequency range (from 20 Hz until 280 Hz approximately), where the single chamber configuration achieve higher TL values. Comparing the performance of the three different surfaces for the four-chamber silencer, at low frequencies the microperforated one reaches the highest TL value in the 360 Hz - 720 Hz frequency range, showing a peak at 540 Hz where the maximum attenuation value is achieved. On the other hand, the dissipative silencer provides more attenuation from 720 Hz until 1240 Hz than the other configurations, while from 1240 Hz until 2640 Hz, the multichamber geometry with sintered ducts shows higher TL than the other two configurations (except for a small range between 2240 Hz and 2320 Hz, where the dissipative silencer provides a better attenuation). Finally, in the 2640 Hz - 3200 Hz frequency range, the transmission loss obtained by the silencer containing absorbent material is again higher, but very close to the sintered configuration. Therefore, these results show that microperforated and sintered surfaces can be good alternatives to dissipative silencers, depending on the frequency range of interest for each particular application.
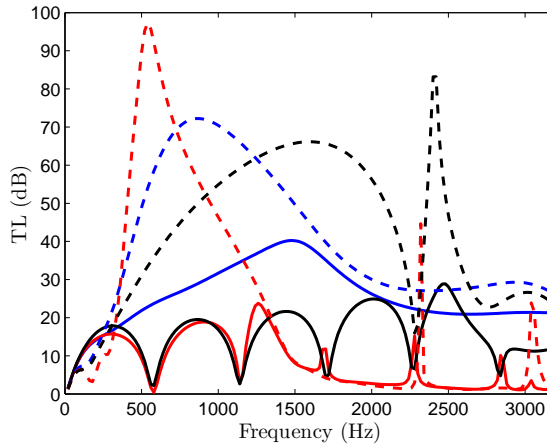
Figure 4.25: Comparison of transmission loss: ——, perforated dissipative silencer, 1 chamber; ——, microperforated duct, 1 chamber; ——, sintered duct, 1 chamber; – – –, perforated dissipative silencer, 4 chambers; – – –, microperforated duct, 4 chambers; – – –, sintered duct, 4 chambers.

Different surfaces can also be combined within a multichamber silencer. A comparison of the results obtained by combining microperforated ducts with sintered surfaces is shown in Figure 4.26. For the geometrical information, see Table 4.17.

Geometry	L_i/L_o (m)	R_d (m)	$L_{ch_{1-4}}$ (m)	$R_{ch_{1-4}}$ (m)	$t_{ch_{1-3}}$ (m)
4 chambers	0.1	0.0268	0.12425	0.075	0.001

Table 4.17: Dimensions of a long multichamber silencer(total length $L_{tot} = 0.5$ m).

The results obtained show that combining surfaces can improve the behaviour of the silencer in those frequencies where other alternatives are better. The dominant surface can be, for example, the one present in a higher number of chambers or the type of the duct associated with the longest chamber, depending on the particular configuration under study. This surface combination is intended to improve the levels of attenuation in the frequency range where the effect of the dominant surface is worse, at the expense of decreasing the maximum attenuation achieved for this kind of screen.
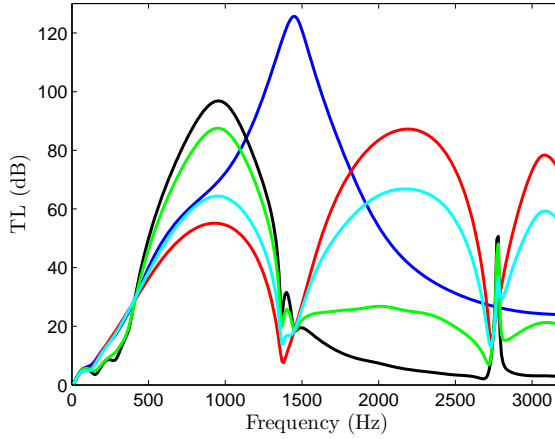
Figure 4.26: TL comparison of several configurations: ———, four chambers with absorbent material and perforated duct; ———, four chambers with sintered duct; ———, four chambers with microperforated duct; ———, three chambers with microperforated duct and one chamber with sintered duct; ———, three chambers with sintered duct and one chamber with microperforated duct.

4.8   Conclusions

In this chapter, a multidimensional FE formulation has been developed to study the acoustic performance of perforated dissipative silencers, in which the propagation media are not homogeneous. The application of this method can be justified due to the lack of accuracy of the plane wave models and other techniques for complex geometries and silencers with non-uniform properties. The aim of this formulation is to bridge some existing deficiencies found in commercial programs when perforated dissipative configurations under more realistic working conditions are considered, such as the presence of high temperature, thermal-induced heterogeneities, non-uniform mean flow as well as other variable properties of the propagation media.

The formulation developed considers a hybrid approach, based on the combination of a velocity potential-based wave equation and a pressure formulation. This permits taking into account a heterogeneous bulk density of the absorbent material, as well as thermal gradients inside the silencer. For that, a suitable form of the wave equation for a moving medium written in terms of velocity potential is required in the central duct to simplify the computations. On the other hand, the corresponding wave equation for the absorbent material domain can be expressed in terms of acoustic pressure

when considering a stationary (non-moving) medium. The coupling between both formulations has been carried out by means of the perforated duct impedance, which also permits the introduction of the absorbent material property variations through the resistivity. The effect of a non-uniform mean flow caused by the presence of thermal gradients within the silencer is also included in the acoustic impedance of the perforated screen. These heterogeneities lead to a spatial variation of the coupling and also to additional convective terms in the wave equations. The main limitations of the method can be, among others: the high computational requirements required by a FE formulation in comparison with analytical and semi-analytical methods on the one hand, and on the other, that the flow noise is not considered due to the low Mach numbers usually found in the exhaust systems (lower than 0.3).

The acoustic behaviour of a dissipative silencer has been studied in the presence of a heterogeneous absorbent material in the outer chamber. In order to validate this approach, several computations have been carried out in the absence of flow to compare the corresponding predictions, with results calculated using a pressure-based wave equation, showing a good agreement. The influence of a number of bulk density distributions on the silencer performance has then been analysed in the presence of mean flow. It has been shown that the density distribution plays an important role in the FE acoustic predictions. Thus, in order to obtain more accurate results, it is reasonable to consider the density distribution instead of an average value if possible. The acoustic impact of the radial density variations has been shown to be more relevant than in the axial case. In addition, if density radially increases, higher transmission loss is obtained, while lower attenuation is achieved for decreasing bulk density in the radial direction.

Also, the acoustic performance of a dissipative silencer subjected to high temperature and thermal gradients has been considered. A detailed analysis of the silencer behaviour has shown that, for an accurate prediction, it is necessary to include the temperature effects when modelling the sound propagation. For high resistivity materials, increasing the mean temperature has been shown to deliver a general reduction in the sound attenuation. Similar conclusions have been found for axial and radial thermal gradients, although axial temperature variations have exhibited a reduced impact. Therefore, a suitable representation of the thermal effects is required to avoid an overestimation of the silencer performance. For less resistive materials, an increase in temperature and/or thermal gradient has led to a slight drop in the silencer performance in the low to mid frequency range but the opposite trend has been found at higher frequencies, the transition point shifting to higher frequencies as the temperature gradient and/or mean flow rise. In general, for some silencer configurations it may be relatively accurate to approximate the temperature field by using a uniform profile considering an average value. It has been shown, however, that this

is not always possible, the model implemented here being primarily intended for use with bulk materials having medium to high airflow resistivities. In this latter case, attenuation overestimation is likely to be predicted if the temperature distribution is not taken into account, justifying the current numerical implementation. In addition, the influence of the mean flow on the transmission loss is consistent with earlier results obtained at room temperature, with higher Mach numbers leading to a drop in the silencer performance.

Finally, an optimization procedure has been carried out to obtain the most suitable configuration of a multichamber silencer in a given frequency range, depending on the particular characteristics of the geometry and the type of surface in the central duct. Silencers incorporating sintered passages have shown to be a good alternative when compared to geometries with microperforated ducts and perforated dissipative configurations in some particular cases. It should be noted that combining several kinds of surfaces, such as microperforated and sintered screens, can be useful from a practical point of view to obtain the suitable configuration for a particular design application.

Chapter 5

Efficient numerical approaches. Point collocation technique and mode-matching method

Summary:

In this chapter, the mode matching method (MM) and the point collocation technique (PC) are applied with the objective of accelerating the traditional FE computations for silencers with high temperature and thermal gradients based on a 3D formulation. Benefit is taken of the fact that, in general, automotive silencers have an arbitrary, but axially uniform, cross section. Under certain assumptions of axial uniformity, several techniques have been developed with a view to reduce the computational effort of a full three-dimensional FE analysis for dissipative silencers with temperature gradients and a central perforated passage carrying mean flow. These approaches are based on a suitable decomposition of the acoustic field into a set of transversal and axial modes within each silencer subdomain, and a matching procedure of the corresponding modal expansions at the silencer geometrical discontinuities through the continuity conditions of the acoustic pressure and axial velocity. The relative computational efficiency and accuracy of predictions for two matching schemes are reviewed here, including point collocation (at nodes and Gauss points) and also mode matching with weighted integration. Both techniques are applied to silencers with variable properties in the cross section and are compared among them, as well as with a general FE formulation, in terms of accuracy and computational cost.

5.1 Introduction

As observed in Chapter 4, the FEM is a very versatile technique, since it permits computing the acoustic performance of a silencer under more realistic working conditions, such as the presence of thermal gradients and the existence of mean flow. In addition, it permits analysing complex geometries. The main drawback of a 3D FE formulation is the high computational cost required to study the acoustic behaviour of a silencer when the number of degrees of freedom (nodal unknowns) increases, which implies certain limitations in design and optimization problems [110, 133, 148]. Kirby [100, 101] took benefit of the fact that most silencers in the automotive industry have an arbitrary, but axially uniform, cross section to set out a quadratic eigenvalue problem associated with the transversal section and to compute the corresponding wavenumbers (eigenvalues) and pressure modes (eigenvectors) using a 2D FE formulation. A suitable decomposition of the solution into transversal and axial modes was combined with the PC technique [100] and the MM method [101] to obtain the complete acoustic fields in all the silencer subdomains considering the continuity of the pressure and axial velocity at the geometric discontinuities. These approaches suppose an important reduction of the computation time; however, as Kirby [100, 101, 105] and Glav [80, 81] noticed, some numerical issues appear, such as those found in the PC technique, where predictions show a high sensitivity to the silencer geometry and the collocation grid.

In this chapter, an extension of the works developed by Kirby [100, 101, 105] is presented to provide some alternatives that are computationally efficient in comparison with a full 3D FE formulation. Thus, the PC technique and MM method are applied considering the existence of transversal temperature gradients and mean flow. The fact of simplifying the temperature field and not considering the axial temperature gradient seems reasonable in a number of practical applications because, as seen in Section 4.7.2, the influence of these gradients on the acoustic behaviour is considerably lower than the transversal ones.

The above-mentioned methods have a common starting point: in both it is necessary to obtain the eigenvalue problem associated with the transversal section of all the silencer subdomains to compute both the wavenumbers and their associated pressure modes. Following this step, how to apply and deal with the continuity conditions of the acoustic fields for both methods is detailed, this being the main difference between the different approaches regarding the algebraic equations required for computing the modal amplitudes of the waves in the involved silencer components. Finally, the silencer TL can be computed after solving the system of equations obtained previ-

ously. In addition, a comparison between these techniques and the 3D FE formulation developed in Section 4.5.2 is presented.

5.2 Quadratic eigenvalue problem associated with the cross section of the silencer

The longitudinal and transversal sections of a perforated dissipative silencer with an arbitrary, but axially uniform, cross section are shown in Figure 5.1. As is usual for this kind of silencers, they are composed of a central perforated duct carrying mean flow and an outer chamber containing dissipative fibre. The geometry is divided into four subdomains: the inlet/outlet pipes and a perforated central airway, denoted as Ω_i, Ω_a and Ω_o, respectively, and an outer chamber Ω_m containing absorbent material. In addition, the perforated surface is denoted as Γ_p. The air ($\Omega_i \cup \Omega_a \cup \Omega_o$) is characterized by means of its density ρ_0 and speed of sound c_0, while the absorbent material is defined by its equivalent density $\rho_m(x, y)$ and speed of sound $c_m(x, y)$, both being complex, frequency-dependent and function of the coordinates because of the transversal variation of the temperature. In principle, no axial temperature variations exist or, if present, they are considered small enough to have a relevant impact on the results. For higher thermal variations along the axis of the silencer, as a first approximation, the transversal thermal gradients could be considered axially uniform with temperature values given by the average of the temperatures at the inlet and outlet sections.
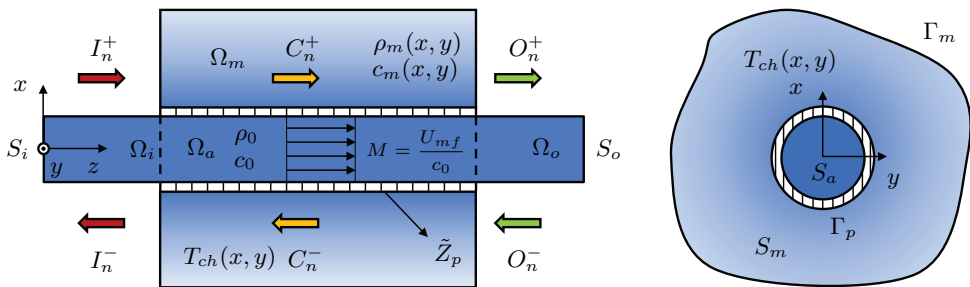

Figure 5.1: Geometry with an arbitrary cross section.

At this point, it should be noted that only the eigenvalue problem associated with the chamber and the perforated duct is detailed for illustration purposes, since once

this procedure is known, obtaining the eigenvalue problem associated with rigid wall pipes such as the inlet and outlet ducts is straightforward. Thus, considering now a pressure formulation, the governing equation of the sound propagation in the air (central duct) can be written as [126]

$$\frac{\partial^2 p_a}{\partial x^2} + \frac{\partial^2 p_a}{\partial y^2} + (1 - M^2)\frac{\partial^2 p_a}{\partial z^2} - 2jMk_0\frac{\partial p_a}{\partial z} + k_0^2 p_a = 0 \tag{5.1}$$

where p_a is the acoustic pressure, k_0 the wavenumber and M the Mach number. In the absorbent material region, the governing wave equation is [16, 63, 149]

$$\nabla\left(\frac{1}{\rho_m}\nabla p_m\right) + \frac{k_m^2}{\rho_m}p_m = 0 \tag{5.2}$$

where p_m is the acoustic pressure, k_m is the equivalent wavenumber and ρ_m the equivalent density of the absorbent material.

The transversal section is axially uniform and therefore, separation of variables can be applied as

$$p(x, y, z) = \Psi^{xy}(x, y)e^{-jk_z z} \tag{5.3}$$

$$\Psi^{xy}(x, y) = \begin{cases} \Psi_a^{xy}(x, y), & (x, y) \in S_a \\ \Psi_m^{xy}(x, y), & (x, y) \in S_m \end{cases} \tag{5.4}$$

where Ψ^{xy} is the transversal pressure mode and k_z the axial wavenumber. Then, substituting expressions (5.3) and (5.4) into (5.1) and (5.2) yields

$$\nabla^2\Psi_a^{xy} + (k_0^2 - 2Mk_0k_z - (1 - M^2)k_z^2)\Psi_a^{xy} = 0 \tag{5.5}$$

$$\nabla\left(\frac{1}{\rho_m}\nabla\Psi_m^{xy}\right) + \frac{1}{\rho_m}(k_m^2 - k_z^2)\Psi_m^{xy} = 0 \tag{5.6}$$

Then, a FE discretization of the silencer cross section is applied, together with the Green's theorem and the weighted residuals method to equations (5.5) and (5.6) leading to

$$\sum_{e=1}^{N_a^e}\left(\int_{S_a}(\nabla[N])^T\nabla[N]\mathrm{d}S + \int_{S_a}(-k_0^2 + 2Mk_0k_z + (1 - M^2)k_z^2)[N]^T[N]\mathrm{d}S\right)\{\Psi_a\}$$

$$= \sum_{e=1}^{N_a^e}\left(\int_{\Gamma_p}[N]^T\frac{\partial\Psi_a}{\partial n}\mathrm{d}\Gamma\right) \tag{5.7}$$

$$\sum_{e=1}^{N_m^e} \left(\int_{S_m} \frac{1}{\rho_m} (\nabla[N])^T \nabla[N] \mathrm{d}S + \int_{S_m} \frac{1}{\rho_m} (k_z^2 - k_m^2)[N]^T[N] \mathrm{d}S \right) \{\Psi_m\}$$
$$= \sum_{e=1}^{N_m^e} \left(\int_{\Gamma_m \cup \Gamma_p} \frac{1}{\rho_m} [N]^T \frac{\partial \Psi_m}{\partial n} \mathrm{d}\Gamma \right)$$
(5.8)

where $[N]$ is the shape functions vector, and $\{\Psi_a\}$ and $\{\Psi_m\}$ are the vectors containing the nodal unknowns related to the air and the absorbent material subdomains. In addition, N_a^e and N_m^e are the number of elements belonging to sections S_a and S_m respectively.

The outer wall of the chamber is rigid and impervious [126], that is

$$\nabla \Psi_m \vec{n}_m = 0, \qquad (x, y) \in \Gamma_m$$
(5.9)

where $\vec{n}_m$ is the outward normal unit vector. Therefore, applying equation (5.9), the integrals corresponding to the load terms of the equations (5.7) and (5.8) are evaluated only over the perforated screen. The coupling of the air and the absorbent material subdomains can be carried out by means of the perforated duct impedance, considering the continuity of the normal acoustic velocity [104, 126]. Thus, the kinematic condition can be written as

$$\vec{u}_a \vec{n}_a = u_{n_a} = -\vec{u}_m \vec{n}_m = -u_{n_m} = u_n$$
(5.10)

u_n being the normal acoustic velocity that can be obtained from the perforated impedance equation as

$$u_n = \frac{\Psi_a - \Psi_m}{\tilde{Z}_p}$$
(5.11)

Thereby taking into account the previous expressions and the relation between the normal acoustic velocity and the normal gradient of the pressure results in

$$\frac{\partial \Psi_a}{\partial n} = -\rho_0 (j\omega u_n - Mc_0 jk_z u_n) = -\rho_0 j\omega \left(1 - Mc_0 \frac{k_z}{\omega} \right) \frac{\Psi_a - \Psi_m}{\tilde{Z}_p}$$
(5.12)

$$\frac{\partial \Psi_m}{\partial n} = -\rho_m j\omega u_{n_m} = \rho_m j\omega u_n = \rho_m j\omega \frac{\Psi_a - \Psi_m}{\tilde{Z}_p}$$
(5.13)

and substituting equations (5.12) and (5.13) in expressions (5.7) and (5.8) respectively, the integral equations defined in (5.14) and (5.15) are obtained.

$$
\sum_{e=1}^{N_a^e} \left(\int_{S_a} (\nabla[N])^T \nabla[N] \mathrm{d}S \right.
$$

$$
+ \int_{S_a} (-k_0^2 + 2Mk_0k_z + (1-M^2)k_z^2)[N]^T[N]\mathrm{d}S \Bigg) \{\Psi_a\}
$$

$$
= \sum_{e=1}^{N_a^e} \left(\int_{\Gamma_p} \left(\frac{-j\omega\rho_0 + jMc_0\rho_0 k_z}{\tilde{Z}_p} \right) [N]^T[N]\mathrm{d}\Gamma \right) \{\Psi_a\} \tag{5.14}
$$

$$
+ \sum_{e=1}^{N_a^e} \left(\int_{\Gamma_p} \left(\frac{j\omega\rho_0 - jMc_0\rho_0 k_z}{\tilde{Z}_p} \right) [N]^T[N]\mathrm{d}\Gamma \right) \{\Psi_m\}
$$

$$
\sum_{e=1}^{N_m^e} \left(\int_{S_m} \frac{1}{\rho_m} (\nabla[N])^T \nabla[N] \mathrm{d}S + \int_{S_m} \frac{1}{\rho_m} (k_z^2 - k_m^2)[N]^T[N]\mathrm{d}S \right) \{\Psi_m\}
$$

$$
= \sum_{e=1}^{N_m^e} \left(\int_{\Gamma_p} \frac{j\omega}{\tilde{Z}_p} [N]^T[N]\mathrm{d}\Gamma \right) \{\Psi_a\} - \sum_{e=1}^{N_m^e} \left(\int_{\Gamma_p} \frac{j\omega}{\tilde{Z}_p} [N]^T[N]\mathrm{d}\Gamma \right) \{\Psi_m\} \tag{5.15}
$$

Thus, after assembling the element matrices related to the air subdomain, equation (5.14) can be written in compact form as

$$
([K_{aa}] + k_z[D_{aa}] + k_z^2[M_{aa}])\{\Psi_a\} + ([K_{am}] + k_z[D_{am}])\{\Psi_m\} = \{0\} \tag{5.16}
$$

where the following global matrices have be defined

$$
[K_{aa}] = \sum_{e=1}^{N_a^e} \left(\int_{S_a} (\nabla[N])^T \nabla[N]\mathrm{d}S - k_0^2 \int_{S_a} [N]^T[N]\mathrm{d}S + \int_{\Gamma_a} \frac{\rho_0 j\omega}{\tilde{Z}_p} [N]^T[N]\mathrm{d}\Gamma \right) \tag{5.17}
$$

$$
[D_{aa}] = 2Mk_0 \sum_{e=1}^{N_a^e} \left(\int_{S_a} [N]^T[N]\mathrm{d}S \right) - \sum_{e=1}^{N_a^e} \left(\frac{\rho_0 jMc_0}{\tilde{Z}_p} \int_{\Gamma_p} [N]^T[N]\mathrm{d}\Gamma \right) \tag{5.18}
$$

$$
[M_{aa}] = (1-M^2) \sum_{e=1}^{N_a^e} \left(\int_{S_a} [N]^T[N]\mathrm{d}S \right) \tag{5.19}
$$

$$
[K_{am}] = -\sum_{e=1}^{N_a^e} \left(\int_{\Gamma_p} \frac{\rho_0 j\omega}{\tilde{Z}_p} [N]^T[N]\mathrm{d}\Gamma \right) \tag{5.20}
$$

$$
[D_{am}] = \sum_{e=1}^{N_a^e} \left(\int_{\Gamma_p} \frac{\rho_0 jMc_0}{\tilde{Z}_p} [N]^T[N]\mathrm{d}\Gamma \right) \tag{5.21}
$$

After assembling the element matrices related to the absorbent material subdomain, equation (5.15) can be represented in compact form as

$$([K_{mm}] + k_z^2 [M_{mm}])\{\Psi_m\} + [K_{ma}]\{\Psi_a\} = \{0\} \tag{5.22}$$

the global matrices being

$$[K_{mm}] = \sum_{e=1}^{N_m^e} \left(\int_{S_m} \frac{1}{\rho_m} (\nabla[N])^T \nabla[N] \mathrm{d}S - \int_{S_m} \frac{k_m^2}{\rho_m} [N]^T [N] \mathrm{d}S \right. \\ \left. + \int_{\Gamma_p} \frac{j\omega}{\tilde{Z}_p} [N]^T [N] \mathrm{d}\Gamma \right) \tag{5.23}$$

$$[M_{mm}] = \sum_{e=1}^{N_m^e} \left(\int_{S_m} \frac{1}{\rho_m} [N]^T [N] \mathrm{d}S \right) \tag{5.24}$$

$$[K_{ma}] = -\sum_{e=1}^{N_m^e} \left(\int_{\Gamma_p} \frac{j\omega}{\tilde{Z}_p} [N]^T [N] \mathrm{d}\Gamma \right) \tag{5.25}$$

Then, the final system of equations yields

$$\left(\begin{bmatrix} [K_{aa}] & [K_{am}] \\ [K_{ma}] & [K_{mm}] \end{bmatrix} + k_z \begin{bmatrix} [D_{aa}] & [D_{am}] \\ [0] & [0] \end{bmatrix} \right. \\ \left. + k_z^2 \begin{bmatrix} [M_{aa}] & [0] \\ [0] & [M_{mm}] \end{bmatrix} \right) \left\{ \begin{matrix} \{\Psi_a\} \\ \{\Psi_m\} \end{matrix} \right\} = \left\{ \begin{matrix} \{0\} \\ \{0\} \end{matrix} \right\} \tag{5.26}$$

that can be rewritten as

$$([K] + k_z[D] + k_z^2[M])\{\Psi\} = \{0\} \tag{5.27}$$

where the following nomenclature has been considered

$$[K] = \begin{bmatrix} [K_{aa}] & [K_{am}] \\ [K_{ma}] & [K_{mm}] \end{bmatrix} \tag{5.28}$$

$$[D] = \begin{bmatrix} [D_{aa}] & [D_{am}] \\ [0] & [0] \end{bmatrix} \tag{5.29}$$

$$[M] = \begin{bmatrix} [M_{aa}] & [0] \\ [0] & [M_{mm}] \end{bmatrix} \tag{5.30}$$

$$\{\Psi\} = \left\{ \begin{matrix} \{\Psi_a\} \\ \{\Psi_m\} \end{matrix} \right\} \tag{5.31}$$

Then, the system of equations can be expressed as follows to solve the eigenvalue problem

$$\begin{pmatrix} [0] & [I] \\ -[M]^{-1}[K] & -[M]^{-1}[D] \end{pmatrix} \begin{Bmatrix} \{\Psi\} \\ k_z\{\Psi\} \end{Bmatrix} = k_z \begin{Bmatrix} \{\Psi\} \\ k_z\{\Psi\} \end{Bmatrix} \qquad (5.32)$$

where $[I]$ is an identity matrix.

Finally, once the eigenvalue problem is solved and the corresponding wavenumbers are obtained, the MM and PC techniques can be applied. According to the imaginary part of the wavenumber k_z, the attenuated waves can be classified as progressive and regressive. In the first, the imaginary part is negative, whereas in the second it is positive to guarantee an attenuated behaviour as the wave propagates. At this point, it should be pointed out that it is necessary to sort the eigenvalues and their associated wavenumbers before applying the above-mentioned methods [100]. This can be done by sorting the eigenvalues of the progressive and regressive waves by the modulus of the imaginary part.

5.3   Continuity of the acoustic fields

In this section, it is detailed how to obtain the full 3D acoustic pressure field, depending on the technique. First, the PC method is described, where the applied continuity conditions at the geometric discontinuities are enforced in a discrete number of points [100], whereas the MM technique considers the continuity conditions weighted and integrated along the sections corresponding to the geometric discontinuities [101]. Both methods consider the continuity of the same acoustic fields: (1) Acoustic pressure; (2) Axial acoustic velocity.

5.3.1   Point collocation technique

The continuity of the acoustic fields is applied pointwise at the area changes between the inlet/outlet ducts and the chamber. The solution of the eigenvalue problem provides information at the nodal level, which permits applying the continuity conditions at the nodes of the FE mesh. However, the number of degrees of freedom and the computational cost associated with the calculations considerably increase as the element size is refined. A possible alternative to reduce the number of collocation points and the computation time is to impose the continuity conditions at a single Gauss point [186] per element. In Section 5.5 the results obtained by using these two approaches are compared.

Compatibility conditions are provided by the physical requirements that acoustic pressure and axial velocity be equal at the expansion/contraction and that axial velocity normal to the rigid endplates be zero [100, 126]. Therefore, at the expansion of the silencer placed between the inlet duct and the chamber, the continuity conditions are

$$p_i(x,y,0) = p_a(x,y,0), \qquad (x,y) \in S_a \quad (\text{or } S_i) \tag{5.33}$$

$$u_{z_i}(x,y,0) = u_{z_a}(x,y,0), \qquad (x,y) \in S_a \quad (\text{or } S_i) \tag{5.34}$$

$$u_{z_m}(x,y,0) = 0, \qquad (x,y) \in S_m \tag{5.35}$$

while at the contraction between the chamber and the outlet yields

$$p_a(x,y,L_m) = p_o(x,y,0), \qquad (x,y) \in S_a \quad (\text{or } S_o) \tag{5.36}$$

$$u_{z_a}(x,y,L_m) = u_{z_o}(x,y,0), \qquad (x,y) \in S_a \quad (\text{or } S_o) \tag{5.37}$$

$$u_{z_m}(x,y,L_m) = 0, \qquad (x,y) \in S_m \tag{5.38}$$

where u_z is the axial velocity of the particle and L_m is the length of the outer chamber. The acoustic pressure and the axial velocity can be written in terms of modal expansions [80, 81, 100, 101, 104], in such a way that for the inlet duct, the sound pressure can be expressed as [100, 126]

$$p_i(x,y,z) = \sum_{n=1}^{\infty} (I_n^+ \Psi_n^+(x,y)e^{-jk_n^{I^+} z} + I_n^- \Psi_n^-(x,y)e^{-jk_n^{I^-} z}) \tag{5.39}$$

whereas the velocity is defined as

$$u_{z_i}(x,y,z) = \frac{1}{\rho_0 c_0} \sum_{n=1}^{\infty} \left(\frac{k_n^{I^+} I_n^+ \Psi_n^+(x,y)e^{-jk_n^{I^+} z}}{k_0 - Mk_n^{I^+}} + \frac{k_n^{I^-} I_n^- \Psi_n^-(x,y)e^{-jk_n^{I^-} z}}{k_0 - Mk_n^{I^-}} \right) \tag{5.40}$$

$k_n^{I^\pm}$ being the axial wavenumber, $I_n^\pm$ the modal amplitude and $\Psi_n^{I^\pm}(x,y)$ the n-th transversal pressure mode. The symbols $+$ and $-$ make reference to the progressive and the regressive wave, respectively.

For the outlet duct, the acoustic fields are

$$p_o(x,y,z) = \sum_{n=1}^{\infty} (O_n^+ \Psi_n^+(x,y)e^{-jk_n^{O^+} z} + O_n^- \Psi_n^-(x,y)e^{-jk_n^{O^-} z}) \tag{5.41}$$

$$u_{z_o}(x,y,z) = \frac{1}{\rho_0 c_0} \sum_{n=1}^{\infty} \left(\frac{k_n^{O^+} O_n^+ \Psi_n^+(x,y)e^{-jk_n^{O^+} z}}{k_0 - Mk_n^{O^+}} + \frac{k_n^{O^-} O_n^- \Psi_n^-(x,y)e^{-jk_n^{O^-} z}}{k_0 - Mk_n^{O^-}} \right) \tag{5.42}$$

It is important to note that progressive and regressive modes are equal when ducts are rigid (even when mean flow exists), and therefore, $\Psi_n^+(x,y) = \Psi_n^-(x,y)$ [126]. The fundamental mode consists of a plane wave, whose associated wavenumber can be expressed as

$$k_1^{I\pm} = \frac{\pm k_0}{1 \pm M} \tag{5.43}$$

As is usual in the computation of the transmission loss, the inlet duct is assumed to contain a incident plane wave only. Thus, equations (5.39) and (5.40) can be written as

$$p_i(x,y,z) = I_1^+ \Psi_1^{I^+} e^{-jk_1^{I^+} z} + \sum_{n=1}^{\infty} I_n^- \Psi_n^-(x,y) e^{-jk_n^{I^-} z} \tag{5.44}$$

$$u_{z_i}(x,y,z) = \frac{1}{\rho_0 c_0} \left(I_1^+ \Psi_1^{I^+} e^{-jk_1^{I^+} z} + \sum_{n=1}^{\infty} \frac{k_n^{I^-} I_n^- \Psi_n^-(x,y) e^{-jk_n^{I^-} z}}{k_0 - M k_n^{I^-}} \right) \tag{5.45}$$

where it can be assumed for simplicity that $I_1^+ \Psi_1^{I^+} = 1$.

Regarding the acoustic fields within the chamber, the acoustic pressure can be expressed as

$$p_c(x,y,z) = \sum_{n=1}^{\infty} (C_n^+ \Psi_n^+(x,y) e^{-jk_{z,n}^+ z} + C_n^- \Psi_n^-(x,y) e^{-jk_{z,n}^- z}) \tag{5.46}$$

where subscript c makes reference to the cross section that includes the chamber and the central duct, so $p_c = p_a$ in S_a and $p_c = p_m$ in S_m. Therefore, the axial acoustic velocity field is [100, 126]

$$u_{z_c}(x,y,z) = \begin{cases} u_{z_a}(x,y,z) = \dfrac{1}{\rho_0 c_0} \displaystyle\sum_{n=1}^{\infty} \left(\dfrac{k_{z,n}^+ C_n^+ \Psi_n^{A+}(x,y) e^{-jk_{z,n}^+ z}}{k_0 - M k_{z,n}^+} \right. \\ \left. + \dfrac{k_{z,n}^- C_n^- \Psi_n^{A-}(x,y) e^{-jk_{z,n}^- z}}{k_0 - M k_{z,n}^-} \right) \quad (x,y,z) \in \Omega_a \\[2em] u_{z_m}(x,y,z) = \dfrac{1}{\rho_m c_m} \displaystyle\sum_{n=1}^{\infty} \left(\dfrac{k_{z,n}^+ C_n^+ \Psi_n^{M+}(x,y) e^{-jk_{z,n}^+ z}}{k_m} \right. \\ \left. + \dfrac{k_{z,n}^- C_n^- \Psi_n^{M-}(x,y) e^{-jk_{z,n}^- z}}{k_m} \right) \quad (x,y,z) \in \Omega_m \end{cases} \tag{5.47}$$

If the acoustic pressure and axial velocity in equations (5.33)-(5.35) are substituted by the corresponding modal expansions defined by equations (5.39) and (5.40), as

well as (5.46) and (5.47), the following expressions are obtained

$$1 + \sum_{n=1}^{\infty} I_n^- \Psi_n^{I^-}(x,y) = \sum_{n=1}^{\infty} (C_n^+ \Psi_n^{A^+}(x,y) + C_n^- \Psi_n^{A^-}(x,y)) \quad (x,y) \in S_a \qquad (5.48)$$

$$\frac{1}{\rho_0 c_0} \left(1 + \sum_{n=1}^{\infty} \frac{k_n^{I^-} I_n^- \Psi_n^{I^-}(x,y)}{k_0 - M k_n^{I^-}} \right)$$
$$= \frac{1}{\rho_0 c_0} \sum_{n=1}^{\infty} \left(\frac{k_{z,n}^+ C_n^+ \Psi_n^{A^+}(x,y)}{k_0 - M k_{z,n}^+} + \frac{k_{z,n}^- C_n^- \Psi_n^{A^-}(x,y)}{k_0 - M k_{z,n}^-} \right) \quad (x,y) \in S_a \qquad (5.49)$$

$$\frac{1}{\rho_m c_m} \sum_{n=1}^{\infty} \left(\frac{k_{z,n}^+ C_n^+ \Psi_n^{M^+}(x,y)}{k_m} + \frac{k_{z,n}^- C_n^- \Psi_n^{M^-}(x,y)}{k_m} \right) = 0 \quad (x,y) \in S_m \qquad (5.50)$$

Equation (5.48) is enforced pointwise at N_a collocation points that will coincide with the nodes of the FE mesh or the Gauss points, depending on the case, in section $S_i \equiv S_a$. Similarly, equations (5.49) and (5.50) are applied at N_a and N_m collocation points belonging to sections S_a and S_m respectively. Besides, the modal expansions are truncated to a suitable number of terms to guarantee the solution of the problem. Then, N_a equations are obtained for the acoustic pressure field continuity condition. Thus, equation (5.48) can be written as follows

$$1 + \sum_{n=1}^{N_a} I_n^- \Psi_{n,q}^{I^-} = \sum_{n=1}^{N_a+N_m} (C_n^+ \Psi_{n,q}^{A^+} + C_n^- \Psi_{n,q}^{A^-}) \qquad (5.51)$$

where the subscript $q = 1, ..., N_a$ and $\Psi_{n,q}^{I^-}$ and $\Psi_{n,q}^{A^\pm}$ refer to the q-th component of the n-th modal pressure eigenvector for the inlet pipe and central passage respectively, while I_n^- and $C_n^\pm$ are the corresponding modal amplitudes. In the same way, equation (5.49) can be written as

$$1 + \sum_{n=1}^{N_a} \frac{k_n^{I^-} I_n^- \Psi_{n,q}^{I^-}}{k_0 - M k_n^{I^-}} = \sum_{n=1}^{N_a+N_m} \left(\frac{k_{z,n}^+ C_n^+ \Psi_{n,q}^{A^+}}{k_0 - M k_{z,n}^+} + \frac{k_{z,n}^- C_n^- \Psi_{n,q}^{A^-}}{k_0 - M k_{z,n}^-} \right) \qquad (5.52)$$

with $q = 1, ..., N_a$. Similarly, the modal summations in the axial acoustic velocity continuity equation (5.50) are truncated and enforced at the collocation points, obtaining N_m equations.

$$\sum_{n=1}^{N_m} \left(k_{z,n}^+ C_n^+ \Psi_{n,q}^{M^+} + k_{z,n}^- C_n^- \Psi_{n,q}^{M^-} \right) = 0 \qquad (5.53)$$

where $q = 1, ..., N_m$ is related to the *q-th* value of the transversal pressure mode associated with the dissipative chamber.

Following a similar approach with equations (5.36)-(5.38) and considering an anechoic termination $(O_n^- = 0 \ \forall n)$, yields

$$\sum_{n=1}^{\infty} \left(C_n^+ \Psi_n^{A^+}(x,y)e^{-jk_{z,n}^+ L_m} + C_n^- \Psi_n^{A^-}(x,y)e^{-jk_{z,n}^- L_m} \right)$$
$$= \sum_{n=1}^{\infty} O_n^+ \Psi_n^{O^+}(x,y) \quad (x,y) \in S_a \tag{5.54}$$

$$\frac{1}{\rho_0 c_0} \sum_{n=1}^{\infty} \left(\frac{k_{z,n}^+ C_n^+ \Psi_n^{A^+}(x,y)e^{-jk_{z,n}^+ L_m}}{k_0 - Mk_{z,n}^+} + \frac{k_{z,n}^- C_n^- \Psi_n^{A^-}(x,y)e^{-jk_{z,n}^- L_m}}{k_0 - Mk_{z,n}^-} \right)$$
$$= \frac{1}{\rho_0 c_0} \left(\sum_{n=1}^{\infty} \frac{k_n^{O^+} O_n^+ \Psi_n^{O^+}(x,y)}{k_0 - Mk_n^{O^+}} \right) \quad (x,y) \in S_a \tag{5.55}$$

$$\frac{1}{\rho_m c_m} \sum_{n=1}^{\infty} \left(\frac{k_{z,n}^+ C_n^+ \Psi_n^{M^+}(x,y)e^{-jk_{z,n}^+ L_m}}{k_m} + \frac{k_{z,n}^- C_n^- \Psi_n^{M^-}(x,y)e^{-jk_{z,n}^- L_m}}{k_m} \right) = 0$$
$$(x,y) \in S_m \tag{5.56}$$

Following the previous truncation criteria, the equations at the collocations points are

$$\sum_{n=1}^{N_a+N_m} (C_n^+ \Psi_{n,q}^{A^+} e^{-jk_{z,n}^+ L_m} + C_n^+ \Psi_{n,q}^{A^-} e^{-jk_{z,n}^- L_m}) = \sum_{n=1}^{N_a} O_n^+ \Psi_{n,q}^{O^+} \tag{5.57}$$

$$\sum_{n=1}^{N_a+N_m} \left(\frac{k_{z,n}^+ C_n^+ \Psi_{n,q}^{A^+} e^{-jk_{z,n}^+ L_m}}{k_0 - Mk_{z,n}^+} + \frac{k_{z,n}^- C_n^- \Psi_{n,q}^{A^-} e^{-jk_{z,n}^- L_m}}{k_0 - Mk_{z,n}^-} \right) = \sum_{n=1}^{N_a} \frac{k_n^{O^+} O_n^+ \Psi_{n,q}^{O^+}}{k_0 - Mk_n^{O^+}} \tag{5.58}$$

$$\frac{1}{\rho_m c_m} \sum_{n=1}^{N_a+N_m} \left(\frac{k_{z,n}^+ C_n^+ \Psi_n^{M^+} e^{-jk_{z,n}^+ L_m}}{k_m} + \frac{k_{z,n}^- C_n^- \Psi_n^{M^-} e^{-jk_{z,n}^- L_m}}{k_m} \right) = 0 \tag{5.59}$$

where $q = 1, ..., N_a$ in equations (5.57) and (5.58), and $q = 1, ..., N_m$ in expression (5.59).

Thus, the resulting algebraic system is composed of $4N_a + 2N_m$ equations, equal to the number of unknowns. This is readily solved for each excitation frequency to obtain the unknown pressure amplitudes I_n^-, C_n^+, C_n^- and O_n^+. Once the amplitudes are known, the attenuation can be determined by means of the transmission loss as [126]

$$TL = -20 \log \left| O_1^+ \Psi_1^{O^+} \right| \tag{5.60}$$

assuming that the outlet duct is long enough to guarantee the rapid decay of higher order evanescent modes.

5.3.2 Mode-matching method

The continuity condition of the pressure and the acoustic velocity fields is enforced at geometric discontinuities along the whole transversal section by means of a weighted integral approach, the weighting functions being the transversal pressure modes or eigenfunctions [104]. This clearly differs from the PC method, where the continuity conditions were enforced pointwise over the collocation points (nodes of the FE mesh or Gauss points). When mean flow is neglected, there exist orthogonality relations between the eigenfunctions that guarantee a convergent system of equations. When mean flow is present, however, the silencer eigenfunctions are not orthogonal; anyway, in the absence of a true orthogonality relation for flow, a convergent system of equations can be established so that its solution reflects the physics of the problem [104].

Therefore, the first condition is given by the continuity of pressure, the weighting function being the eigenfunction associated with the incident wave, which leads to the following expressions

$$\int_{S_i} p_i \Psi_n^{I^+}(x, y) \mathrm{d}S = \int_{S_a} p_a \Psi_n^{I^+}(x, y) \mathrm{d}S \tag{5.61}$$

$$\int_{S_a} p_a \Psi_n^{I^+}(x, y) \mathrm{d}S = \int_{S_o} p_o \Psi_n^{I^+}(x, y) \mathrm{d}S \tag{5.62}$$

where equations 5.61 and 5.62 are related to the expansion and contraction respectively, $n = 1, ..., N_{max}$ referring to the n-th transversal pressure mode. It is worth noting that in equation (5.62), in general, the weighting function chosen should be the eigenfunction associated with the progressive wave of the outlet duct [157]. However, in this case, $\Psi_n^{I^+}(x, y) = \Psi_n^{O^+}(x, y)$ and therefore, the result is not affected.

The second condition is a kinematic relationship that considers the continuity of the axial acoustic velocity and the condition of rigid lateral wall. In this case, the eigenfunctions associated with the incident wave at the chamber have been chosen as weighting function, obtaining [101, 104]

$$\int_{S_i} u_{z_i} \Psi_n^+(x,y)\mathrm{d}S = \int_{S_a \cup S_m} u_{z_c} \Psi_n^+(x,y)\mathrm{d}S \qquad (5.63)$$

$$\int_{S_a \cup S_m} u_{z_c} \Psi_n^+(x,y)\mathrm{d}S = \int_{S_o} u_{z_o} \Psi_n^+(x,y)\mathrm{d}S \qquad (5.64)$$

where expressions (5.63) and (5.64) are related to the expansion and the contraction, respectively, with $n = 1, ..., N_{max}$.

Then, developing equations (5.61)-(5.64) and considering the corresponding modal expansions (5.39)-(5.42) and (5.46)-(5.47) developed in Section 5.3, it yields

$$\int_{S_i} \Psi_n^{I^+} dS + \sum_{n=1}^{\infty} \int_{S_i} I_n^- \Psi_n^{I^-} \Psi_n^{I^+} dS = \sum_{n=1}^{\infty} \int_{S_a} (C_n^+ \Psi_n^{A^+} + C_n^- \Psi_n^{A^-})\Psi_n^{I^+} dS \qquad (5.65)$$

$$\sum_{n=1}^{\infty} \int_{S_a} \left(C_n^+ \Psi_n^{A^+} e^{-jk_{z,n}^+ L_m} + C_n^- \Psi_n^{A^-} e^{-jk_{z,n}^- L_m} \right) \Psi_n^{I^+} dS = \sum_{n=1}^{\infty} \int_{S_o} O_n^+ \Psi_n^{O^+} \Psi_n^{I^+} dS \qquad (5.66)$$

$$\int_{S_i} \frac{1}{\rho_0 c_0} \Psi_n^+ dS + \sum_{n=1}^{\infty} \int_{S_i} \frac{1}{\rho_0 c_0} \frac{k_n^{I^-} I_n^- \Psi_n^{I^-}}{k_0 - M k_n^{I^-}} \Psi_n^+ dS$$

$$= \sum_{n=1}^{\infty} \int_{S_a} \frac{1}{\rho_0 c_0} \left(\frac{k_{z,n}^+ C_n^+ \Psi_n^{A^+}}{k_0 - M k_{z,n}^+} + \frac{k_{z,n}^- C_n^- \Psi_n^{A^-}}{k_0 - M k_{z,n}^-} \right) \Psi_n^+ dS \qquad (5.67)$$

$$+ \sum_{n=1}^{\infty} \int_{S_m} \frac{1}{\rho_m c_m} \left(\frac{k_{z,n}^+ C_n^+ \Psi_n^{M^+}}{k_m} + \frac{k_{z,n}^- C_n^- \Psi_n^{M^-}}{k_m} \right) \Psi_n^+ dS$$

$$\sum_{n=1}^{\infty} \int_{S_a} \frac{1}{\rho_0 c_0} \left(\frac{k_{z,n}^+ C_n^+ \Psi_n^{A^+} e^{-jk_{z,n}^+ L_m}}{k_0 - M k_{z,n}^+} + \frac{k_{z,n}^- C_n^- \Psi_n^{A^-} e^{-jk_{z,n}^- L_m}}{k_0 - M k_{z,n}^-} \right) \Psi_n^+ dS$$

$$+ \sum_{n=1}^{\infty} \int_{S_m} \frac{1}{\rho_m c_m} \left(\frac{k_{z,n}^+ C_n^+ \Psi_n^{M^+} e^{-jk_{z,n}^+ L_m}}{k_m} + \frac{k_{z,n}^- C_n^- \Psi_n^{M^-} e^{-jk_{z,n}^- L_m}}{k_m} \right) \Psi_n^+ dS \quad (5.68)$$

$$= \sum_{n=1}^{\infty} \int_{S_o} \frac{1}{\rho_0 c_0} \left(\frac{k_n^{O^+} O_n^+ \Psi_n^{O^+}}{k_0 - M k_n^{O^+}} \right) \Psi_n^+ dS$$

Now, the modal expansions (5.65)-(5.68) are truncated at suitable number of terms N_{max} to guarantee the convergence of the solution and the same number of equations and unknowns. This leads to the following expressions

$$\int_{S_i} \Psi_n^{I^+} dS + \sum_{n=1}^{N_{max}} \int_{S_i} I_n^- \Psi_n^{I^-} \Psi_n^{I^+} dS = \sum_{n=1}^{N_{max}} \int_{S_a} (C_n^+ \Psi_n^{A^+} + C_n^- \Psi_n^{A^-}) \Psi_n^{I^+} dS \quad (5.69)$$

$$\sum_{n=1}^{N_{max}} \int_{S_a} \left(C_n^+ \Psi_n^{A^+} e^{-jk_{z,n}^+ L_m} + C_n^- \Psi_n^{A^-} e^{-jk_{z,n}^- L_m} \right) \Psi_n^{I^+} dS = \sum_{n=1}^{N_{max}} \int_{S_o} O_n^+ \Psi_n^{O^+} \Psi_n^{I^+} dS$$

$$(5.70)$$

$$\int_{S_i} \frac{1}{\rho_0 c_0} \Psi_n^+ dS + \sum_{n=1}^{N_{max}} \int_{S_i} \frac{1}{\rho_0 c_0} \frac{k_n^{I^-} I_n^- \Psi_n^{I^-}}{k_0 - M k_n^{I^-}} \Psi_n^+ dS$$

$$= \sum_{n=1}^{N_{max}} \int_{S_a} \frac{1}{\rho_0 c_0} \left(\frac{k_{z,n}^+ C_n^+ \Psi_n^{A^+}}{k_0 - M k_{z,n}^+} + \frac{k_{z,n}^- C_n^- \Psi_n^{A^-}}{k_0 - M k_{z,n}^-} \right) \Psi_n^+ dS \quad (5.71)$$

$$+ \sum_{n=1}^{N_{max}} \int_{S_m} \frac{1}{\rho_m c_m} \left(\frac{k_{z,n}^+ C_n^+ \Psi_n^{M^+}}{k_m} + \frac{k_{z,n}^- C_n^- \Psi_n^{M^-}}{k_m} \right) \Psi_n^+ dS$$

$$\sum_{n=1}^{N_{max}} \int_{S_a} \frac{1}{\rho_0 c_0} \left(\frac{k_{z,n}^+ C_n^+ \Psi_n^{A^+} e^{-jk_{z,n}^+ L_m}}{k_0 - Mk_{z,n}^+} + \frac{k_{z,n}^- C_n^- \Psi_n^{A^-} e^{-jk_{z,n}^- L_m}}{k_0 - Mk_{z,n}^-} \right) \Psi_n^+ dS$$

$$+ \sum_{n=1}^{N_{max}} \int_{S_m} \frac{1}{\rho_m c_m} \left(\frac{k_{z,n}^+ C_n^+ \Psi_n^{M^+} e^{-jk_{z,n}^+ L_m}}{k_m} + \frac{k_{z,n}^- C_n^- \Psi_n^{M^-} e^{-jk_{z,n}^- L_m}}{k_m} \right) \Psi_n^+ dS$$

$$= \sum_{n=1}^{N_{max}} \int_{S_o} \frac{1}{\rho_0 c_0} \left(\frac{k_n^{O^+} O_n^+ \Psi_n^{O^+}}{k_0 - Mk_n^{O^+}} \right) \Psi_n^+ dS \tag{5.72}$$

Finally, the weighted integrals (5.69)-(5.72) are numerically evaluated after the aforementioned truncation at N_{max} modal terms. These modes have to guarantee a suitable representation of the acoustic fields [1]. In addition, the consideration of an anechoic termination ($O_n^- = 0\ \forall n$) and an incident wave amplitude $I_1^+ = 1$, $I_n^+ = 0$ $\forall n \neq 0$ leads to a system composed of $4N_{max}$ equations and unknowns, which permits obtaining the pressure modal amplitudes. Once these wave amplitudes are obtained, the transmission loss can be computed as [101]

$$TL = -20 \log \left| O_1^+ \right| \tag{5.73}$$

5.4   Temperature variation

In this chapter, a simplified temperature field is considered in order to apply the PC technique and the MM method. Transversal thermal gradients are retained while the temperature is assumed to be axially uniform, its value being the average between the inlet and the outlet sections. This assumption seems plausible, since radial thermal gradients can considerably affect the acoustic performance of the silencer, the influence of axial gradients being small enough to have a relevant impact on the results in a number of interesting situations (see Section 4.7.2).

5.4.1   Absorbent material

As previously shown [10], an absorbent material can be defined by its equivalent acoustic properties, e.g. the characteristic impedance Z_m and wavenumber k_m. These parameters are coordinate-dependent, since they are affected by temperature. Thus,

similarly to the procedure detailed in Section 3.3.1, the empirical law of Delany and Bazley [57] can be modified to obtain

$$Z_m(x,y) = Z_0 \left(1 + a_5 \left(\frac{f\rho_0}{R(x,y)} \right)^{a_6} - ja_7 \left(\frac{f\rho_0}{R(x,y)} \right)^{a_8} \right) \quad (5.74)$$

$$k_m(x,y) = k_0 \left(1 + a_3 \left(\frac{f\rho_0}{R(x,y)} \right)^{a_4} - ja_1 \left(\frac{f\rho_0}{Rx,y)} \right)^{a_2} \right) \quad (5.75)$$

The coefficients and exponents a_1, ..., a_8, are obtained by fitting a curve to the experimental data. Also, they are considered constant at high temperatures (see Section 3.3 for further details) and resistivity $R = R(x,y)$ can be updated at each integration point by means of the Christie's expression [41]

$$R(T(x,y)) = R(T_0) \left(\frac{T(x,y) + 273.15}{T_0 + 273.15} \right)^{0.6} \quad (5.76)$$

$R(T_0)$ being the resistivity at the reference temperature T_0 and $T(x,y)$ the temperature at the corresponding integration point. For a given point, the corresponding temperature can be obtained, for example, from the simplified thermal field under consideration, the latter being computed from the one detailed in Section 3.3.1, assuming that axial variations are negligible. Thus, the temperature is considered axially uniform in the current analysis and equal to the average value at the inlet and the outlet sections, whereas the radial variations can be modelled as $T(r) = c_0 + c_1 r + c_2 r^2$, r being the radius of the integration point that can be obtained from the x and y coordinates as $r = \sqrt{x^2 + y^2}$, and c_0, c_1 and c_2 are the coefficients defining the temperature field. These coefficients are obtained from the temperature values at the central duct radius, and the mid and outer radii of the chamber. This latter definition fits satisfactorily the logarithmic function that characterizes the heat transfer in a cylindrical duct [90].

Once the above-mentioned two material properties Z_m and k_m are obtained, the equivalent acoustic density and speed of sound can be computed. These values are introduced in equations of Section 5.3.1 associated with the PC method and of Section 5.3.2 related to the MM scheme for obtaining the corresponding final system of equations in each case.

5.4.2   Impedance of the perforated duct

In this Thesis, the model developed by Lee and Ih [108] is used to calculate the characteristic impedance of the perforated surface. Therefore, the dimensionless impedance

of the perforated duct in the presence of a tangential mean flow can be expressed by the expression (2.149), which is repeated here for convenience.

$$\tilde{Z}_p(x,y) = \rho_0 c_0 \left(\xi_p' + \frac{j0.425 k_0 d_h \left(\frac{\rho_m(x,y)}{\rho_0} - 1 \right) F(\sigma)}{\sigma} \right)$$

In this case, the acoustic impedance of the perforated duct does not explicitly depend on the axial coordinate z, since the duct is parallel to the z axis and any possible axial variation of the temperature has been substituted by a constant value obtained as the average between the temperatures at the inlet and outlet sections.

5.5 Application to axisymmetric dissipative silencers

In this section, the PC and the MM techniques are applied to perforated dissipative silencers subjected to transversal thermal gradients. The geometry of the configuration under study is detailed in Table 5.1. In addition, the perforated duct is defined by $\sigma = 0.1$, $d_h = 0.0035$ m and $t_p = 0.001$ m. In all the cases the mean flow Mach number is $M = 0.1$ and the dissipative fibre considered is E fibreglass, whose resistivity is $R = 30716$ rayl/m at 25°C.

Geometry	L_i/L_o (m)	R_d (m)	L_{ch} (m)	R_{ch} (m)
1	0.1	0.0268	0.3	0.091875

Table 5.1: Geometry under study: L, length; R, radius; i, inlet; o, outlet; d, duct; ch, chamber.

All the temperature distributions considered in the computations are listed in Table 5.2 (for further information see Figure 3.3). Simplified *equivalent* temperature distributions are denoted by a, while b is used for the corresponding temperature fields including radial and axial thermal gradients.

Some of the results presented hereafter have been published in reference [151]. In addition, further details of the PC technique applied at nodes can be found in [63].

Case	$T_{r_1}(R_d)$	$T_{r_2}(R_m)$	$T_{r_3}(R_{ch})$	$T_{r_4}(R_d)$	$T_{r_5}(R_m)$	$T_{r_6}(R_{ch})$
1a	250	185.48	150	250	185.48	150
2a	325	228.22	175	325	228.22	175
3a	400	270.96	200	400	270.96	200
1b	300	235.48	200	200	135.48	100
2b	400	303.22	250	250	153.22	100
3b	500	370.96	300	300	170.96	100

Table 5.2: Temperatures (°C) for the definition of temperature fields.

5.5.1 Point collocation in nodes and Gauss points

In order to validate the PC approach presented in this Thesis, several analyses have been carried out considering the simplified temperature distributions detailed in Table 5.2. The numerical test problem has been computed three times for each temperature field, including the PC technique at nodes and Gauss points, and a full FE formulation (see Section 4.5.2). For the latter, two possibilities are taken into account: (1) The in-house hybrid formulation developed in Section 4.5.2; and (2) the commercial FE software COMSOL Multiphysics®. The hybrid formulation allows the consideration of both axial and radial thermal gradients, as well as the variations of the mean flow due to these gradients, while the commercial program has only been used to validate the PC technique when a uniform temperature field of 200 °C is considered in the whole silencer, in the absence of mean flow. In the rest of the cases a mean flow Mach number of $M = 0.1$ is taken into account.

The results obtained, according to Figure 5.2, show that good agreement is found between the results predicted by the full FE formulation and the PC approach for both nodes and Gauss points. It can be observed that increasing temperature gradients and mean flow lead to lower attenuation in almost all the frequency range, shifting the maximum value of transmission loss to higher frequencies, which agrees with the results obtained in Section 4.7.1.

Figure 5.3 depicts the comparison of the transmission loss achieved considering a full FE approach for configurations b detailed in Table 5.2, with axial and radial thermal gradients, and the PC technique (using the FE nodes of the transversal mesh) for configurations a with only radial temperature variations. From a practical point of view, these discrepancies are not very relevant. It can be observed that considering only the radial gradient produces a slight overestimation of the TL. Also, the differences between the attenuation curves computed with a complex temperature
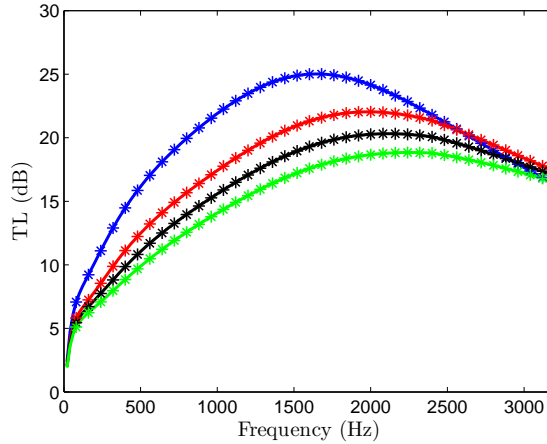
Figure 5.2: Transmission loss of a dissipative silencer with radial thermal gradients: ——, uniform, 200 °C, COMSOL; × × ×, uniform, 200 °C, PC, nodes; +++, uniform, 200 °C, PC, Gauss points; ——, 1a, full FE formulation; × × ×, 1a, PC, nodes; +++, 1a, PC, Gauss points; ——, 2a, full FE formulation; × × ×, 2a, PC, nodes; +++, 2a, PC, Gauss points; ——, 3a, full FE formulation; × × ×, 3a, PC, nodes; +++, 3a, PC, Gauss points.

field and those obtained with a simplified variation increase as the thermal gradients are higher. For example, the maximum discrepancy between cases 1a and 1b is 0.56 dB, whereas in cases 2a and 2b the difference is approximately 0.66 dB, and in cases 3a and 3b is about 0.78 dB. Thus, the slight influence of substituting the axial temperature gradient by its average value is clearly compensated by the benefits of an important reduction of the computational cost associated with PC approach. More details about the computation time will be provided in Section 5.5.3.

5.5.2 Mode-matching

In this section, the attenuation curves obtained with the MM method are compared with the transmission loss results computed by means of the full FE hybrid formulation in Figure 5.4, where it can be observed that good agreement appears between both methods. In order to obtain higher accuracy, six modes have been considered in the computations (further details about the number of modes and the error associated with the FE discretization are given later). The temperature fields under study are defined in Table 5.2, and the value of mean flow considered is given by $M = 0.1$. In addition, it can be observed that the main conclusions related to the TL in Figure 5.3, are repeated here.
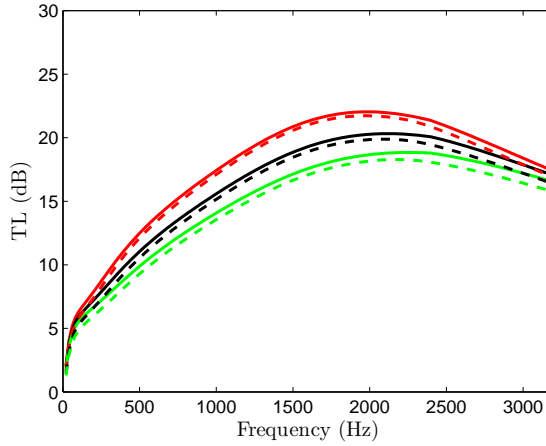
Figure 5.3: Transmission loss comparison for a dissipative silencer with axial/radial and only radial temperature gradients: ——, 1a, simplified field, PC; – – –, 1b, full FE formulation; ——, 2a, simplified field, PC; – – –, 2b, full FE formulation; ——, 3a, simplified field, PC; – – –, 3b, full FE formulation.
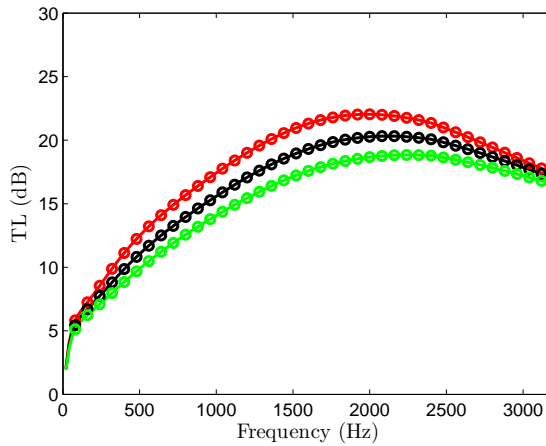

Figure 5.4: Transmission loss of a dissipative silencer with radial thermal gradients: ——, 1a, full FE formulation; ooo, 1a, MM; ——, 2a, full FE formulation; ooo, 2a, MM; ——, 3a, full FE formulation; ooo, 3a, MM.

5.5.3 Study and comparison of the error convergence between the PC technique and the MM approach

To study the convergence of the PC and the MM approaches, several analyses have been carried out with an increasing refinement of the 2D transversal FE mesh associated with the silencer cross section. As the element size is refined, the number of nodes included in the calculations is higher, which improves the accuracy of the solution of the eigenvalue problem leading to a better computation of the silencer transmission loss.

Both methods obtain good agreement when compared with the full FE hybrid formulation. However, a study of convergence is required to compare the PC technique with the MM method. The impact of the element size is studied refining the FE mesh and computing the associated relative error. This can be achieved comparing the transmission loss obtained through the PC and the MM techniques with a reference solution computed via the hybrid formulation presented in this Thesis (see Section 4.5.2). The mesh used in this reference computation is composed of 8-node quadratic quadrilateral elements, their size being 0.001 m, which permits obtaining an accurate solution. This provides about 100 elements per wavelength for the maximum frequency $f_{max} = 3200$ Hz considered in the computations [75]. The time required to calculate the acoustic performance can be usually more than an hour due to the considerable number of nodes (101688). The meshes associated with the transversal discretizations of the PC and the MM approaches are composed of 3-node quadratic one-dimensional elements, since the geometry under analysis is axisymmetric and, therefore, the silencer cross section can be represented by a line. The relative error of the transmission loss associated with these FE discretizations for both approaches can be computed as

$$Error(\%) = 100\sqrt{\sum_{i=1}^{n_{freq}} (TL_i - TL_i^{ref})^2 \Big/ \sum_{i=1}^{n_{freq}} (TL_i^{ref})^2} \qquad (5.77)$$

TL_i being the value of the transmission loss obtained by the PC and the MM methods and TL_i^{ref} the corresponding value given by the full FE formulation with the aforementioned reference mesh. All the computations have been done considering case 1a (see Table 5.2) and a mean flow Mach number $M = 0.1$.

Figure 5.5 represents the average relative error (%) previously defined versus the number of nodes for the meshes under study, considering case 1a. The parameters related to the meshes are listed in Table 5.3.

Element size (m)	Number of nodes
0.002	96
0.003	64
0.004	50
0.005	42
0.006	34
0.007	30
0.008	28
0.009	24
0.01	22
0.0125	20
0.015	16
0.02	14
0.032	8
0.065	6

Table 5.3: Number of nodes of each finite element mesh.

Figure 5.5: Average relative error (%) versus number of nodes for different meshes considering case 1a: ——, MM, 1 mode; ——, MM, 2 modes; ——, MM, 3 modes; ——, MM, 4 modes; ——, MM, 5 modes; ——, MM, 6 modes; – – –, PC, nodes; – – –, PC, Gauss points.

From figure 5.5 it can be deduced that, from a practical point of view, the average error is negligible if a reasonable number of nodes (more than 10) is used, since its value does not exceed the 0.2% in any case for both the PC and the MM approaches

when a mesh of more than fourteen nodes is used. Therefore, it can be concluded that the good agreement shown before between these techniques and a full finite element formulation is confirmed. Nevertheless, it is worth noting that as the number of degrees of freedom increases, the algebraic system of equations is worse conditioned, which can generate numerical problems. For example, when applying the MM method, the error decreases as the number of modes increases, except for the case of four and five modes. This can be due to the fact that the problem starts to be ill-conditioned for five modes and the error consequently increases at this point, decreasing again for six modes. It is also observed that for a given number of modes, as the number of nodes increases the error tends to an asymptotic value. On the other hand, when applying the nodal PC technique for meshes with an element size of 0.003 m or lower, it has been impossible to obtain values of transmission loss because of the ill-conditioning of the problem. However, considering the same FE mesh, the number of Gauss points is lower than the number of nodes, which makes possible to solve the problem. In addition, when considering solvable problems for both nodal and gaussian PC, the discretization error for a given FE mesh is lower for the former, since the dimension of the system of equations is larger.

Figure 5.6 shows some curves related to the computational effort. As the number of modes considered in the MM technique is higher, the error decreases at the expense of increasing the computation time. It should be noted that the PC and the MM errors are comparable if six modes are considered in the latter technique, but the collocation techniques have a certain advantage in terms of computational expenditure. The errors obtained using the nodes of the finite element mesh as collocation points are slightly lower than those obtained with one Gauss point per element. The most time-consuming operation of these methods is related to the assembly of the final system of equations when a standard matrix process is followed. In this case, the PC method at Gauss points requires a lower computational cost. To improve the computation time, the MATLAB® function *bsxfun* has been used to avoid some time-consuming loops in the code when assembling the final system of equations in all the methodologies presented here. This fact supposes that the computation times are quite similar if the MM approach with one mode and the PC approaches (nodes and Gauss points) are compared, although the error of the former is considerably higher (see Figure 5.5). The computation cost increases with a higher number of degrees of freedom, as well as with a larger number of weighting functions in the case of the MM method. As can be seen, the error is higher when using this latter method for a given computational expenditure.
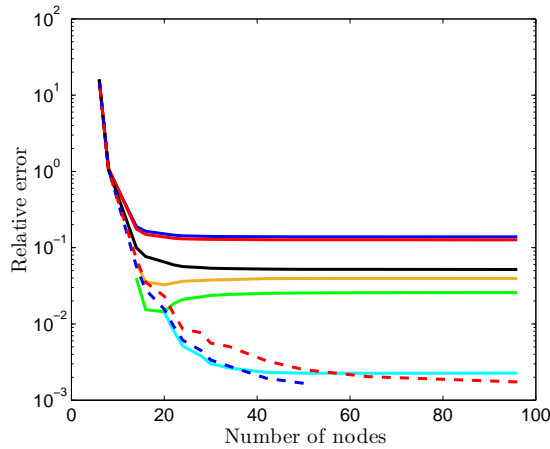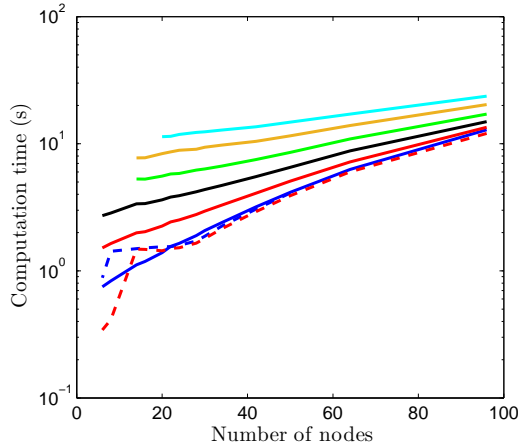
Figure 5.6: Computation time (s) versus number of nodes for different meshes considering case 1a: ——, MM, 1 mode; ——, MM, 2 modes; ——, MM, 3 modes; ——, MM, 4 modes; ——, MM, 5 modes; ——, MM, 6 modes; - - -, PC, nodes; - - -, PC, Gauss points.

The relative error calculated at 320 Hz and 3200 Hz is depicted in Figures 5.7 and 5.8, respectively. The tendencies shown at each one of these frequencies are relatively similar to the behaviour presented by the average relative error (see also Figure 5.5). Nevertheless, there is an important oscillation in the relative error for the gaussian point collocation at 320 Hz, while at 3200 Hz the trend shown by the error is smoother and no relevant oscillations appear. If the error obtained at 3200 Hz using the nodes as collocation points is compared with the error associated with Gauss points, it is found that the error is slightly higher for the latter approach. When the PC and the MM techniques are compared, the error observed at 3200 Hz for the nodal PC is similar to the one shown by the MM method when six modes are considered. However, the relative error at 320 Hz is higher for the latter approach. In spite of the fact that it is difficult to extract general conclusions from single frequencies, it seems that at low frequencies the PC technique shows more accuracy, while at high frequencies both the nodal PC and the MM methods exhibit a similar behaviour.

Figure 5.7: Relative error (%) at 320 Hz versus number of nodes for different meshes considering case 1a: ——, MM, 1 mode; ——, MM, 2 modes; ——, MM, 3 modes; ——, MM, 4 modes; ——, MM, 5 modes; ——, MM, 6 modes; – – –, PC, nodes; – – –, PC, Gauss points.
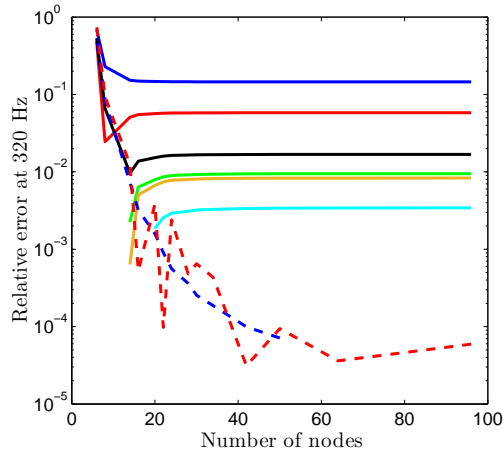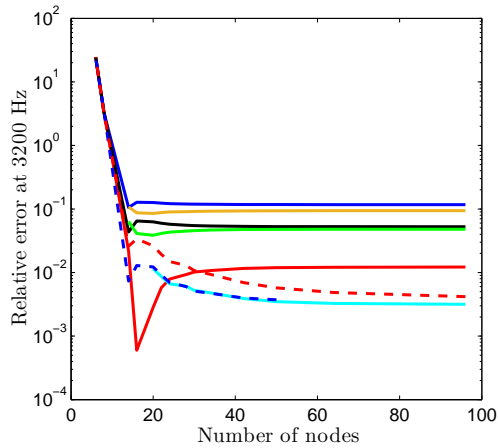

Figure 5.8: Relative error (%) at 3200 Hz versus number of nodes for different meshes considering case 1a: ——, MM, 1 mode; ——, MM, 2 modes; ——, MM, 3 modes; ——, MM, 4 modes; ——, MM, 5 modes; ——, MM, 6 modes; – – –, PC, nodes; – – –, PC, Gauss points.

5.6 Conclusions

Two computationally efficient numerical approaches, based on the MM method and the PC technique, have been applied to study the acoustic behaviour of perforated dissipative silencers of arbitrary, but axially uniform, cross sections with thermal gradients in the absorbent material. Also, the presence of mean flow in the central perforated duct has been considered in the model. The main advantage of the proposed methodologies is that they reduce the computational effort when compared to a full FE formulation. Both approaches combine axial and transversal solutions of the wave equation in the different regions of the silencer. The transversal pressure modes and their corresponding wavenumbers are obtained by means of a transversal finite element analysis of the eigenvalue problem associated with the cross section. Since the presence of temperature gradients leads to a non-homogeneous absorbent material, an adapted version of the wave equation has been considered. In the numerical cases under study, it is supposed that the transversal thermal gradients have more influence on the acoustic behaviour of the silencer than the axial ones. Thus, the transversal gradient has been retained in the formulation, while the axial temperature variations have been substituted by a uniform temperature field, its value being the average between the inlet and outlet sections. Considering the compatibility equations of the acoustic pressure and the axial velocity at the geometric discontinuities, and applying the MM/PC methods, the modal pressure amplitudes are obtained at the chamber as well as at the inlet/outlet ducts. Although more accuracy is expected with the mode-matching method, the computational cost required rapidly increases with the number of modes. For a given computational effort, the most precise approach seems to be the nodal PC technique, which has a slight advantage over Gauss collocation.

Chapter 6

Conclusions and future works

Summary:

In this chapter, the main conclusions extracted from this work are detailed, highlighting those related to the objectives of the Thesis. The more relevant contributions are pointed out and possible future works are proposed in order to continue the research line presented here.

6.1 Conclusions

The conclusions obtained in the present Thesis, related to the development and implementation of general and efficient methods for the design and acoustic modelling of automotive silencers are presented here.

- It has been shown that plane wave models are not valid for silencers in the usual working range of frequencies for reciprocating internal combustion engines. This justifies the need to use more general and accurate models based on numerical techniques, such as the FEM and other numerical approaches that combine the mode-matching method and the point collocation technique with the FEM, to efficiently study the acoustic behaviour of silencers.

- Perforated dissipative silencers present a good acoustic performance in the mid and high frequency range. However, the absorbent materials can be swept by the exhaust gases from the engine, which can have harmful effects on human health. This justifies the need to find new materials and design solutions as an alternative to perforated dissipative silencers.

- The characterization of the acoustic impedance of sintered surfaces has been carried out as a possible alternative to the traditional perforated dissipative silencers. A possible additional advantage can be related to the reduction of the weight associated with dissipative configurations. The results obtained show a nearly constant normalized acoustic resistance of the sintered screen, while the imaginary part of the acoustic impedance shows a slight dependence on the frequency and its numerical value is lower than the real one up to relatively high frequencies. Therefore, as a first approximation, it can be modelled by a real-valued constant impedance. In addition, several analyses have been done to study the acoustic behaviour of these sintered plates, showing good attenuation properties. Thus, it seems a potential alternative to dissipative configurations in some practical applications.

- In order to simulate the 3D acoustic behaviour of perforated dissipative silencers under more realistic conditions such as the existence of high temperature, thermal gradients, variations of the absorbent material properties and the presence of mean flow, a hybrid FE model has been presented.

- For the consideration of an absorbent material with variable bulk density, two different formulations have been applied and combined. In the central duct a suitable equation for a moving medium in terms of velocity potential is considered, while in the outer chamber, the suitable form of the wave equation for a

non-moving medium in terms of pressure is taken into account. The coupling between both subdomains has been carried out by means of the perforated duct impedance, considering the continuity of the velocity. The acoustic impedance is variable due to the variation of the absorbent material density that modifies the steady airflow resistivity of the fibre. Therefore, the usual definition of the acoustic impedance has been modified to include the spatial variation of the properties.

- Once the previous model has been implemented in an in-house code, the acoustic behaviour of perforated dissipative silencers carrying an absorbent material with heterogeneous bulk density has been studied. The results show that the radial variation of the bulk density has a higher influence on the attenuation achieved by the silencer than the axial distribution. When radial variations are considered and the fibre density is higher near the perforated surface, the transmission loss is dramatically reduced. However, if the density is higher near the outer radius of the chamber, the transmission loss considerably increases. It is also worth noting that the influence of a variable density distribution seems to have more impact on the acoustic performance as the fibre considered is more resistive.

- High temperature and thermal gradients can appear within a silencer provoking spatial variations of the propagation media properties, as well as of the mean flow. As in the previous case, two different formulations have been combined. In the central duct a suitable equation for a moving medium in terms of velocity potential is required. The potential formulation permits including the flow variations due to the temperature gradients and reducing the number of variables. A pressure-based wave equation for stationary medium is applied in the dissipative outer chamber. Both subdomains have been coupled through the perforated duct acoustic impedance; this depends on the thermal-induced material heterogeneities and mean flow. The resistivity plays a key role in the model, and it is computed pointwise via Christie's power law, once the temperature field has been defined.

- The effect of temperature and associated gradients on the acoustic behaviour of dissipative silencers has been studied. The analysis shows that high temperatures have a great influence on the acoustic performance. In addition, transversal gradients seem to have a higher impact on the transmission loss than axial variations. It is worth noting that thermal gradients have more impact on the transmission loss as the material resistivity increases. Therefore, for less resistive materials, an increase in temperature and/or thermal gradient has led to a slight drop in the silencer performance in the low to mid frequency range but the opposite trend has been found at higher frequencies, the transition point shifting to higher frequencies as the temperature gradient and/or

mean flow rise. This involves that, for some silencer configurations containing low resistivity materials, the temperature field can be approximated by using a uniform profile considering an average value. On the contrary, for absorbent materials having medium to high airflow resistivities the consideration of the full temperature field is required to obtain accurate and reliable computations. In this latter case, attenuation overestimation is likely to be predicted if the temperature distribution is not taken into account, thus justifying the numerical implementation presented in this Thesis.

- An optimization procedure has been applied to multichamber silencers in order to find a useful design tool with a view to obtaining the most suitable configuration for each application. Also the acoustic performance of different surfaces has been assessed, showing that microperforated and sintered surfaces can be good alternatives to dissipative silencers, depending on the frequency range of interest. The most important aspects for silencer optimization depend on each particular application. Nevertheless, parameters as the transversal and axial dimensions are important factors. Also, the geometrical characteristics of the perforated/sintered plates and the parameters defining the absorbent material play a key role in the corresponding computational procedure.

- Two numerical techniques have been developed and implemented in the corresponding in-house code with the objective of accelerating the finite element computations (based on a 3D full formulation) for perforated dissipative silencers with high temperature and thermal gradients. These techniques take benefit from the fact that, in general, the silencers have an arbitrary, but axially uniform, cross-section. The methods developed are based on the point collocation technique (at nodes of the finite element mesh and also at Gauss points) and the mode-matching method. In these approaches the computation of the pressure modes and the wavenumbers of the different cross sections that compose the silencer is carried out by means of a transversal finite element eigenvalue problem. Then, the transversal solutions corresponding to the different subdomains are coupled at the silencer geometric discontinuities through the above-mentioned techniques. These numerically efficient approaches have been compared, showing that the mode-matching method is more accurate if a reasonable number of modes is considered. However, its computational cost is higher when the number of nodes increases, which implies that the point collocation technique is a little faster. When comparison is carried out between nodal and Gaussian collocation, it can be observed that the former are slightly more accurate. Finally, it is worth noting that the relative error is below 1% in all the computations carried out for both methods (mode-matching and point collocation), and therefore the two techniques are suitable from a practical point of view.

6.2   Future works

Two different parts can be distinguished in this Thesis. On the one hand, modelling and experimental work has been carried out to characterize new materials and surfaces to avoid the main drawbacks of perforated dissipative silencers. On the other hand, several numerical models have been developed and implemented for silencer optimization purposes and also to study the acoustic performance of perforated dissipative silencers in the presence of propagation media with variable properties. Following the previous ideas, some possible future works could be, among others:

- More accurate and detailed characterization of sintered surfaces, including the presence of mean flow and high pressure levels.

- Search and characterization of new materials as an alternative to the traditional fibrous silencer configurations, e.g. open cell metallic foams.

- Study of the coupling between sintered surfaces and absorbent materials.

- Development and extension of the existing numerical models for other exhaust devices, such as catalytic converters and diesel particulate filters, to include thermal gradients and variable properties of ceramic monoliths, as well as the effects of wall vibrations and non-potential flows.

- Development of accurate and efficient numerical methods, based on the mode-matching method and the point collocation technique, to model the acoustic behaviour of catalytic converters and diesel particulate filters.

- Extension of some numerical techniques, developed by the research group, to the acoustic problem in exhaust devices: FEM with non-conforming meshes, Cartesian grids, error estimation of the FE solution, exact integration over the boundary (which permits the use of CAD silencer models), etc.

Bibliography

[1] M. Åbom. Derivation of four-pole parameters including higher order mode effects for expansion chamber mufflers with extended inlet and outlet. *Journal of Sound and Vibration*, 137(3):403–418, 1990.

[2] M. Åbom. Determination of porous material data via two-port measurements. *The Journal of the Acoustical Society of America*, 105(2):1385–1385, 1999.

[3] A.L. Abrahamson. A finite element formulation for sound propagation in axisymmetric ducts containing compressible mean flow. Technical report, American Institute of Aeronautics and Astronautics, 1977.

[4] T. Airaksinen and E. Heikkola. Multiobjective muffler shape optimization with hybrid acoustic modeling. *The Journal of the Acoustical Society of America*, 130(3):1359–1369, 2011.

[5] I. Akseli. *The application of aluminum foam for the heat and noise reduction in automobiles*. PhD thesis, İzmir Institute of Technology, 2005.

[6] J. Albelda, F.D. Denia, A. Broatch, and F.J. Fuenmayor. Modelado acústico de silenciadores con flujo medio y placas perforadas mediante elementos finitos. In *SEMNI, Seville*, 1999.

[7] S. Allam and M. Åbom. Sound propagation in an array of narrow porous channels with application to diesel particulate filters. *Journal of Sound and Vibration*, 291(3):882–901, 2006.

[8] S. Allam and M. Åbom. A new type of muffler based on microperforated tubes. *Journal of Vibration and Acoustics*, 133(3):1–8, 2011.

[9] S. Allam, Y. Guo, and M. Åbom. Acoustical study of micro-perforated plates for vehicle applications. Technical report, SAE Technical Paper, 2009.

[10] J. Allard and N. Atalla. *Propagation of sound in porous media: modelling sound absorbing materials*. John Wiley & Sons, 2009.

[11] J.F. Allard, A. Aknine, and C. Depollier. Acoustical properties of partially reticulated foams with high and medium flow resistance. *Journal of the Acoustical Society of America*, 79(6):1734–1740, 1986.

[12] J.F. Allard, R. Bourdier, and A. L'Esperance. Anisotropy effect in glass wool on normal impedance in oblique incidence. *Journal of Sound and Vibration*, 114(2):233–238, 1987.

[13] ANSYS-Fluent. Fluent 14.5 user's guide. *ANSYS Inc*, 2011.

[14] A.G. Antebas. *Contribución al modelado acústico de la línea de escape en motores de combustión. Aplicación a silenciadores y catalizadores.* PhD thesis, Departamento de Ingeniería Mecánica y de Materiales, Universitat Politècnica de València, Valencia, 2010.

[15] A.G. Antebas, F.D. Denia, A.M. Pedrosa, and F.J. Fuenmayor. Modelado analítico multidimensional del comportamiento acústico en silenciadores de escapes de cámara reversa con material absorbente y placa perforada. In *V Congreso Ibérico de Acústica, XXIX Congreso Español de Acústica. Tecni-acústica 2008,.* Coimbra, 2008.

[16] A.G. Antebas, F.D. Denia, A.M. Pedrosa, and F.J. Fuenmayor. A finite element approach for the acoustic modeling of perforated dissipative mufflers with non-homogeneous properties. *Mathematical and Computer Modelling*, 57(78):1970–1978, 2013.

[17] A.G. Antebas, F.D. Denia, E.M. Sánchez-Orgaz, and F.D. Fuenmayor. Numerical transmission loss calculations for perforated dissipative mufflers containing heterogeneous material and mean flow. In *Société Française d'Acoustique. Acoustics 2012.* Nantes, 2012.

[18] J.P. Arenas and M.J. Crocker. Recent trends in porous sound-absorbing materials. *Sound and vibration*, 44(7):12–18, 2010.

[19] R.J. Astley and W. Eversman. The application of finite element techniques to acoustic transmission in lined ducts with flow. In *AIAA 5th Aeronautics Conference.* Seattle, 1979.

[20] N. Atalla and F. Sgard. Modeling of perforated plates and screens using rigid frame porous models. *Journal of sound and vibration*, 303(1):195–208, 2007.

[21] K. Attenborough. Acoustical characteristics of rigid fibrous absorbents and granular materials. *Journal of the Acoustical Society of America*, 73(3):785–799, 1983.

[22] Y. Aurégan and M. Leroux. Failures in the discrete models for flow duct with perforations: an experimental investigation. *Journal of Sound and Vibration*, 265(1):109–121, 2003.

[23] Y. Aurégan and M. Leroux. Experimental evidence of an instability over an impedance wall in a duct with flow. *Journal of Sound and Vibration*, 317(3):432–439, 2008.

[24] R. Barbieri and N. Barbieri. The technique of active/inactive finite elements for the analysis and optimization of acoustical chambers. *Applied Acoustics*, 73(2):184–189, 2012.

[25] A.B. Bauer. Impedance theory and measurements on porous acoustic liners. *Journal of Aircraft*, 14(8):720–728, 1977.

[26] D.E. Baxa. *Noise control in internal combustion engines.* John Wiley & Sons, New York, 1982.

[27] J.L. Bento. *Acoustic characteristics of perforate liners in expansion chambers.* PhD thesis, University of Southampton, Southampton, 1983.

[28] L.L. Beranek. Acoustical properties of homogeneous, isotropic rigid tiles and flexible blankets. *Journal of the Acoustical Society of America*, 19(4):556–568, 1947.

[29] L.L. Beranek. *Noise reduction.* Peninsula Pub, California, 1988.

[30] L.L. Beranek. *Acoustics.* Acoustical Society of America, Woodbury, 1996.

[31] E.H. Berger. *The noise manual.* Aiha, 2003.

[32] M.A. Biot. Theory of propagation of elastic waves in a fluid-saturated porous solid. Higher frequency range. *Journal of the Acoustical Society of America*, 28(2):179–191, 1956.

[33] M.A. Biot. Theory of propagation of elastic waves in a fluid-saturated porous solid. Low-frequency range. *Journal of the Acoustical Society of America*, 28(2):168–178, 1956.

[34] R.H. Bolt. On the design of perforated facings for acoustic materials. *The Journal of the Acoustical Society of America*, 19(5):917–921, 1947.

[35] A. Broatch, X. Margot, A. Gil, and F.D. Denia. A CFD approach to the computation of the acoustic response of exhaust mufflers. *Journal of Computational Acoustics*, 13(02):301–316, 2005.

[36] D.B. Callaway and L.G. Ramer. The use of perforated facings in designing low frequency resonant absorbers. *The Journal of the Acoustical Society of America*, 24(3):309–312, 1952.

[37] M.C. Chiu. Shape optimization of multi-chamber mufflers with plug-inlet tube on a venting process by genetic algorithms. *Applied Acoustics*, 71(6):495–505, 2010.

[38] M.C. Chiu and Y.C. Chang. Numerical studies on venting system with multi-chamber perforated mufflers by GA optimization. *Applied Acoustics*, 69(11):1017–1037, 2008.

[39] M.C. Chiu and Y.C. Chang. Shape optimization of multi-chamber cross-flow mufflers by SA optimization. *Journal of Sound and Vibration*, 312(3):526–550, 2008.

[40] P.W. Christensen and A. Klarbring. *An introduction to structural optimization*, volume 153. Springer Science & Business Media, 2008.

[41] D.R.A. Christie. Measurement of the acoustic properties of a sound absorbing material at high temperatures. *Journal of Sound and Vibration*, 46(3):347–355, 1976.

[42] T.J. Cox and P. D'Antonio. *Acoustic absorbers and diffusers: theory, design and application*. CRC Press, 2009.

[43] J.P. Coyette. Flow acoustics using finite elements. Technical background and application to muffler systems. Technical report, LMS International, 1995.

[44] A. Craggs. The use of simple three-dimensional acoustic finite elements for determining the natural modes and frequencies of complex shaped enclosures. *Journal of Sound and Vibration*, 23(3):331–339, 1972.

[45] A. Craggs. An acoustic finite element approach for studying boundary flexibility and sound transmission between irregular enclosures. *Journal of Sound and Vibration*, 30(3):343–357, 1973.

[46] A. Craggs. A finite element method for damped acoustic systems. An application to evaluate the performance of reactive mufflers. *Journal of Sound and Vibration*, 48(3):377–392, 1976.

[47] A. Craggs. A finite element method for modelling dissipative mufflers with a locally reactive lining. *Journal of Sound and Vibration*, 54(2):285–296, 1977.

[48] I.B. Crandall. *Theory of vibrating systems and sound*. D. Van Nostrand Company, New York, 1926.

[49] M.J. Crocker. *Handbook of Acoustics.* John Wiley & Sons, New York, 1998.

[50] A. Cummings. Sound transmission at sudden area expansions in circular ducts, with superimposed mean flow. *Journal of Sound and Vibration*, 38(1):149–155, 1975.

[51] A. Cummings. The effects of grazing turbulent pipe-flow on the impedance of an orifice. *Acustica*, 61(4):233–242, 1986.

[52] A. Cummings. A segmented Rayleigh-Ritz method for predicting sound transmission in a dissipative exhaust silencer of arbitrary cross-section. *Journal of Sound and Vibration*, 187(1):23–37, 1995.

[53] A. Cummings and I.J. Chang. Internal mean flow effects on the characteristics of bulk-reacting liners in circular ducts. *Acta Acustica united with Acustica*, 64(4):169–178, 1987.

[54] W.A. Davern. Perforated facings backed with porous materials as sound absorbers: an experimental study. *Applied Acoustics*, 10(2):85–112, 1977.

[55] P.O.A.L. Davies. Practical flow duct acoustics. *Journal of Sound and Vibration*, 124(1):91–115, 1988.

[56] K. Fonseca de Lima, A. Lenzi, and R. Barbieri. The study of reactive silencers by shape and parametric optimization techniques. *Applied Acoustics*, 72(4):142–150, 2011.

[57] M.E. Delany and E.N. Bazley. Acoustical properties of fibrous absorbent materials. *Applied Acoustics*, 3(2):105–116, 1970.

[58] F.D. Denia. *Modelado del comportamiento acústico de silenciadores de escape mediante técnicas analíticas y el método de elementos finitos.* PhD thesis, Departamento de Ingeniería Mecánica y de Materiales, Universitat Politècnica de València, Valencia, 2004.

[59] F.D. Denia, A.G. Antebas, A. Selamet, and A.M. Pedrosa. Acoustic characteristics of circular dissipative reversing chamber mufflers. *Noise Control Engineering Journal*, 59(3):234–246, 2011.

[60] F.D. Denia, A.Selamet, M.J. Martínez, and F.J. Fuenmayor. Sound attenuation of a circular multi-chamber hybrid muffler. *Noise Control Engineering Journal*, 56(5):356–364, 2008.

[61] F.D. Denia, F.J. Fuenmayor, and J. Albelda. Three-dimensional analysis of mufflers with conical ducts. analytical, numerical and experimental studies. In J. G. Ih, editor, *The 32nd International Congress and Exposition on Noise Control Engineering, INTER-NOISE 2003*, pages 1–8. Jeju, 2003.

[62] F.D. Denia, F.J. Fuenmayor, A.J. Torregrosa, and A. Selamet. Numerical modelling of thermal effects on the acoustic attenuation of dissipative mufflers. In *41st International Congress and Exposition on Noise Control Engineering 2012, INTER-NOISE 2012*, pages 9376–9387, 2012.

[63] F.D. Denia, E.M. Sánchez-Orgaz, L. Baeza, and R. Kirby. Point collocation scheme in silencers with temperature gradient and mean flow. *Journal of Computational and Applied Mathematics*, 291:127–141, 2016.

[64] F.D. Denia, E.M. Sánchez-Orgaz, F.J. Fuenmayor, and D. J. Busquets. 3D acoustic modelling of multichamber silencers with microperforated surfaces and constant impedance ducts. In *41st International Congress and Exposition on Noise Control Engineering 2012, INTER-NOISE 2012*, pages 5010–5021, 2012.

[65] F.D. Denia, E.M. Sánchez-Orgaz, J. Martínez-Casas, and R. Kirby. Finite elements based acoustic analysis of dissipative silencers with high temperature and thermal-induced heterogeneity. *Finite Elements in Analysis and Design*, 101(4-5):46–57, 2015.

[66] F.D. Denia, A. Selamet, F.J. Fuenmayor, and R. Kirby. Acoustic attenuation performance of perforated dissipative mufflers with empty inlet/outlet extensions. *Journal of Sound and Vibration*, 302(4-5):1000–1017, 2007.

[67] N.S. Dickey, A. Selamet, and J.M. Novak. The effect of high-amplitude sound on the attenuation of perforated tube silencers. *The Journal of the Acoustical Society of America*, 108(3):1068–1081, 2000.

[68] E. Dokumaci. Transmission of sound in uniform pipes carrying hot gas flows. *Journal of Sound and Vibration*, 195(2):257–266, 1996.

[69] E. Dokumaci. A note on transmission of sound in a wide pipe with mean flow and viscothermal attenuation. *Journal of Sound and Vibration*, 208(4):653–655, 1997. abstract.

[70] V. Easwaran and M.L. Munjal. Plane wave analysis of conical and exponential pipes with incompressible mean flow. *Journal of Sound and Vibration*, 152(1):73–93, 1992.

[71] M. Ehsan, M.Z. Shah, M. Hasan, and S.M.R. Hasan. Study of temperature profile in automotive exhaust systems for retrofitting catalytic converters. In *Proceedings of the International Conference on Mechanical Engineering*. Dhaka, 2005.

[72] T. Elnady, M. Åbom, and S. Allam. Modeling perforates in mufflers using two-ports. *Journal of Vibration and Acoustics*, 132(6):061010, 2010.

[73] L.J. Eriksson. Higher order mode effects in circular ducts and expansion chambers. *Journal of the Acoustical Society of America*, 68(2):545–550, 1980.

[74] H.V. Fuchs. *Applied Acoustics: Concepts, Absorbers, and Silencers for Acoustical Comfort and Noise Control*. Springer, 2013.

[75] F.J. Fuenmayor, F.D. Denia, J. Albelda, and E. Giner. H-adaptive refinement strategy for acoustic problems with a set of natural frequencies. *Journal of Sound and Vibration*, 255(3):457–479, 2002.

[76] G.D. Garrison, A.C. Schnell, C.D. Baldwin, and P.R. Russell. Suppression of combustion oscillations with mechanical damping devices. Technical report, Pratt and Whitney Aircraft, 1969.

[77] G.M.L. Gladwell. A variational formulation of damped acousto-structural vibration problems. *Journal of Sound and Vibration*, 4(2):172–186, 1966.

[78] G.M.L. Gladwell and V. Mason. Variational finite element calculation of acoustic response of a rectangular panel. *Journal of Sound and Vibration*, 14(1):115–135, 1971.

[79] G.M.L. Gladwell and G. Zimmermann. On energy and complementary energy formulations of acoustic and structural vibration problems. *Journal of Sound and Vibration*, 3(3):233–241, 1966.

[80] R. Glav. The point-matching method on dissipative silencers of arbitrary cross-section. *Journal of Sound and Vibration*, 189(1):123–135, 1996.

[81] R. Glav. The transfer matrix for a dissipative silencer of arbitrary cross-section. *Journal of Sound and Vibration*, 236(4):575–594, 2000.

[82] G.R. Gogate and M.L. Munjal. Analytical and experimental aeroacoustic studies of open-ended three-duct perforated elements used in mufflers. *The Journal of the Acoustical Society of America*, 97(5):2919–2927, 1995.

[83] Y. Guo, S. Allam, and M. Åbom. Micro-perforated plates for vehicle application. In *The 37th International Congress and Exposition on Noise Control Engineering, INTER-NOISE 2008*. Shangai, 2008.

[84] F. Han, G. Seiffert, Y. Zhao, and B. Gibbs. Acoustic absorption behaviour of an open-celled aluminium foam. *Journal of Physics D: Applied Physics*, 36(3):294, 2003.

[85] H.S. Han, S.S. Chae, and Y.C. Kim. Analytical design of muffler based on transmission loss calculation. In *Fisita World Automotive Congress*. Seoul, 2000.

[86] D. Havelock, S. Kuwano, and M. Vorländer. *Handbook of signal processing in acoustics*. Springer Science & Business Media, 2008.

[87] X. Hou, X. Guo, Z. Liu, F. Yan, and F. Peng. Flow field analysis and improvement of automobile exhaust system cold end. In *International Conference on Computational Intelligence and Software Engineering*. Wuhan, 2010.

[88] N.T. Huff. Materials for absorptive silencer systems. Technical report, SAE Technical Paper, 2001.

[89] W.F. Hughes and E.W. Gaylord. *Basic equations in engineering science*. McGraw-Hill, New York, 1964.

[90] F.P. Incropera. *Fundamentals of heat and mass transfer*. John Wiley & Sons, 2011.

[91] K.U. Ingard. On the design of acoustic resonators. *Journal of the Acoustical Society of America*, 25(4):1037–1061, 1953.

[92] K.U. Ingard and H. Ising. Acoustic nonlinearity of an orifice. *Journal of the Acoustical Society of America*, 42(1):6–17, 1967.

[93] U. Ingard. Perforated facing and sound absorption. *Journal of the Acoustical Society of America*, 26(2):151–154, 1954.

[94] U. Ingard and R.H. Bolt. Absorption characteristics of acoustic material with perforated facings. *Journal of the Acoustical Society of America*, 23(5):533–540, 1951.

[95] K. Jayaraman and K. Yam. Decoupling approach to modeling perforated tube muffler components. *Journal of the Acoustical Society of America*, 69(2):390–396, 1981.

[96] F.C. Karal. The analogous acoustical impedance for discontinuities and constrictions of circular cross section. *The Journal of the Acoustical Society of America*, 25(2):327–334, 1953.

[97] B. Karthik, B.M. Kumar, and R.I. Sujith. Exact solutions to one-dimensional acoustic fields with temperature gradient and mean flow. *The Journal of the Acoustical Society of America*, 108(1):38–43, 2000.

[98] Y.H. Kim and J.W. Choi. General solution of acoustic wave equation for circular reversing chamber with temperature gradient. *Journal of vibration and acoustics*, 113(4):543–550, 1991.

[99] Y.H. Kim, J.W. Choi, and B.D. Lim. Acoustic characteristics of an expansion chamber with constant mass flow and steady temperature gradient (theory and numerical simulation). *Journal of Vibration and Acoustics*, 112(4):460–467, 1990.

[100] R. Kirby. Transmission loss predictions for dissipative silencers of arbitrary cross section in the presence of mean flow. *Journal of the Acoustical Society of America*, 114(1):200–209, 2003.

[101] R. Kirby. A comparison between analytic and numerical methods for modelling automotive dissipative silencers with mean flow. *Journal of Sound and Vibration*, 325(3):565–582, 2009.

[102] R. Kirby and A. Cummings. The impedance of perforated plates subjected to grazing gas flow and backed by porous media. *Journal of Sound and Vibration*, 217(4):619–636, 1998.

[103] R. Kirby and A. Cummings. Prediction of the bulk acoustic properties of fibrous materials at low frequencies. *Applied Acoustics*, 56(2):101–125, 1999.

[104] R. Kirby and F.D. Denia. Analytic mode matching for a circular dissipative silencer containing mean flow and a perforated pipe. *Journal of the Acoustical Society of America*, 122(6):3471–3482, 2007.

[105] R. Kirby and J.B. Lawrie. A point collocation approach to modelling large dissipative silencers. *Journal of Sound and Vibration*, 286(1):313–339, 2005.

[106] J.W. Kooi and S.L. Sarin. An experimental study of the acoustic impedance of Helmholtz resonator arrays under a turbulent boundary layer. In *AAIA 7th Aeroacoustics Conference*. Palo Alto, 1981.

[107] I. Lee, A. Selamet, and N.T. Huff. Acoustic impedance of perforations in contact with fibrous material. *Journal of the Acoustical Society of America*, 119(5):2785–2797, 2006.

[108] S.H. Lee and J.G. Ih. Empirical model of the acoustic impedance of a circular orifice in grazing mean flow. *Journal of the Acoustical Society of America*, 114(1):98–113, 2003.

[109] J. Li, S. Zhao, and K. Ishihara. Study on acoustical properties of sintered bronze porous material for transient exhaust noise of pneumatic system. *Journal of Sound and Vibration*, 332(11):2721–2734, 2013.

[110] S. López-Real. Optimización de componentes mecánicos mediante algoritmo genético y software comercial de elementos finitos. Master's thesis, Departamento de Ingeniería Mecánica y de Materiales, Universitat Politècnica de València, Valencia, 2007.

[111] T.J. Lu, A. Hess, and M.F. Ashby. Sound absorption in metallic foams. *Journal of Applied Physics*, 85(11):7528–7539, 1999.

[112] D.Y. Maa. Microperforated-panel wideband absorbers. *Noise Control Engineering Journal*, 29(3):77–84, 1987.

[113] D.Y. Maa. Microperforated panel at high sound intensity. In *The 23th International Congress and Exposition on Noise Control Engineering, INTER-NOISE 1994*. Yokohama, 1994.

[114] D.Y. Maa. General theory and design of microperforated-panel absorbers. *Acta Acustica*, 5, 1997.

[115] D.Y. Maa. Potential of microperforated panel absorber. *Journal of the Acoustical Society of America*, 104(5):2861–2866, 1998.

[116] M.J. Martínez-Bordes. *Modelado analítico-numérico y caracterización experimental de silenciadores de escape híbridos*. PhD thesis, Departamento de Ingeniería Mecánica y de Materiales, Universitat Politècnica de València, Valencia, 2010.

[117] F.P. Mechel. Extension to low-frequencies of formulas of delany and bazley for absorbing materials. *Acustica*, 35(3):210–213, 1976.

[118] F.P. Mechel. Model theory for fibrous absorber .1. regular fiber arrangements. *Acustica*, 36(2):53–64, 1976.

[119] F.P. Mechel. Model theory for fibrous absorber .2. model consisting of elementary cells and numerical results. *Acustica*, 36(2):65–89, 1976.

[120] F.P. Mechel. *Formulas of acoustics*, volume 2. Springer Science & Business Media, 2002.

[121] O.Z. Mehdizadeh and M. Paraschivoiu. A three-dimensional finite element approach for predicting the transmission loss in mufflers and silencers with no mean flow. *Applied Acoustics*, 66(8):902–918, 2005.

[122] T.H. Melling. Impedance tube for precision-measurement of acoustic impedance and insertion loss at high sound pressure levels. *Journal of Sound and Vibration*, 28(1):23–54, 1973.

[123] G. Montenegro, A. Della Torre, A. Onorati, and R. Fairbrother. A nonlinear quasi-3D approach for the modeling of mufflers with perforated elements and sound-absorbing material. *Advances in Acoustics and Vibration*, 2013, 2013.

[124] T. Mores, J. Morel, and D.A. Blaser. Fluid dynamic and acoustic modeling of concentric-tube resonators/silencers. In *SAE Paper 910071. International Congress and Exposition*. Rio de JaneiroDtroit, 1991.

[125] P.M. Morse and K.U. Ingard. *Theoretical acoustics*. McGraw-Hill, New York, 1968.

[126] M.L. Munjal. *Acoustics of ducts and mufflers, 2nd Edition*. John Wiley & Sons, New York, 2014.

[127] M.L. Munjal and M.G. Prasad. On plane-wave propagation in a uniform pipe in the presence of a mean flow and a temperature gradient. *Journal of the Acoustical Society of America*, 80(5):1501–1506, 1986.

[128] J.E. Murphy and S.A. Chin-Bing. A finite-element model for ocean acoustic propagation and scattering. *The Journal of the Acoustical Society of America*, 86(4):1478–1483, 1989.

[129] E. Nadal. *Cartesian grid FEM (cgFEM): High performance h-adaptive FE analysis with efficient error control. Application to structural shape optimization*. PhD thesis, Departamento de Ingeniería Mecánica y de Materiales, Universitat Politècnica de València, Valencia, 2014.

[130] E. Nadal, J.J. Ródenas, E.M. Sánchez-Orgaz, S. López-Real, and J. Martí-Pellicer. On the use of Cartesian grid finite element code in structural optimization. *Revista Internacional de Métodos Numéricos para Cálculo y Diseño en Ingeniería*, 30(3):155–165, 2014.

[131] B. Nennig, E. Perrey-Debain, and M.B. Tahar. A mode matching method for modeling dissipative silencers lined with poroelastic materials and containing mean flow. *Journal of the Acoustical Society of America*, 128(6):3308–3320, 2010.

[132] The Ceramic Society of Japan. *Advanced Ceramic Technologies & Products*. Springer Science & Business Media, 2012.

[133] E. Pahl. Optimization, an attempt at describing the state of the art. *International Center for Numerical Methods in Engineering (CIMNE), Barcelona*, 2004.

[134] F. Payri, A. Broatch, J.M. Salavert, and D. Moreno. Acoustic response of fibrous absorbent materials to impulsive transient excitations. *Journal of Sound and Vibration*, 329(7):880–892, 2010.

[135] F. Payri, A.J. Torregrosa, and R. Payri. Evaluation through pressure and mass velocity distributions of the linear acoustical description of IC engine exhaust systems. *Applied Acoustics*, 60(4):489–504, 2000.

[136] K.S. Peat. Evaluation of four-pole parameters for ducts with flow by the finite element method. *Journal of Sound and Vibration*, 84(3):389–395, 1982.

[137] K.S. Peat. The acoustical impedance at discontinuities of ducts in the presence of a mean flow. *Journal of Sound and Vibration*, 127(1):123–132, 1988.

[138] K.S. Peat and K.L. Rathi. A finite element analysis of the convected acoustic wave motion in dissipative silencers. *Journal of Sound and Vibration*, 184(3):529–545, 1995.

[139] A.M. Pedrosa. *Desarrollo de herramientas experimentales para la caracterización acústica de silenciadores en presencia de flujo medio.* PhD thesis, Departamento de Ingeniería Mecánica y de Materiales, Universitat Politècnica de València, Valencia, 2015.

[140] A.D. Pierce. Wave-equation for sound in fluids with unsteady inhomogeneous flow. *Journal of the Acoustical Society of America*, 87(6):2292–2299, 1990.

[141] S. Pole. MOGA-II: An improved Multi-Objective Genetic Algorithm. Technical report, Esteco, Trieste, 2003.

[142] D. Potente. General design principles for an automotive muffler. In *Proceedings of Acoustics*, pages 153–158, 2005.

[143] K.N. Rao and M.L. Munjal. Experimental evaluation of impedance of perforates with grazing flow. *Journal of Sound and Vibration*, 108(2):283–295, 1986.

[144] L. Rayleigh. *The theory of sound.* Dover Publications, 1945.

[145] D.F. Ross. A finite element analysis of perforated component acoustic systems. *Journal of Sound and Vibration*, 79(1):133–143, 1981.

[146] S. Rossetti, P. Gardonio, and M.J. Brennan. A wave model for rigid-frame porous materials using lumped parameter concepts. *Journal of Sound and Vibration*, 286(1):81–96, 2005.

[147] A.D. Sahasrabudhe, M.L. Munjal, and S. Anantha Ramu. Analysis of inertance due to the higher order mode effects in a sudden area discontinuity. *Journal of Sound and Vibration*, 185(3):515–529, 1995.

[148] E.M. Sánchez-Orgaz. Evaluación de estrategias de parametrización geométrica y de la medida de control de la velocidad de convergencia en metodologías de optimización de forma basadas en algoritmos evolutivos. Master's thesis, Departamento de Ingeniería Mecánica y de Materiales, Universitat Politècnica de València, Valencia, 2012.

[149] E.M. Sánchez-Orgaz, F.D. Denia, J. Martínez-Casas, and L. Baeza. 3D acoustic modelling of dissipative silencers with nonhomogeneous properties and mean flow. *Advances in Mechanical Engineering*, 6(537935):1–10, 2014.

[150] E.M. Sánchez-Orgaz, F.D. Denia, J. Martínez-Casas, and F.J. Fuenmayor. FE computation of sound attenuation in dissipative silencers with temperature gradients and non-uniform mean flow. In *42nd International Congress and Exposition on Noise Control Engineering 2013, INTER-NOISE 2013: Noise Control for Quality of Life*. Innsbruck, 2013.

[151] E.M. Sánchez-Orgaz, F.D. Denia, J. Martínez-Casas, and L. Baeza. Comparison of numerical approaches for the acoustic modelling of dissipative silencers with temperature gradients and mean flow. In *44th International Congress and Exposition on Noise Control Engineering 2015, INTER-NOISE 2015*, pages 1–12, 2015.

[152] H. Schlichting and K. Gersten. *Boundary-layer theory*. Springer Science & Business Media, 2000.

[153] A. Selamet, F.D. Denia, and A.J. Besa. Acoustic behavior of circular dual-chamber mufflers. *Journal of Sound and Vibration*, 265(5):967–985, 2003.

[154] A. Selamet, H. Kim, and N.T. Huff. Leakage effect in helmholtz resonators. *The Journal of the Acoustical Society of America*, 126(3):1142–1150, 2009.

[155] A. Selamet, I.J. Lee, and N.T. Huff. Acoustic attenuation of hybrid silencers. *Journal of Sound and Vibration*, 262(3):509–527, 2003.

[156] A. Selamet, I.J. Lee, Z.L. Ji, and N.T. Huff. Acoustic attenuation performance of perforated absorbing silencers. Technical report, SAE Paper 2001-01-1435, 2001.

[157] A. Selamet and P.M. Radavich. The effect of length on the acoustic attenuation performance of concentric expansion chambers: An analytical, computational and experimental investigarion. *Journal of Sound and Vibration*, 201(4):407–426, 1997.

[158] A. Selamet, M.B. Xu, I.J. Lee, and N.T. Huff. Analytical approach for sound attenuation in perforated dissipative silencers. *Journal of the Acoustical Society of America*, 115(5):2091–2099, 2004.

[159] A. Selamet, M.B. Xu, I.J. Lee, and N.T. Huff. Analytical approach for sound attenuation in perforated dissipative silencers with inlet/outlet extensions. *Journal of the Acoustical Society of America*, 117(4):2078–2089, 2005.

[160] A. Selamet, M.B. Xu, I.J. Lee, and N.T. Huff. Dissipative expansion chambers with two concentric layers of fibrous material. *International Journal of Vehicle Noise and Vibration*, 1(3):341–357, 2005.

[161] A. Selamet, M.B. Xu, I.J. Lee, and N.T. Huff. Effect of voids on the acoustics of perforated dissipative silencers. *International Journal of Vehicle Noise and Vibration*, 2(4):357–372, 2006.

[162] A.F. Seybert and D.F. Ross. Experimental determination of acoustic properties using a two-microphone random-excitation technique. *Journal of the Acoustical Society of America*, 61(5):1362–1370, 1977.

[163] R.K. Sigman, R.K. Majjigi, and B.T. Zinn. Determination of turbofan inlet acoustics using finite-elements. *AIAA Journal*, 16(11):1139–1145, 1978.

[164] L.J. Sivian. Acoustic impedance of small orifices. *Journal of the Acoustical Society of America*, 7(2):94–101, 1935.

[165] J. Sokolowski and J.P. Zolesio. *Introduction to shape optimization*. Springer, 1992.

[166] B.H. Song and J.S. Bolton. A transfer-matrix approach for estimating the characteristic impedance and wave number of limpid and rigid porous materials. *Journal of the Acoustical Society of America*, 107(3):1131–1152, 2000.

[167] R.I. Sujith. Transfer matrix of a uniform duct with an axial mean temperature gradient. *The Journal of the Acoustical Society of America*, 100(4):2540–2542, 1996.

[168] J.W. Sullivan. Method for modeling perforated tube muffler components. I. Theory. *Journal of the Acoustical Society of America*, 66(3):772–778, 1979.

[169] J.W. Sullivan. Method for modeling perforated tube muffler components. II. Applications. *Journal of the Acoustical Society of America*, 66(3):779–788, 1979.

[170] J.W. Sullivan. Some gas-flow and acoustic pressure measurements inside a concentric-tube resonator. *Journal of the Acoustical Society of America*, 76(2):479–484, 1984.

[171] J.W. Sullivan and M.J. Crocker. Analysis of concentric-tube resonators having unpartitioned cavities. *Journal of the Acoustical Society of America*, 64(1):207–215, 1978.

[172] X. Sun, X. Jing, H. Zhang, and Y. Shi. Effect of grazing-bias flow interaction on acoustic impedance of perforated plates. *Journal of Sound and Vibration*, 254(3):557–573, 2002.

[173] Z. Tao, D.W. Herrin, and A.F. Seybert. Measuring bulk properties of sound-absorbing materials using the two-source method. Technical report, SAE Technical Paper, 2003.

[174] A.J. Torregrosa, A. Broatch, A. Gil, and D. Moreno. Analysis of acoustic networks including cavities by means of a linear finite volume method. *Journal of Sound and Vibration*, 331(20):4575–4586, 2012.

[175] O. Umnova, K. Attenborough, and K.M. Li. Cell model calculations of dynamic drag parameters in packings of spheres. *Journal of the Acoustical Society of America*, 107(6):3113–3119, 2000.

[176] O. Umnova, K. Attenborough, and K.M. Li. A cell model for the acoustical properties of packings of spheres. *Acta Acustica*, 87(2):226–235, 2001.

[177] C.N. Wang. Numerical decoupling analysis of a resonator with absorbent material. *Applied Acoustics*, 58(2):109–122, 1999.

[178] C.N. Wang, Y.N. Chen, and J.Y. Tsai. The application of boundary element evaluation on a silencer in the presence of a linear temperature gradient. *Applied Acoustics*, 62(6):707–716, 2001.

[179] F.M. White. *Fluid Mechanics*. McGraw-Hill, New York, 2003.

[180] P.T. Williams, R. Kirby, C. Malecki, and J. Hill. Measurement of the bulk acoustic properties of fibrous materials at high temperatures. *Applied Acoustics*, 77:29–36, 2014.

[181] T.W. Wu. *Boundary element acoustics*. WIT Press, Southampton, 2000.

[182] X.Yu, L.Cheng, and X.You. Hybrid silencers with micro-perforated panels and internal partitions. *The Journal of the Acoustical Society of America*, 137(2):951–962, 2015.

[183] L.Y. Yeh, Y.C. Chang, M.C. Chiu, and G.J. Lai. GA optimization on multi-segments muffler under space constraints. *Applied Acoustics*, 65(5):521–543, 2004.

[184] C.I.J. Young and M.J. Crocker. Prediction of transmission loss in mufflers by the finite-element method. *The Journal of the Acoustical Society of America*, 57(1):144–148, 1975.

[185] C.I.J. Young and M.J. Crocker. Acoustical analysis, testing, and design of flow-reversing muffler chambers. *The Journal of the Acoustical Society of America*, 60(5):1111–1118, 1976.

[186] O.C. Zienkiewicz and R.L. Taylor. *The Finite Element Method. Volume 1.* Elsevier Butterworth-Heinemann, Oxford, 2000.

List of publications

Some relevant contributions related to the present PhD Thesis are listed below:

1. International journals (JCR)

I. F.D. Denia, E.M. Sánchez-Orgaz, L. Baeza and R. Kirby. Point collocation scheme in silencers with temperature gradient and mean flow. *Journal of Computational and Applied Mathematics*, 291:127-141, 2016.
DOI: http://dx.doi.org/10.1016/j.cam.2015.02.007

II. F.D. Denia, E.M. Sánchez-Orgaz, J. Martínez-Casas and R. Kirby. Finite element based acoustic analysis of dissipative silencers with high temperature and thermal-induced heterogeneity. *Finite Elements in Analysis and Design*, 101(4-5):46-57, 2015.
DOI: http://dx.doi.org/10.1016/j.finel.2015.04.004

III. E.M. Sánchez-Orgaz, F.D. Denia, J. Martínez-Casas, L. Baeza. 3D acoustic modelling of dissipative silencers with non-homogeneous properties and mean flow. *Advances in Mechanical Engineering*, 6(537935):1-10, 2014.
DOI: http://dx.doi.org/10.1155/2014/537935

IV. E. Nadal, J.J. Ródenas, E.M. Sánchez-Orgaz, S. López-Real and J. Martí-Pellicer. Sobre la utilización de códigos de elementos finitos basados en mallados cartesianos en optimización estructural. *Revista Internacional de Métodos Numéricos para el Cálculo y Diseño en Ingeniería*, 30(3):155-165, 2014.
DOI: http://dx.doi.org/10.1016/j.rimni.2013.04.009

2. International congresses

I. E.M. Sánchez-Orgaz, F.D. Denia, J. Martínez-Casas and L. Baeza. Comparison of numerical approaches for the acoustic modelling of dissipative silencers with temperature gradients and mean flow. In *44th International Congress and Exposition on Noise Control Engineering (Inter-noise 2015)*, San Francisco, 2015.

II. E.M. Sánchez-Orgaz, F.D. Denia, J. Martínez-Casas and L. Baeza. Comparación de técnicas basadas en colocación puntual y ajuste modal para la caracterización acústica de silenciadores disipativos con gradientes transversales de temperatura y flujo medio. In *IX Congreso Iberoamericano de Acústica (FIA 2014)*, Valdivia, 2014.

III. E.M. Sánchez-Orgaz, F.D. Denia, L. Baeza and R. Kirby. Numerical mode matching in dissipative silencers with temperature gradients and mean flow. In *7th Forum Acusticum 2014*, Krakow, 2014.

IV. E.M. Sánchez-Orgaz, F.D. Denia, L. Baeza and R. Kirby. Point collocation scheme in silencers with temperature gradient and mean flow. In *Mathematical Modelling in Engineering & Human Behaviour 2014. 16th Edition of the Mathematical Modelling Conference Series at the Institute for Multidisciplinary Mathematics*, Valencia, 2014.

V. E.M. Sánchez-Orgaz, F.D. Denia, F.J. Fuenmayor and R. Kirby. An efficient technique based on numerical mode matching for the acoustic characterization of dissipative silencers with thermal gradients. In *11th World Congress on Computational Mechanics (WCCM 2014)*, Barcelona, 2014.

VI. E.M. Sánchez-Orgaz, F.D. Denia, J. Martínez-Casas and F.J. Fuenmayor. FE computation of sound attenuation in dissipative silencers with temperature gradients and non-uniform mean flow. In *42nd International Congress and Exposition on Noise Control Engineering (Inter-noise 2013)*, Innsbruck, 2013.

VII. F.D. Denia, E.M. Sánchez-Orgaz, F.J. Fuenmayor and D.J. Busquets. 3D acoustic modelling of multichamber silencers with microperforated surfaces and constant impedance ducts. In *41st International Congress and Exhibition on Noise Control Engineering (Inter-noise 2012)*, New York, 2012.

VIII. A.G. Antebas, F.D. Denia, E.M. Sánchez-Orgaz and F.J. Fuenmayor. Numerical transmission loss calculations for perforated dissipative mufflers containing heterogeneous material and mean flow. In *Annual Institute of Acoustics Meeting (Acoustics 2012)*, Nantes, 2012.

3. National congresses

I. F.D. Denia, E.M. Sánchez-Orgaz, J. Carballeira and F. J. Fuenmayor. Modelado del comportamiento acústico de catalizadores cónicos mediante colocación puntual. In *Tecni-acústica 2015. 46° Congreso Español de Acústica. 9° Encuentro Ibérico de Acústica. Simposio Europeo sobre Acústica Virtual y Ambisonics*, Valencia, 2015.

II. E.M. Sánchez-Orgaz, F.D. Denia, L. Baeza and F. J. Fuenmayor. Técnica eficiente basada en ajuste modal para la caracterización de silenciadores disipativos con gradientes transversales de temperatura. In *Tecni-acústica 2014. 45° Congreso Español de Acústica. 8° Congreso Ibérico de Acústica. Simposio Europeo sobre Ciudades Inteligentes y Acústica Ambiental*, Murcia, 2014.

III. E.M. Sánchez-Orgaz, F.D. Denia, F. J. Fuenmayor and R. Kirby. Técnica numérica de colocación puntual para la caracterización acústica eficiente de silenciadores disipativos con gradientes térmicos. In *XX Congreso Nacional de Ingeniería Mecánica*, Málaga, 2014.

IV. E.M. Sánchez-Orgaz, F.D. Denia, J. Martínez-Casas and F.J. Fuenmayor. Modelado numérico del comportamiento acústico de dispositivos de escape de vehículos con gradiente de temperatura y flujo medio no uniforme. In *44° Congreso Español de Acústica. Encuentro Ibérico de Acústica. EAA Simposio Europeo de Acústica Ambiental y Mapas de Ruido (Tecni-acústica 2013)*, Valladolid, 2013.

V. F.D. Denia, E.M. Sánchez-Orgaz, F.J. Fuenmayor and D.J. Busquets. Modelado acústico 3D de silenciadores de escape multicámara con superficies microperforadas y de impedancia constante. In *XIX Congreso Nacional de Ingeniería Mecánica*, Castellón, 2012.